

**ADENOVIRUS STRATEGIES FOR ALTERING THE CELLULAR ENVIRONMENT
IN FAVOR OF INFECTION**

Christin Herrmann

A DISSERTATION

in

Cell and Molecular Biology

Presented to the Faculties of the University of Pennsylvania

in

Partial Fulfillment of the Requirements for the

Degree of Doctor of Philosophy

2019

Supervisor of Dissertation

Matthew D. Weitzman, Ph.D.

Professor of Pathology and Laboratory Medicine

Graduate Group Chairperson

Daniel S. Kessler, Ph.D.

Associate Professor of Cell and Developmental Biology

Dissertation Committee

Carolina B. Lopez, Ph.D., Associate Professor of Microbiology and Immunology

Sara Cherry, Ph.D., Professor of Microbiology

Paul M. Lieberman, Ph.D., Professor of Gene Expression and Regulation

Paul F. Bates, Ph.D., Professor of Microbiology

**ADENOVIRUS STRATEGIES FOR ALTERING THE CELLULAR ENVIRONMENT IN
FAVOR OF INFECTION**

COPYRIGHT

2019

Christin Herrmann

This work is licensed under the
Creative Commons Attribution-
NonCommercial-ShareAlike 4.0
License

To view a copy of this license, visit

<https://creativecommons.org/licenses/by-nc-sa/4.0/us/>

Ich widme diese Arbeit meinen Eltern,
die mich immer darin unterstützt haben
meinen eigenen Weg zu gehen.

ACKNOWLEDGMENTS

I want to thank everyone that has contributed to this great experience of curiosity, inventiveness, learning, many mistakes, and exhilarating successes that is grad school and science in general. I am exceedingly grateful to all of you for your support!

I especially want to thank my advisor Matt. His mentorship, high expectations, and unwavering support have helped me become a better scientist. Matt has taught me the importance of asking the right questions and to always have high expectations of myself. His guidance has enabled me to successfully drive my own research projects, making me ready to face the challenges that are waiting for me as I continue my scientific career. I also want to thank the members of the Weitzman lab, past and present, for their friendship and support - I would not have made it so far without you! I want to especially thank Daphne, who has been a wonderful mentor, helping me understand all the intricacies necessary for being a great scientist, especially writing and designing rigorous experiments. Daphne's attention to detail nicely complemented Matt's big picture view of my scientific development, supporting my development as a well-rounded scientist. I am also very grateful to Jen and Joe; whose help made the second project of this thesis possible. Additionally, I want to thank Alex and Matt C for many great and often crazy discussions inside the lab and out. They always reminded me what I love about science - that your craziest hypotheses are often the best, you just have to come up with a way to test them. Furthermore, I am thankful to our numerous collaborators, especially the members of the Garcia lab that have made my projects feasible with the magic that is mass spectrometry.

I want to thank my committee members, Carolina Lopez, Sara Cherry, Paul Lieberman, and Paul Bates, for scientific input on my projects and their help in my career development. I am also exceedingly grateful to the amazing communities in CAMB, Microbiology, Protective Immunity, and Cancer Pathobiology for the exposure to great science and insightful discussions. A special thank-you goes to the CAMB office, Anna Kline, Meagan Schofer, Kathy O'Connor-Cooley, and Christina Strathearn, who have always been exceedingly helpful in anything grad school related, particularly in navigating Penn bureaucracy.

I want to thank my previous mentors for helping me on my way to grad school. This is especially true for Walther Mothes, my advisor for my master's thesis. Without his encouragement I would never have gone to Penn. Thank you for guiding me in the right direction!

I also want to thank my friends back home and all the amazing people I have met here during my time at Penn. You have made grad school an amazing experience! I have met too many amazing people to possibly thank them all - but I want to give a special shout out to Annie, Priya, Chris, Steve, the other Steve, Devin, Terra, Colleen, David, Somdutta, Ian, Kayla, and Vineet!

Most importantly, I would like to thank my parents and my family. Without them this thesis, and the work it represents, would not have been possible. I know it has not always been easy for them that I chose to follow my dream on the other side of the world, but I would like to let them know how grateful I am for their unwavering support. I am also extremely grateful to my boyfriend Bobby for his love and support - I look forward to starting our next big adventure together! I also want to thank Bobby's family for welcoming me into their midst. Finally, I want to thank my cat Cooper who has always been able to distract me when I most needed it. While he might not be entirely sane himself, he has definitely saved what is left of my sanity.

ABSTRACT

ADENOVIRUS STRATEGIES FOR ALTERING THE CELLULAR ENVIRONMENT IN FAVOR OF INFECTION

Christin Herrmann

Matthew D. Weitzman, Ph.D.

Viruses, as obligate intracellular pathogens, rely on their host cell for successful replication. Viruses have evolved different strategies to hijack and redirect cellular processes to benefit infection and overcome host immune responses. Understanding the mechanisms by which viruses exploit their host cells will reveal new targets for antiviral therapies. In addition, these studies can provide insights into the regulation of fundamental cellular processes. While much progress has been made in this area, many unexpected nuances of virus-host interaction are still being discovered. Here, we employed several strategies to uncover new aspects of viral manipulation of the host environment by adenovirus, a nuclear-replicating DNA virus that commonly infects humans.

The first project focused on how viral histone-like proteins impact cellular chromatin. Adenovirus encodes the small, basic protein VII that coats and condenses viral genomes. The effect of this viral DNA-binding protein on host chromatin structure and function had remained unexplored. Here we demonstrated that protein VII interacts with host nucleosomes and is sufficient to alter nuclear morphology. We also identified post-translational modifications of protein VII that regulate chromatin association. Through a proteomics analysis of chromatin composition, we revealed that protein VII causes nuclear retention of HMGB1, a host alarmin, and reduces downstream inflammation.

The second project examined roles of viral-mediated ubiquitination during infection. Ubiquitination of host proteins, mediated by adenovirus proteins E1B55K and E4orf6, is important for viral RNA processing. However, previously identified substrates of viral-mediated

ubiquitination do not explain this phenotype. Here we used a proteomics approach to define new substrates of the E1B55K/E4orf6 complex. We uncovered viral-mediated ubiquitination of RNA-binding proteins (RBPs) which, unlike ubiquitination of other substrates, does not result in proteasomal degradation. We furthermore demonstrated that ubiquitination of RBPs RALY and hnRNP-C decreases their binding to viral RNA and relieves a restriction these host proteins exert on adenovirus RNA processing.

Our study of adenovirus proteins revealed new strategies employed by viruses to alter host functions: manipulating host chromatin through viral histone-like proteins to dampen immune responses and regulating RNA processing by non-degradative ubiquitination of cellular RBPs.

TABLE OF CONTENTS

DEDICATION	III
ACKNOWLEDGMENTS	IV
ABSTRACT	VI
TABLE OF CONTENTS	VIII
LIST OF TABLES	X
LIST OF ILLUSTRATIONS	XI
CHAPTER 1: INTRODUCTION	1
1.1 Virus vs. Host	1
1.2 Adenovirus	2
1.2.1 Adenovirus virion structure	2
1.2.2 The adenovirus life cycle	3
1.2.3 Adenovirus as a model system to study virus-host interaction	5
1.3 Viruses, histones, and chromatin	6
1.3.1 Histones and cellular chromatin	7
1.3.2 Viral manipulation of histones	8
1.3.3 Ad protein VII as a viral histone-like protein	10
1.4 Viruses and the ubiquitin system	13
1.4.1 The host ubiquitin system	13
1.4.2 Viral manipulation of the host ubiquitin system.....	14
1.4.3 Adenovirus E1B55K/E4orf6 and the ubiquitin system	16
1.5 Figures	20
CHAPTER 2: A CORE VIRAL PROTEIN BINDS HOST NUCLEOSOMES TO SEQUESTER IMMUNE DANGER SIGNALS	33
2.1 Abstract	33
2.2 Introduction	34
2.3 Results	34
2.4 Figures	40
2.5 Methods	55

CHAPTER 3: VIRAL-MEDIATED UBIQUITINATION IMPACTS INTERACTIONS OF HOST PROTEINS WITH VIRAL RNA AND PROMOTES VIRAL RNA PROCESSING.	67
3.1 Abstract.....	67
3.2 Introduction	68
3.3 Results	69
3.4 Discussion	79
3.5 Figures	82
3.6 Materials and Methods	99
CHAPTER 4: CONCLUSIONS AND FUTURE DIRECTIONS	111
4.1 Summary.....	111
4.2 Viral histone-like proteins and the manipulation of host chromatin	113
4.3 Non-degradative ubiquitination during viral infection and RNA processing	118
4.4 Implications for oncolytic virus design	127
4.5 Concluding remarks	129
4.6 Figures	130
APPENDIX.....	131
Appendix 1: Differential Salt Fractionation of Nuclei to Analyze Chromatin-associated Proteins from Cultured Mammalian Cells.....	131
Appendix 2: Mapping the protein VII-HMGB1 interaction and determining the role of HMGB1 for intracellular steps of Ad infection	149
BIBLIOGRAPHY	165

LIST OF TABLES

Table A1.1 Preparation of different fractions for Western blot.....	145
---	-----

LIST OF ILLUSTRATIONS

Figure 1.1 Virus vs. host.	20
Figure 1.2 Schematic of the Ad virion structure.	21
Figure 1.3 Schematic of the Ad life cycle highlighting the different stages of virus replication. ...	22
Figure 1.4 Schematic of the Ad genome structure.	23
Figure 1.5 Schematic of the replication of the Ad genome.	24
Figure 1.6 The basic structure of cellular chromatin.	25
Figure 1.7 Different viral strategies to exploit cellular histones and chromatin.	26
Figure 1.8 Change in nuclear architecture during Ad infection.	27
Figure 1.9 Rationale for project 1.	28
Figure 1.10 The host ubiquitin system.	29
Figure 1.11 Different viral strategies to hijack the cellular ubiquitin system.	30
Figure 1.12 Schematic of the E1B55K/E4orf6 ubiquitin ligase complex.	31
Figure 1.13 Rationale for project 2.	32
Figure 2.1 Protein VII is sufficient to alter chromatin and directly binds nucleosomes.	40
Figure 2.S1 Adenovirus protein VII distorts chromatin.	41
Figure 2.S2 Protein VII associates tightly with chromatin and binds DNA and nucleosomes in vitro.	42
Figure 2.S3 Bioanalyzer examination of MNase-digested nucleosomes and protein-VII-nucleosome complexes.	43
Figure 2.2 Post-translational modifications on protein VII contribute to chromatin localization. ...	44
Figure 2.S4 Purification of protein VII from infected cells.	45
Figure 2.S5 Representative mass spectra.	46
Figure 2.S6 Acetylated protein VII spectra from virus particles and analysis of total histone PTM changes upon protein VII expression.	47
Figure 2.3 Protein VII directly binds HMGB1 and is necessary for retention of the alarmin in cellular chromatin.	49
Figure 2.S7 Bioinformatic analysis of proteins enriched in the high-salt fraction upon protein VII expression.	50
Figure 2.S8 Protein VII retains HMGB1 and HMGB2 in chromatin.	51
Figure 2.S9 Protein VII is necessary and sufficient for chromatin retention of HMGB1 in human and mouse cells.	52
Figure 2.4 Protein VII prevents HMGB1 release.	53
Figure 2.S10 Transduction of mouse lungs demonstrating expression of GFP or protein-VII-GFP.	54
Figure 3.1 E1B55K deletion or inhibition of Cullin-mediated ubiquitination decreases adenovirus late RNA splicing and RNA processing overall.	82

Figure 3.S1 E1B55K deletion or inhibition of Cullin-mediated ubiquitination does not decrease viral early RNA levels or splicing.....	83
Figure 3.2 Unbiased proteomics reveals RNA-binding proteins among putative non-degraded substrates of the Ad ubiquitin ligase.	84
Figure 3.S2 Quantification of number of peptides and proteins identified in di-glycine remnant profiling and whole cell proteome data sets.....	85
Figure 3.S3 Di-glycine remnant profiling and whole cell proteome data for RNA-binding proteins enriched within the predicted E1B55K/E4orf6 substrates.....	86
Figure 3.S4 Network analysis of predicted E1B55K/E4orf6 substrates identifies a “RALY/hnRNP-C module” enriched for RNA-binding proteins.	87
Figure 3.S5 MS2 evidence for ubiquitination site localization in RALY (a) and hnRNP-C (b-f) peptides.....	90
Figure 3.3 RALY and hnRNP-C are non-degraded substrates of the Ad ubiquitin ligase.	91
Figure 3.S6 RALY and hnRNP-C are not decreased upon transduction in multiple cell lines. ...	93
Figure 3.4 Knock-down of RALY and hnRNP-C rescues the RNA processing defect caused by the absence of a functional viral ubiquitin ligase.	94
Figure 3.S7 RALY and hnRNP-C single knock-down rescue late protein, RNA and splice efficiency during infection with Ad Δ E1B.....	95
Figure 3.5 The interaction of hnRNP-C with viral late RNA increases in the absence of a functional viral ubiquitin ligase.	96
Figure 3.S8 No dramatic difference in protein localization and protein-complex formation of RALY and hnRNP-C between Ad WT and Δ E1B infection.....	97
Figure 3.6 Non-degradative ubiquitination of RNA-binding proteins promotes efficient adenoviral RNA processing.	98
Figure 4.1 Thesis summary.....	130
Figure A1.1 Schematic of nuclear fractionation and example Western blot.	142
Figure A1.2 Fractionation of nuclear protein HMGB1 can differ depending on the method of nuclear isolation.	143
Figure A1.3 Intermediate steps of nuclear isolation.....	144
Figure A1.4 Digestion of cellular DNA using MNase.	146
Figure A2.1 The Ad5 but not MAV-1 protein VII interacts with HMGB1.	156
Figure A2.2 The N-terminus of Ad5 protein VII interacts with HMGB1.....	157
Figure A2.3 Protein VII interacts with the HMGB1 A-box in cells.	158
Figure A2.4 HMGB1 C-terminus interacts with protein VII in vitro.....	159
Figure A2.5 Deletion of HMGB1 does not impact Ad5 infection.	160
Figure A2.6 Protein VII suppresses IFN β expression through HMGB1.....	161

CHAPTER 1: INTRODUCTION

A portion of this chapter has been adapted from:

Dybas JM, **Herrmann C**, Weitzman MD. Ubiquitination at the interface of tumor viruses and DNA damage responses. *Curr Opin Virol* **32**, 40-47 (2018). **PMID: 30261451**.¹

AND

Charman M, **Herrmann C**, Weitzman MD. Viral and Cellular Interactions During Adenovirus DNA Replication. 2019. *FEBS Letters*. Submitted.

1.1 Virus vs. Host

Viruses are obligate intracellular pathogens that rely on host cell components for successful infection and have evolved sophisticated mechanisms to alter the cellular environment to their advantage (**Figure 1.1**). This takeover can disrupt host processes with detrimental outcomes for the infected cell and the organism as a whole. Accordingly, host cells have developed different layers of defense against viral infection that can interfere with each step of the viral life cycle, from entry to virus release. Cells can sense molecules that contain foreign patterns introduced by viruses, such as aberrant RNA or DNA structures. The recognition of these pathogen-associated molecular patterns (PAMPs) activates a multifaceted antiviral response, including the interferon pathway that can stimulate an antiviral state in an autocrine and paracrine fashion to directly antagonize viral processes and prevent a spread of the infection²⁻⁴. Viruses in turn use diverse strategies to overcome these host barriers, leading to an arms race of evolution between viruses and their hosts⁵. This coevolution makes viruses an excellent model system to understand regulation of cellular processes as these pathogens have evolved to exploit host cells for their own replication using as minimal machinery as possible^{5,6}. Understanding virus-host interaction will also allow for development of better antiviral drugs as well as treatment of unrelated human diseases, as viruses can be used as a platform for oncolytic cancer treatment, gene therapy, and vaccine development. While viruses have evolved numerous different strategies to manipulate

the host cell environment, there are commonalities to be found as many viruses target the same cellular pathways. For example, many DNA and RNA viruses interact with host chromatin components to regulate their own replication and transcription^{7,8}. Another common target for viral manipulation is the host ubiquitin machinery. The main focus in studying this virus-host interaction has been traditionally proteasomal degradation of host factors restrictive to viral infection^{1,9,10}. This thesis will examine new aspects of virus-host interaction on the level of chromatin and viral-mediated ubiquitination.

1.2 Adenovirus

Adenovirus (Ad) was originally isolated from pediatric adenoid tissue in 1953¹¹. It comprises a family of small, non-enveloped double-stranded DNA (dsDNA) viruses that replicate in the nucleus of host cells¹². There are at least 56 human Ad serotypes, all with similar genome structure and encoding homologous proteins¹³. These serotypes can be classified into 7 subgroups, A through G. Depending on the serotype, Ad causes mild respiratory disease, conjunctivitis, or infantile gastroenteritis, but can be life-threatening in immunocompromised individuals. Ad is also of particular interest for the healthcare research community as it provides an attractive delivery method, both *in vitro* and *in vivo*, for genetic information. Its ~36 kb genome is relatively easy to manipulate, which allows for inactivation viral gene expression and insertion of other genes of interest. These features make Ad an excellent platform for gene therapy, vaccines, and oncolytic viruses used in cancer therapy¹⁴⁻¹⁷. Most studies have used either Ad2 or Ad5, two closely related serotypes in subgroup C that commonly infect the human respiratory tract. The work described in this thesis was carried out using Ad5 unless otherwise noted.

1.2.1 Adenovirus virion structure

Ad virions are non-enveloped, with an outer capsid and an inner core comprised exclusively of viral proteins and nucleic acid (**Figure 1.2**)¹⁸⁻²⁰. The icosahedral capsid contains the major capsid proteins hexon, penton, and fiber^{21,22}. Minor capsid proteins IIIa, VIII, and IX further stabilize the structure^{18,19}. The core contains many additional viral proteins. The small, basic core proteins V,

VII, and μ interact with the dsDNA genome ranging in size from 25 to 45 kb and likely contribute to condensation of the DNA²³⁻²⁶. One copy of the terminal protein, which serves as a primer during viral genome replication, is covalently attached to the 5' end of each DNA strand^{27,28}. In addition, the core also contains the viral protease that is involved in maturation of viral particles as well as virion entry into the cell^{29,30}, and protein IVa2 that is implicated in packaging³¹.

1.2.2 The adenovirus life cycle

There are two phases of the Ad life cycle: an early and a late phase that are separated by the onset of viral DNA replication (**Figure 1.3**)¹². The virus is taken up into host cells through receptor mediated endocytosis. First, virions make a low-affinity interaction with integrins on the cell surface^{32,33}, followed by a high-affinity interaction of fiber with the viral receptor³⁴. Receptor usage differs between the subgroups: A, C, D, E, and F bind to the tight junction protein CAR (Coxsackie B, Adenovirus Receptor)³⁵ while subgroup B viruses bind to CD46³⁶. The interaction with their respective receptors induces clathrin-mediated endocytosis of the virions^{37,38}. In the endosomes, acidification activates the viral protease that cleaves protein VI³⁰. Cleaved protein VI then facilitates release of the virions into the cytoplasm. Transport of the virions to the nucleus occurs on microtubules through the interaction of hexon with dynein motor proteins^{39,40}. Uncoating of the virions begins with the loss of fiber at the cell surface with further uncoating in the endosome, thought to be triggered by acidification³⁸. At the nuclear pore, final disassembly is triggered and the genome is imported coated only with protein VII and covalently attached to two copies of the terminal protein⁴¹.

The Ad genome is divided into early and late transcription units (**Figure 1.4**). The early proteins expressed before the onset of DNA replication mainly fulfill three functions: 1) facilitating entry of the infected cell into S-phase to ensure all the necessary resources for virion assembly are present, 2) protection from the immune response triggered by infection, and 3) initiation of viral genome replication¹².

The first viral protein expressed is E1A, due to the strong promoter of this gene^{42,43}. The E1A transcript produces two different major isoforms, called small and large E1A. Large E1A functions

as a transactivator for the E1A gene and other viral early transcription units through recruitment of cellular transcription factors to the viral genome^{44,45}. In addition, both small and large E1A are capable of inducing cellular entry into S-phase to ultimately support viral DNA replication, which occurs through interaction with the Rb family of proteins. E1A binding removes Rb from the E2F family of transcription factors, which is required for entry into S-phase⁴⁶. Both E1A isoforms also alter the transcriptional landscape, upregulating proviral and downregulating antiviral genes to further support viral replication⁴⁷. For example, E1A inhibits the induction of interferon stimulated genes (ISGs) by preventing activating histone marks at these specific loci⁴⁸⁻⁵¹. The E1B region encodes two major proteins, E1B19K and E1B55K. E1B19K is an anti-apoptotic homolog of the BCL2-family member MCL-1 and blocks cell death induced as a consequence of E1A functions⁵². E1B55K can also block apoptosis and alter the cellular environment to support viral infection - discussed in detail in Chapter 1.4.3⁵³.

The E2 region encodes the three viral proteins necessary for genome replication^{28,54}: the pre-terminal protein that serves as primer for DNA replication²⁷, the Ad DNA polymerase, and the single-strand DNA-binding protein DBP that stabilizes single-stranded DNA (ssDNA) and promotes strand separation during DNA replication^{55,56}. The E3 region encodes several proteins that are important for inhibiting innate and adaptive immune responses towards the virus⁵⁷. The E4 region encodes 6 distinct proteins: orf1, orf2, orf3, orf4, orf6, and orf6/7. These early proteins are involved in regulating several cellular processes including transcription, mRNA splicing, translation, apoptosis, protein turnover, and the host DNA damage repair (DDR) towards the Ad genomes^{58,59}. The most important gene products are E4orf3 and E4orf6, as deletion of both together severely reduces virus replication^{60,61}. E4orf3 interacts with PML nuclear bodies, a nuclear structure involved in antiviral immune responses, transcription, apoptosis, and the DDR⁶². The association with E4orf3 rearranges PML nuclear bodies into tracks^{63,64}. E4orf3 then recruits cellular proteins into these tracks, including several proteins involved in the DDR. This suppresses recognition of the viral DNA by these DNA repair factors that would otherwise induce degradation or concatemerization of the genomes⁶³⁻⁶⁷. E4orf6 associates with E1B55K and

several host proteins to form a viral ubiquitin ligase, the function of which is discussed in detail in Chapter 1.4.3 below.

The replication of the Ad genome occurs in viral replication centers that can be visualized by staining for DBP⁶⁸. Several host proteins, in addition to the viral gene products of the E2 region, are involved in replicating the viral DNA^{28,69}. This process occurs in two rounds. First, one DNA strand is replicated while the second strand is displaced as the nascent DNA strand is elongated. Second, the displaced strand circularizes by self-annealing of the complementary ends, forming a panhandle structure. This DNA structure allows for replication of the second strand via a similar mechanism as the first round (**Figure 1.5**)^{12,28}.

The late genes are only expressed upon onset of genome replication⁷⁰. Most late transcripts are expressed through the major late promoter (MLP). The MLP is heavily alternatively spliced to 5 distinct transcription units with separate poly(A) sites that encode at least 14 distinct late mRNA species (**Figure 1.4**)⁷¹. These gene products include structural components of viral particles, proteins involved in DNA condensation, and proteins that facilitate virion formation. Assembly of new particles occurs in the nucleus where virions accumulate until release through lysis of the host cell^{20,72,73}. Overall, one infected cell produces tens of thousands new virus particles and a large excess of structural proteins¹².

1.2.3 Adenovirus as a model system to study virus-host interaction

Ad is commonly used in research in part because of its easy propagation in cell culture and ability to synchronously infect many different cell types. In addition, the Ad genome can be easily manipulated to create different mutant viruses. This makes Ad an excellent model system to not only study virus-host interaction but also investigate the regulation of fundamental cellular processes⁶. Ad was instrumental in the discovery of RNA splicing. This fundamental cellular process was discovered while trying to map the regions of the Ad genome encoding the hexon protein to the corresponding late mRNA^{74,75}. In addition, work with Ad has enabled a better understanding of the processes involved in cellular transformation and cancer development. Ad was the first human virus shown to induce tumor formation, even though these experiments were

carried out in rodents⁷⁶. This is one reason Ad is sometimes classified as a tumor virus although there is no evidence to link Ad to cancer in humans. Several Ad proteins by themselves are sufficient to facilitate entry into the cell cycle and transform human cells in culture⁷⁷. For example, HEK293 cells were generated through integration of part of the Ad DNA containing the E1 region into the cellular genome, resulting in immortalization of these cells^{77,78}. The E1A protein induces entry of these cells into the cell cycle and reprograms transcription^{46,47}. E1B19K as a homolog of anti-apoptotic protein MCL-1 prevents cell death⁵². E1B55K also counteracts apoptosis through inactivation of the tumor suppressor p53⁷⁹⁻⁸¹. In addition, E1B55K was actually the second viral protein, after SV40 large T antigen, to be shown to interact with p53⁸². The DDR is another area of research that benefitted greatly from studying Ad. As mentioned earlier, Ad has several mechanisms to overcome the host DDR that would otherwise recognize and antagonize viral genomes. The virus causes ubiquitin-dependent degradation or mislocalization of the MRN complex, which consists of MRE11, RAD50, and NBS1, and is important in recognition and processing of dsDNA breaks⁶⁷. These findings not only enabled the study of these host proteins in context of the DDR towards viral genomes but also studies to define their role in DNA repair in general⁸³⁻⁸⁶.

These examples highlight the value of Ad as a model system to examine cellular processes at the interface of virus-host interaction. The work in this thesis focuses on defining additional ways Ad employs viral proteins to alter the host cell environment in favor of infection. Project 1, described in Chapter 2, investigates the manipulation of host chromatin by an Ad histone-like protein. Project 2, which forms the basis for Chapter 3, examines how hijacking the host ubiquitin machinery contributes to viral RNA processing.

1.3 Viruses, histones, and chromatin

Cellular histones not only serve to condense DNA but also modulate global genome structure and accessibility to regulate DNA replication, DNA repair, and gene expression⁸⁷⁻⁹⁰. This contributes to processes such as cell differentiation and immune responses⁹¹⁻⁹⁵. Viruses have

evolved many different ways to use host chromatin components to regulate their own genomic material and alter the host transcriptome^{7,8}. At the same time viruses have to overcome ways the host uses chromatin components to block viral genome replication and to suppress viral transcription^{7,8,83-86}. This section will highlight the regulation of host chromatin, different strategies viruses have developed to exploit cellular histones, and discuss how viral proteins with similar functions to histones may in turn impact host DNA.

1.3.1 Histones and cellular chromatin

In human cells, 2 meters of DNA are condensed into a nucleus with an average of 6 μm diameter while the organization necessary for proper gene expression, DNA replication, and repair is maintained. The basic structure that makes this possible is the nucleosome: 147 bp of DNA wrapped around an octamer of core histones, containing two copies each of histones H2A, H2B, H3, and H4⁹⁶⁻⁹⁸. The tight wrapping of DNA in nucleosomes is possible through the interaction of the small, highly basic histones with the positively charged phosphate backbone of DNA. The linker histone H1 associates with the core nucleosome and linker DNA to stabilize higher-order chromatin structure such as fibers (**Figure 1.6**)^{99,100}. Nucleosomes compact the genome but also regulate access to the DNA, serve as platforms for epigenetic signaling, and regulate the formation of higher order structures. There are two basic types of chromatin, heterochromatin and euchromatin. In transcriptionally silent heterochromatin nucleosomes form more compact structures, limiting access of transcription factors. Euchromatin, on the other hand, is more accessible and transcriptionally active. Chromatin is dynamically regulated through DNA modifications, histone modifications, and chromatin remodeling complexes. DNA can be methylated at CpG motifs throughout the genome, especially at CpG islands, resulting in silencing of associated chromatin¹⁰¹. While the C-terminal globular domains of histones form the central core of nucleosome, the N-terminal tails of histones are unstructured, extend from the core, and can be modified with more than 200 different histone marks including acetylation, methylation, ubiquitination, and phosphorylation¹⁰². This forms the basis for the histone code, which is the principle that different histone marks and their combination determine the protein

occupancy and transcriptional state of the associated DNA sequence⁸⁷⁻⁹⁰. More than 150 different cellular histone-modifying enzymes have been identified so far¹⁰³. Modifications of histones can alter the local chromatin compaction, impact nucleosome dynamics, and serve as binding platforms for chromatin-associated proteins. Several histone marks have been associated with more open and active chromatin such as acetylation (e.g. acetylation of histone H3 at lysine 9, abbreviated H3K9Ac) and methylation (e.g. H3K4me1 or H3K4me3). Methylation of other lysine residues within histones, such as H3K27me3 or H3K9me3, are associated with more tightly-packed and thus silent chromatin⁸⁷⁻⁸⁹. Some histone modifications can also play a role in other processes, such as phosphorylation of histone H2A variant H2A.X (γ H2A.X) which is important for DDR signaling^{104,105}. Histone marks can be read out by chromatin remodeling complexes. More than 100 proteins have been identified as components of these complexes, which use ATP to mobilize nucleosomes and change chromatin structure^{89,106}.

1.3.2 Viral manipulation of histones

Viruses have evolved different strategies to exploit histones and chromatin regulatory mechanisms to facilitate successful infection^{7,8}. Viruses need to regulate the chromatin components such as chromatin remodelers, transcription factors, and histone chaperones associated with their genomes to their advantage while avoiding detrimental effects such as viral genome silencing or activation of an aberrant DDR^{7,8,83-86}. Cellular histones can fulfill different roles during virus infection. This includes functions such as condensing viral genomes to regulating viral gene expression and ensuring propagation of viral genomes to the two daughter cells during cell division (**Figure 1.7**). This section highlights some examples of viral strategies employed to harness cellular histones and host chromatin.

Viruses have to condense their genetic information for packaging into viral particles and have evolved different strategies to achieve this. Papillomaviruses such as HPV and polyomaviruses including SV40 package their circular dsDNA genomes into virions as 'minichromosomes' using the four core histones as well as linker histone H1 from host cells (**Figure 1.7a**)^{107,108}. This allows for condensation of the viral genetic material and eliminates the need to remove histones during

packaging. For SV40 it has been demonstrated that the packaged histones contain different post-translational modifications (PTMs) to optimize compaction and transcription upon infection¹⁰⁹⁻¹¹².

Herpesviruses (e.g. HSV, KSHV, and EBV) and many other DNA viruses are devoid of histones in viral particles. However, viral genomes become rapidly chromatinized upon entry into the nucleus (**Figure 1.7b**). Initially, repressive chromatin marks are deposited to silence the viral genomes. This is followed by viral-mediated remodeling of histone marks and activation of viral transcription¹¹³⁻¹¹⁵. Herpesviruses can undergo both lytic and latent infection, and the chromatin state associated with viral genomes differ under these conditions¹¹⁶. For HSV, lytic or productive infection occurs in epithelial cells with active transcription of lytic genes and more euchromatin-like histone modifications¹¹³⁻¹¹⁵. In neurons, HSV is predominantly latent and there is a progressive association of heterochromatin marks with the viral genome as latency is established¹¹⁷. In addition, different regions of the Herpesvirus DNA are associated with distinct types of histones marks under these conditions. Latency genes are actively transcribed and associated with more active chromatin marks. Lytic genes, on the other hand, are silenced. Immediate early genes are in a poised chromatin state with both active and repressive histone modifications, or active chromatin marks but repression of transcription elongation. Late genes are associated with facultative heterochromatin that is silent but poised for reactivation^{118,119}.

Viruses that integrate into the host genome, including HIV, are also associated with cellular histones. For these viruses, the integration site and surrounding host chromatin in part regulate the activity of integrated proviruses¹²⁰. Latently infected cells with silenced proviruses represent a major reservoir for HIV and are a barrier for curing infection¹²¹. Some latent proviruses can be reactivated by altering the repressive chromatin marks associated with viral genomes. A proposed strategy to cure HIV is to use drugs to reactivate the proviruses that make up the viral reservoir, resulting in recognition and clearance of infected cells by the immune system¹²². For example, histone deacetylase (HDAC) inhibitors that increase histone acetylation can reactivate a subset of latent proviruses^{123,124}. However, not all proviruses are reactivated through this treatment and additional strategies will be needed for a successful cure¹²⁵.

Certain viruses that undergo viral latency, including HPV, KSHV, and EBV, have evolved mechanisms to tether their genomes to host chromatin to facilitate partitioning of viral genomes to daughter cells during cell division (**Figure 1.7c**). HPV protein E2 directly links viral genomes to active regions of host chromatin throughout the cell cycle. In addition to facilitating genome distribution during mitosis, this also allows access to transcription factors and prevents silencing of the viral DNA by the host^{126,127}.

While RNA viruses do not package their genomes using nucleosomes, studies suggest that nuclear-replicating RNA viruses can interact with cellular histones and host chromatin. Replication of influenza virus has been proposed to occur in DNase-insensitive nuclear fractions at the nuclear matrix, and influenza proteins M1 and NP have been shown to associate with nucleosomes¹²⁸⁻¹³⁰. In addition, one serotype of influenza has been shown to alter cellular transcription by mimicking cellular histones. The NS1 protein of influenza serotype H3N2 contains a short histone-like sequence at its C-terminus that recruits the PAF1 transcription elongation complex. This association blocks the function of the host complex and reduces antiviral gene expression¹³¹.

1.3.3 Ad protein VII as a viral histone-like protein

Although some viruses use cellular histones for condensing their genomes inside virions^{107,108}, many viruses use alternative strategies. HSV, for example, has little or no protein associated with the DNA in virus particles. Instead it uses the highly basic polyamine spermine to condense its genomic information¹³². Other viruses encode their own small basic proteins that are thought to function similarly to histones¹³³⁻¹³⁷.

Ad encodes a small, basic protein named protein VII that condenses viral DNA inside virions¹³³⁻¹³⁵. Protein VII is an Ad late protein expressed from the L2 region of the viral genome (**Figure 1.4**) and its functions have been extensively studied in the context of association with viral genomes. Like many other Ad proteins, protein VII is produced as a precursor and then cleaved by the viral protease during virion maturation¹³⁸. Protein VII contributes to many stages of

the Ad life cycle such as transcription¹³⁹⁻¹⁴³, evasion of the DDR¹⁴⁴, and, of course, condensation of the viral DNA in virions^{133,134}. These functions of protein VII are summarized below.

There are conflicting reports about the role of protein VII in viral transcription. Condensation of the genome is essential for packaging, but impedes transcription once imported into the nucleus^{140,142}. It is thought that displacement of protein VII is necessary for transcription to occur. Indeed, over time the levels of protein VII on viral genomes decrease while the amount of cellular histones on the viral DNA increases^{139,145-148}. Initially, the histone variant H3.3 is loaded onto the Ad genome in a replication-independent manner by the histone chaperone HIRA^{149,150}. This results in nucleosome spacing on viral genomes comparable to that found on cellular chromatin by 6 hours post infection (hpi)¹⁴⁹. Later during infection, when viral DNA replication has been initiated, the association with histone H3 decreases and the nucleosome pattern is less structured¹⁵⁰. There is evidence that remodeling of protein VII regulates the timing of transcription. At 6 hpi, protein VII is still largely associated with the transcriptionally silent MLP region of the genome, and association with the highly transcribed E1A region is decreased¹³⁹. While these observations suggest that protein VII functions as a transcriptional repressor, there are reports that association of protein VII with DNA can facilitate transcription and that this viral core protein can recruit the E1A transactivator to the genome to support gene expression^{139,143}.

Protein VII also interacts with the cellular protein SET (also known as TAF-I - template-activating factor-I)¹³⁹⁻¹⁴². SET promotes dissociation of protein VII from viral DNA to support early gene expression and genome replication¹³⁹⁻¹⁴². It was recently shown that SET also contributes to the protein VII-mediated protection of the incoming genome from the host DDR^{144,151}.

Protein VII is the major core component of viral particles with about 800 copies per virion and is thought to contribute to condensation of viral DNA in capsids^{22,152}. Interestingly, protein VII is dispensable for the actual packaging process¹⁵³. Viral particles containing genomes are still made in the absence of protein VII, suggesting that other viral proteins can condense the viral DNA. However, virions lacking protein VII do not properly uncoat upon infection of the next cell and do not escape the endosome¹⁵³. Viral DNA isolated from virions is coated with protein VII and

exhibits a beads-on-a-string pattern reminiscent of host DNA wrapped around cellular histones^{134,154}. This observation further highlights the similarity between Ad protein VII and histones. Protein VII is expressed in large excess during infection, which is thought to contribute to assembly of new virions. Yet, what are the consequences of producing large amounts of excess protein VII, a viral protein designed to bind to and change the structure of DNA?

While many studies have examined the effect of cellular histones on viral genomes^{7,8}, little is known about the association of viral histone-like proteins, like Ad protein VII, with cellular chromatin. What we do know is that large structural changes of the host nucleus and chromatin occur upon infection by numerous viruses¹⁵⁵⁻¹⁵⁸. During Ad infection, for example, the nucleus of host cells increases in size over time and chromatin structure, visualized by DAPI, changes from a pan-nuclear staining to a more speckled pattern with large areas of less dense DNA (**Figure 1.8**)¹⁵⁸. While this phenomenon has been observed for different viruses, whether viral histone-like proteins, such as Ad protein VII, contribute to these drastic changes in nuclear architecture and how this impacts infection has not been examined. We hypothesized that protein VII, in addition to its functions on Ad genomes mentioned above^{41,133,134,139-144}, interacts with and manipulates cellular chromatin (**Figure 1.9**). In Chapter 2 of this thesis, we first examined whether protein VII, as a viral histone-like protein, could interact with components of host chromatin. We found that protein VII tightly associates with host chromatin and nucleosomes, and that expression of this viral protein alone is sufficient to alter nuclear morphology. We also discovered that protein VII, similar to cellular histones, can be modified by different PTMs and these modifications regulate the association of protein VII with host chromatin. Next, we used a proteomics approach to characterize protein VII-mediated changes in protein composition of cellular chromatin. This revealed that protein VII sequesters a family of cellular alarmins in the nucleus, resulting in a blunted immune response. As such, our work examines a novel aspect of virus-host interaction and serves as a proof-of-principle study regarding the association of viral histone-like proteins with host DNA and the contribution of this interaction to virus infection by assisting immune evasion.

1.4 Viruses and the ubiquitin system

Viruses have evolved many different strategies to shape the host cell environment to their advantage. One way is to use PTMs such as ubiquitination to manipulate host cell processes^{1,9,10}. It is becoming increasingly apparent that ubiquitination can fulfill many functions in addition to induction of protein turnover, including altering protein localization, protein-protein interactions, and complex stability¹⁵⁹⁻¹⁶¹. This diversity in function makes hijacking the host ubiquitin machinery an attractive means for viruses to manipulate host cells.

1.4.1 The host ubiquitin system

Ubiquitin is a 76 amino acid protein that can be covalently attached to primary amines through its C-terminus. The new isopeptide bond is typically formed with lysine residues in the substrate, although ubiquitination of other amino acids and the substrate N-terminus have been reported¹⁶². This is accomplished by a three-enzyme cascade involving E1 ubiquitin-activating enzymes, E2 conjugating enzymes, and E3 ubiquitin ligases (**Figure 1.10a**). The protein family of E3 ubiquitin ligases is subdivided into the HECT (homologous to the E6AP carboxyl terminus) and RING (really interesting new gene) type ligases. The HECT type ligases form an intermediary bond with the ubiquitin protein before passing it on to the substrate. The RING type ligases mediate a direct transfer of ubiquitin from the E2 to the substrate without forming a catalytic intermediate with the ubiquitin protein. The substrate specificity is provided by the E3 ubiquitin ligases. An estimated 500-1000 different E3 enzymes are encoded in the human genome, while only 2 E1 enzymes and 35 E2 enzymes have been identified.

In addition to simple mono- and multi-mono ubiquitination of substrates, ubiquitin itself can be ubiquitinated at any of the 7 lysine residues within its sequence (K6, K11, K27, K29, K33, K48, and K63) as well as at the N-terminus (linear or M1-linked ubiquitin) (**Figure 1.10b**)¹⁵⁹⁻¹⁶¹. This can lead to the formation of ubiquitin chains with distinct topologies that can be recognized by proteins with ubiquitin-binding domains¹⁶³. These domains are able to distinguish between different forms of ubiquitination and can provide the readout and function for different forms of ubiquitination. The most well-studied linkages are K48 and K63, which are also the linkages most

commonly found in cells¹⁵⁹. We are just starting to understand the diverse functions of the less abundant linkages¹⁶⁴. Below are examples for proposed functions for each of the different ubiquitin-linkages. The proteasome contains several subunits that specifically bind to K48-linked chains containing at least four ubiquitin proteins¹⁶⁵. This induces subsequent proteasomal degradation of the substrate to small peptides while the ubiquitin molecules are recycled¹⁶⁶. As such, K48-linked ubiquitin plays a major role in protein recycling and turn over¹⁶⁷. Ubiquitin chains containing K11 have also been associated with substrate degradation¹⁶⁸⁻¹⁷⁰. Other ubiquitin-linkages, such as K63 and M1, are important for signaling cascades by forming platforms for complex assembly. Both of these chain types are important for NFκB signaling¹⁷¹⁻¹⁷³. K63-linked ubiquitin chains are also involved in DNA repair^{174,175}, protein sorting^{176,177}, and oxidative stress^{178,179}. K6 is thought to contribute to the DDR¹⁸⁰ and the removal of damaged mitochondria from cells^{181,182}, while K27 regulates DNA repair¹⁸³ and is involved in host immune responses¹⁸⁴. K29 is linked to Wnt/β-catenin signaling¹⁸⁵, and K33 regulates trafficking through the trans-Golgi network¹⁸⁶. Mono and multi-mono ubiquitination can alter protein-protein interactions and are involved in membrane trafficking, endocytosis and the DDR^{177,187,188}. Furthermore, ubiquitination can occur in functional domains of proteins, such as a nuclear localization sequence (NLS)¹⁸⁹, and thereby impact protein function and localization. In addition to ubiquitin chains composed of a single linkage type, there also exist chains with mixed linkages or even branched chains. Furthermore, ubiquitin chains can also contain other ubiquitin-like proteins such as SUMO, NEDD8, and ISG15¹⁶⁰. Ubiquitination is highly dynamic and can be reversed by deubiquitinating enzymes (DUBs)¹⁹⁰. These enzymes can be specific for processing one or multiple different ubiquitin chain types. This section highlights just how complex ubiquitination is and that we are only just beginning to understand the functions mediated by this system¹⁶⁰.

1.4.2 Viral manipulation of the host ubiquitin system

Many different viruses exploit the host ubiquitin system to alter the host environment in favor of viral infection. Commonly targeted pathways include the immune response such as NFκB signaling or antigen presentation by MHC molecules, apoptosis, transcription, and the DDR.

There are many different viral strategies to alter ubiquitination (for more examples of the different strategies see **Figure 1.11**)^{1,9,10}.

Some viruses encode their own E3 ubiquitin ligases that facilitate ubiquitination of substrates (**Figure 1.11 Type I**). HSV, for example, encodes the RING-type ubiquitin ligase ICP0 that induces the degradation of host E3 ligases RNF8 and RNF168. These host proteins are involved in the DDR and without degradation they could facilitate recruitment of the host DNA repair machinery to viral genomes^{191,192}. Other substrates of ICP0 include PML and SP100^{193,194}. Degradation of these host proteins results in disruption of PML nuclear bodies that could otherwise repress viral infection¹⁹⁵.

Other viruses encode viral proteins that hijack host Cullin complexes (**Figure 1.11 Type II**). Cullin ubiquitin ligase complexes are the largest family of cellular E3 ubiquitin ligases and have been extensively studied in context of protein turnover mediated through K48-linked ubiquitin chains¹⁹⁶. They belong to the RING type family of E3 ligases and recruit an E2 for ubiquitination of the substrates. Multiple viruses encode proteins that assume the substrate adapter function of the Cullin ubiquitin ligase complexes, recruiting host proteins for ubiquitination. For example, the HIV protein Vif associates with a Cullin complex composed of Cullin5, Elongin B, Elongin C, and RBX2. By hijacking this cellular E3 ubiquitin ligase, Vif induces the degradation of APOBEC3G, a cellular cytidine deaminase that can restrict HIV infection by editing the RNA/DNA intermediate during reverse transcription of the viral RNA¹⁹⁷⁻²⁰¹. In addition to hijacking of the Cullin complexes, some viral proteins can indirectly mediate ubiquitination through interaction with host E3 ubiquitin ligases (**Figure 1.11 Type III**). For instance, the HPV E6 oncoprotein interacts with the host E3 ligase E6AP (E6 associated protein) to mediate ubiquitination and subsequent degradation of the tumor suppressor p53²⁰²⁻²⁰⁴.

Furthermore, viruses can alter deubiquitination by either encoding their own DUBs or interacting with cellular DUBs that then alter the removal of ubiquitin from substrates (**Figure 1.11 Type IV**). The EBNA1 protein of EBV, for example, competes with p53/MDM2 for binding to the

host DUB USP7, resulting in p53 destabilization and reduction of DNA-damage associated apoptosis^{205,206}.

The best-characterized function of ubiquitination is facilitating degradation of substrates by the proteasome and this is also the most well-studied in the context of virus-host interaction. The use of non-degradative ubiquitination is clearly widespread within cells and thus is likely exploited by viruses. However, there are only few known examples of viral-mediated non-degradative ubiquitination^{207,208}. For instance, while KSHV proteins K3 and K5 have been shown to facilitate ubiquitination of MHC class I with K63-linked chains this still results in degradation of the substrate, in this case by the lysosome instead of the proteasome²⁰⁹. Use of non-degradative ubiquitination could vastly increase the ways viruses can alter the host cell environment through altering protein localization, protein-protein interactions, and protein functions independent of changes in protein abundance. One possible explanation for the shortage in studies on viral-mediated ubiquitination without subsequent degradation is the limited availability of experimental techniques that allow for detection of non-degradative ubiquitination events. Advances in proteomics such as di-glycine remnant profiling now allow for global detection of ubiquitinated proteins^{210,211}. Combining these techniques with a whole cell proteome analysis enables the identification of both degraded and non-degraded substrates of viral-mediated ubiquitination. One example of how this approach can be used to define new substrates of a viral ubiquitin ligase can be found in Chapter 3 of this thesis.

1.4.3 Adenovirus E1B55K/E4orf6 and the ubiquitin system

Ad also exploits the host ubiquitin machinery to support successful viral infection. The two early proteins E1B55K and E4orf6 recruit cellular proteins to form a viral E3 ubiquitin ligase complex (**Figure 1.4**)²¹²⁻²¹⁵. E1B55K is thought to function as the substrate recognition component and recruits cellular proteins for ubiquitination²¹³. E4orf6, on the other hand, hijacks a cellular E3 ubiquitin ligase complex of the Cullin family that consists of Cullin5, Elongin B, Elongin C, and RBX1 (**Figure 1.12**, see Chapter 1.4.2 for details on Cullin ligases)^{212,213}. This is facilitated through two BC box motifs in the E4orf6 sequence which directly interact with the Elongin

proteins²¹⁶⁻²¹⁸. E1B55K contains several highly disordered regions within its structure that are important for substrate binding, and interaction with different substrates requires distinct residues within the viral protein²¹⁹. E1B55K expressed by itself remains cytoplasmic and the interaction with E4orf6 is required for the nuclear localization of the complex²²⁰. It has been demonstrated that this viral ubiquitin ligase marks host proteins for proteasomal degradation, and K48-linked ubiquitin chains have been shown for one substrate^{67,212,213,221-223}.

Several substrates of the Ad ubiquitin ligase have been identified. One such substrate is the tumor suppressor p53 that is degraded to prevent the cell cycle arrest and apoptosis, induced as a consequence of forced entry into the cell cycle by E1A^{212,213,224,225}. Interestingly, both E1B55K and E4orf6 can interact with and suppress p53-mediated transcription independently of their function in the ubiquitin ligase complex. E4orf6 can also interact with and repress the function of p73, a homolog of p53^{226,227}. E1B55K suppresses p53 by binding to the N-terminal transcriptional activation domain⁷⁹⁻⁸¹ while E4orf6 binds to the C-terminus^{226,228}, resulting in inhibition of different subsets of p53 target genes²²⁷. Several substrates of E1B55K/E4orf6 are components of the host DDR, including the MRN complex⁶⁷, Bloom Helicase (BLM)²²¹, and Ligase IV (LIG4)²²². The MRN complex recognizes dsDNA breaks and is important for initial processing of breaks prior to repair by homologous recombination or non-homologous end joining²²⁹. BLM is important for unwinding DNA during repair, while LIG4 functions at the ligation step in the repair of dsDNA breaks during non-homologous end joining^{230,231}. As described in Chapter 1.2.2, the DDR is also antagonized by E4orf3, highlighting the importance of preventing the interaction of the host repair machinery with viral dsDNA for Ad infection. Failure to antagonize these host proteins results in partial digest of viral DNA, concatemerization of the genome, problems in DNA replication, and defects in packaging of Ad DNA into virions^{65,67,232-237}. Another substrate of the Ad ubiquitin ligase is integrin $\alpha 3$ ^{223,238}. This surface protein is important for interactions between cells and its degradation may promote release and spread of Ad. E1B55K/E4orf6 substrates have mostly been identified using Ad5 and it has been demonstrated that substrate specificity of the E1B55K/E4orf6 complex differs between different serotypes^{239,240}.

While multiple substrates of the Ad ubiquitin ligase have been identified, there are several unexplained phenotypes that have been observed upon inhibition of the Ad ubiquitin ligase function. E1B55K-deleted viruses (Δ E1B) have been developed for oncolytic therapy as it was thought that their replication would rely on the inactivation of p53 that commonly occurs in cancer cells. While Δ E1B viruses indeed replicate efficiently in certain cancer cells as opposed to untransformed cells, the phenotype displayed is inconsistent with induction of apoptosis and has been shown to be independent of the p53 status of the cells^{78,241,242}. Instead, deletion of E1B55K decreases late protein expression and progeny production with only mild impact on early gene expression and DNA replication. This defect has been mapped to a step in nuclear RNA processing of specifically viral late RNA transcripts, with little difference observed in RNA transcription or decay rates^{243,244}. The original study by Babiss *et al.* from 1985 concluded that deletion of E1B55K results in a failure to export viral late RNA²⁴³. Furthermore, during the late stage of Ad wild-type (WT) infection, the export of cellular as well as viral early RNA is inhibited to enable exclusive export of viral late RNA species^{243,245,246}. This switch does not occur upon deletion of E1B55K. The decrease in viral late mRNA results in reduced expression of viral late proteins. This is further potentiated by low levels of L4-100K, an Ad late protein, that normally inhibits cap dependent translation^{247,248} and enhances cap independent translation of the late RNA species through ribosome shunting facilitated by the tripartite leader present in all late transcripts^{249,250}. Deletion of E4orf6, mutation of the BC box motifs in E4orf6 to prevent ubiquitin ligase assembly, expression of a dominant negative Cullin5, or inhibition of the ubiquitin ligase complex all show a similar phenotype^{60,216,242,246,251,252}. This highlights that it is E1B55K/E4orf6-mediated ubiquitination, and not an E1B55K function independent of the ubiquitin ligase complex, that contributes to viral late RNA processing.

The currently known substrates for the E1B55K/E4orf6 complex are involved in apoptosis (p53) and the host DDR (MRN complex, Lig4, and BLM)^{67,212,213,221,222,224,225}. Activation of these cellular pathways do not explain the RNA processing defects observed for E1B55K- or E4orf6 mutant viruses, as it has been demonstrated that defects in Ad late RNAs still occur in cells that

are p53-deficient or do not possess a functional DDR^{241,242}. This suggests that additional unidentified substrates of the Ad ubiquitin ligase exist, and that ubiquitination of these host proteins is important for viral RNA processing. Several different strategies have been previously employed to identify new substrates and interaction partners of the Ad ubiquitin ligase complex that may contribute to viral RNA processing. These experiments included immunoprecipitation of the viral proteins followed by mass spectrometry (IP-MS)^{212,213,253}, 2D-gel electrophoresis followed by MS²³⁸, and whole cell proteomics coupled with a transcriptome analysis comparing WT and Δ E1B viruses^{254,255}. However, none of these approaches have identified substrates of E1B55K/E4orf6 that explain the RNA processing defect. One possible explanation is that these experiments were only designed to identify degraded substrates of the Ad ubiquitin ligase, potentially missing any substrates that are not degraded by the proteasome upon ubiquitination. Furthermore, it has been revealed that while IP-MS studies can identify regulators of ubiquitin ligases, the interaction with substrates is often too transient to be reliably detected with this method^{256,257}. This indicates that different approaches are necessary for identification of additional substrates of the E1B55K/E4orf6 complex that are responsible for proper processing of viral late RNA.

In Chapter 3 of this thesis we employed an alternative strategy to identify substrates of the Ad ubiquitin ligase. We used a combined proteomics approach to identify proteins ubiquitinated upon expression of the E1B55K/E4orf6 complex and assessed resulting changes in protein abundance by whole cell proteome profiling (**Figure 1.13**). We furthermore demonstrated that two of the newly identified substrates of E1B55K/E4orf6 are indeed involved in processing of viral late RNA. Interestingly, we showed that these host proteins were not degraded upon Ad-mediated ubiquitination, but that instead their binding to viral RNA was altered. These findings revealed an unexpected function of non-degradative ubiquitination during virus infection.

1.5 Figures

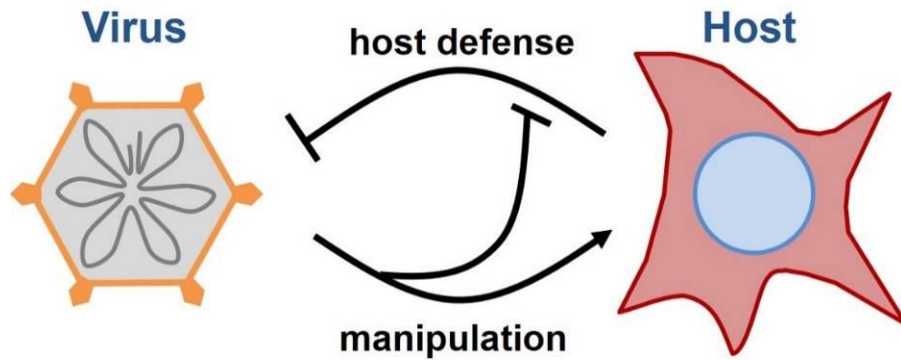


Figure 1.1 | Virus vs. host. Viruses rely on manipulating the environment of their host cell for their own replication. In addition, viruses have to overcome antiviral responses developed by the host to counteract infections.

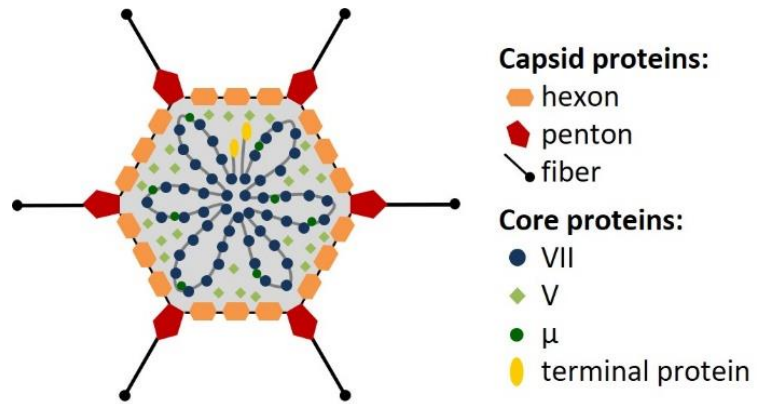


Figure 1.2 | Schematic of the Ad virion structure. Viral particles consist of an outer capsid and inner core.

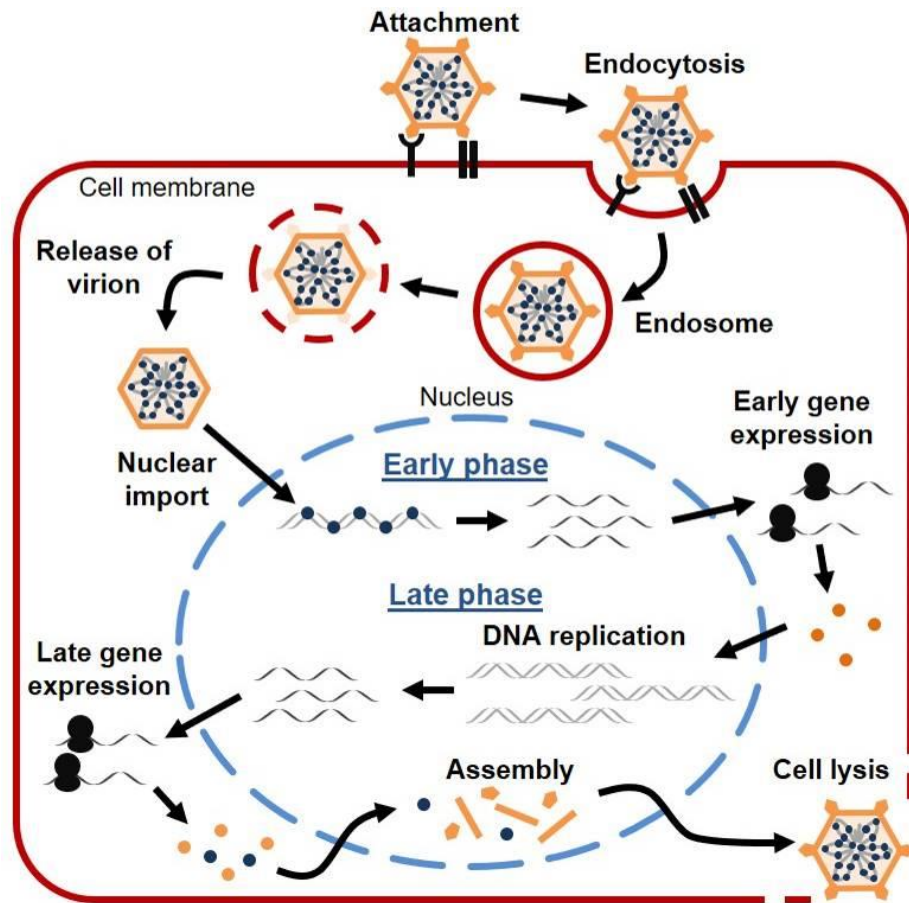


Figure 1.3 | Schematic of the Ad life cycle highlighting the different stages of virus replication. During the early phase of infection, early proteins rewire host processes towards late protein production. In the late phase the viral genome is replicated, and the structural late proteins are produced and assembled into virions.

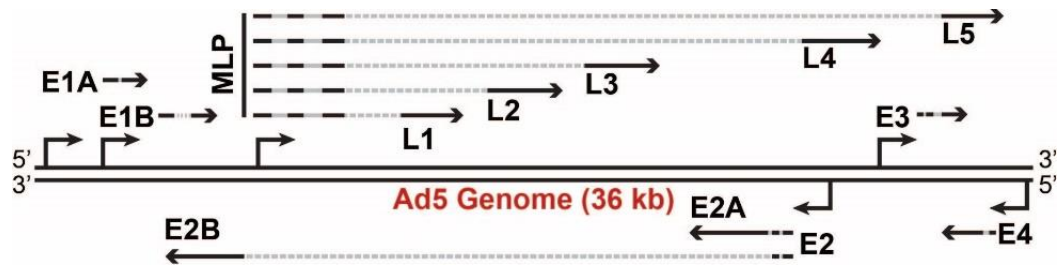


Figure 1.4 | Schematic of the Ad genome structure. There are four early (E1-E4) transcription units that encode the proteins expressed during the early phase of infection. The five late transcription units (L1-L5) are expressed from one common major late promoter (MLP) and encode mainly structural proteins and those involved in virion assembly. *Schematic courtesy of AM Price.*

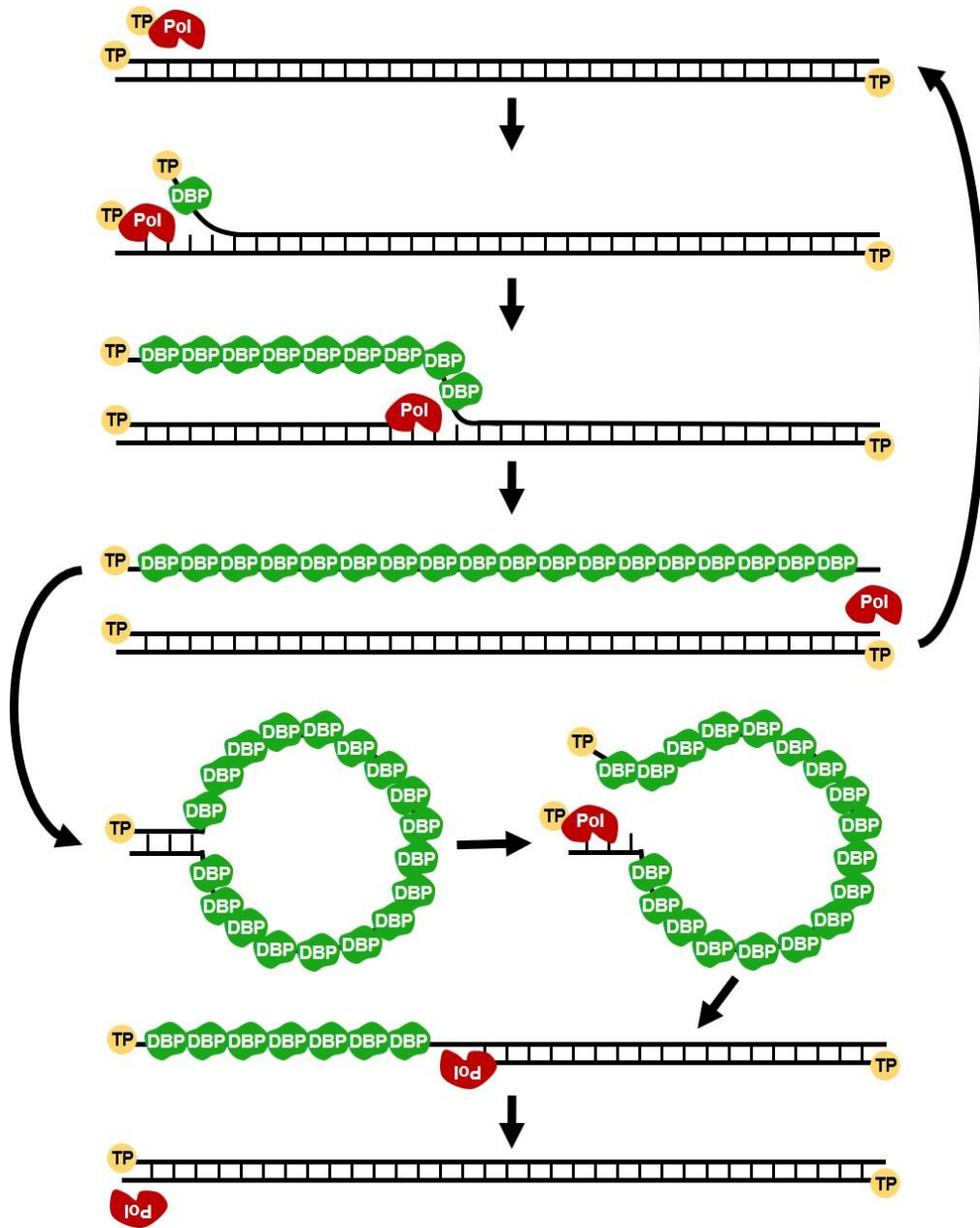


Figure 1.5 | Schematic of the replication of the Ad genome. Three viral proteins (pre-terminal protein - TP, Ad DNA polymerase - Pol, single-strand DNA binding protein - DBP) are essential for the replication of the Ad genome. Replication is initiated through a protein priming mechanism, in which TP is covalently linked to the first nucleotide of the new strand and serves for a primer for Pol. DBP binds to the displaced single-stranded DNA that circularizes through the inverted terminal repeats. This panhandle structure has the same structure and sequence as the original replication origin, enabling replication by the same mechanism as the first strand. The pre-terminal protein is processed into its mature form by the viral protease during virion maturation.

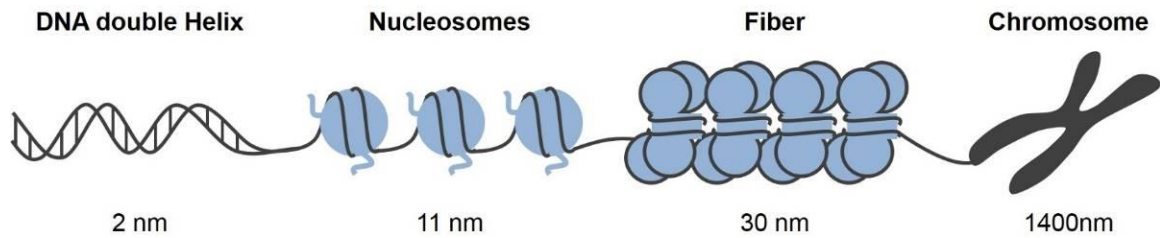
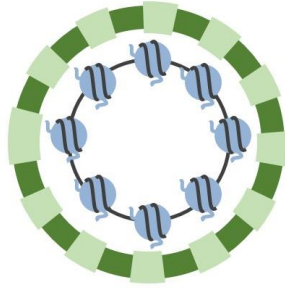


Figure 1.6 | The basic structure of cellular chromatin. Double-stranded DNA is wrapped around an octamer of histones to form nucleosomes as the basic component of chromatin. Nucleosomes then form higher order structures such as fibers that are intertwined in the nucleus and can be further condensed to distinct chromosomes during cell division.

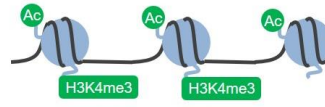
a Packaging



HPV, SV40

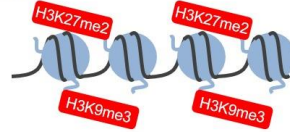
b Regulation of gene expression

Acute



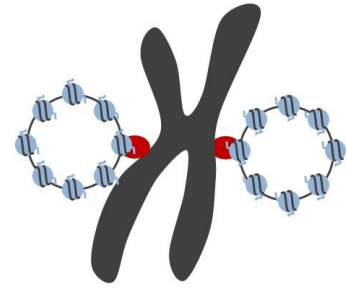
Ad, HSV, EBV

Latent



HSV, EBV, KSHV, HIV

c Genome propagation



HPV, KSHV, EBV

Figure 1.7 | Different viral strategies to exploit cellular histones and chromatin. **a**, Viruses such Papillomavirus and Polyomavirus use cellular histones to condense the viral genomes inside virions. **b**, Other DNA viruses are not packaged with cellular histones but associate with histones within the host cell. The structure of viral chromatin and associated histone marks differs between actively replicating and latent infection and is exploited to regulate viral gene expression. **c**, Tethering to host chromatin enables even distribution of viral genomes to the daughter cells during division of the host cell.

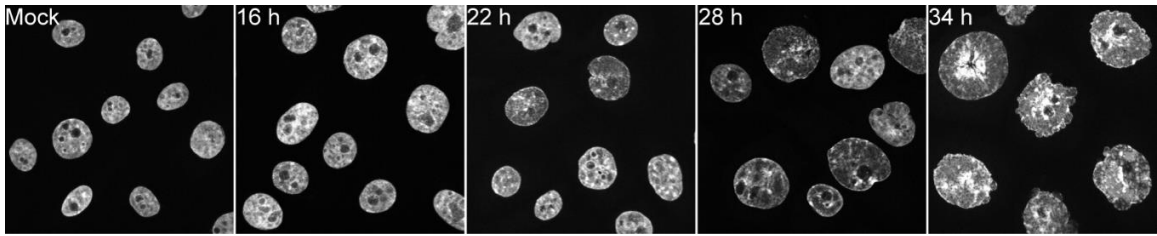


Figure 1.8 | Change in nuclear architecture during Ad infection. Changes in nuclear architecture and size upon infection of primary-like HBE3C-KT with Ad WT (multiplicity of infection/MOI = 20) over a time course visualized by immunofluorescence staining of DNA with DAPI (grey). *Figure courtesy of M Charman.*

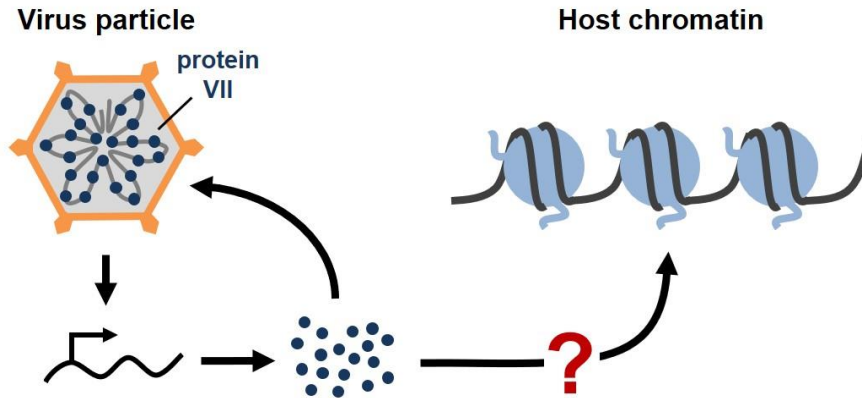


Figure 1.9 | Rationale for project 1. The Ad histone-like protein VII that condenses the viral genome inside virions is produced in large quantities during infection for packaging of new virus particles. Considering the ability of protein VII to bind DNA and that it is produced in large excess to what is needed for production of new virions, we hypothesized that this viral protein can interact with and manipulate the cellular chromatin, contributing to the distortion of the host cell nucleus observed during infection, forming the basis for Chapter 2 of this thesis.

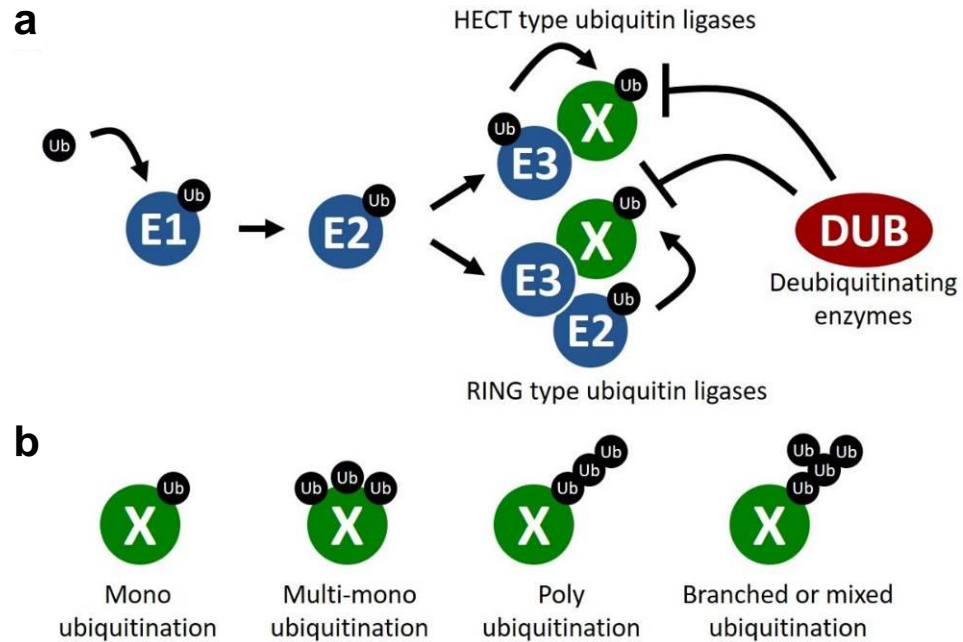


Figure 1.10 | The host ubiquitin system. **a**, Ubiquitination is a three-step cascade facilitated by the E1, E2, and E3 enzymes. Substrate specificity is conferred by the E3 enzymes that can be divided into HECT and RING type ligases. Ubiquitination can be reversed by deubiquitinating enzymes (DUBs). **b**, There are different forms of ubiquitination such as mono and multi-mono ubiquitination in addition to ubiquitin chains that can contain one specific linkage, multiple linkages or even be branched.

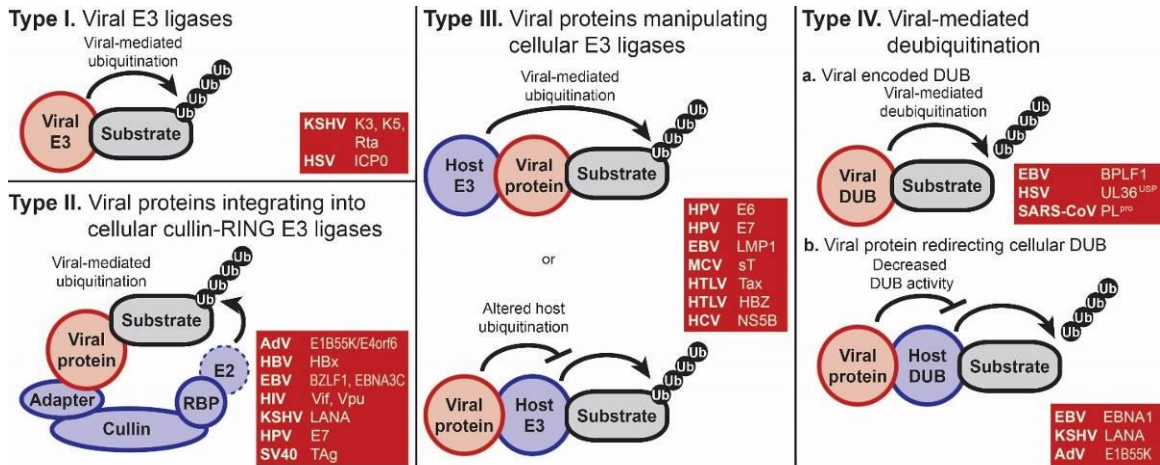


Figure 1.11 | Different viral strategies to hijack the cellular ubiquitin system. Type I, viruses encode proteins with E3 ubiquitin activity that directly ubiquitinate cellular substrates. **Type II**, viral proteins integrate into cellular Cullin E3 ubiquitin ligase complexes and assume the substrate adaptor function to dictate cellular substrates that are ubiquitinated. **Type III**, viral proteins interact with cellular E3 ligases to direct ubiquitination of cellular substrates or alter cellular E3 ligase activity. **Type IV**, viruses can impart the opposite function of E3 ligases by directing deubiquitination of cellular substrates either by encoding viral proteins with DUB activity or by interacting with cellular DUBs.

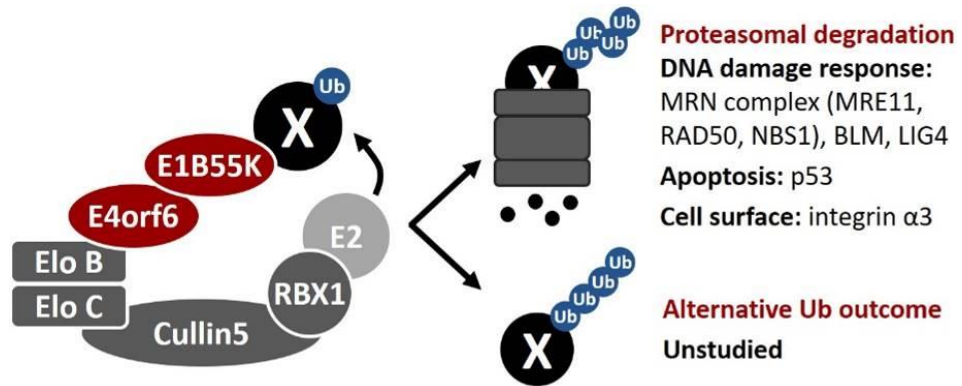


Figure 1.12 | Schematic of the E1B55K/E4orf6 ubiquitin ligase complex. E1B55K recruits cellular proteins for ubiquitination facilitated by the Cullin5 complex hijacked by E4orf6. All currently identified substrates of the Ad ubiquitin ligase are subsequently degraded by the proteasome while alternative outcomes of ubiquitination by E1B55K/E4orf6 have remained unexplored.

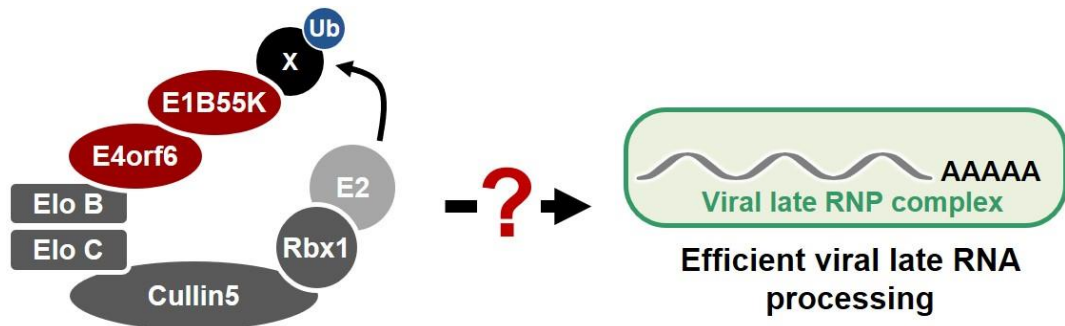


Figure 1.13 | Rationale for project 2. It has long been known that Ad-mediated ubiquitination is important for proper processing of Ad late RNA. This phenotype is unexplained by the currently known substrates for the Ad ubiquitin ligase complex. We therefore hypothesize that ubiquitination of one or several undiscovered E1B55K/E4orf6 substrates is critical for processing of viral late RNA, forming the basis of Chapter 3 of this thesis.

CHAPTER 2: A CORE VIRAL PROTEIN BINDS HOST NUCLEOSOMES TO SEQUESTER IMMUNE DANGER SIGNALS

This chapter has been published as:

Avgousti DC, **Herrmann C**, Kulej K, Pancholi NJ, Sekulic N, Petrescu J, Molden RC, Blumenthal D, Paris AJ, Reyes ED, Ostapchuk P, Hearing P, Seeholzer SH, Worthen GS, Black BE, Garcia BA, Weitzman MD. A core viral protein binds host nucleosomes to sequester immune danger signals. *Nature* **535**, 173-177 (2016). **PMID: 27362237**.²⁵⁸

2.1 Abstract

Viral proteins mimic host protein structure and function to redirect cellular processes and subvert innate defenses²⁵⁹. Small basic proteins compact and regulate both viral and cellular DNA genomes. Nucleosomes are the repeating units of cellular chromatin and play an important part in innate immune responses⁹². Viral-encoded core basic proteins compact viral genomes, but their impact on host chromatin structure and function remains unexplored. Adenoviruses encode a highly basic protein called protein VII that resembles cellular histones¹³³. Although protein VII binds viral DNA and is incorporated with viral genomes into virus particles^{23,24}, it is unknown whether protein VII affects cellular chromatin. Here we show that protein VII alters cellular chromatin, leading us to hypothesize that this has an impact on antiviral responses during adenovirus infection in human cells. We find that protein VII forms complexes with nucleosomes and limits DNA accessibility. We identified post-translational modifications on protein VII that are responsible for chromatin localization. Furthermore, proteomic analysis demonstrated that protein VII is sufficient to alter the protein composition of host chromatin. We found that protein VII is necessary and sufficient for retention in the chromatin of members of the high-mobility-group protein B family (HMGB1, HMGB2 and HMGB3). HMGB1 is actively released in response to inflammatory stimuli and functions as a danger signal to activate immune responses^{260,261}. We showed that protein VII can directly bind HMGB1 *in vitro* and further demonstrated that protein VII

expression in mouse lungs is sufficient to decrease inflammation-induced HMGB1 content and neutrophil recruitment in the bronchoalveolar lavage fluid. Together, our *in vitro* and *in vivo* results show that protein VII sequesters HMGB1 and can prevent its release. This study uncovers a viral strategy in which nucleosome binding is exploited to control extracellular immune signaling.

2.2 Introduction

As viruses commandeer cellular functions to promote viral production, they induce numerous cellular changes. Manipulation of host chromatin is important for viral takeover of cellular functions^{7,131,259,262,263}. Although there are known examples of viral control by manipulating gene expression^{47,92,131}, an alternative strategy for immune evasion could exploit cellular chromatin to affect extracellular signaling. Genomes of DNA viruses are compacted and packaged into virus particles with small basic proteins encoded by the host or virus. Adenoviruses encode protein VII, a small basic protein packaged with viral genomes^{23,24,133}. We hypothesized that protein VII contributes to host chromatin manipulation.

2.3 Results

We investigated protein VII localization during infection, and found it present in both viral replication centers stained for viral DNA-binding protein (DBP; **Figure 2.1a** and **Figure 2.S1a**), and in cellular chromatin stained for histone H1 and 4',6-diamidino-2-phenylindole (DAPI; **Figure 2.1b**). These observations suggest that protein VII functions on both viral and host genomes. To determine the impact of protein VII on cellular chromatin, we generated cell lines with inducible expression. In multiple cell types we observed that protein VII accumulation altered nuclear DNA into a punctate appearance (**Figure 2.1c** and **Figure 2.S1b, c**). We tested whether other basic proteins produce similar effects on chromatin. Viral core protein V and the precursor of protein VII (preVII) localized to nucleoli and did not affect chromatin appearance (**Figure 2.S1d**). Human protamine PRM1, a basic protein involved in sperm DNA compaction²⁶⁴, also localized to nucleoli and did not affect chromatin appearance (**Figure 2.S1d**). Taken together, our data demonstrate

that protein VII is sufficient to alter cellular chromatin and is distinct from other small basic proteins.

To affect cellular chromatin at the nucleosome level during infection, we reasoned that protein VII must be abundant and associated with histones. Acid extraction of histones^{265,266} from infected cells revealed viral proteins VII and V isolated with cellular histones (**Figure 2.1d**), as verified by western blot (**Figure 2.S2a**) and mass spectrometry (MS). Protein VII abundance was comparable to cellular histone levels (**Figure 2.1d**). We further analyzed association of protein VII with cellular chromatin by salt fractionation of nuclei²⁶⁷. We found protein VII with cellular histones and DNA in high-salt fractions (**Figure 2.1e** and **Figure 2.S2b-d**). Ectopically expressed protein VII is also found in high-salt fractions, in contrast to other viral proteins that elute at low salt (**Figure 2.1e** and **Figure 2.S2b**). These data suggest that protein VII is highly abundant and tightly associated with cellular chromatin.

We hypothesized that protein VII interacts with chromatin by forming complexes with DNA, histones, or nucleosomes, and examined protein VII interactions in vitro. Purified recombinant protein VII binds to DNA²⁴ (**Figure 2.S2e, f**). We reconstituted nucleosomes in vitro with recombinant histone proteins on 195 base pairs (bp) of DNA²⁶⁸. Protein VII changed nucleosome mobility upon native gel electrophoresis (**Figure 2.1f** and **Figure 2.S2g**). We analyzed native gel bands by denaturing SDS-polyacrylamide gel electrophoresis (SDS-PAGE), and confirmed that complexes contained core histones with protein VII (**Figure 2.1f**, bottom). Unlike protamines²⁶⁴, protein VII forms complexes with nucleosomes but does not appear to replace histones. Next, we examined whether protein VII association with nucleosomes affects DNA wrapping using micrococcal nuclease (MNase) digestion followed by DNA fragment analysis²⁶⁸. We found that protein VII pauses nucleosomal DNA digestion at ~165 bp, the point at which DNA strands cross over the nucleosome dyad (**Figure 2.1g** and **Figure 2.S3a**). By contrast, nucleosome digestion alone paused with core particles at ~150 bp, suggesting that protein VII encumbers DNA access. Unlike linker histone binding that is dependent on DNA length²⁶⁹, protein VII protects against MNase digestion on the nucleosome core particle of 147 bp (**Figure 2.S3b**). Protein VII alone

protects DNA from MNase digestion, as would be expected given its role in the viral core. Together, these data demonstrate that protein VII binds directly to nucleosomes and limits DNA accessibility at the DNA entry/exit site.

Post-translational modifications (PTMs) on histones are central to regulating chromatin structure^{90,265}. Owing to the histone-like nature of protein VII¹³³, we hypothesized that it is subject to post-translational modification similar to histones. PreVII was previously proposed to be acetylated by N-terminal addition during protein synthesis²⁷⁰. We noted that protein VII contains conserved lysine residues within an AKKRS motif²⁷¹, similar to the commonly modified canonical histone motif ARKS⁹⁰. We therefore purified protein VII from histone extracts over an adenovirus infection time course by reverse-phase high-performance liquid chromatography (RP-HPLC; **Figure 2.2a** and **Figure 2.S4**). Consistent with observations from histone extracts (**Figure 2.1d**), protein VII levels were comparable to endogenous histones. We digested purified protein VII and preVII with chymotrypsin to distinguish the two proteins, and analyzed peptides by tandem mass spectrometry (MS/MS). We identified several PTMs, with two acetylation sites and three phosphorylation sites the most abundant modifications (**Figure 2.2b** and **Figures 2.S5, 2.S6b**). Interestingly, we identified acetylation sites on ectopically expressed protein VII but not on protein VII in virus particles (**Figure 2.S6a**). We speculate that this provides a possible mechanism for distinguishing protein VII bound to cellular chromatin from protein destined for packaged virus. To investigate the relevance of the identified PTMs, we mutated modified sites in protein VII. An alanine-replacement mutant for all five PTM sites localized to nucleoli instead of cellular chromatin (**Figure 2.2c**). Results with individual point mutations suggest that the K3 residue is important for chromatin localization, and employing glutamine as an acetylation mimic (K3Q) mirrored the pattern of wild-type protein (**Figure 2.2c**). Effects induced by protein VII are not due to global alteration of histone PTMs since only six PTMs on histones H3 and H4 showed minor but significant changes (**Figure 2.S6c-e**). These data suggest that protein VII modification has critical roles during virus infection.

To determine whether protein VII manipulation of cellular chromatin is part of a strategy to counteract host defenses, we employed MS to examine changes in the protein composition of nuclear fractions. We compared the total chromatin proteome in the presence and absence of protein VII (**Figure 2.3a**). We identified 20 proteins that changed significantly across three biological replicates (**Figure 2.S7**). The categories of proteins most significantly changed upon protein VII expression were related to immune responses (**Figure 2.S7c**). The top four proteins enriched in chromatin fractions by protein VII were SET (also known as TAF-1), a protein previously shown to interact with protein VII^{141,145}, and HMGB1, HMGB2, and HMGB3 (Fig. 3a). The HMGB proteins are alarmins with multiple functions as activators of immunity and inflammation^{260,261}. HMGB1 is a nuclear protein normally only transiently associated with chromatin^{272,273}. Cells also release HMGB1 as an extracellular danger signal that promotes immune responses after injury or infection²⁷⁴. We confirmed increased chromatin association of HMGB1 and HMGB2 by analysis of fractionated nuclei, upon protein VII expression and during adenovirus infection (**Figure 2.3b**). We verified that these changes are not due to altered HMGB1 expression levels (**Figure 2.S8a, b**). We demonstrated direct binding of recombinant protein VII to HMGB1 in vitro and confirmed HMGB1 co-immunoprecipitation with protein VII (**Figure 2.3c**). We visually observed reorganization of HMGB1 and HMGB2 distribution upon protein VII expression, and at late stages of infection (**Figure 2.3d-f** and **Figure 2.S8c-e**). We also showed reorganization of HMGB1 distribution by vector transduction to express protein-VII-green fluorescent protein (GFP; **Figure 2.3g** and **Figure 2.S8f**). The effect of protein VII on HMGB1 is also conserved across human adenovirus serotypes (**Figure 2.S8g**). We further defined the effects of protein VII on HMGB1 mobility by fluorescence recovery after photobleaching (FRAP) and found decreased HMGB1 diffusion (**Figure 2.3h**). We next investigated whether protein VII is necessary for chromatin retention of HMGB1 during virus infection. We used a replication-competent adenovirus with loxP sites inserted on either side of the protein VII gene, allowing deletion of protein VII during infection of cells expressing Cre recombinase (**Figure 2.3i, j** and **Figure 2.S9a, b**). We fractionated nuclei from infected cells and found that HMGB1 and HMGB2

were no longer retained in chromatin when protein VII was deleted (**Figure 2.3k** and **Figure 2.S9c**). Together, these data indicate that protein VII is necessary and sufficient to promote chromatin association and immobilization of HMGB1.

We hypothesized that protein VII retains HMGB1 in chromatin during natural infection to prevent cellular release and abrogate host immune responses. We therefore visualized endogenous HMGB1 during adenovirus infection in precision-cut lung slices²⁷⁵ from human donors (**Figure 2.4a**). Consistent with cell culture experiments, we demonstrate that protein VII is sufficient to relocalize endogenous HMGB1. We then tested whether protein VII prevents HMGB1 release in cell culture and in vivo models. We expressed GFP or protein-VII-GFP in macrophage-like THP-1 cells, and confirmed that protein-VII-GFP was sufficient to alter chromatin and HMGB1 localization (**Figure 2.S9d**). Cells were treated to stimulate inflammasomes, and HMGB1 content was analyzed in supernatants. Protein VII expression resulted in reduced levels of HMGB1 and HMGB2 in supernatants (**Figure 2.4b, c**). Subsequently, we employed a murine model of lipopolysaccharide (LPS)-induced lung injury²⁷⁶ to investigate the impact of protein VII on HMGB1 release and neutrophil recruitment in vivo (**Figure 2.4d**). We confirmed that protein VII was expressed in transduced mouse lungs (**Figure 2.S10a-c**) and retained mouse HMGB1 (**Figure 2.S9e, f**). We exposed mice to inhaled LPS to induce HMGB1 release and neutrophil recruitment to alveoli. Bronchoalveolar lavage fluid obtained 24 h after LPS exposure showed that mice transduced to express protein VII had significantly less HMGB1 and fewer neutrophils than mice expressing GFP (**Figure 2.4d-f**). Together, these data suggest that protein VII functions in cellular chromatin to retain HMGB1 as a mechanism to blunt immune responses.

In addition to known roles on packaged viral DNA^{143,144}, we show that protein VII interacts with cellular chromatin and binds nucleosomes. We suggest that protein VII PTMs contribute to chromatin localization, and that protein VII affects the chromatin association of host proteins. Finally, we show that protein VII in cellular chromatin leads to sequestration of HMGB family members, contributing to abrogated immune responses (**Figure 2.S10d**). Our study reveals that

chromatin retention of signaling molecules by a viral protein may represent a previously unrecognized immune evasion strategy.

2.4 Figures

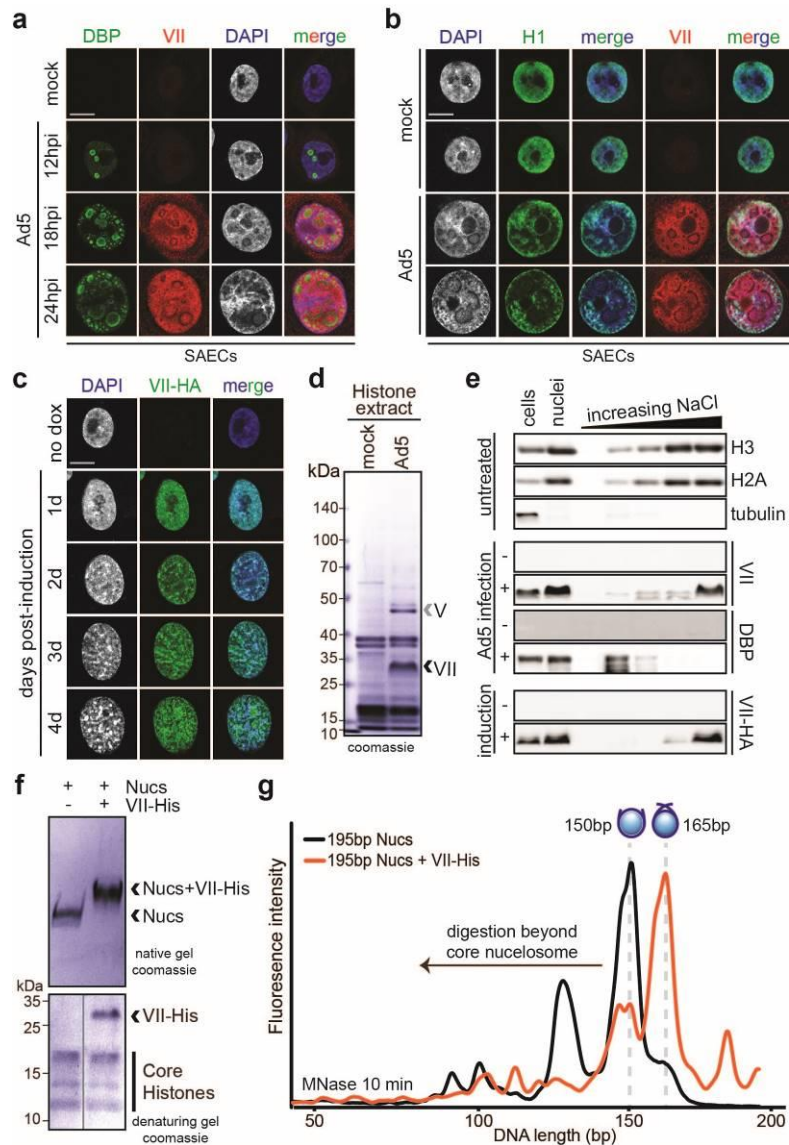


Figure 2.1 | Protein VII is sufficient to alter chromatin and directly binds nucleosomes. **a**, **b**, Adenovirus serotype 5 (Ad5)-infected small airway epithelial cells (SAECs) stained for protein VII (red) with DBP (**a**) or histone H1 (**b**) (green), and DAPI (grey, blue in merge). hpi, hours post-infection. **c**, Protein-VII-haemagglutinin (HA)-induced cells over 4 days showing HA (green) and DAPI (grey, blue in merge). dox, doxycycline. **a-c**, Scale bars, 10 μ m. **d**, SDS-PAGE of histone extract from Ad5-infected cells showing protein V and protein VII. **e**, Western blot of chromatin fractionation from nuclei of Ad5-infected cells, induced for protein-VII-HA, or untreated. **f**, Protein VII binds to nucleosomes (Nucs). Protein bands from native gel stained with Coomassie (top) were subjected to two-dimensional analysis by SDS-PAGE (bottom). **g**, Protein VII protects nucleosome complexes from MNase digestion. Bioanalyzer curves represent nucleosomes alone (black) or protein-VII-nucleosome complexes (orange). *Panels a-d and f-g by DC Avgousti.*

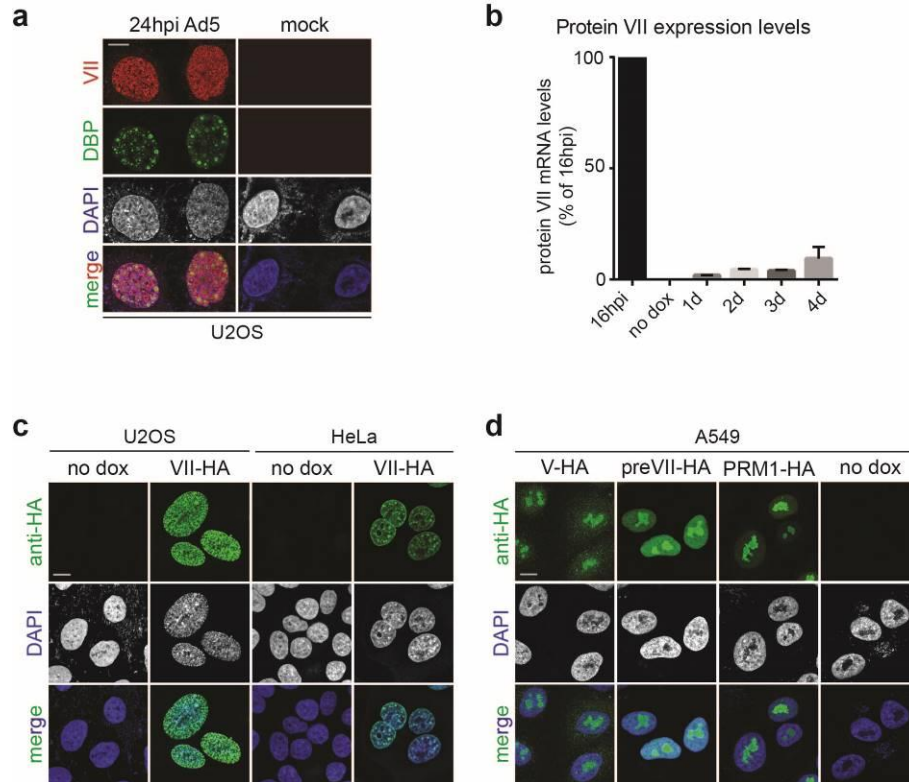


Figure 2.S1 | Adenovirus protein VII distorts chromatin. **a**, Protein VII localizes to cellular chromatin and viral replication centers in U2OS cells similarly to SAECs in Figure 2.1a. **b**, Protein VII messenger RNA levels measured by quantitative PCR showing that after 4 days of induction in the A549 cell line, the level of protein VII transcripts is approximately 10% of that measured during infection at 16 hpi. Despite the low relative level, this amount of protein VII is sufficient to cause dramatic changes in the nucleus (graph shows mean \pm s.d., $n = 3$ biological replicates). **c**, Inducible cell lines of U2OS and HeLa expressing protein-VII-HA show chromatin localization and distortion, similar to A549 cells in Figure 2.1c. **d**, Inducible A549 cell lines expressing viral protein V, the precursor for protein VII (preVII) or cellular protamine PRM1 with C-terminal HA tags. Although all three proteins possess a large number of charged residues, none are sufficient to distort cellular chromatin or increase nuclear size as observed with mature protein VII. Scale bars, 10 μ m. *Panels a, c, and d by DC Avgousti, panel b by NJ Pancholi.*

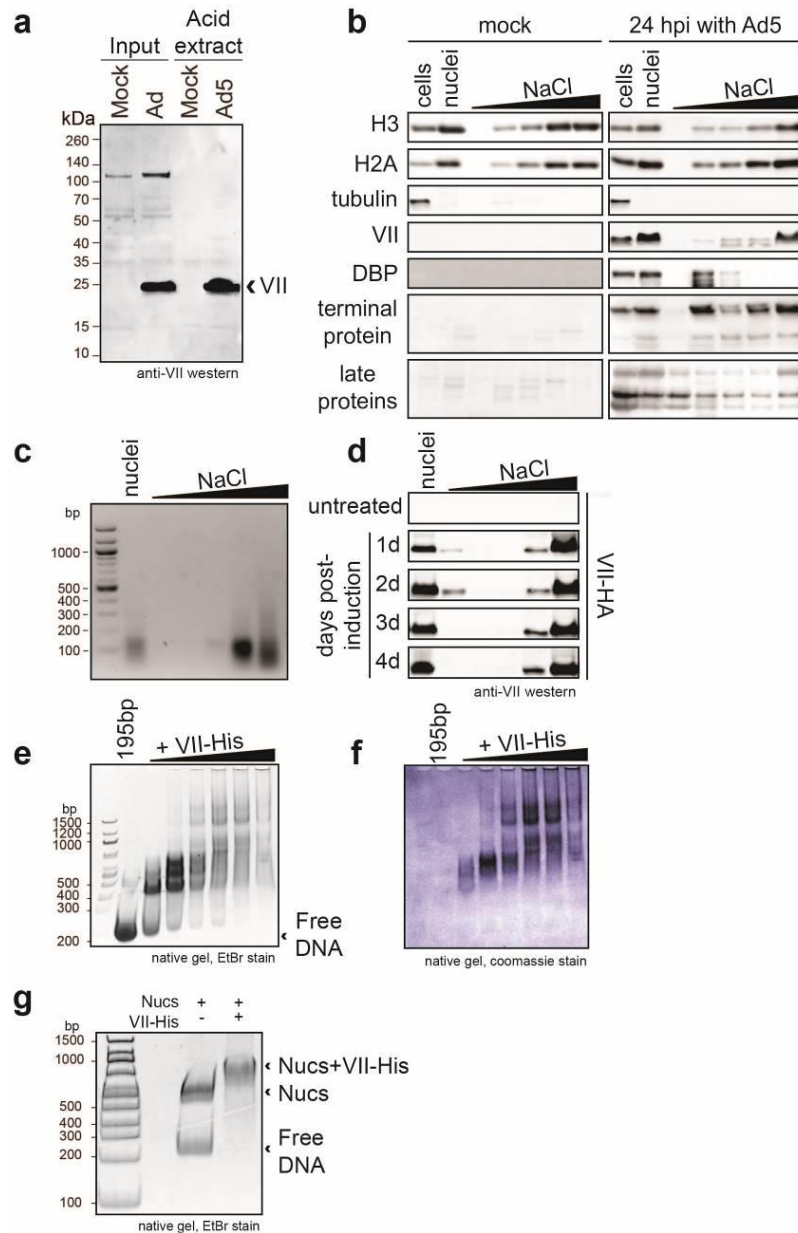


Figure 2.S2 | Protein VII associates tightly with chromatin and binds DNA and nucleosomes in vitro. **a**, Western blot analysis showing protein VII in histone extracts from infected HeLa cells at 24 hpi. **b**, Chromatin fractionation of lysates from A549 cells that were uninfected (mock) or infected for 24 h with Ad5. Viral and cellular proteins were detected by western blotting with various antibodies as indicated. **c**, Agarose gel analysis of DNA extracted from nuclear fractionation experiments, indicating that the size of DNA is between 100 and 200 bp and elutes predominantly in the higher-salt fractions. **d**, Chromatin fractionation of cells induced to express protein VII, indicating that protein VII is present in the highest-salt fraction from the first day of induction. **e**, **f**, Recombinant protein-VII-His binds DNA. Incubating increasing molar amounts of protein VII with 195 bp DNA results in shifts by native gel electrophoresis, indicating protein-VII-DNA complex formation. Staining with either ethidium bromide (**e**) or Coomassie (**f**) are shown to verify the presence of DNA and protein, respectively. **g**, Ethidium bromide staining shows DNA content of nucleosome shifts from gel in Figure 2.1f. *Panels a and e-g by DC Avgousti.*

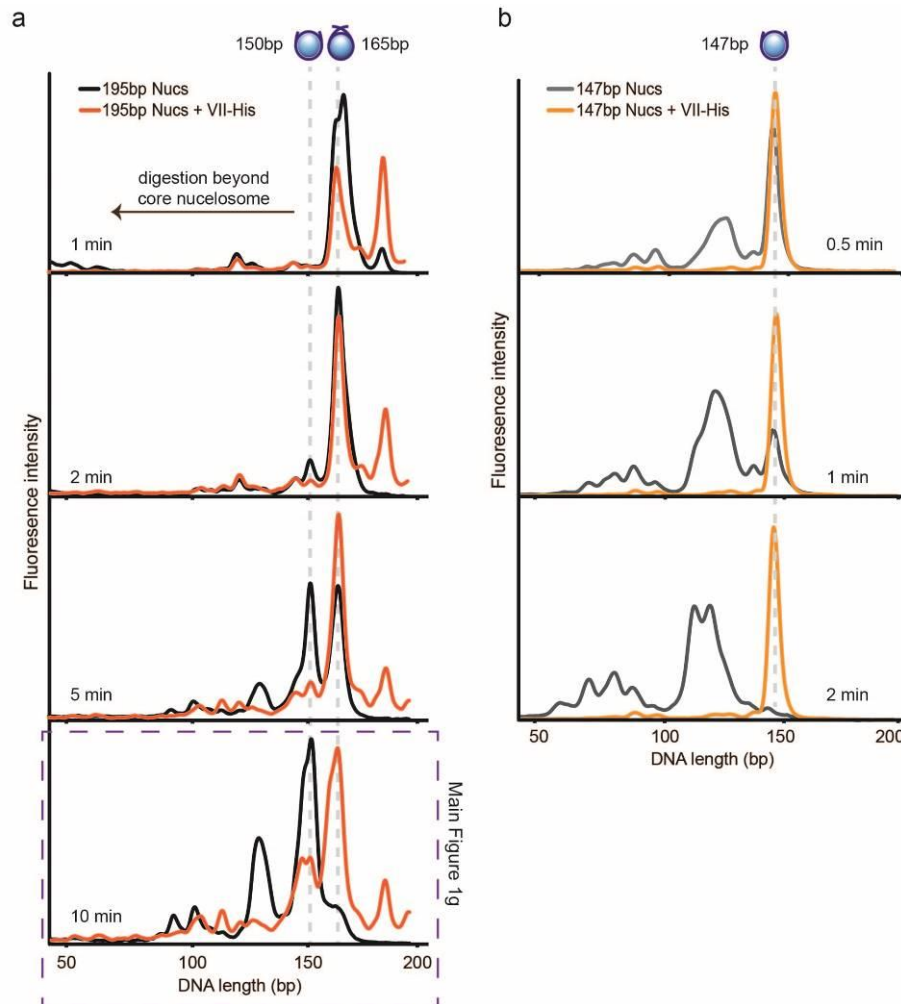


Figure 2.S3 | Bioanalyzer examination of MNase-digested nucleosomes and protein-VII-nucleosome complexes. **a**, 195 bp nucleosomes or protein-VII-nucleosome complexes were incubated with MNase for the indicated times, the reaction was stopped, DNA was extracted and analyzed. As in Figure 2.1g, nucleosomes are shown in black and protein-VII-nucleosome complexes in orange. The presence of protein VII pauses digestion at 165 bp, suggesting that protein VII is blocking access to the DNA. **b**, 147 bp nucleosomes or protein-VII-nucleosome complexes were incubated with MNase for the indicated times, the reaction was stopped, DNA was extracted and analyzed. Graphs show nucleosomes in grey and protein-VII-nucleosome complexes in orange. The presence of protein VII completely blocks digestion even after nucleosomes alone have been digested well beyond the core particle. In contrast to what would be expected for linker histones, protein VII protects the core nucleosome particle from digestion. These data indicate that protein VII may be masking the substrate for MNase through complex formation. This represents a unique mechanism of nucleosome binding and suggests a model for blocking DNA access in cellular chromatin during infection. *Panels a and b by DC Avgousti.*

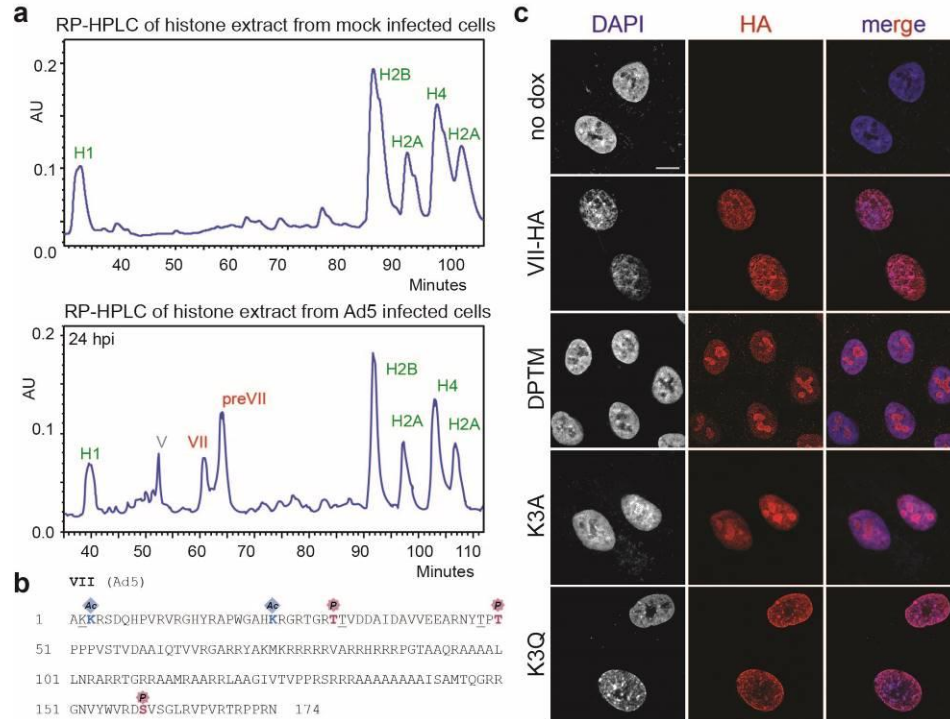


Figure 2.2 | Post-translational modifications on protein VII contribute to chromatin localization. **a**, RP-HPLC analysis of histone extracts. Viral proteins V, VII and preVII are indicated at 24 hpi. **b**, Primary sequence of protein VII with modified residues identified in infected cells. Underlined residues represent moieties that may also be modified in identified peptides (see Extended Data Fig. 5). ac, acetylated; P, phosphorylated. **c**, Immunofluorescence showing DAPI (grey, blue in merge) and protein VII (red) as wild type or with alanine substitutions at PTM sites (Δ PTM), K3A or K3Q. Scale bar, 10 μ m. *Panels a-c by DC Avgousti.*

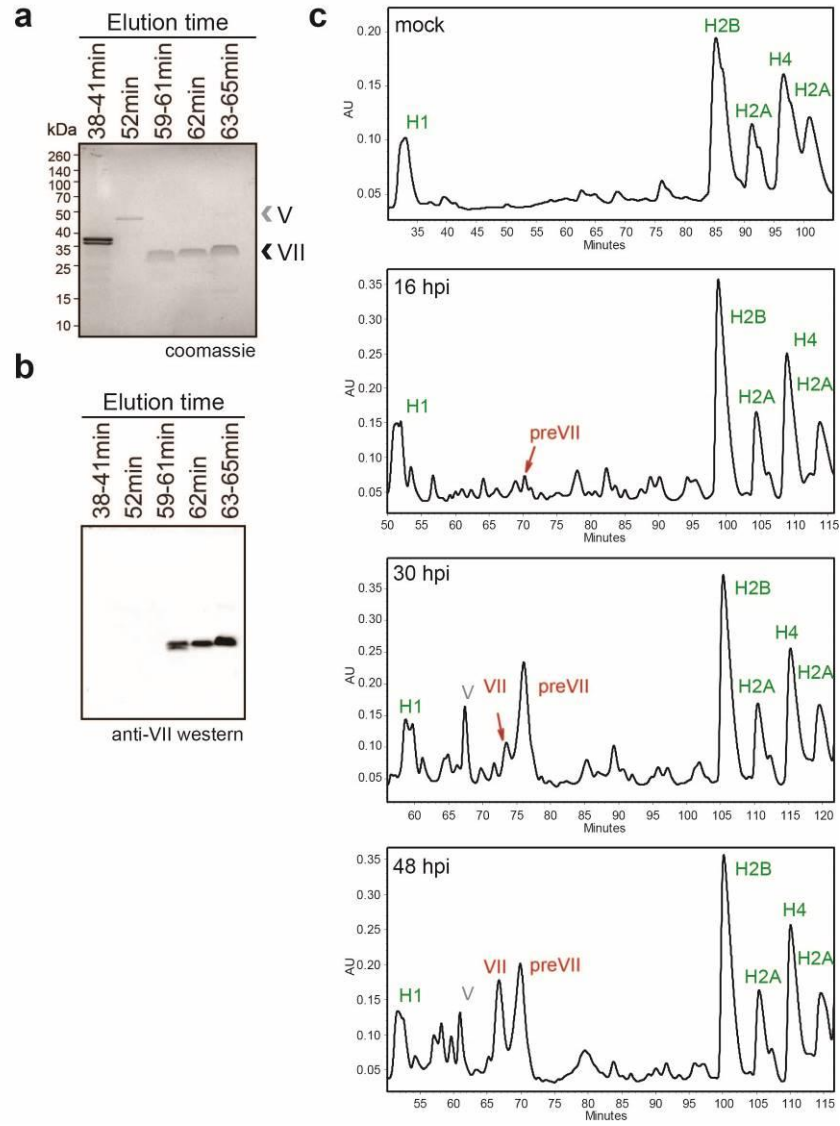


Figure 2.S4 | Purification of protein VII from infected cells. **a**, Coomassie-stained SDS-PAGE analysis of fractions from RP-HPLC in Figure 2.2a. The bands in fraction 38-41 min correspond to histone H1. Protein VII and V, as indicated, were verified by MS analysis (data not shown). The slight upward shift of the protein VII bands in the later peak corresponds to the higher abundance of protein preVII, as seen by HPLC in Figure 2.2a. **b**, Western blot analysis of protein VII in HPLC fractions from **a**. **c**, Time course of infection followed by histone extraction and HPLC analysis. MS analysis verified peaks in each sample as indicated. *Panels a-c by DC Avgousti and K Kulej.*

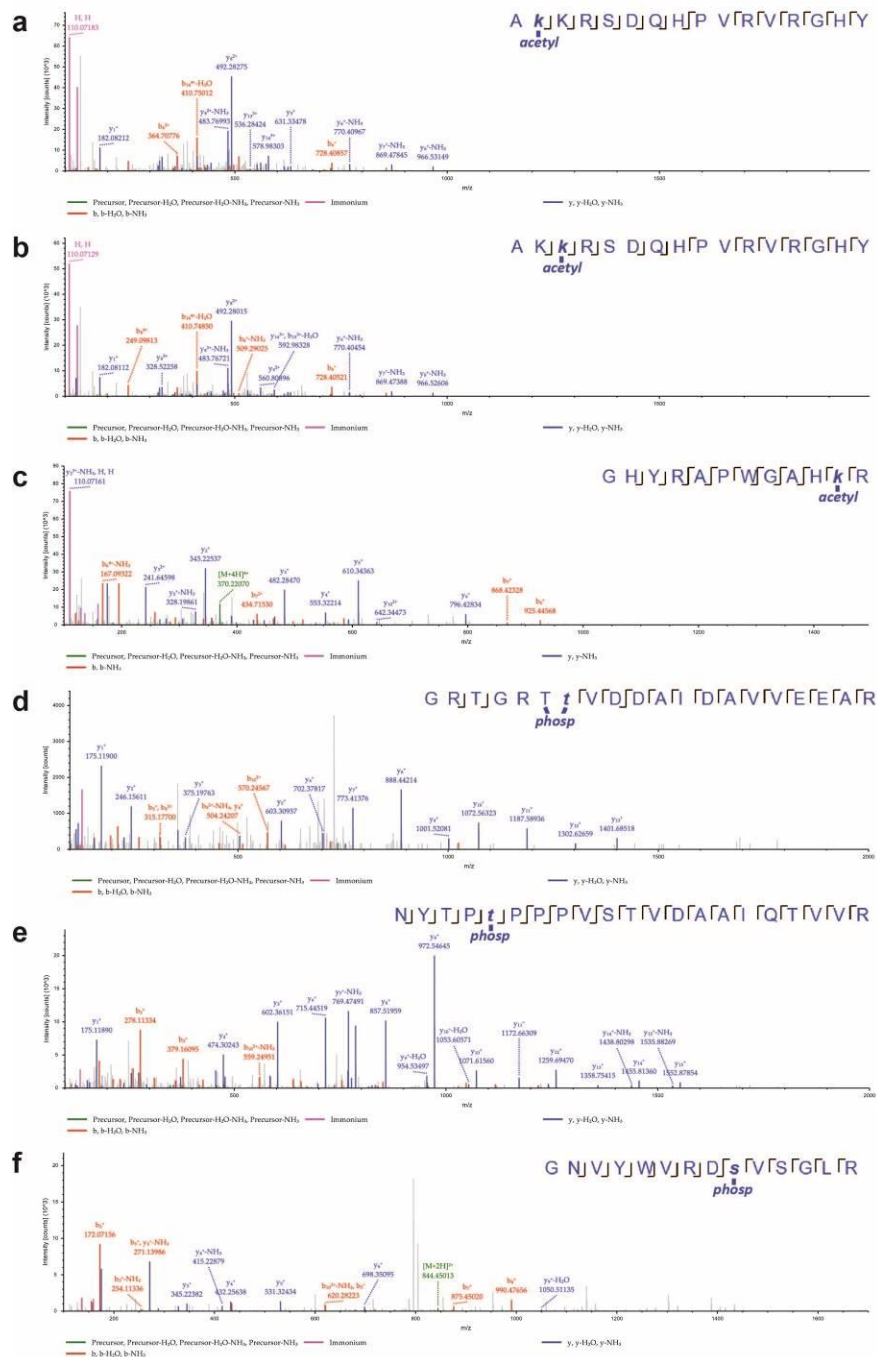


Figure 2.S5 | Representative mass spectra. **a-f**, Annotated MS/MS spectra of identified peptides of protein VII containing PTMs (**a-c**, acetylated peptides; **d-f**, phosphorylated peptides). The images represent the observed fragment ions collected using MS/MS collision-induced dissociation (CID). Colored lines represent matches between observed and expected fragment ions of the given peptides. Specifically, green lines represent not fragmented precursor mass, blue lines represent matches with y-type fragments, red lines with b-type fragments, and yellow boxed masses represent fragments containing PTM neutral losses (for example, ions that lost the phosphorylation during fragmentation). *Panels a-f by DC Avgousti and K Kulej.*

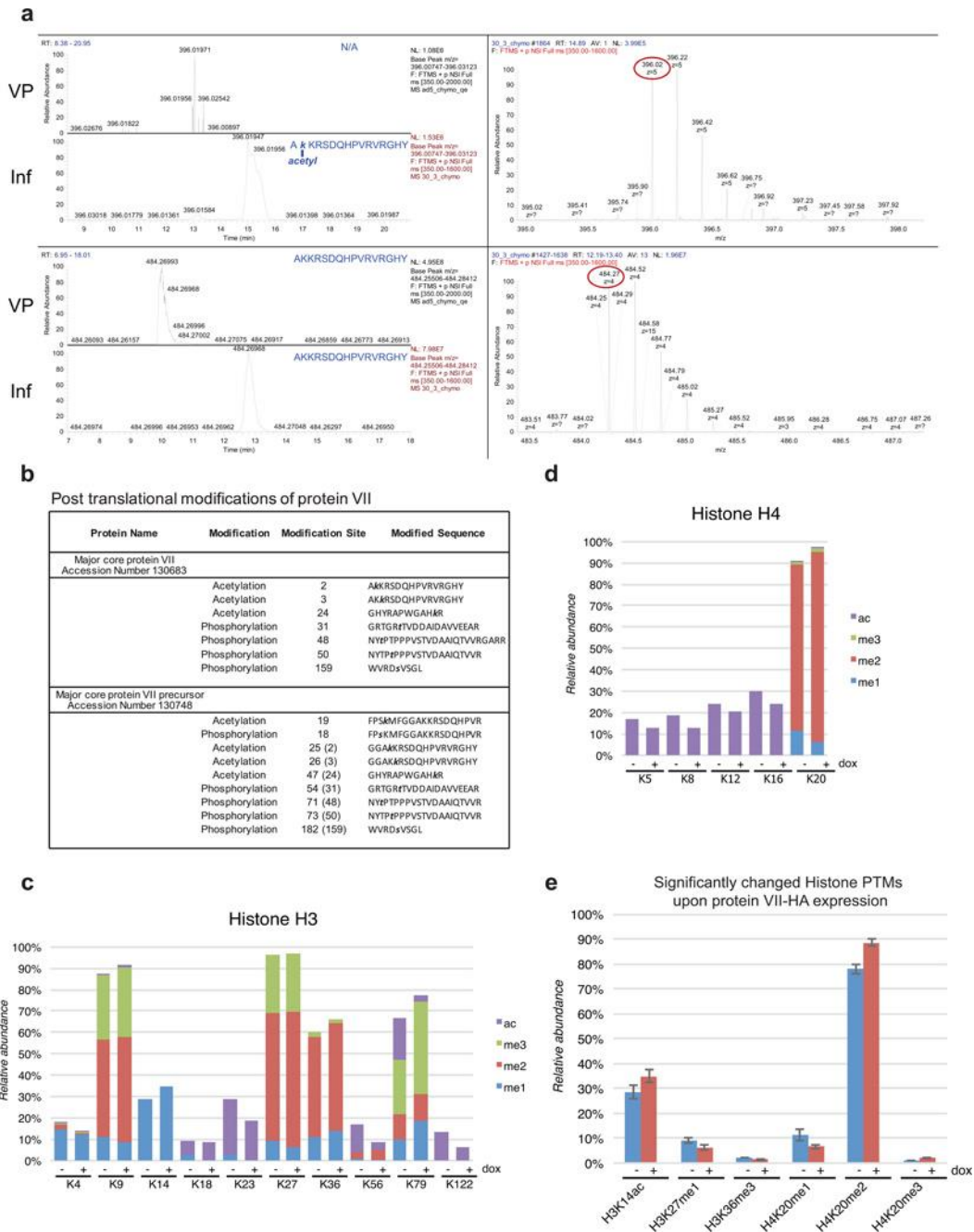


Figure 2.S6 | Acetylated protein VII spectra from virus particles and analysis of total histone PTM changes upon protein VII expression. **a**, Liquid chromatography-mass spectrometry (LC-MS) analysis of unmodified and modified chymotryptic peptide AKKRSDQHPVVRVGRGHY. On the left, nano-LC-MS-extracted ion chromatograms of protein VII peptides identified in the histone extracts of adenovirus infected cells (Inf) or viral particles (VP). The top left represents the modified form, while the bottom left represents the unmodified form. Non-modified forms were detected in both conditions for Inf and VP, while the acetylated form was unique for the infected sample only (Inf). On the right, full MS spectrum of the modified (top) and unmodified (bottom) peptide. Circled mass represents the monoisotopic signal of the peptide. **b**, Summary of post-translational modifications detected on protein VII. Peptides shown

were identified during infection at various time points with the mature protein VII in the top row and preVII in the bottom row. The numbers in brackets for preVII indicate the location of the same moiety in mature protein VII. Acetylation sites were detected in approximately 3% of peptides for mature protein VII and 2% of peptides in preVII. Phosphorylation was detected in approximately 1% of peptides for mature protein VII and preVII. **c, d**, Quantification of histone H3 (**c**) and H4 (**d**) PTMs in protein-VII-HA-induced (+dox) and -uninduced (-dox) A549 cells from the analysis of crude histone mixtures ($n = 3$ biological replicates). Positions of PTMs are listed along the x axis. Modification type is indicated by color as shown. y Axis represents the cumulative extent of PTMs relative to the total histone H3 or H4, respectively. **e**, Breakdown of the histone marks (H3K14ac, H3K27me1, H3K36me3, H4K20me1, H4K20me2 and H4K20me3) found to be significantly different ($n = 3$ biological replicates) in terms of relative abundance between the protein-VII-HA-induced and -uninduced states (<5% homoscedastic two-tailed t -test). Mean \pm s.d. *Panels a-e by DC Avgousti and K Kulej.*

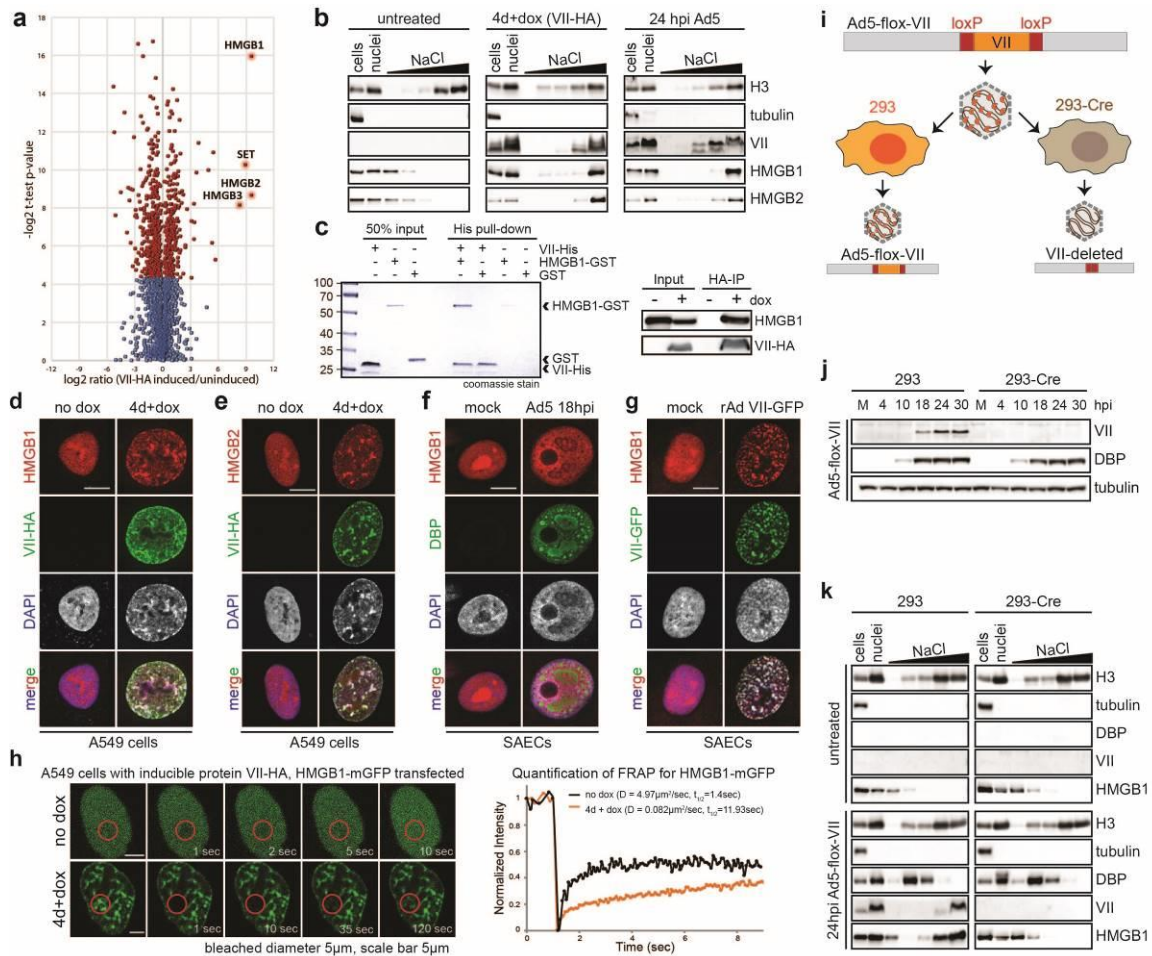


Figure 2.3 | Protein VII directly binds HMGB1 and is necessary for retention of the alarmin in cellular chromatin. **a**, Volcano plot for proteomics analysis of one representative biological replicate of the high-salt fraction. The y axis represents $-\log_2$ statistical P value and the x axis represents \log_2 protein fold-change between uninduced or protein-VII-expressing cells (homoscedastic two-tailed t-test, $P < 0.05$ red dots; $n = 3$ technical replicates). **b**, Nuclear fractionation shows that HMGB1 and HMGB2 normally elute from nuclei at low salt concentrations but are retained in high-salt fractions by protein-VII-HA. d, day; dox, doxycycline. **c**, Protein VII interacts with HMGB1 in pull-down of recombinant HMGB1-glutathione S-transferase (GST) (left, Coomassie-stained SDS-PAGE) and immunoprecipitation of HMGB1 (right, western blots). **d**, **e**, Protein VII expression alters localization of HMGB1 (**d**) and HMGB2 (**e**). Immunofluorescence shows protein-VII-HA (green) colocalized with HMGB1 (**d**) and HMGB2 (**e**) (red) in cellular chromatin (DAPI, grey, blue in merge). **f**, Same as **d** at 18 hpi with Ad5 DBP (green). **g**, Protein-VII-GFP relocalizes HMGB1 (red) to chromatin with DAPI (grey, blue in merge). rAd, recombinant adenovirus. **d-g**, Scale bars, 10 μm . **h**, FRAP experiment with HMGB1-monomeric GFP (mGFP). Recovery of FRAP signal in time-course images (left) with quantification and diffusion coefficients (right). Scale bar, 5 μm . D, diffusion coefficient; $t_{1/2}$, half-time of recovery. **i**, Schematic showing loxP strategy for deleting protein VII. **j**, Western blots comparing 293 and 293-Cre cells infected with Ad5-flox-VII virus. **k**, Salt fractionation in nuclei from **j**. Analysis of panel a by K Kulej, panels c-h by DC Avgousti, and panels i and j by NJ Pancholi.

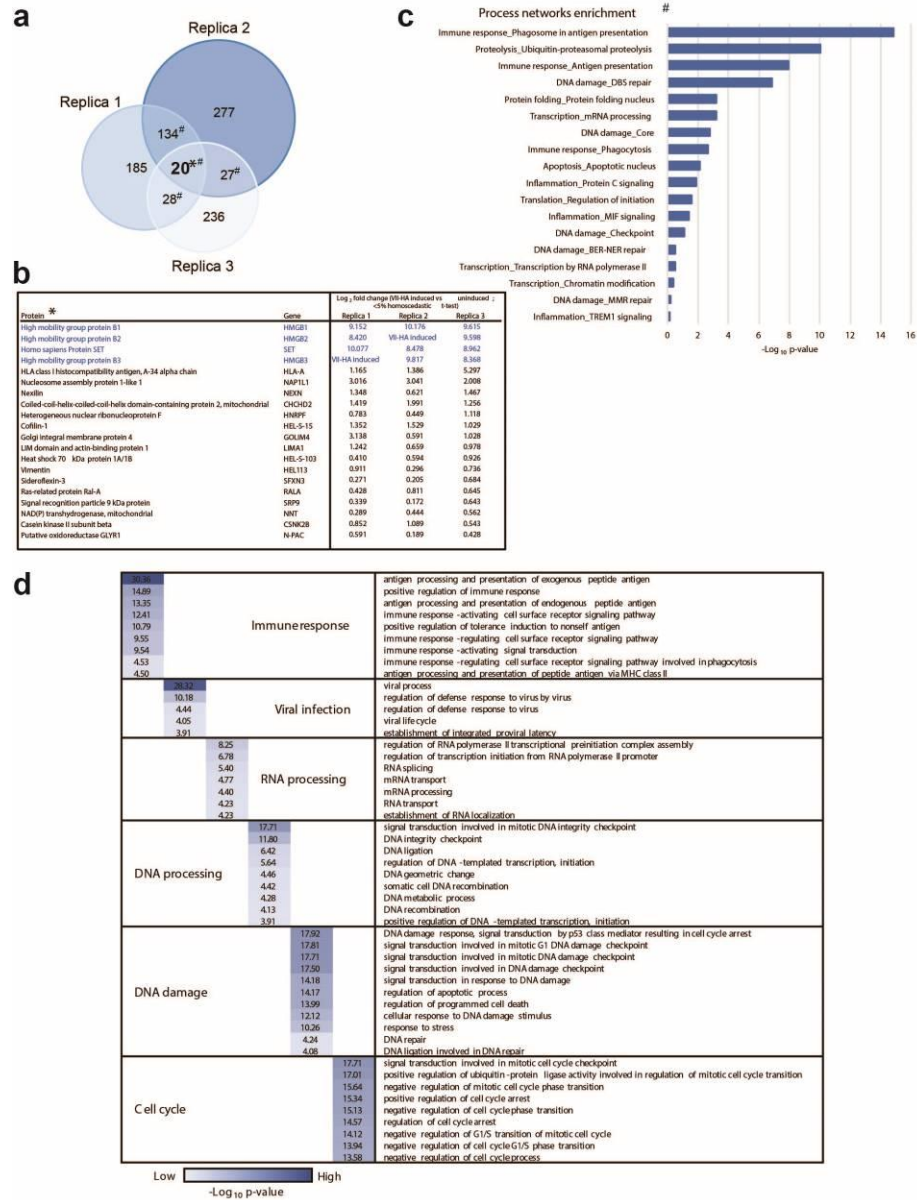


Figure 2.S7 | Bioinformatic analysis of proteins enriched in the high-salt fraction upon protein VII expression. **a**, Venn diagram showing overlap between three biological replicates of high-salt-fraction proteins significantly enriched compared with uninduced cells. **b**, Proteins found significantly enriched in the protein-VII-HA-induced state compared with uninduced (<5% homoscedastic *t*-test) in all three biological replicates ("VII-HA induced" indicates proteins identified only in protein-VII-HA-induced condition). **c**, **d**, Classification of proteins significantly enriched in minimum two out of three biological replicates (protein-VII-HA-induced versus uninduced) according to process network enrichment and Gene Ontology biological process (GeneGo MetaCore pathways analysis package; false discovery rate (FDR) < 5%); each Gene Ontology term was ranked using *P*-value enrichment. *Analysis of panel a-d by K Kulej.*

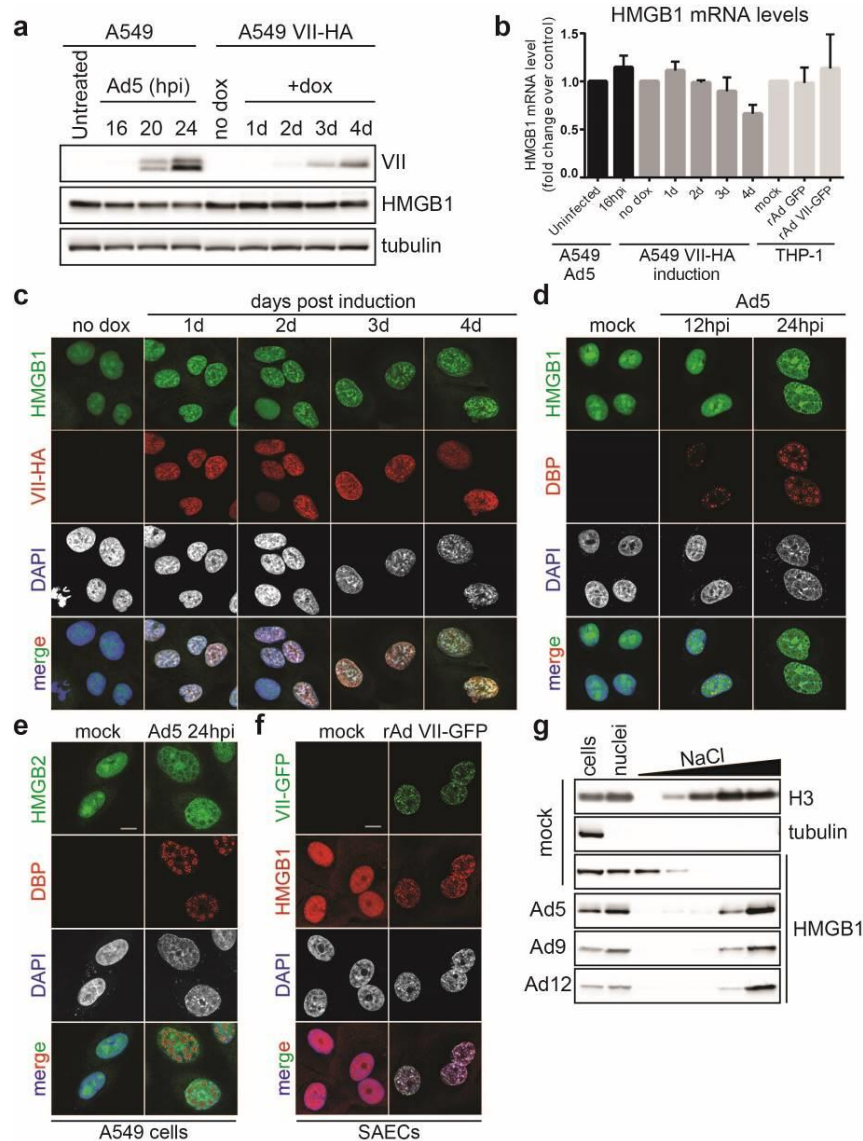


Figure 2.S8 | Protein VII retains HMGB1 and HMGB2 in chromatin. **a**, Western blot of adenovirus-infected or doxycycline-treated A549 cells showing the relative levels of protein VII expression. HMGB1 levels do not change upon infection or protein VII expression. Tubulin is shown as a loading control. **b**, Quantitative PCR analysis of mRNA transcripts of *HMGB1* in various cell types as indicated (for A549, $n = 3$ biological replicates; for THP-1, $n = 2$ biological replicates; mean \pm s.d.). The levels of HMGB1 do not significantly change. **c**, Immunofluorescence analysis of a time course of protein-VII-HA (red) induction shown with HMGB1 (green) and DAPI (grey, blue in merge) in A549 cells. Expression of protein-VII-HA results in a change to the HMGB1 distribution upon expression. **d**, HMGB1 (green) localization changes between 12 and 24 hpi of wild-type adenovirus in A549 cells, and adopts a pattern similar to protein VII as in Figure 2.1a. DBP (red) is shown as a marker of infection, DNA is stained with DAPI (blue in merge). **e**, Same as **d** showing that HMGB2 adopts the same pattern as HMGB1 during Ad5 infection at 24 hpi. **f**, Multiple cells showing the same pattern of HMGB1 relocalization upon expressing protein-VII-GFP as in Figure 2.3g. **g**, HMGB1 retention in the high-salt fraction is conserved across adenovirus serotypes. Western blot analysis of HMGB1 from salt-fractionated A549 cells infected with Ad5, Ad9 or Ad12 as shown. Scale bars, 10 μ m. Panels **a** and **b** by NJ Pancholi, panels **c-f** by DC Avgousti.

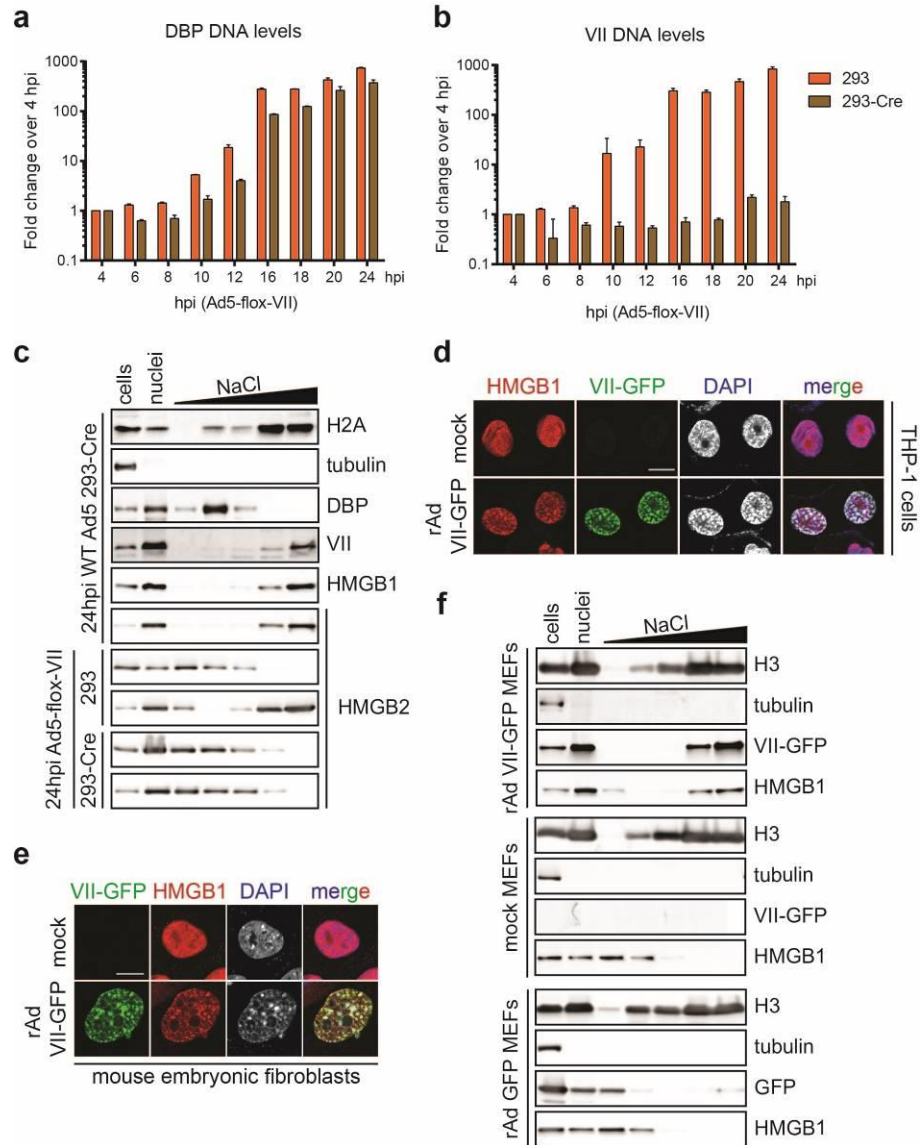


Figure 2.S9 | Protein VII is necessary and sufficient for chromatin retention of HMGB1 in human and mouse cells. **a**, **b**, Replication of Ad5-flox-VII virus on 293 or 293-Cre cells. Quantitative PCR analysis of viral genomic DNA over a time course of infection (**a**) shows the DBP gene is increasing exponentially in 293 and 293-Cre cells when infected with Ad5-flox-VII virus. In contrast, PCR for the protein VII gene (**b**) demonstrates deletion in 293-Cre cells ($n = 2$ biological replicates, mean \pm s.d.). **c**, Salt fractionation of 293-Cre cells infected with wild-type Ad5, indicating that the Cre recombinase does not interfere with the ability of protein VII to retain HMGB1 in the high-salt chromatin fraction. Protein VII is also necessary for the chromatin retention of HMGB2. **d**, THP-1 cells transduced to express protein-VII-GFP results in chromatin distortion and HMGB1 retention in chromatin. Immunofluorescence of transduced PMA-treated THP-1 cells showing protein-VII-GFP (green), HMGB1 (red) and DNA (grey, blue in merge). **e**, Transduction to express protein-VII-GFP is sufficient to relocalize mouse HMGB1 in mouse embryonic fibroblast (MEF) cells. **f**, Salt fractionation of mouse embryonic fibroblast cells transduced to express protein-VII-GFP. Human Ad5 protein VII is sufficient to retain mouse HMGB1 in the high-salt fraction in MEF cells. The control vector expressing GFP alone does not have this effect. *Panels a and b by NJ Pancholi, panels d and e by DC Avgousti.*

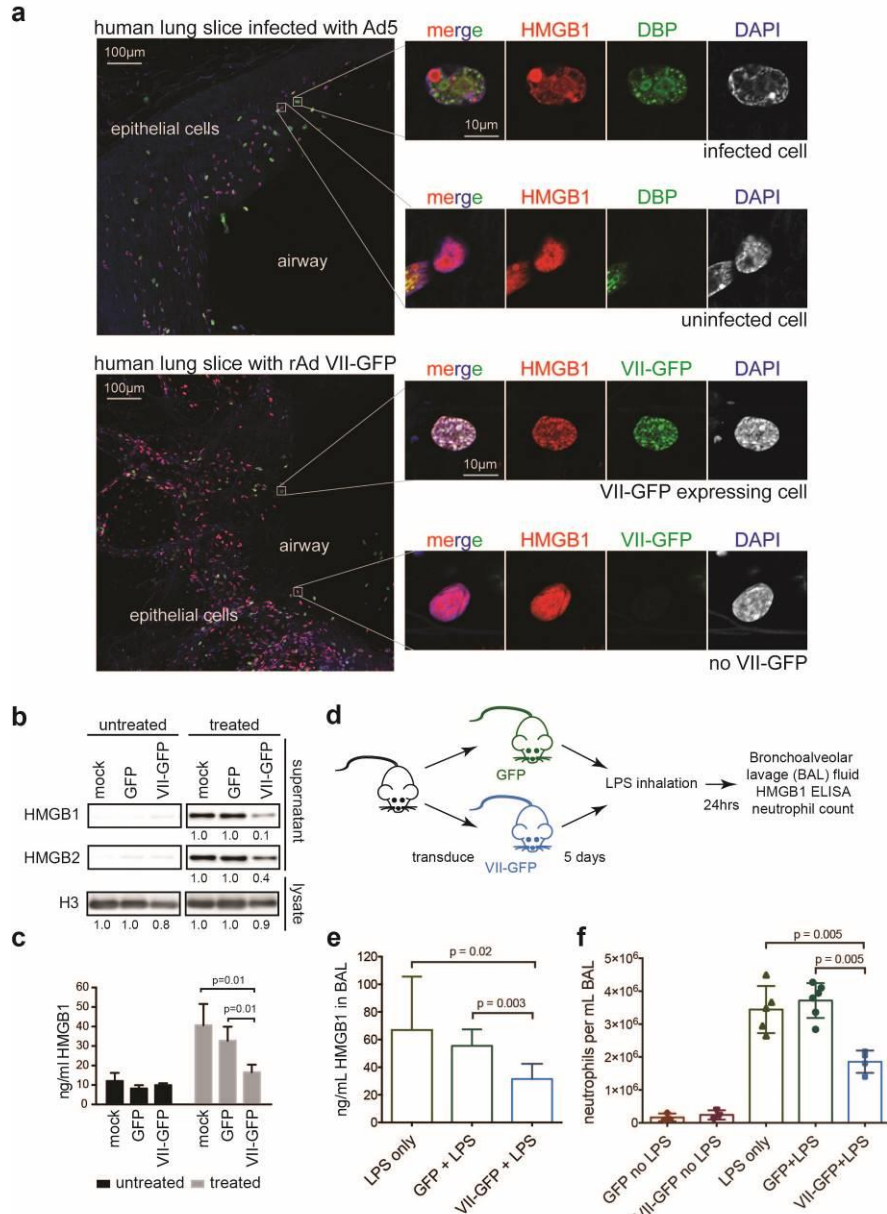


Figure 2.4 | Protein VII prevents HMGB1 release. **a**, Precision-cut lung slices infected with Ad5 or transduced to express protein-VII-GFP. Endogenous HMGB1 (red) is redistributed in cells with virus (DBP, top) and protein-VII-GFP (bottom). **b**, Protein-VII-GFP is sufficient to inhibit HMGB1 and HMGB2 release in THP-1 cells. Numbers indicate relative intensities of bands quantified with ImageJ. **c**, Enzyme-linked immunosorbent assay (ELISA)-based quantification of HMGB1 in supernatants from **b**. Mean \pm standard deviation (s.d.), $n = 4$ technical replicates, homoscedastic one-tailed t-test. **d**, Schematic for investigating protein VII in a mouse lung injury model. **e**, Expression of protein-VII-GFP decreases HMGB1 in mouse BAL fluid as quantified by ELISA. Mean \pm s.d., biological replicates: nLPS = 4, nGFP+LPS = 6, nVII-GFP+LPS = 7, homoscedastic one-tailed ($P = 0.02$) or two-tailed ($P = 0.003$) t-test. **f**, Neutrophils in bronchoalveolar lavage (BAL) fluid are significantly fewer in mice expressing protein-VII-GFP. Mean \pm s.d., biological replicates: nGFP+LPS = 6, nVII-GFP+LPS = 4, nLPS = 5, nGFP = 3, nVII-GFP = 3, homoscedastic two-tailed t-test. *Panels a, and d-f by DC Avgousti, panels e and f with help of GS Worthen and AJ Paris.*

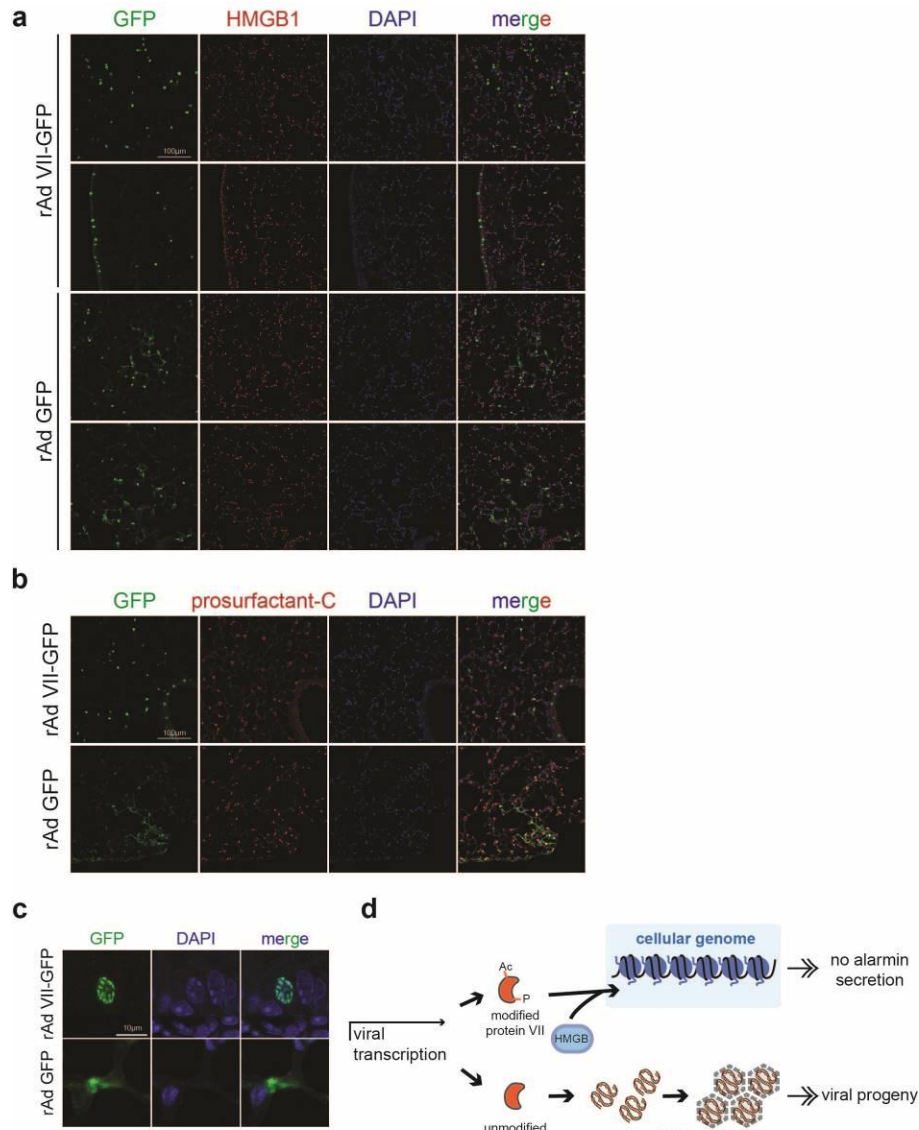


Figure 2.S10 | Transduction of mouse lungs demonstrating expression of GFP or protein-VII-GFP. a, Sections of mouse lungs transduced to express protein-VII-GFP or GFP co-stained for HMGB1. GFP signal shows multiple cell types transduced in both cases. Protein-VII-GFP has a more distinct nuclear signal than GFP, which also appears cytoplasmic. Two sections for each condition are shown to indicate transduction efficiency. **b,** Same as **a** but co-stained for prosurfactant-C to mark type II pneumocytes. Some cells are positive for both, confirming that multiple cell types were transduced. **c,** Zoomed images of individual epithelial cells from mouse lungs showing the characteristic protein-VII-GFP pattern colocalizing with DAPI in the nucleus. GFP only is mostly cytoplasmic. **d,** Schematic summarizing function of protein VII during infection. Newly synthesized protein VII late during infection can be post-translationally modified and binds to HMGB1, sequestering it on the cellular chromatin and preventing its release. Unmodified protein VII is packaged in viral progeny. *Panels a-d by DC Avgousti.*

2.5 Methods

2.5.1 Cells

Primary SAECs, U2OS, HeLa, 293, THP-1 and A549 cells were obtained from the American Type Culture Collection (ATCC) and grown according to the provider's instructions. Cell lines were not authenticated or tested for mycoplasma. Acceptor cells for generation of inducible cell lines were provided by E. Makeyev and used as previously reported^{277,278}. Protein VII, preVII and V were cloned from genomic DNA isolated from HeLa cells infected with adenovirus type 5 and inserted into the inducible plasmid cassette with a C-terminal HA tag using restriction enzymes BsrGI and AgeI (primer sequences available upon request). Positive clones were selected in DH5 α cells, sequenced, and transfected into A549, U2OS or HeLa acceptor cells along with plasmid expressing the Cre recombinase. Recombined clones were selected by puromycin resistance (1 μ g/ml) and induced with doxycycline (0.2 μ g/ml) to express the desired protein. Protein expression was verified by immunofluorescence and western blot. All figures shown are after 4 days of induction unless otherwise stated. Protein VII and preVII were also verified by HPLC purification and MS analysis. Point mutations were generated by gene synthesis from Genewiz. 293-Cre cells were provided by P. Hearing.

2.5.2 Viruses and infections

Wild-type Ad5, Ad9, Ad12 and recombinant adenovirus vectors expressing only GFP were propagated in 293 cells as previously described²⁷⁸. Recombinant adenovirus vector with protein-VII-GFP replaced in the E1 region was a gift from D. Curiel²⁷⁹. Infections were carried out as described previously²²¹ using a multiplicity of infection of 10 for primary cells and cell lines for Ad5 infections. Ad9 and Ad12 infections were carried out with a multiplicity of infection of 50 and 20, respectively. Ad5-flox-VII was generated by P. Hearing and also prepared using standard methods in 293 cells. loxP sites were added flanking protein VII in the Ad5 genome resulting in protein VII deletion during infection of 293 cells expressing Cre recombinase.

2.5.3 Antibodies

Primary antibodies were purchased from Covance (HA MMS-101R), Abcam (H1 ab4269, H3 ab1791, HMGB1 ab18256, HMGB2 ab67282), Millipore (H2A 07-146, prosurfactin-C AB3786), and Santa Cruz (Ku86 sc5280, tubulin sc69969). The antibodies to DBP, adenoviral late proteins, terminal protein and protein VII were gifts from A. Levine²⁸⁰, J. Wilson²⁷⁸, R. Hay and L. Gerace, respectively. Secondary antibodies for immunoblotting were obtained from Jackson ImmunoResearch and secondary antibodies for immunofluorescence were obtained from Life Technologies.

2.5.4 Immunofluorescence

Cells were grown on glass coverslips in 24-well plates and either infected or induced with doxycycline (0.2 µg/ml). Cells were harvested for immunofluorescence at the indicated time points, washed in PBS, fixed in 4% paraformaldehyde for 15 min and post-fixed with 100% ice-cold methanol for 5 min. Coverslips were then blocked and stained as previously described³⁶ and mounted using ProLong Gold Antifade Reagent (Life Technologies). Immunofluorescence was visualized using a Zeiss LSM 710 Confocal microscope (Cell and Developmental Microscopy Core at UPenn) and ZEN 2011 software. Images were processed using ImageJ and assembled with Adobe CS6.

2.5.6 Immunoblotting

Western blot analysis was carried out using standard methods. Briefly, equal amounts of total protein lysates were separated by SDS-PAGE and transferred to a nitrocellulose membrane (Millipore) for at least 30 min at 30 V. Membranes were stained with ponceau to confirm protein loading and blocked in 5% milk in TBST containing 0.1% azide. Membranes were incubated with primary antibodies overnight, washed for 30 min in TBST and incubated with secondary antibodies conjugated to horseradish peroxidase (Jackson Laboratories) for 1 h. Membranes were washed again and proteins were visualized with Pierce ECL Western Blotting Substrate (Thermo Scientific) and detected using a Syngene G-Box.

2.5.7 Mice

All mice were housed in specific-pathogen-free (SPF) conditions in an animal facility at the Children's Hospital of Philadelphia. All studies in mice were carried out in accordance with the recommendations in the Guide for the Care and Use of Laboratory Animals of the National Institutes of Health and approved by the Institutional Animal Care and Use Committee, Children's Hospital of Philadelphia Animal Welfare Assurance Number A3442-01. C57BL/6J male mice aged 8-10 weeks were used for experiments. Mice were sedated with ketamine and xylazine. Once sedated, mice underwent orotracheal intubation, as previously described²⁸¹, with a 20G angiocatheter from BD. Mice subsequently received 5×10^{10} genome copies (GC) of recombinant adenovirus expressing protein-VII-GFP or GFP purified by the Penn Vector Core. Four days after infection, mice were exposed to aerosolized LPS, 3 mg/ml for 30 min as previously described²⁸². One day after LPS exposure, bronchoalveolar lavage (BAL) and lung tissue were harvested as previously detailed²⁸³ and examined for HMGB1 content (ELISA, Chondrex 6010) and neutrophil count (haematoxylin and eosin stain kit EMD 65044/93). Immunostaining was carried out by the CHOP Pathology Core using standard methods. A minimum of four biological replicates were used for each condition studied. Mice were assigned a random number and color at the start of the experiment and were randomized. Technicians carrying out the experiments were blinded to the identity of the samples. Tissue samples were assigned a random study number such that the technician performing the analysis was blinded. Unblinding for the purpose of data analysis occurred only after all data had been collected.

2.5.8 Salt fractionation of nuclei

Salt fractionation of nuclei was adapted from established protocols^{267,284}. Briefly, $2-4 \times 10^7$ cells were collected and resuspended in 2 ml of ice-cold buffer I (0.32 M sucrose, 60 mM KCl, 15 mM NaCl, 5 mM MgCl₂, 0.1 mM EGTA, 15 mM Tris, pH 7.5, 0.5 mM dithiothreitol (DTT), 0.1 mM PMSF and protease inhibitor cocktail from Roche). To dissolve the plasma membrane, 2 ml ice-cold buffer I supplemented with 0.1% IGEPAL were added and samples were incubated on ice for 10 min. The 4 ml of nuclei was layered on 8 ml of ice-cold buffer II (1.2 M sucrose, 60 mM KCl, 15 mM NaCl, 5 mM MgCl₂, 0.1 mM EGTA, 15 mM Tris, pH 7.5, 0.5 mM DTT, 0.1 mM

PMSF and protease inhibitor cocktail from Roche) and centrifuged for 20 min at 10,000 g and 4 °C. The pelleted nuclei were resuspended in 400 µl buffer III (10 mM Tris pH 7.4, 2 mM MgCl₂, 0.1 mM PMSF) supplemented with 5 mM CaCl₂ and the DNA was digested to mononucleosomes by addition of 1 unit of MNase (Sigma-Aldrich, N3755). The reaction was incubated at 37 °C for 30 min and then stopped by addition of 25 µl of 0.1 M EGTA. The samples were centrifuged for 10 min, 350 g, at 4 °C, and supernatants were set aside for western blot analysis. The pellet was resuspended in 400 µl of buffer IV (70 mM NaCl, 10 mM Tris pH 7.4, 2 mM MgCl₂, 2 mM EGTA, 0.1% Triton X-100, 0.1 mM PMSF) with 80 mM salt and rotated for 30 min at 4 °C. The sample was centrifuged for 10 min at 350 g, 4 °C, and the supernatant collected for western blot analysis. This step was repeated for salt concentrations in buffer IV of 150 mM, 300 mM and 600 mM. The final pellet was resuspended in 400 µl H₂O and all samples were analyzed together by western blot. An aliquot of each supernatant was set aside for DNA purification using a PCR purification kit (Qiagen) and analyzed by agarose gel electrophoresis. Alternatively, 4 × 10⁷ cells were resuspended in 400 µl hypotonic buffer (10 mM HEPES pH 7.9, 1.5 mM MgCl₂, 10 mM KCl, 1:1,000 PMSF, 0.5 mM DTT) and incubated on ice for 30 min. The cells were transferred to a 1 ml dounce tissue grinder and the cell membranes were gently disrupted with 40 strokes of a tight-fitting pestle. The samples were centrifuged for 5 min at 1,500 g and 4 °C. The pelleted nuclei were resuspended in 400 µl buffer III and the fractionation was continued as described earlier.

2.5.9 Preparation of salt fractions for MS analysis

All chemicals used for preparation of MS samples were of at least sequencing grade and purchased from Sigma-Aldrich, unless otherwise stated. Only the 600 mM salt fraction was used for LC-MS/MS analysis. The 0.1% Triton X-100 detergent was removed from samples before MS analysis by precipitation using chloroform (CHCl₃)-methanol (MeOH) precipitation²⁸⁵. The protein pellet from CHCl₃-MeOH precipitation was resuspended in 6 M urea and 2 M thiourea in 50 mM ammonium bicarbonate. Samples were reduced with 10 mM DTT for 1 h at room temperature and then carbamidomethylated with 20 mM iodoacetamide for 30 min at room temperature in the dark. Afterwards, alkylated proteins were digested first with endopeptidase Lys-C (Wako, MS grade) for

3 h, after which the solution was diluted 10 times with 20 mM ammonium bicarbonate. Subsequently, samples were digested with trypsin (Promega) at an enzyme-to-substrate ratio of approximately 1:50 for 12 h at room temperature. The samples were acidified with 5% formic acid (FA) to $\text{pH} \leq 3$ and desalted using Poros Oligo R3 RP columns (PerSeptive Biosystems) packed in a P200 stage tip with C18 3M plug (3M Bioanalytical Technologies). Purified peptide samples were dried by lyophilization and stored at -20°C until further analysis. This procedure was carried out for three biological replicas.

2.5.10 Nano-LC-MS/MS and analysis of salt fractions

Samples were loaded onto a 16 cm C18-AQ column (inner diameter $75\ \mu\text{m}$, $3\ \mu\text{m}$ beads, Dr, Maisch GmbH, Germany) using an Easy nano-flow HPLC system (Thermo Fisher Scientific). The nano-LC was coupled to an Orbitrap Fusion Tribrid Mass Spectrometer (Thermo Fisher Scientific) via a nanoelectrospray ion source (Thermo Fisher Scientific). Peptides were loaded in buffer A (0.1% formic acid) and eluted with a 120 min linear gradient from 2-30% buffer B (95% acetonitrile, 0.1% formic acid). After the gradient, the column was washed with 90% buffer B. Mass spectra were acquired using a data-dependent acquisition method with the TopSpeed set with 3-s cycle. Spectra were acquired in the Orbitrap analyzer with mass range of 350-1,200 m/z and 120,000 resolution (200 m/z), with a maximum injection time of 50 ms and an AGC target of 5×10^5 . Signals with 2-5 charges were selected for HCD fragmentation using a normalized collision energy of 27, a maximum injection time of 120 ms and an AGC target of 10,000. Fragments were analyzed in the ion trap. Raw MS files were analysed by MaxQuant (v.1.5.2.8)²⁸⁶ (<http://www.maxquant.org>). MS/MS spectra were searched against the UniProt-human database (version June 2014, 59,345 entries). All used search parameters were default, with the exception of including the match between runs (1 min window) and the intensity-based absolute quantification (iBAQ) label-free quantification²⁸⁷. The search included variable modifications of methionine oxidation and N-terminal acetylation, and fixed modification of carbamidomethyl cysteine. Each iBAQ value was \log_2 transformed and subsequently normalized by the average protein abundance within each run. Biological process association analysis and process network

enrichment were performed using the GeneGo MetaCore pathways analysis package with FDR < 5%; each Gene Ontology term was ranked using P-value enrichment.

2.5.11 Purification of recombinant protein-VII-His

Protein VII was cloned from genomic DNA isolated from adenovirus-infected HeLa cells into a pET21a backbone to generate a C-terminal hexahistidine tag. Positive clones were selected in DH5 α cells, sequenced, and transformed into BL21 (DE3) cells (NEB C25271). The purification of insoluble protein-VII-His was adapted from existing protocols to purify histone proteins from *Escherichia coli*^{97,288}. Briefly, BL21 cells were inoculated from overnight cultures and grown to an optical density of 0.5-0.6 OD_{260 nm}, induced with 0.1 mM isopropyl- β -d-thiogalactoside (IPTG; Sigma) and harvested after 4 h at 37 °C. Cell pellets were resuspended in a mild buffer (50 mM Tris-HCl pH 8.0, 500 mM NaCl, 1 mM PMSF, 5% glycerol, 2.5 μ g/ml aprotinin, leupeptin and pepstatin) and disrupted by sonication using a Branson 250 sonifier. The lysate was then centrifuged at 27,000 g for 20 min at 4 °C. The supernatants were discarded, and pellets were resuspended in a denaturing buffer (50 mM Tris-HCl, pH 8.0, 500 mM NaCl, 5% glycerol, 8 M urea). The suspension was centrifuged again to eliminate insoluble cell debris and the His-tagged protein was isolated using a cobalt resin (ThermoScientific 89964) according to the manufacturer's instructions for denaturing conditions. The purified protein was then dialysed against water and lyophilized. Purified protein was verified by western blot and MS.

2.5.12 In vitro binding assays

HMGB1-GST (Abnova) or GST (Sigma) were combined with recombinant protein-VII-His at equimolar ratios and incubated at 4 °C for 1 h. Complexes were then mixed with a cobalt resin (ThermoScientific 89964) to bind protein-VII-His and any associated protein and washed three times in the binding buffer (50 mM Tris pH 8, 300 mM NaCl, 0.1% IGEPAL). The beads were then boiled in sample buffer, separated on a 4-12% NuPage gel and visualized by Coomassie staining.

2.5.13 Nucleosome in vitro binding and MNase digestion assays

Gel shift and MNase digestion assays were carried out as previously described^{268,289,290}. Briefly, nucleosomes were reconstituted by incubating purified recombinant histones with '601'

DNA of either 195 or 147 bp over a series of dialysis. Recombinant protein-VII-His was then combined with nucleosomes at various molar ratios, incubated at room temperature for 15 min, and analyzed by native gel electrophoresis. Complexes were also digested with MNase (Affymetrix) by addition of 1 unit per μg of DNA for 147 bp nucleosome experiments and 0.1 unit per μg of DNA for 195 bp nucleosome experiments, incubated at 22 °C for varying amounts of time followed by the addition of EGTA and guanidine thiocyanate to stop the reaction. The DNA fragments were then purified using a MinElute PCR purification kit (Qiagen) and analyzed on an Agilent 2100 Bioanalyzer as previously described²⁶⁸.

2.5.14 Release assay of HMGB1 in THP-1 cells

THP-1 cells were seeded at a density of 2×10^5 cells per well in a 24-well plate, and stimulated into macrophage-like cells by addition of 10 ng/ml PMA for 48 h. Cells were washed in PBS and transduced with recombinant adenovirus vectors expressing only GFP or protein-VII-GFP such that >90% of cells were GFP positive. At 48 h after transduction, cells were washed and 200 μl of serum-free RPMI was added. To stimulate the inflammasome, LPS (Sigma-Aldrich L2880) with a final concentration of 0.5 $\mu\text{g}/\text{ml}$ was added to wells and incubated for 2 h, then nigericin (Sigma-Aldrich N7143) was added with a final concentration of 10 μM for 1 h. Supernatants were collected and proteins precipitated overnight at 4 °C with a final concentration of 20% trichloroacetic acid (Sigma), washed with acetone, dried, and resuspended in 1 \times LDS sample buffer with reducing agent (Invitrogen). For ELISA analysis, supernatants were harvested directly and HMGB1 content was detected by the manufacturer's instructions (Chondrex 6010). Cells were also harvested by the addition of 1 \times LDS sample buffer with reducing agent (Invitrogen) and boiled. Supernatants and lysates were analyzed together by western blot.

2.5.15 Acid extraction and RP-HPLC

Histones were prepared for MS analysis as detailed previously²⁹¹. Nuclei were isolated and histones from infected cells were extracted by acid as previously described²⁶⁵. The preVII and protein VII variants were fractionated using an offline RP-HPLC. Briefly, $\sim 100 \mu\text{g}$ proteins were resuspended in buffer A (0.1% trifluoroacetic acid (TFA) in HPLC-grade water) and loaded onto a

C18 5 μm column (4.6 mm internal diameter \times 250 mm, Vydac) using a Beckman Coulter (System GoldA) HPLC (buffer A: 0.1% TFA; buffer B: 95% acetonitrile, 0.08% TFA). The proteins were separated using a gradient from 30 to 45% buffer B in 100 min at a flow rate of 0.2 ml/min. The fractions containing the proteins of interest were collected using an automatic fraction collector and individual peaks were combined based on their ultraviolet signal. The fractions were subsequently dried by vacuum centrifugation and prepared for MS (see later). Protein VII was purified from three biological replicates and analyzed as follows for MS.

2.5.16 MS analysis of protein VII PTMs

2.5.16.1 Sample preparation/protein VII

RP-HPLC-purified samples of protein VII variants were reduced in 10 mM DTT in 50 mM ammonium bicarbonate for 1 h at 56 °C. After cooling to room temperature, samples were alkylated in 20 mM iodoacetamide in 50 mM ammonium bicarbonate for 30 min in the dark. Samples were digested with chymotrypsin or Arg-C, at an enzyme-to-substrate ratio of approximately 1:20 for 8 h at 37 °C. The samples were acidified to a final concentration of 5% formic acid to $\text{pH} \leq 3$ and desalted using P200 stage tip columns packed with C18 3M plug (3M Bioanalytical Technologies). Purified peptide samples were dried by lyophilization and stored at -20 °C until further analysis.

2.5.16.2 Nano-LC-MS/MS analysis of histone PTMs

The nano-LC-MS/MS analysis was performed as previously described²⁹¹.

2.5.16.3 Nano-LC-MS/MS analysis of protein VII peptides

The nano-LC-MS/MS analysis was performed in triplicate for each sample. Samples were loaded onto a 16 cm C18-AQ column (inner diameter 75 μm , 3 μm beads, Dr. Maisch GmbH) using an Easy nano-flow HPLC system (Thermo Fisher Scientific). The nano-LC was coupled to an Orbitrap Velos Pro Mass Spectrometer (Thermo Fisher Scientific) via a nanoelectrospray ion source (Thermo Fisher Scientific). Peptides were loaded in buffer A (0.1% formic acid) and eluted with a 45 min linear gradient from 2 to 30% buffer B (95% acetonitrile, 0.1% formic acid). After the gradient, the column was washed with 90% buffer B. Mass spectra were acquired using a data-

dependent acquisition method with the top 15 most intense ions. Spectra were acquired in the Orbitrap analyzer with mass range of 350-1,600 m/z and 60,000 resolution (400 m/z), with a maximum injection time of 10 ms and an AGC target of 10×10^6 . Signals above 1,000 count charges were selected for HCD fragmentation using normalized collision energy of 36, a maximum injection time of 100 ms and an AGC target of 50,000. Fragments were analyzed in the orbitrap.

2.5.17 Data processing of protein VII spectra

Raw mass spectrometer files were analyzed using Proteome Discoverer (v.1.4, Thermo Scientific). MS/MS spectra were converted to .mgf files and searched against the UniProt adenovirus C serotype 5 database using Mascot (v.2.5, Matrix Science). Database searching was performed with the following parameters: precursor mass tolerance 10 p.p.m.; MS/MS mass tolerance 0.05 Da; enzyme chymotrypsin (Promega) or Arg-C (Roche), with two missed cleavages allowed; fixed modification was cysteine carbamidomethylation; variable modifications were methionine oxidation, serine/threonine/tyrosine phosphorylation, lysine acetylation and methylation, asparagine and glutamine deamidation. Specifically, phosphorylation, acetylation, and methylation were searched separately, not as co-existing modifications. Peptides were filtered for <1% FDR, Mascot ion score >20 and peptide rank 1.

2.5.18 Co-immunoprecipitation of protein-VII-HA

A549 cells were induced to express protein VII with doxycycline for 4 days as described earlier. Approximately 4×10^7 cells were harvested and pelleted for each immunoprecipitation reaction. Cell pellets were resuspended in 500 μ l of IC wash buffer with protease inhibitors (20 mM HEPES pH 7.9, 110 mM KOAc, 2 mM MgCl₂, 150 mM NaCl, 0.1% Tween-20, 0.1% Triton X-100) and incubated on ice for 10 min with intermittent vortexing to disrupt cells. Samples were then incubated on ice for 1 h with 5 μ l of benzonase (Millipore) added to each sample to digest DNA to ~150 bp, which was confirmed by DNA isolation and agarose gel analysis. Samples were then sonicated in a Diagenode Biorupter for 30 s on and 30 s off for five rounds at 4 °C and centrifuged at 14,000 g for 15 min at 4 °C. Supernatants were then incubated rotating for 1 h at

4 °C with 30 µl of HA-conjugated magnetic beads (Thermo Scientific) and washed three times for 5 min in IC buffer. Isolated proteins were eluted with 100 µl of 2 mg/ml HA peptide (Thermo Scientific) for 20 min rotating at 37 °C and separated on an SDS-PAGE gel. For protein separation by SDS-PAGE the NuPAGE 1DE System was used (NuPAGE Novex 4-12% Bis-Tris 1.0 mm gels, Invitrogen). Uninduced cells were used as a negative control. The immunoprecipitation was carried out in biological triplicate and pull-down of protein-VII-HA and HMGB1 was confirmed by western blotting standard techniques as described earlier.

2.5.19 Quantitative PCR

Genomic DNA was isolated using the PureLink Genomic DNA kit (Thermo Scientific). Quantitative PCR was performed using primers specific for viral DBP (5'-GCCATTGCGCCCAAGAAGAA and 5'-CTGTCCACGATTACCTCTGGTGAT), protein VII (5'-GCGGGTATTGTCACTGTGC and 5'-CACCCAATACACGTTGCCC), and cellular tubulin (5'-CCAGATGCCAAGTGACAAGAC and 5'-GAGTGAGTGACAAGAGAAGCC). Values for DBP and protein VII were normalized internally to tubulin and to the 4 h time point to control for any variation in virus input. RNA was isolated using the RNeasy Mini Kit (Qiagen) and reverse transcribed using the High Capacity RNA to cDNA Kit (Applied Biosystems). Quantitative PCR was performed using primers specific for HMGB1 (5'-TAACTAAACATGGGCAAAGGAG and 5'-TAGCAGACATGGTCTTCCAC) and β -actin (5'-GCACCACACCTTCTACAATGAG and 5'-GGTCTCAAACATGATCTGGGTC). Quantitative PCR was performed using the standard protocol for Sybr Green (Thermo Scientific) and analyzed using the ViiA 7 Real-Time PCR System (Thermo Scientific).

2.5.20 Precision-cut lung slice immunofluorescence

Precision-cut lung slices were obtained and prepared as previously described^{275,292}. De-identified human lung tissue from donors was obtained from the National Disease Research Interchange. Analysis of human samples was approved by the University of Pennsylvania Internal Review Board. Samples were infected with 10⁸ plaque-forming units (p.f.u.) of Ad5 per slice or 109 GC of rAd protein-VII-GFP for 24 h. Samples were fixed in 4% PFA at room temperature for

15 min and washed three times in PBS. Samples were permeabilized with 0.5% Triton X-100 and washed twice more in PBS. Samples were then incubated with 3% BSA and 0.03% Triton X-100 in PBS for 1 h to block. Primary antibodies (DBP or HMGB1) were incubated in the same buffer for 1 h and then samples were washed three times in PBS with 3% BSA, incubated with secondary antibodies and DAPI for 1 h, and washed three more times. Whole slices were mounted on slides with mounting solution and imaged by confocal microscopy.

2.5.21 FRAP

Full-length HMGB1 was cloned from pcDNA3.1 Flag-hHMGB1 (Addgene 31609) into pEGFP-N1 containing a L221K mutation to prevent dimerization of GFP molecules²⁹³. A549 cells were induced to express protein VII for 4 days with doxycycline in glass-bottom dishes. Cells were then transfected with the construct that constitutively expresses HMGB1 with a monomeric GFP C-terminal tag. FRAP was carried out using standard methods on a Zeiss LSM 710 confocal microscope. Diffusion coefficients were calculated using the 'simFRAP' algorithm (<http://imagej.nih.gov.proxy.library.upenn.edu/ij/plugins/sim-frap/index.html>), a simulation based approach to FRAP analysis²⁹⁴.

2.5.22 Statistical analyses

Statistical details are reported in each figure legend. Statistical analyses were performed on at least three different biological replicates, unless otherwise stated in the figure legend. The sample size was chosen to provide enough statistical power to apply parametric tests (one- or two-tailed homoscedastic t-test). The t-test was considered a valuable statistical test since binary comparisons were performed and the number of replicates was limited. Furthermore, we applied the homoscedastic t-test assuming that the variance between the two data sets would remain homogeneous due to the use of the same cell lines in culture with and without protein VII expression. No samples were excluded as outliers (this applies to all proteomics analyses described in this manuscript). Proteins with a P value smaller than 0.05 were considered to be significantly altered between the two tested conditions for two-tailed and one-tailed t-test. Data

distribution was assumed to be normal but this was not formally tested. The nano-LC-MS/MS analysis was performed in triplicate for each sample to determine technical variation.

CHAPTER 3: VIRAL-MEDIATED UBIQUITINATION IMPACTS INTERACTIONS OF HOST PROTEINS WITH VIRAL RNA AND PROMOTES VIRAL RNA PROCESSING

This chapter has been adapted from the following manuscript being considered for publication:

Herrmann C, Dybas JM, Liddle JC, Price AM, Charman M, Kim ET, Garcia BA, Weitzman MD. Viral-mediated ubiquitination impacts interactions of host proteins with viral RNA and promotes viral RNA processing. *Nature Microbiology*. In revision.

3.1 Abstract

Viruses promote infection by hijacking the host ubiquitin machinery to counteract or redirect cellular processes. Adenovirus encodes two early proteins, E1B55K and E4orf6, that together co-opt a cellular ubiquitin ligase complex to overcome host defenses and promote virus production. Adenovirus mutants lacking E1B55K or E4orf6 display defects in viral RNA processing and protein production, but previously identified substrates of the ligase do not explain these phenotypes. Here we used a quantitative proteomics approach to identify substrates of E1B55K/E4orf6 that are ubiquitinated to facilitate RNA processing. While cellular proteins known as substrates of E1B55K/E4orf6 are degraded by the proteasome, we uncovered RNA-binding proteins (RBPs) as predicted substrates which are not decreased in overall abundance. We focused on two predominant RBPs, RALY and hnRNP-C, which we confirm are ubiquitinated without degradation. Knockdown of RALY and hnRNP-C rescued levels of viral RNA splicing, protein, and progeny production during infection with E1B55K-deleted virus. Furthermore, deletion of E1B55K resulted in increased interaction of hnRNP-C with viral RNA and attenuation of viral RNA processing. These data suggest viral-mediated ubiquitination of RALY and hnRNP-C relieves a restriction on viral RNA processing, revealing an unexpected role for non-degradative ubiquitination in the manipulation of cellular processes during virus infection.

3.2 Introduction

Viruses have evolved extensive mechanisms to alter cellular pathways to their advantage and facilitate inactivation of host defenses. One way this can be achieved is through viral factors that redirect host post-translational protein modification such as ubiquitin, in order to regulate protein function and turnover. Viruses interface with the host ubiquitin system by encoding their own ubiquitin ligases, redirecting cellular ubiquitin ligases, or altering the removal of ubiquitin by deubiquitinating enzymes^{1,9,10}. Ubiquitin can be employed as a signal for diverse outcomes, including proteasome-mediated degradation, protein localization, and regulating interactions with other proteins or nucleic acids^{159,164,295,296}. This diversity of function makes hijacking the host ubiquitin machinery an attractive approach for viruses to manipulate multiple cellular pathways.

The nuclear-replicating Adenovirus (Ad) encodes two early proteins (E1B55K and E4orf6) which integrate into an existing host ubiquitin ligase complex containing Elongin B and C, Cullin5, and RBX1^{212,213}. The cellular ligase is recruited through E4orf6, and the E1B55K protein is involved in substrate recognition to redirect the ligase activity²¹³. The importance of hijacking the host ubiquitin machinery for productive virus infection has been demonstrated using Ad deletion mutants or expression of dominant negative Cullin5, which all severely limit virus production^{60,216,243-246,251,252,297}. A number of cellular proteins have been identified as targets for proteasomal degradation after expression of the Ad serotype 5 (Ad5) E1B55K/E4orf6 complex, including MRE11, RAD50, NBS1, DNA Ligase IV, BLM, Integrin α 3, and the tumor suppressor p53^{67,212,221-224}. Degradation of these proteins represses DNA damage signaling and apoptosis during infection^{219,234,298}. However, the E1B55K/E4orf6 complex also stimulates export of viral late mRNAs and synthesis of viral late proteins^{60,243,244,246,251,252}. Viral mutants defective for either E1B55K or E4orf6 show similar phenotypes but none of the known substrates have been shown to account for the defects in viral RNA processing and late protein synthesis^{60,243-246,251,252}.

In this study, we used an unbiased global proteomics approach to identify new cellular substrates of the ubiquitin ligase activity directed by the Ad5 E1B55K/E4orf6 complex. We used di-glycine remnant profiling (K- ϵ -GG)^{210,211} to quantify changes to the cellular ubiquitinome upon

expression of E1B55K and E4orf6, and predicted the impact of ubiquitination on protein abundance by employing whole cell proteomics (WCP). This combined approach enabled us to identify many potential E1B55K/E4orf6 substrates, and classify these proteins as predicted degraded or non-degraded substrates. Our analysis suggests that the E1B55K/E4orf6 complex can redirect ubiquitination onto substrates in multiple ways, and reveals that the majority of cellular substrates are ubiquitinated without significant changes in their protein abundance. Among the cellular substrates predicted to be ubiquitinated without degradation, we found an enrichment for cellular RNA-binding proteins (RBPs). We further validated the importance of the highly ubiquitinated RBPs RALY and hnRNP-C as two host proteins modified by the virus to overcome a restriction for late viral transcript production. We identify the first substrates to provide a mechanistic link between the E1B55K/E4orf6 ubiquitin ligase function and its known role in Ad5 viral RNA processing. Furthermore, these studies highlight a viral approach to exploit ubiquitination without degradation as a strategy to manipulate host pathways.

3.3 Results

3.3.1 The Ad E1B55K/E4orf6 ubiquitin ligase is required for viral late RNA splicing

Given that cellular ubiquitination can have degradative or non-degradative outcomes, we hypothesized that ubiquitination mediated by E1B55K/E4orf6 redirecting the Cullin5 ligase can either target cellular proteins for proteasomal degradation, as seen for all currently known substrates such as MRE11, RAD50, and BLM^{67,221}, or could impact function without affecting protein abundance (**Figure 3.1a**). We assessed the role of the Ad5 ubiquitin ligase on RNA processing and late protein accumulation by inactivating the ligase through deletion of the E1B55K gene or chemical inhibition of the Cullin5 ubiquitin ligase activity²⁹⁹. Infection with an E1B55K mutant virus resulted in decreased levels of viral late proteins (hexon, penton, fiber and protein VII) but had minimal impact on viral early protein production (DBP) when compared to wild-type (WT) Ad5 infection (**Figure 3.1b**). The Cullin5 hijacked by E1B55K/E4orf6 requires post-translational modification by the ubiquitin-like protein NEDD8 to form a functional ubiquitin

ligase complex^{300,301}. We used a small molecule inhibitor of the neddylation activating enzyme (NEDDi; MLN4924²⁹⁹) to block Cullin-mediated ubiquitination during infection. Inhibition of Cullin neddylation was observed by a decrease in abundance of the slower-migrating modified Cullin5 (**Figure 3.1b**). Inhibition of the viral ubiquitin ligase was confirmed by a block of MRE11 and BLM degradation, two previously identified substrates of viral-mediated degradation. NEDDi treatment during WT Ad5 infection substantially decreased levels of viral late proteins (hexon, penton, fiber and protein VII) but only marginally decreased production of the viral early protein DBP (**Figure 3.1b**). Furthermore, NEDDi treatment did not further alter the late protein defect observed with E1B55K deletion (**Figure 3.1b**). We then assessed several steps of viral RNA processing during viral ligase inhibition or E1B55K deletion. We observed decreased accumulation of viral late mRNA for transcripts containing the major late promoter (MLP) and fiber gene during NEDDi treatment of WT Ad5 infection, similar to decreases detected with E1B55K deletion (**Figure 3.1c**). We used quantitative reverse transcription PCR (RT-qPCR) to determine the ratio of spliced to unspliced transcript as a surrogate for splicing efficiency (**Figure 3.S1a**). This analysis revealed that both NEDDi treatment and E1B55K deletion decreased splicing efficiency of viral late transcripts (MLP and fiber) without negatively impacting an early transcript (E1A) (**Figure 3.1d; Figure 3.S1b, c**). We also examined RNA export by fluorescence *in situ* hybridization (FISH) for fiber transcripts. This experiment demonstrated that less fiber RNA reaches the cytoplasm upon E1B55K deletion, which was recapitulated by NEDDi inhibition (**Figure 3.1e; Figure 3.S1d**). Failure to splice transcripts correctly causes retention in the nucleus and subsequent degradation^{302,303}. Incorrect splicing could explain the observed RNA export defect and decrease in RNA levels observed for late viral transcripts. These data demonstrated by chemical inhibition of neddylation that Cullin ligase inactivation recapitulates the effects of E1B55K deletion, highlighting that E1B55K/E4orf6-mediated ubiquitination of substrates is important for RNA splicing, RNA export, and protein production from viral late transcripts during Ad5 infection. None of the previously identified cellular substrates of E1B55K/E4orf6-mediated ubiquitination explain these phenotypes.

3.3.2 Proteomics reveals enrichment of RNA-binding proteins among cellular substrates of E1B55K/E4orf6

To identify cellular substrates of the Ad5 ubiquitin ligase we conducted global profiling of the ubiquitinome and associated whole cell proteome (WCP) over a time course of transduction of HeLa cells with viral vectors encoding E1B55K and E4orf6 of Ad5^{224,304} (**Figure 3.2a**; **Figure 3.S2**). Using non-replicating viral vectors allowed us to identify substrates specific to the activity of the viral E1B55K/E4orf6 complex outside the context of Ad5 infection. We assayed the degradation kinetics of known cellular substrates of the Ad5 ligase by immunoblotting to determine when proteins were most likely to be modified but still detectable (**Figure 3.S2a**). We subsequently sampled for ubiquitin modification at 6, 8, and 10 hours post transduction (hpt) and at 10 hpt for protein abundance. We employed di-glycine remnant profiling combined with mass spectrometry (K- ϵ -GG)^{210,211} to quantify ubiquitination of host proteins upon expression of E1B55K/E4orf6 (**Figure 3.2a**). We performed three replicates for each sample and identified a similar number of peptides in untransduced cells (2,328 peptides) and those transduced by E1B55K/E4orf6 (2,254 to 2,419 peptides) (**Figure 3.S2b**). The identified di-glycine remnant peptides corresponded to ~1,100 proteins (**Figure 3.S2b**). Changes in peptide modification were then normalized to changes in protein abundance in order to assess differential ubiquitination over the time course. Expression of E1B55K/E4orf6 induced a significant increase in ubiquitination ($p < 0.05$ and \log_2 fold-change > 1) for 55 peptides (**Figure 3.2b**). Additionally, 51 peptides were ubiquitinated upon expression of E1B55K/E4orf6 but were not identified as ubiquitinated in untransduced cells, and therefore do not have a calculated fold-change or associated p-value. Peptides that exhibited increased or unique ubiquitination upon E1B55K/E4orf6 expression included known protein substrates MRE11 (4 peptides) and RAD50 (5 peptides). The whole cell proteome quantified a similar overall number of proteins in untransduced cells (6,126 proteins) and cells transduced by E1B55K/E4orf6 (6,147 proteins) (**Figure 3.S2c**). The whole cell proteome data showed that E1B55K/E4orf6 expression induced significant changes in abundance for several proteins, with 67 proteins decreased at least 2-fold.

Consistent with previous studies, we observed significant decreases for the known substrates MRE11, NBS1, RAD50, and LIG4 upon E1B55K/E4orf6 expression (**Figure 3.2b**).

To compare K- ϵ -GG and WCP datasets, the peptide-level K- ϵ -GG data were transformed into protein-based K- ϵ -GG abundance changes by calculating the abundance-weighted average of the K- ϵ -GG peptide log₂ fold-changes for all modified peptides detected for that protein. Resulting protein-based K- ϵ -GG log₂ fold-changes were plotted against their associated WCP fold-changes (**Figure 3.2c**). We implemented a threshold for protein-based K- ϵ -GG increase of > 2 fold and identified 119 host proteins as putative substrates of the Ad5 ubiquitin ligase. Proteins that were ubiquitinated and also decreased in abundance by more than 1 standard deviation (s.d.) from the mean proteome change were predicted to be degraded substrates of E1B55K/E4orf6. Conversely, proteins that exhibited abundance changes within 1 s.d. of the mean WCP abundance change were predicted to be ubiquitinated by E1B55K/E4orf6 but unchanged in abundance (**Figure 3.2c**, blue shading). In total, 25 cellular proteins were classified as predicted to be degraded as a result of ubiquitination by E1B55K/E4orf6, including known targets MRE11 and RAD50 (**Figure 3.2c**, red shading). In contrast, 90 cellular proteins were predicted to be ubiquitinated by E1B55K/E4orf6 without concomitant decreases in protein abundance, suggesting that these cellular substrates can be classified as non-degraded (**Figure 3.S3a**). These data provide the first evidence that the Ad5 ubiquitin ligase facilitates non-degradative ubiquitination and suggest that the majority of potential E1B55K/E4orf6 substrates fall into this category.

We further analyzed the predicted E1B55K/E4orf6 cellular substrates for gene functions. Gene ontology analysis revealed significant enrichment of “poly(A) RNA binding” and “RNA-binding” GO annotations (**Figure 3.2d**). Since E1B55K deletion has been shown to induce RNA processing defects, we focused on the 26 proteins included within the RNA-binding GO terms (**Figure 3.S3b**). There were 7 RBPs predicted to be ubiquitinated only in the presence of E1B55K/E4orf6. Among these, RALY stands out as the RBP with the greatest increase in ubiquitination over the time-course of E1B55K/E4orf6 expression, and its homolog and interaction partner hnRNP-C has the largest number of sites that increase in ubiquitination among RBPs

(**Figure 3.2e**; **Figure 3.S3c**). We used the Reactome³⁰⁵ protein-protein interaction database to analyze interactions among all predicted E1B55K/E4orf6 substrates, and found RALY and hnRNP-C together in an interaction module with other RBPs (**Figure 3.S4**). Both RALY and hnRNP-C are expressed at high levels in all tissues³⁰⁶ and are implicated in multiple steps of RNA processing, including RNA splicing and export³⁰⁷⁻³¹². Additionally, it has been reported that hnRNP-C binds to Ad transcripts encoding late proteins³¹³. We therefore chose to further validate RALY and hnRNP-C as cellular substrates of the ubiquitin ligase activity redirected by E1B55K/E4orf6 and to characterize their impact on Ad5 biology.

3.3.3 RALY and hnRNP-C are ubiquitinated but not degraded upon E1B55K/E4orf6 expression

RALY and hnRNP-C are ~43% homologous, with the highest homology (63%) in the coiled-coil (CC) domain, which contains all the lysine residues that show increased ubiquitination upon E1B55K/E4orf6 expression (**Figure 3.3a**; **Figure 3.S5**). The lysine residue of hnRNP-C that shows the highest increase in ubiquitination (K204 as shown in **Figure 3.2e**) is homologous to the only detected ubiquitination site in RALY (K198). Since E1B55K is the substrate recognition component of the Ad ligase, we examined interaction of E1B55K with the two host RBPs during Ad5 virus infection (**Figure 3.3b**). We performed immunoprecipitation (IP) of E1B55K, RALY and hnRNP-C for mock, Ad5 WT and Δ E1B infection conditions followed by immunoblotting for viral and host proteins. Negative controls included antibodies to a viral protein (DBP) and cellular protein (Tubulin) which were not isolated with any condition. IP of E1B55K isolated RALY and hnRNP-C from cells infected with WT virus but not the Δ E1B mutant. In the reciprocal experiment, E1B55K was detected upon IP of RALY and hnRNP-C during WT virus infection, confirming interaction between the Ad ligase and the two host RBPs (**Figure 3.3b**). The cellular hnRNP-C and RALY proteins interact in reciprocal IPs, as reported previously³¹⁴, and this association was not impacted by virus infection. To confirm ubiquitination of RALY and hnRNP-C by the Ad ligase, we expressed Flag-tagged proteins together with HA-tagged ubiquitin and E4orf6 by transfection of HEK293 cells (this cell line contains a genomic integration of Ad5 E1B55K⁷⁸). After IP for the HA epitope on ubiquitin, immunoblotting for Flag revealed an increase

in high molecular weight ubiquitin-complexes of RALY and hnRNP-C in the presence of E4orf6 (**Figure 3.3c**). We saw similar results with hnRNP-C2, an alternative isoform of hnRNP-C (**Figure 3.S6a**). To demonstrate that Cullin complexes are involved in ubiquitination of RALY and hnRNP-C by the Ad5 ligase, we performed experiments in the presence of NEDDi. The elevated ubiquitination of RALY and hnRNP-C detected by expression of E4orf6 and HA-ubiquitin was decreased upon NEDDi treatment (**Figure 3.3d**). We also verified that hnRNP-C was ubiquitinated during Ad5 WT infection but not with the Δ E1B mutant (**Figure 3.3e**). The RALY antibody quality precluded our ability to detect the endogenous protein in this assay. Our whole cell proteome analysis showed that RALY and hnRNP-C are not decreased in abundance during infection (**Figure 3.S3b**). Lack of degradation was confirmed by immunoblotting of RALY and hnRNP-C protein levels over a time course of Ad5 WT infection or transduction with E1B55K/E4orf6 vectors (**Figure 3.3f**; **Figure 3.S6b**). We observed a rapid decrease for the known degraded targets MRE11 and RAD50, but there was no substantial change in RALY and hnRNP-C levels (**Figure 3.3f**). Similar observations were made upon transduction of A549 and U2OS cells with E1B55K/E4orf6 vectors, as well as transfection of HEK293 cells with an E4orf6 expression vector (**Figure 3.S6c**). RALY and hnRNP-C could be degraded in the context of continually increasing transcript abundance and protein synthesis, which could account for the observed consistent total abundance during infection (**Figure 3.3f**). To rule out this possibility, we examined the effect of infection on RALY and hnRNP-C turnover by quantifying protein abundances over a time course of cycloheximide treatment (**Figure 3.3g**). While MRE11 and RAD50 turnover increased upon infection, RALY and hnRNP-C protein levels remained relatively stable during infection in the presence of cycloheximide. We also found no significant change in mRNA levels for RALY and hnRNP-C as measured by RT-qPCR during a time course of Ad WT infection (**Figure 3.S6d**). We therefore propose that E1B55K/E4orf6 can induce ubiquitination that has both degradative and non-degradative outcomes. To support this hypothesis further, we investigated differences in ubiquitination of MRE11, RAD50, RALY, and hnRNP-C induced by E1B55K/E4orf6. Proteasome inhibition by drugs such as MG132 leads to accumulation of

ubiquitinated proteins that would otherwise be degraded. Ubiquitination assays were performed by transfection of HEK293 cells with and without MG132-mediated inhibition of the proteasome (**Figure 3.3h**). Expression of E4orf6 increased ubiquitination of MRE11 and the ubiquitination was further increased during proteasome inhibition, consistent with MRE11 being a known degraded substrate of the viral ubiquitin ligase. In contrast, expression of E4orf6 increased ubiquitination of RALY and hnRNP-C but there was no further increase upon treatment with MG132. The fact that MG132 treatment did not alter ubiquitination of RALY and hnRNP-C suggests that ubiquitination of these substrates does not result in degradation by the proteasome, supporting a non-degradative function of viral-mediated ubiquitination. Since the effect of proteasomal inhibition varies between E1B55K/E4orf6 substrates, we examined the ubiquitin chains attached to RALY and hnRNP-C as compared to MRE11 and RAD50. The ubiquitin linkage most commonly associated with proteasomal degradation is K48. Therefore, we hypothesize that the E1B55K/E4orf6 complex generates K48 polyubiquitin chains on MRE11 and RAD50. Furthermore, since our data suggest that hnRNP-C and RALY are not degraded, we hypothesize that these substrates are marked with non-K48 ubiquitin chains. To determine whether K48-linked ubiquitin is attached to the MRE11, RAD50, RALY, or hnRNP-C we performed native IPs of HA-ubiquitin, expressed in HEK293 cells together with E4orf6, and then compared the degree of ubiquitination after treatment with deubiquitinating enzymes (DUBs) that cleave either all ubiquitin linkages (DUB^{Pan}) or only K48-linked ubiquitin chains (DUB^{K48})¹⁹⁰ (**Figure 3.3i**). The previously identified degradation substrates, MRE11 and RAD50, showed a clear decrease of high molecular weight ubiquitin chains upon treatment with both DUBs. This indicates that K48-linked ubiquitin is attached to these E1B55K/E4orf6 substrates to induce proteasomal degradation. In contrast, ubiquitination of RALY and hnRNP-C only decreased with the DUB^{Pan} but not the more specific DUB^{K48}. This suggests that RALY and hnRNP-C are substrates for non-K48 linked ubiquitination that is distinct from the K48-linked ubiquitin chains on degraded substrates MRE11 and RAD50. Together, these data validate RALY and hnRNP-C as the first non-degraded cellular substrates identified for the E1B55K/E4orf6 Ad5 ligase.

3.3.4 RALY and hnRNP-C are detrimental for viral late RNA processing in the absence of a functional Ad ubiquitin ligase

To determine whether RALY and hnRNP-C impact Ad infection, we used siRNA to knockdown these host proteins in HeLa and primary-like HBEC3-KT cells, and then infected with WT Ad5 and Δ E1B viruses (**Figure 3.4**). Although RALY and hnRNP-C are not degraded, this approach allowed us to determine whether these RBPs are beneficial or detrimental to virus infection. Knockdown of RALY and hnRNP-C did not affect viral protein levels during WT Ad5 infection, suggesting that in the context of infection with a fully competent virus their presence does not have a significant impact. Infection with Δ E1B mutant virus generated reduced viral late protein levels as compared to WT Ad5 (**Figure 3.4a**). Depletion of RALY and hnRNP-C rescued this viral late protein defect almost to the level observed in WT Ad5 (**Figure 3.4a**; **Figure 3.S7a**). We examined whether knockdown of RALY and hnRNP-C also affects progeny production of the mutant virus (**Figure 3.4b**). There was no difference between WT Ad5 and Δ E1B at 8 hours post infection (hpi), before production of new infectious virions, confirming comparable virus input and entry. By 24 hpi the E1B55K mutant virus produced > 100-fold fewer viral particles than WT Ad5. Knockdown of RALY and hnRNP-C had no effect on WT Ad5, but significantly increased progeny production for the mutant virus (**Figure 3.4b**). Similar rescue of the E1B55K mutant virus was observed with RALY and hnRNP-C knockdown prior to infection in HBEC3-KT cells (**Figure 3.4b**). These data suggest that RALY and hnRNP-C are detrimental to Ad infection and that E1B55K/E4orf6-mediated ubiquitination relieves their restriction on virus production. Since RALY and hnRNP-C are involved in RNA splicing and export, we hypothesized that their depletion selectively increases late RNA processing without affecting DNA replication and early viral RNAs. We therefore examined viral DNA replication by quantitating genome accumulation using qPCR (**Figure 3.4c**). We observed a modest decrease (2-fold) in DNA replication for the Δ E1B virus as compared to WT Ad5, in agreement with prior reports³¹⁵. Viral DNA accumulation for both WT Ad5 and Δ E1B was not significantly affected by depletion of RALY and hnRNP-C (**Figure 3.4c**), confirming that their effects are mediated at a step after viral genome replication. We then

quantified RNA levels of both early (E1A) and late (MLP and fiber) viral transcripts (**Figure 3.4d**). We observed reduced levels of late but not early transcripts upon infection with the Δ E1B virus, which shows qualitative correlation with the decrease in late proteins shown in **Figure 3.1b**. Depletion of RALY and hnRNP-C rescued mRNA levels for both MLP and fiber at both 18 hpi and 24 hpi during infection with the Δ E1B virus, to levels observed in WT Ad5 (**Figure 3.4d**) without impacting the E1A transcript (**Figure 3.S7b**). We observed a similar pattern when we examined splicing efficiency of viral transcripts. The Δ E1B mutant virus displayed a reduction in splicing efficiency of MLP and fiber that was rescued to WT Ad5 levels upon knockdown of RALY and hnRNP-C (**Figure 3.4e**; **Figure 3.S7c**). We also used FISH to examine the effect of RALY and hnRNP-C depletion on export of fiber mRNA into the cytoplasm. siRNA treatment increased the amount of cytoplasmic fiber RNA visible in Δ E1B infection, while not impacting WT Ad5 (**Figure 3.4f**). We also verified that knockdown of either RALY or hnRNP-C alone rescued late RNA and protein defects of the Δ E1B virus. Depletion of either RBP by itself increased viral late protein, RNA levels, and splicing efficiency of the mutant virus, with hnRNP-C knockdown having a more dramatic effect than RALY knockdown (**Figure 3.S7d-f**). To connect the impact of RALY and hnRNP-C depletion on late stages of Ad infection with Cullin-dependent ubiquitination by E1B55K/E4orf6, we combined siRNA-mediated knockdown with NEDDi treatment during WT Ad5 infection. The NEDDi treatment decreased viral late RNA levels, splicing efficiency, and protein production (**Figure 3.4g-i**). Knockdown of RALY and hnRNP-C completely rescued this defect caused by inhibition of Cullin function without impacting viral early proteins or RNA (**Figure 3.4g-i**; **Figure 3.S7g, h**). These data suggest that RALY and hnRNP-C are detrimental to the late stages of Ad5 infection in the absence of a functional viral ubiquitin ligase.

3.3.5 Ubiquitination of hnRNP-C specifically reduces interaction with viral late RNA

Our data suggest that ubiquitination of RALY and hnRNP-C relieves a restriction on viral late RNA processing without the need for proteasomal degradation. Non-degradative ubiquitination has been reported to alter protein localization, for example by obscuring nuclear localization sequences and preventing nuclear import¹⁸⁹. We examined localization of RALY and hnRNP-C by

immunofluorescence (IF) in untreated HeLa cells and during infection with either WT Ad5 or Δ E1B virus (**Figure 3.S8a**). Both RALY and hnRNP-C showed a diffuse nuclear pattern in uninfected HeLa cells, in accordance with the reported localization of both proteins³⁰⁶. Upon infection, both proteins were excluded from viral replication centers marked by DBP or USP7 in a pattern that matches viral RNA and other RBPs^{316,317}. However, there was no obvious difference in localization between WT Ad5 and Δ E1B infection, suggesting that viral-induced ubiquitination does not specifically change their cellular localization. Since both RALY and hnRNP-C are ubiquitinated within the coiled-coil domain that is involved in multimerization and protein-RNA interaction (**Figure 3.3a**), we examined whether overall protein complex formation and RNA association are affected during Ad5 infection. To examine complex formation, we treated HeLa cells with disuccinimidyl suberate (DSS) at various concentrations during mock, WT Ad5 or Δ E1B infection (**Figure 3.S8b**). DSS is a cell-permeable crosslinker that forms stable amide bonds between lysine residues in close proximity (less than 11.4 Å), crosslinking protein complexes. DSS treatment caused a mobility shift of hnRNP-C and RALY, consistent with multimerization and previous reports of dimers and tetramers³¹⁸. During WT Ad5 or Δ E1B infections these patterns did not change noticeably, suggesting that viral-induced ubiquitination does not significantly affect overall protein complex formation of hnRNP-C or RALY. Finally, to examine the effect of ubiquitination on interaction of hnRNP-C with viral RNA we performed crosslinking-immunoprecipitation (CLIP) followed by RT-qPCR for several viral and cellular transcripts (**Figure 3.5a, Figure 3.S8c**). Commercially available antibodies for RALY were not suitable for this technique (data not shown). The hnRNP-C transcript itself served as a positive control, while the GAPDH RNA was a negative control (according to ENCODE data of hnRNP-C eCLIP-Seq.). This approach was validated by detection of the hnRNP-C transcript upon CLIP-qPCR with hnRNP-C antibody in both WT Ad5 and Δ E1B infections, with very low signal for GAPDH (**Figure 3.5b**). All viral late transcripts were detected above background under WT Ad5 conditions, however, there was a 2 to 4-fold increase in the amount of late RNA detected during Δ E1B infection. There was however no significant difference in the level of early RNAs detected between WT Ad5 and

mutant virus. This indicates that viral-induced ubiquitination of hnRNP-C specifically decreases the interaction with viral late transcripts. To confirm that this difference between WT and Δ E1B virus was caused by ubiquitination, we repeated the hnRNP-C CLIP-qPCR with inhibition of Cullin-dependent ubiquitination during WT Ad5 infection (**Figure 3.5c**, **Figure 3.S8d**). Following the trend with Δ E1B infection, the interaction of hnRNP-C with viral late transcripts increased at least 2-fold upon treatment with NEDDi, while there were only minor differences for viral early and cellular transcripts. This experiment confirms that hnRNP-C interacts specifically with viral late RNAs in the absence of the functional viral ubiquitin ligase.

3.4 Discussion

Viruses commonly adapt cellular regulatory mechanisms towards efficient viral production. The E1B55K/E4orf6 complex is known to interact with the cellular Cullin5 ubiquitin ligase to redirect ubiquitination and to stimulate viral late mRNA nuclear export and late protein synthesis. A number of prior studies identified binding partners of the complex and a limited number of substrates^{67,212,213,221-224,238,253-255}, however, these studies did not enrich for proteins specifically ubiquitinated by the E1B55K/E4orf6 or explicitly link potential cellular substrates to effects on viral RNA processing. Here we employed a systematic proteomics approach to identify cellular substrates of the E1B55K/E4orf6 viral ubiquitin ligase by combining quantification and analysis of the ubiquitinome and the associated whole cell proteome upon expression of E1B55K/E4orf6. We identified 119 potential substrates, with specific enrichment of RBPs that may be involved in viral RNA processing. In addition to RNA processing, functional analysis of the predicted substrates highlights other host pathways that may be manipulated by Ad5-mediated ubiquitination: ubiquitin machinery and de-ubiquitinating enzymes, antigen presentation, protein folding, cellular transport, and cell signaling (**Figure 3.S4a**). We focused on two of the most highly ubiquitinated RBPs, RALY and hnRNP-C, which we demonstrated to be the first non-degraded substrates of the Ad5 ligase. We demonstrated differential interaction of hnRNP-C with viral late transcripts in the presence of E1B55K/E4orf6 ligase activity, supporting a model in which ubiquitinated RALY and

hnRNP-C are excluded from viral late ribonucleoprotein (RNP) complexes, to promote efficient processing of late RNA (**Figure 3.6**). Since hnRNP-C and RALY have reported roles in alternative splicing^{307,309,310}, we propose that their ubiquitination by the Ad5 ligase results in exclusion from viral RNP complexes to promote splicing of late viral RNAs. Substrates of the E1B55K/E4orf6 complex can vary across human Ad serotypes, although some target proteins fall within the same cellular pathway^{239,240}. It will be interesting to determine whether RBPs are similarly modified between serotypes or whether effects on RNA processing are achieved through different substrates. There is a precedent for post-translational modification regulating hnRNP-C affinity for RNA, with conjugation of the ubiquitin-like protein SUMO decreasing the affinity of hnRNP-C for RNA³¹⁹. Ubiquitin and related proteins have emerging roles in regulating splicing by altering the properties and dynamics of spliceosomal complexes through altered protein-protein interactions³²⁰. It is likely that RBPs such as RALY and hnRNP-C are also functionally regulated through ubiquitination by cellular ubiquitin ligase. Correlating changes to host splicing induced as a result of the impact of ubiquitination during Ad infection may provide insights into host pathways that are altered by ubiquitination of these RBPs.

Manipulation of the host ubiquitin machinery during virus infection has traditionally been studied in the context of proteasomal degradation and there are very few known examples of viruses directing ubiquitin towards cellular substrates that are not subsequently degraded^{1,9,10}. This has been true for the Cullin5 ligase redirected by Ad E1B55K/E4orf6 which was previously shown to induce degradation of proteins involved in the cellular DNA damage response and apoptosis^{67,212,221,222,224}. Our observation that the majority of potential cellular substrates of the E1B55K/E4orf6 viral ligase appear to be ubiquitinated without significant decrease in abundance suggests that a major aspect of the activity of this ligase is non-degradative ubiquitination. This finding highlights the need to combine ubiquitinome analysis together with whole cell proteome quantification when identifying outcomes of ubiquitination. Future studies of other viral ligases should include this type of analysis of non-degradative ubiquitination in order to ensure that all aspects of viral manipulation by ubiquitin are identified. We propose that ubiquitination without the

need for proteasome-mediated degradation provides increased flexibility and more rapid approaches to counter host responses and redirect cellular processes. Viral ubiquitin ligases may present particularly good model systems to study how ubiquitin ligases in general can facilitate both degradative and non-degradative ubiquitination of distinct substrates. Given the increasing appreciation that cellular ubiquitin ligases (such as the Cullin ligase hijacked by Ad) can facilitate the formation of multiple different types of ubiquitin chains³²¹⁻³²³, viral infections provide systems to decipher the rules that govern outcomes of ubiquitination.

In addition to its contributions to fundamental knowledge of cellular and molecular biology, Ad has also been developed as a vector for gene delivery and oncolytic cancer treatment. Mutant viruses that lack E1B55K have been shown to replicate conditionally in cancer cells, with selectivity that was initially suggested to be based on p53 inactivation but is more likely due to preferential viral late mRNA export^{241,242,324}. Since many cancers have altered RNA processing, the Ad Δ E1B used for oncolytic therapies may be complemented by defects in E1B55K/E4orf6 substrates. Our work suggests that alterations in these substrates, such as the RBPs RALY and hnRNP-C, may make tumor cells more susceptible to Δ E1B-based oncolytic viruses.

3.5 Figures

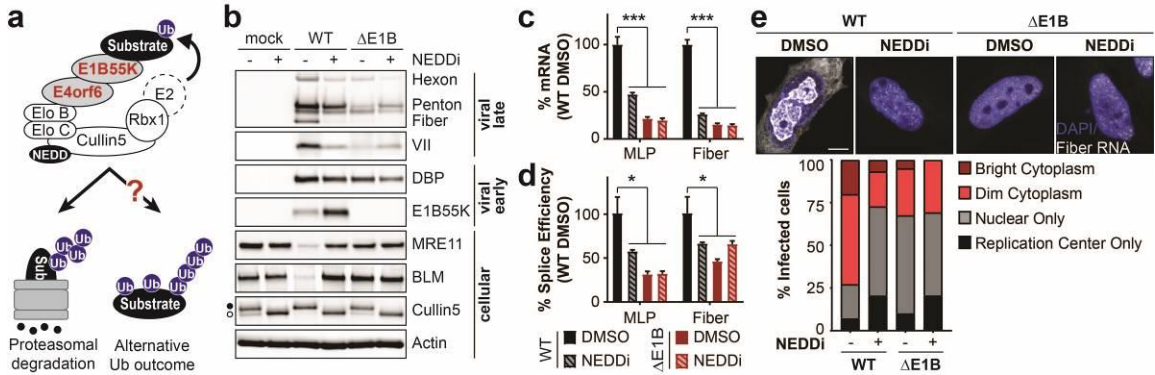


Figure 3.1 | E1B55K deletion or inhibition of Cullin-mediated ubiquitination decreases adenovirus late RNA splicing and RNA processing overall. **a**, The E1B55K/E4orf6 complex redirects substrate recognition of the host Cullin5 ubiquitin ligase to target proteins for proteasomal degradation or lead to alternative outcomes of ubiquitination. **b-e**, HeLa cells infected with wild-type (WT) or E1B55K-deleted (Δ E1B) Ad5 at multiplicity of infection (MOI) of 10. Cells were treated with either DMSO or NEDDi (neddylation inhibitor MLN2449) at 8 hours post-infection (hpi) and assayed at 24 hpi. **b**, Immunoblot analysis of viral and cellular protein abundance. The neddylated (\bullet) and unmodified (\circ) forms of Cullin5 are indicated. Results are representative of three biological experiments. **c**, Bar graph representing spliced RNA levels of viral late transcripts for the major late promoter (MLP) and fiber by quantitative reverse transcription PCR (RT-qPCR). Shown is mean+s.d., n equals three biological experiments. **d**, Bar graph representing splicing efficiency as the ratio of spliced to unspliced transcripts of MLP and fiber relative to the WT DMSO control by RT-qPCR. Shown is mean+s.d., n equals three biological experiments. **e**, RNA FISH visualizing the localization of fiber transcripts (white) in relation to nuclear DNA stained with DAPI (blue) and quantification of observed pattern for > 50 HeLa cells. Scale bar 10 μ m. Statistical significance was calculated using an unpaired, two-tailed Student's t-test, * $p < 0.05$, *** $p < 0.005$. Panel e by AM Price.

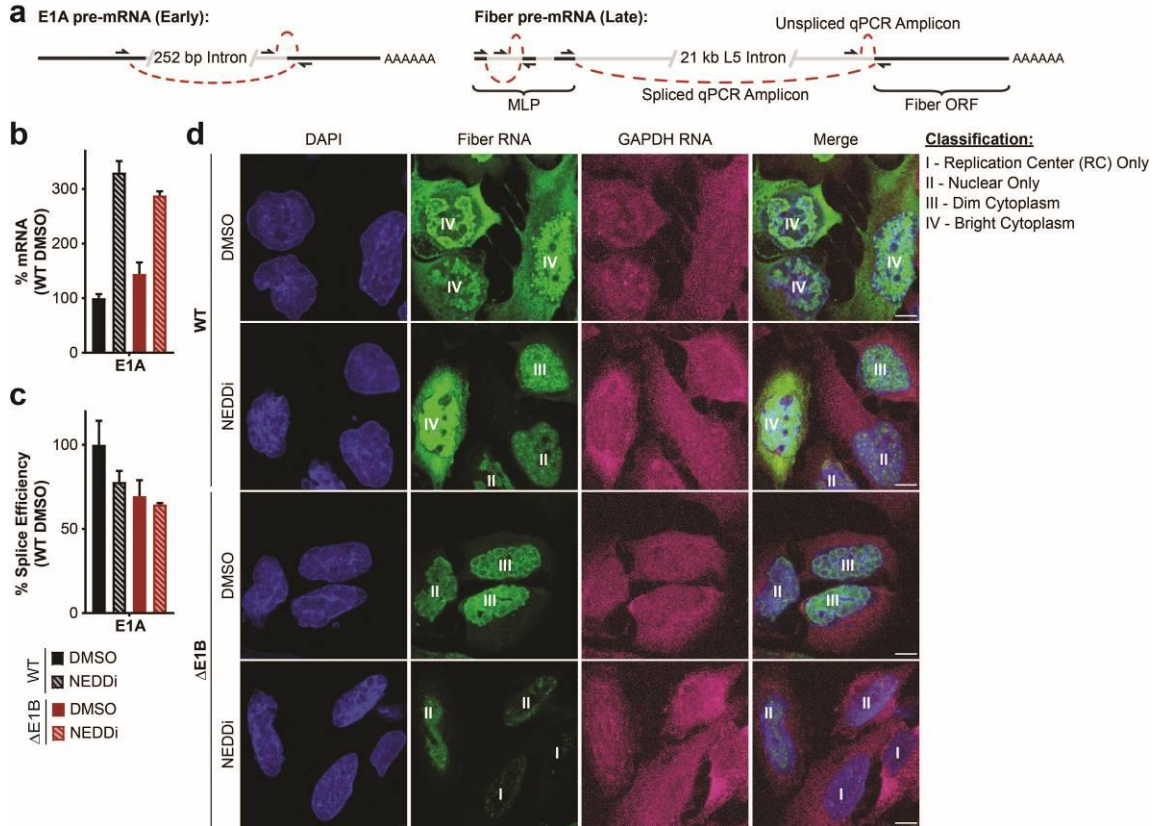


Figure 3.S1 | E1B55K deletion or inhibition of Cullin-mediated ubiquitination does not decrease viral early RNA levels or splicing. **a**, Schematic illustrating primer design to differentiate spliced and unspliced viral transcripts. **b-d**, HeLa cells infected with wild-type (WT) or E1B55K-deleted (Δ E1B) Ad5 (MOI=10) in the presence of DMSO or NEDDi (neddylation inhibitor MLN2449) added at 8 hours post-infection (hpi). Cells were harvested for RNA analysis at 24 hpi. **b**, Bar graph representing spliced RNA levels of viral early transcripts E1A by RT-qPCR, shown is mean+s.d., n equals three biological experiments. **c**, Bar graph representing splicing efficiency as the ratio of spliced to unspliced transcripts of E1A relative to the WT DMSO control by RT-qPCR, shown is mean+s.d., n equals three biological experiments. **d**, RNA FISH visualizing the localization of fiber (green) and GAPDH (magenta) transcripts in relation to nuclear DNA stained with DAPI (blue). Nuclei are labeled with the classification of each cell according to the pattern of fiber used for Figure 1d. Scale bar 10 μ m. *Panels a and d by AM Price.*

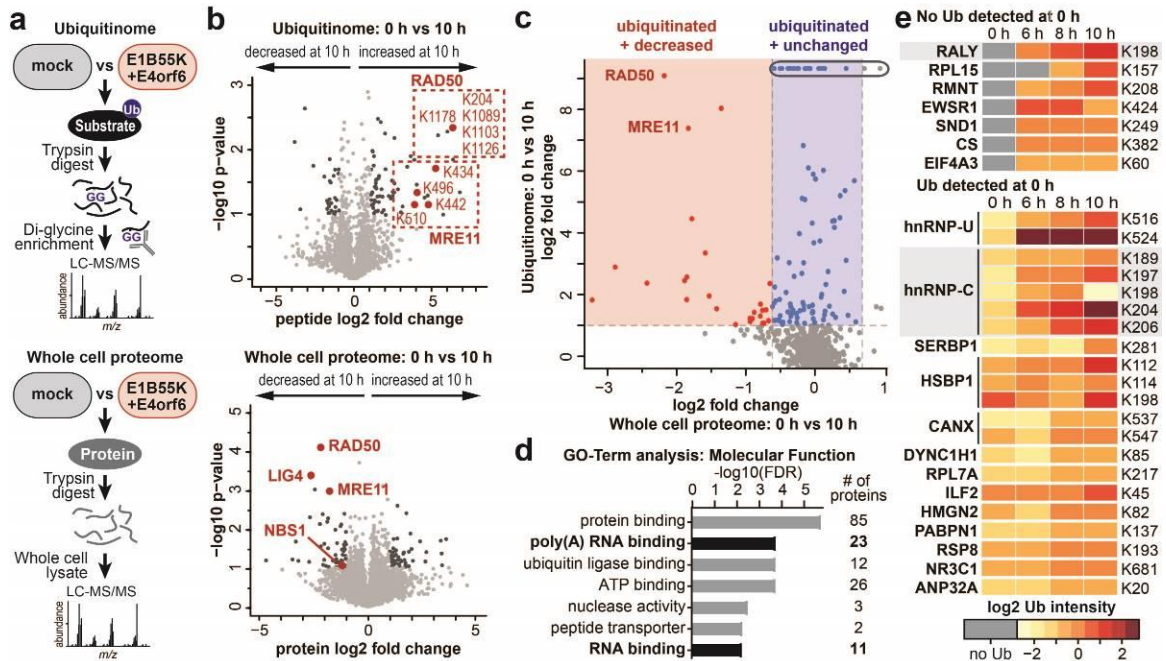


Figure 3.2 | Unbiased proteomics reveals RNA-binding proteins among putative non-degraded substrates of the Ad ubiquitin ligase. **a**, Proteomics workflow for identification of E1B55K/E4orf6 substrates. HeLa cells were transduced with recombinant Ad vectors expressing E1B55K and E4orf6 (MOI=10), and subjected to both di-glycine remnant profiling (K-ε-GG) to identify ubiquitinated lysine residues and whole cell proteomics to determine protein abundance. **b**, Volcano plots showing log₂ fold-changes between 0 h and 10 h for ubiquitination (above) and protein abundance (below). For ubiquitination, individual peptides containing the modified lysine residues are normalized to protein abundance. Peptides and proteins with a fold change > ±s.e.m. and p-value < 0.05 are considered significantly changed and highlighted in dark grey. Ubiquitinated peptides and proteins corresponding to known E1B55K/E4orf6 substrates are highlighted in red. n equals three biological replicates. **c**, Scatter plot integrating changes in protein abundance (X-axis) and ubiquitination (Y-axis). Putative degraded substrates are shown in red (increased ubiquitination, decreased protein abundance), putative non-degraded substrates are shown in blue (increased ubiquitination, no significant change in protein abundance). Known degraded substrates MRE11 and RAD50 are indicated. Blue dots circled at the top indicate proteins that were only ubiquitinated upon expression of E1B55K/E4orf6 and were not detected as ubiquitinated in mock conditions. **d**, Bar graph representing gene ontology (GO) analysis of all predicted substrates by molecular functions. Categories containing RNA-binding proteins are highlighted. **e**, Heat map of all ubiquitinated lysine residues within RNA-binding proteins with a normalized log₂ abundance z-score > -0.5 and maximum log₂ fold-change > 1 over the time course of E1B55K/E4orf6 transduction. The colors in the heat map correspond to the average z-score of the ubiquitination and are indicated in the accompanying scale. Highly ubiquitinated proteins RALY and hnRNP-C are highlighted. *Panels b-e with help of JM Dybas and JC Liddle.*

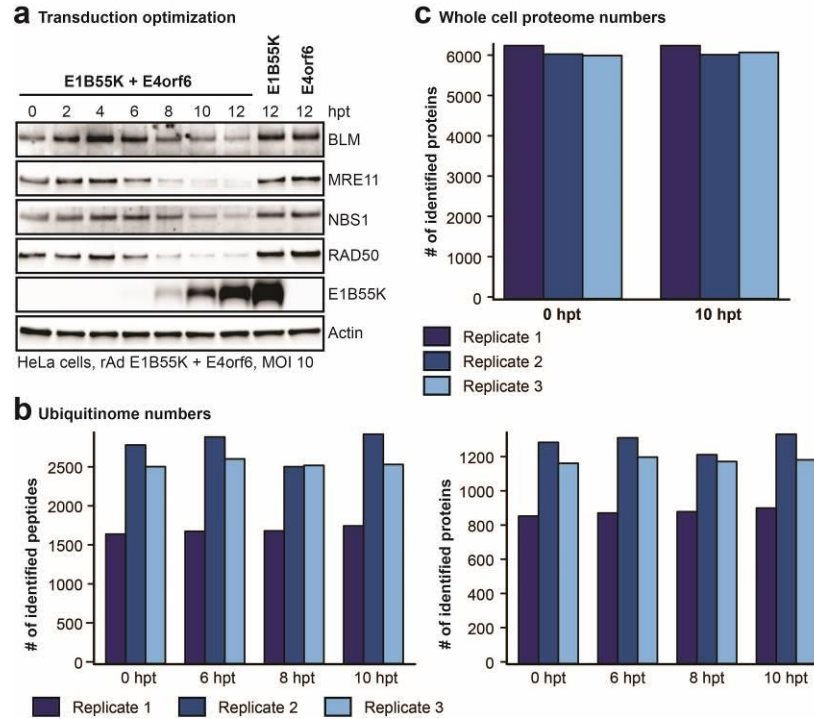


Figure 3.S2 | Quantification of number of peptides and proteins identified in di-glycine remnant profiling and whole cell proteome data sets. a-c, HeLa cells transduced with rAd E1B55K/E4orf6 at an MOI of 10. **a,** Immunoblot of time course of E1B55K/E4orf6 expression showing degradation kinetics of known substrates. hpt = hours post transduction. **b,** Numbers of peptides and corresponding proteins identified following K- ϵ -GG antibody enrichment in di-glycine remnant combined with mass spectrometry analysis at 0, 6, 8, and 10 hours post E1B55K/E4orf6 expression. **c,** Number of proteins identified by whole cell proteomics analysis at time 0 and 10 hours post E1B55K/E4orf6 expression. **b,c,** Dark blue, medium blue, and light blue bars indicate the counts for three individual biological replicates. *Analysis in panels b and c by JM Dybas.*

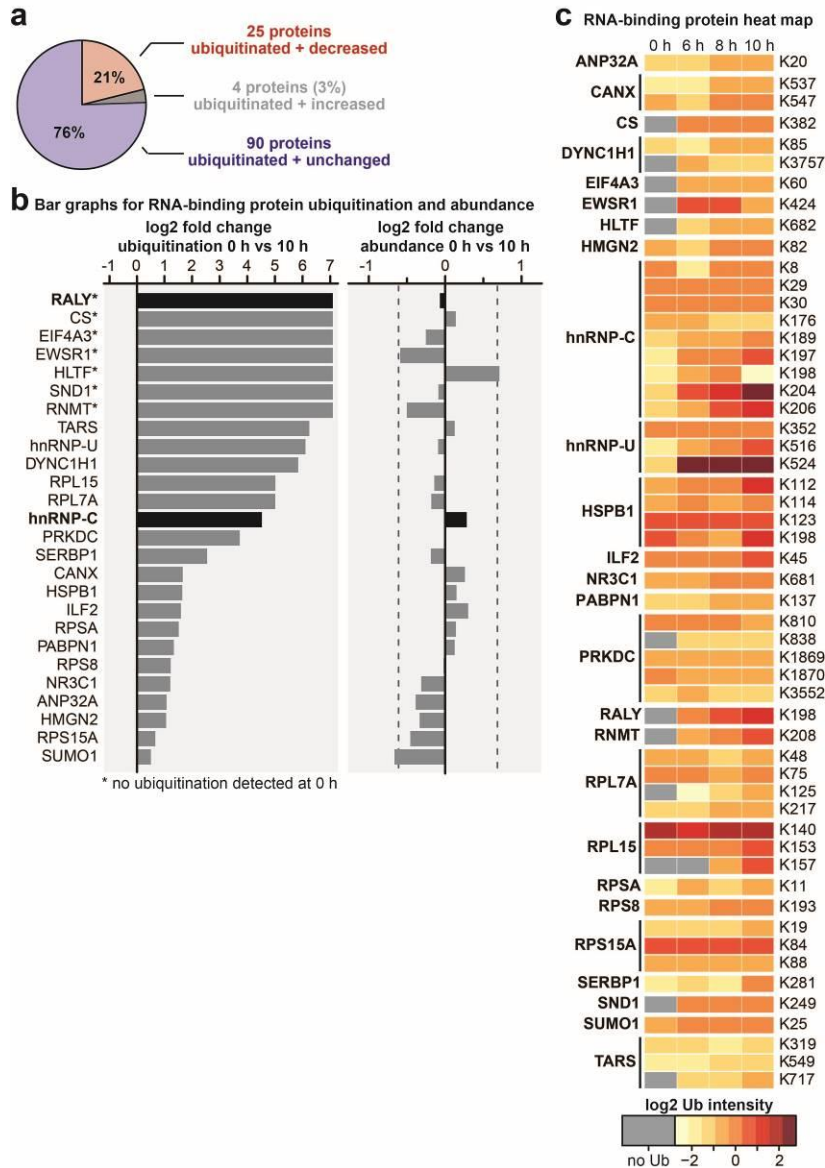


Figure 3.S3 | Di-glycine remnant profiling and whole cell proteome data for RNA-binding proteins enriched within the predicted E1B55K/E4orf6 substrates. a, Predicted substrates that either decrease (red), increase (grey) or remain unchanged (blue) in their protein abundance during expression of E1B55K/E4orf6. **b-c,** Gene ontology analysis identified RNA-binding proteins enriched in the set of proteins that exhibited an increase in normalized protein-based ubiquitin abundance of log₂ fold change > 1 following 10 h transduction of E1B55K/E4orf6. **b,** Enriched RNA-binding protein, ubiquitination log₂ fold changes (left) and whole cell protein abundance log₂ fold changes (right) following 10 h transduction by E1B55K/E4orf6. **c,** Heat map showing relative ubiquitination of the respective lysine residues quantified by di-glycine remnant profiling analysis at 0, 6, 8, and 10 h of E1B55K/E4orf6 expression for peptides within enriched RNA-binding proteins. Heat map color gradient is based on low (yellow) to high (red) ubiquitin abundance and grey indicates “not identified” at that time point. *Analysis in panels a-c by JM Dybas.*

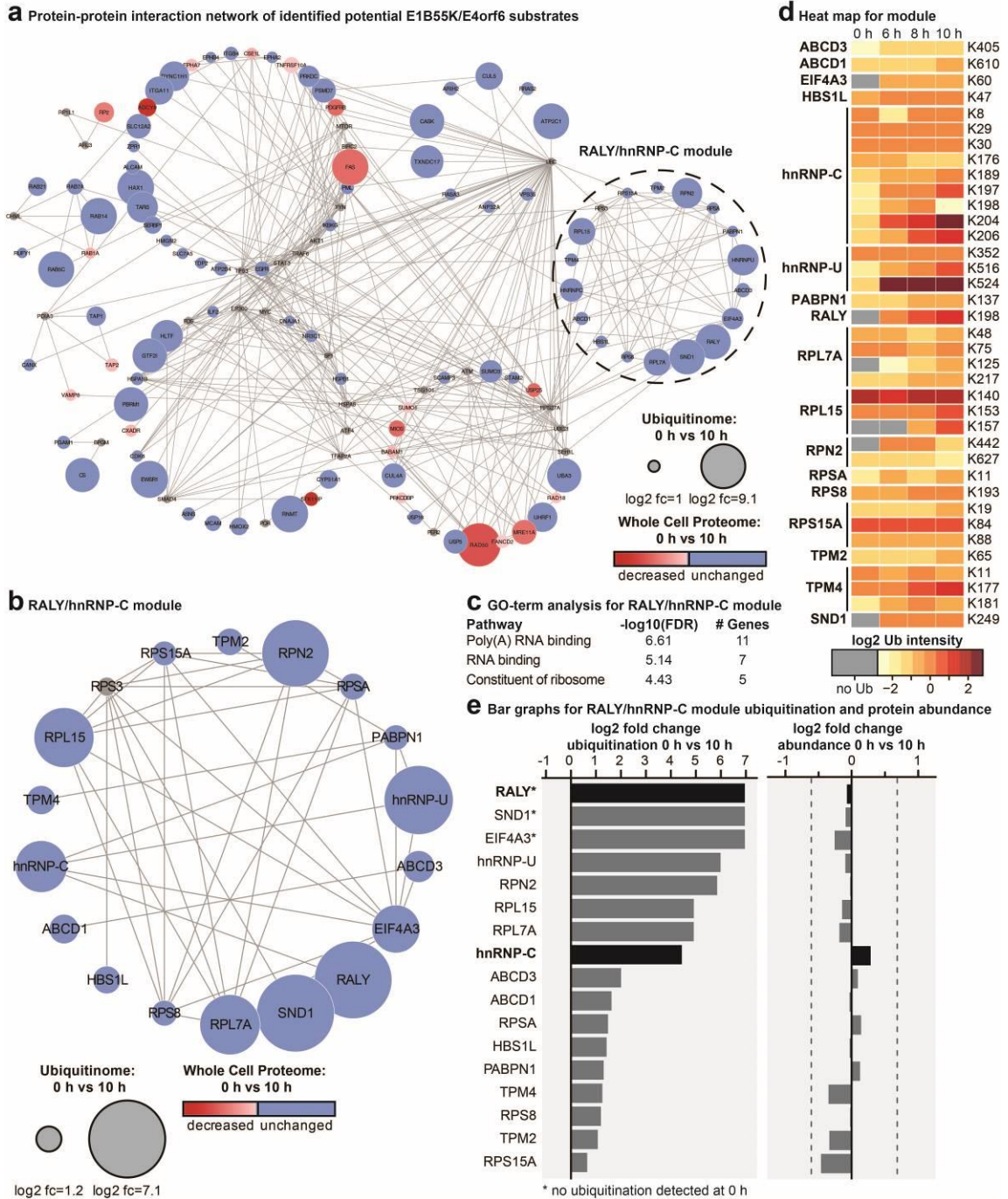


Figure 3.S4 | Network analysis of predicted E1B55K/E4orf6 substrates identifies a “RALY/hnRNP-C module” enriched for RNA-binding proteins. a,b, The Reactome-FI application in Cytoscape was utilized to generate a protein-protein interaction network in which nodes represent proteins and edges represent Reactome-based protein-protein interactions. Node size corresponds to relative protein-based ubiquitination \log_2 fold change and node color corresponds to whole cell proteome \log_2 fold change following 10 h transduction of E1B55K/E4orf6. a, Protein-protein interaction network of proteins that exhibited normalized protein-based ubiquitin abundance \log_2 fold change > 1 following 10 h transduction of E1B55K/E4orf6. Reactome-FI interaction module analysis was performed to generate clusters of

highly interacting proteins. **b**, RALY and hnRNP-C are contained within a single module. **c**, Gene ontology analysis for molecular function identified enrichment of RNA-binding and Poly(A) RNA-binding proteins within the RALY/hnRNP-C network module. **d**, Heat map showing relative ubiquitin abundance quantified by di-glycine remnant profiling analysis at 0, 6, 8, and 10 h post E1B55K/E4orf6 transduction for peptides from proteins within the RALY/hnRNP-C network module. Heat map color gradient is based on low (yellow) to high (red) ubiquitination and grey indicates “not identified” at that time point. **e**, RALY/hnRNP-C network module protein ubiquitin log₂ fold changes (left) and whole cell protein abundance log₂ fold changes (right) comparing 0 and 10 h post transduction with E1B55K/E4orf6. *Analysis in Panels a-e by JM Dybas.*

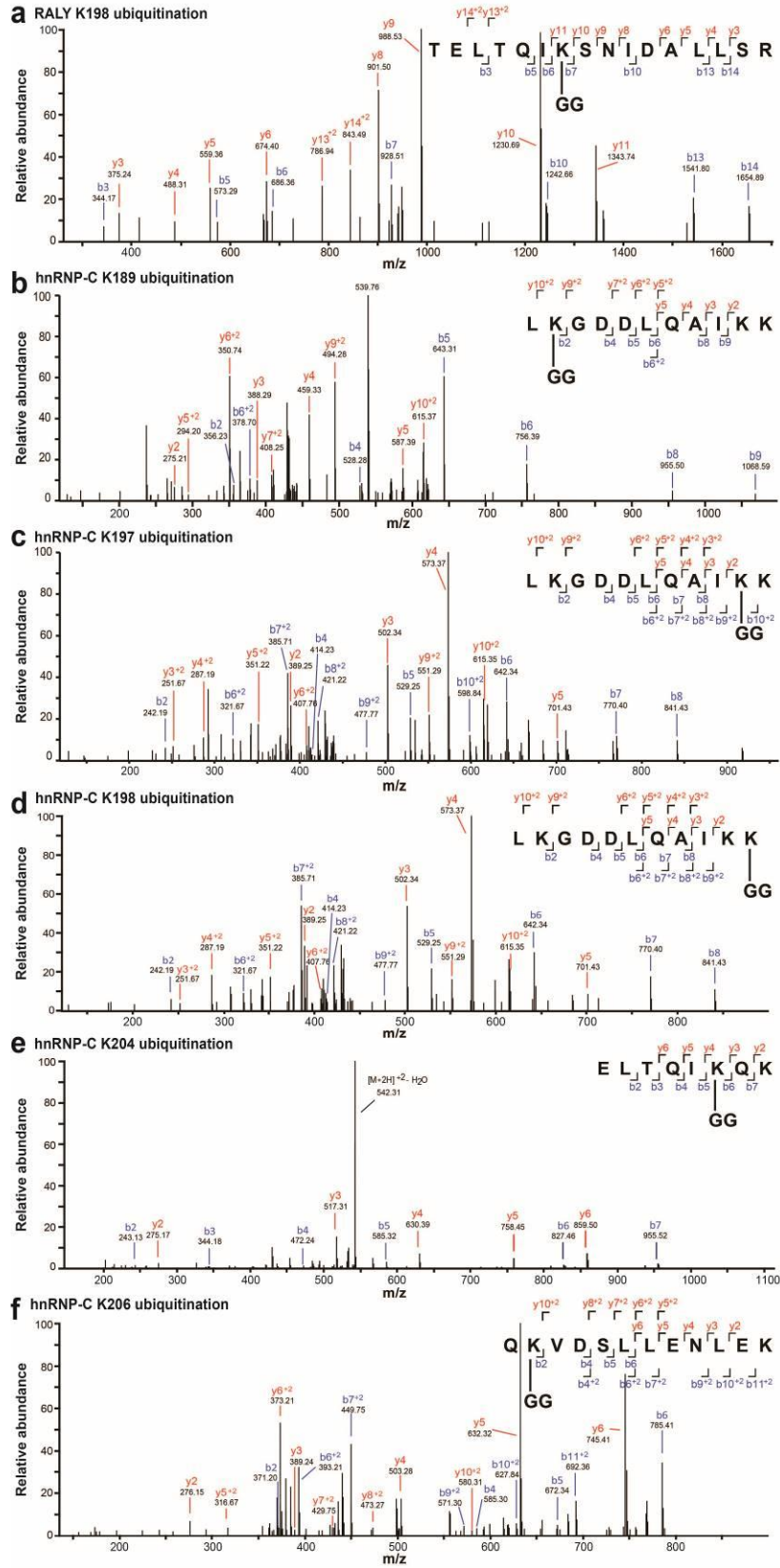


Figure 3.S5 | MS2 evidence for ubiquitination site localization in RALY (a) and hnRNP-C (b-f) peptides. Spectra were obtained from LC-MS/MS analyses using collision-induced dissociation (CID) at 35%, and identified in MaxQuant 1.6.0.1. All modified residues can be confidently identified by confirming ions, except for hnRNP-C K198 (d), which lacks ions to distinguish between K197 and K198. Best evidence spectra were selected for annotation of b-ion (blue) and y-ion (red) series and their masses for singly- and doubly-charged fragments. *Analysis in panels a-f by JC Liddle.*

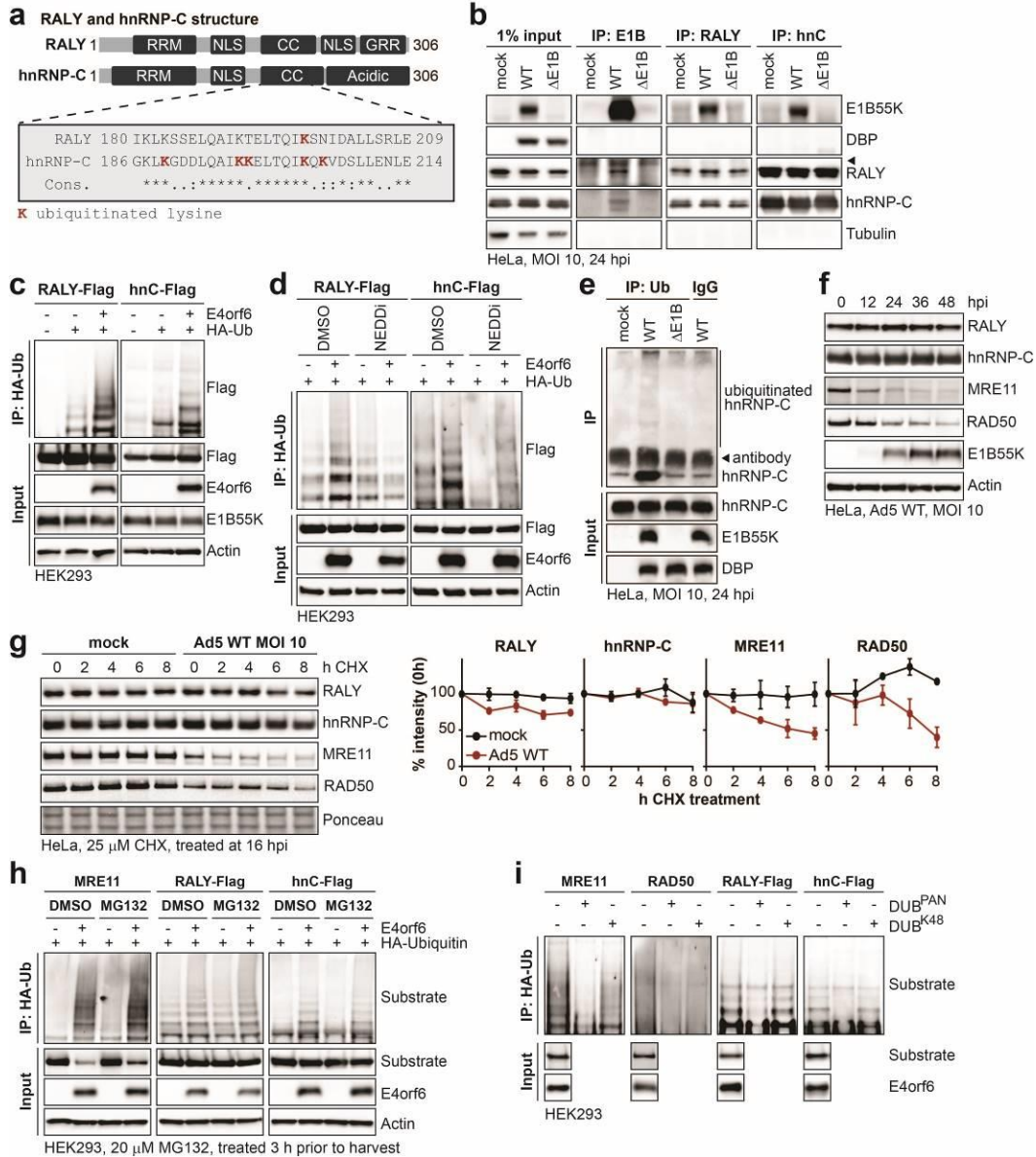


Figure 3.3 | RALY and hnRNP-C are non-degraded substrates of the Ad ubiquitin ligase. **a**, Domain structure of RALY and hnRNP-C. RRM = RNA recognition motif, NLS = nuclear localization sequence, CC = coiled-coil region, GRR = glycine rich region. CC region shown below contains all the lysine residues with increased ubiquitination upon E1B55K/E4orf6 expression highlighted in red. **b**, Immunoblot analysis of E1B55K, RALY, and hnRNP-C immunoprecipitations (IP) probing for pull-down of viral and cellular proteins during mock, WT and ΔE1B infection of HeLa cells at MOI of 10 for 24 hpi. ◀ denotes the signal of the antibody heavy chain. **c**, HEK293 cells transfected with the indicated constructs for 24 h followed by denaturing IP with HA antibody and immunoblot analysis of RALY-Flag or hnRNP-C-Flag. **d**, HEK293 cells transfected with the indicated constructs for 24 h and treated with DMSO or NEDDi 6 h prior to harvest followed by denaturing IP with HA antibody and immunoblot analysis of RALY-Flag or hnRNP-C-Flag. **e**, Immunoblot of denaturing hnRNP-C IP probing for ubiquitin during mock, WT and ΔE1B infections at MOI of 10 for 24 h. ◀ indicates non-specific signal of the antibody heavy chain. **f**, Immunoblot analysis of protein levels over a time course of Ad5 WT infection (MOI=10) of HeLa cells. **g**, Immunoblot analysis and quantification of RALY, hnRNP-C,

MRE11, and RAD50 over a time course of cycloheximide (CHX) treatment of mock or Ad5 WT infected HeLa cells. Quantification showing mean+s.d. of two biological replicates. **h**, HEK293 cells transfected with the indicated constructs for 24 h and treated with DMSO or proteasome inhibitor MG132 3 h prior to harvest followed by denaturing IP with HA antibody and immunoblot analysis of MRE11, RALY-Flag, and hnRNP-C-Flag. **i**, HEK293 cells transfected with the indicated constructs for 24 h followed by denaturing IP with HA antibody, treatment with the indicated deubiquitinating enzymes (DUBs) and immunoblot analysis of MRE11, RAD50, RALY-Flag, and hnRNP-C-Flag. All immunoblots are representative of at least three biological replicates. *Panels b and e with help of ET Kim and panel d with help of JC Liddle.*

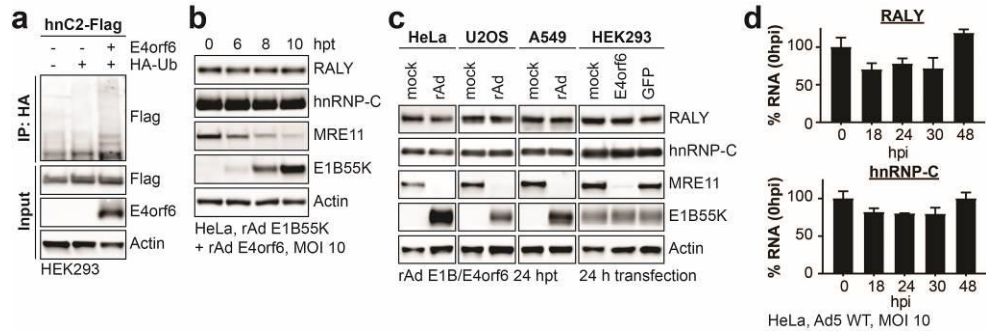


Figure 3.S6 | RALY and hnRNP-C are not decreased upon transduction in multiple cell lines. **a**, HEK293 cells transfected with the indicated constructs for 24 h followed by denaturing IP with HA antibody and immunoblot analysis of hnRNP-C2-Flag. **b**, Immunoblot analysis of protein levels in HeLa cells over a time course of transduction with recombinant Ad vectors expressing only E1B55K and E4orf6 (MOI=10). **c**, Immunoblot analysis of protein levels in HeLa, U2OS, A549 and HEK293 cells. HeLa, U2OS and A549 cells were transduced with recombinant Ad vectors expressing only E1B55K and E4orf6 for 24 h. HEK293 cells, which contain an endogenous copy of E1B55K, were mock transfected or transfected with plasmids expressing E4orf6 or GFP. **d**, Bar graphs of RALY and hnRNP-C RNA levels over a time course of infection with Ad5 WT (MOI=10) relative to mock as determined by RT-qPCR, shown is mean+s.d, n equals three biological replicates. All immunoblots are representative of at least three biological replicates.

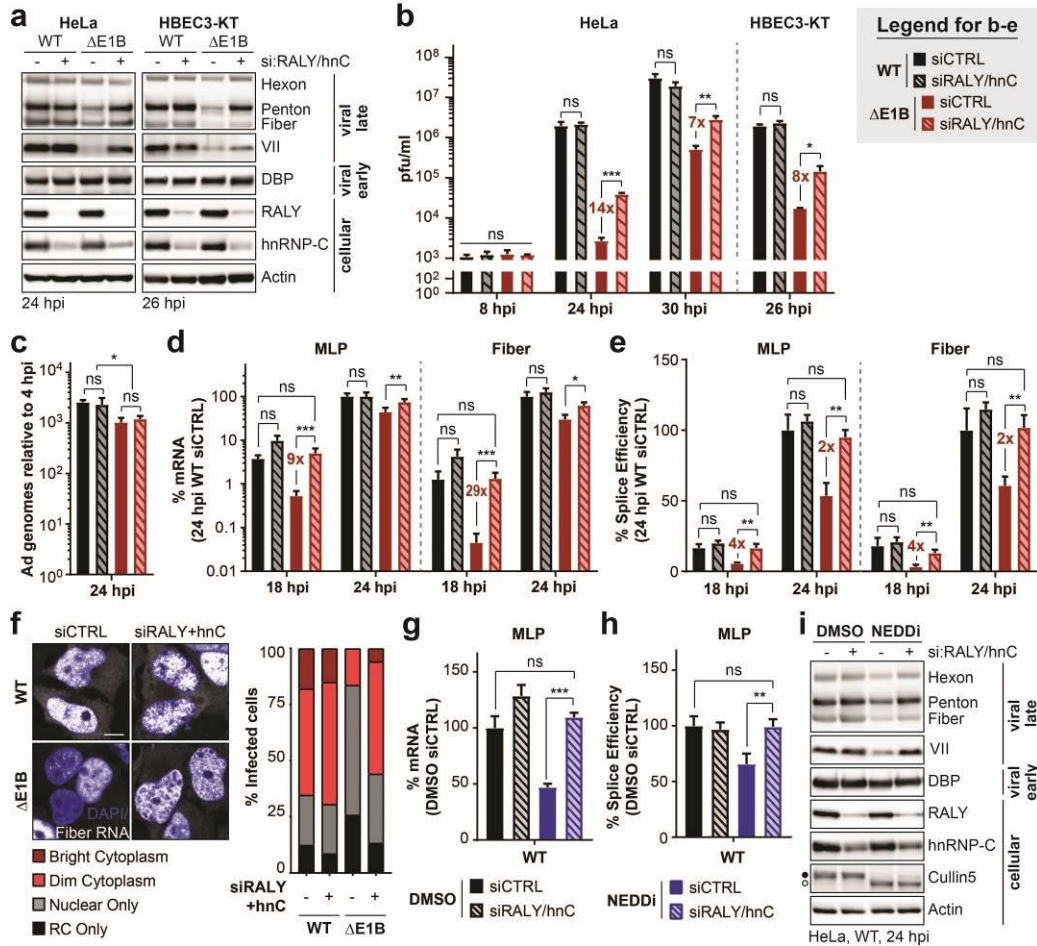


Figure 3.4 | Knock-down of RALY and hnRNP-C rescues the RNA processing defect caused by the absence of a functional viral ubiquitin ligase. a-f, HeLa cells or HBEC3-KT (only a,b) transfected with control (siCTRL) or RALY and hnRNP-C (siRALY/hnC) siRNA 24 h prior to infection with Ad5 WT or Δ E1B (MOI 10), harvested at respective time points. a, Immunoblot analysis of viral and cellular protein levels. b, Bar graph representing plaque assays for viral progeny. c, Bar graph representing qPCR of viral genomes normalized to input. d, Bar graph representing spliced RNA levels of viral late transcripts MLP and fiber measured by RT-qPCR. e, Bar graph representing splicing efficiency as defined as the ratio of spliced to unspliced transcripts of MLP and fiber measured by RT-qPCR. f, RNA FISH visualizing the localization of fiber transcripts (white) in relation to nuclear DNA stained with DAPI (blue) and quantification of observed pattern for > 100 HeLa cells. RC - replication center. Scale bar 10 μ m. g-i. HeLa cells transfected with control (siCTRL) or RALY and hnRNP-C (siRALY/hnC) siRNA 24 h prior to infection with Ad5 WT (MOI=10), treated with either DMSO or NEDDi at 8 hpi and processed at 24 hpi. g, Bar graph representing spliced RNA levels of MLP measured by RT-qPCR. h, Bar graph representing splicing efficiency as defined as the ratio of spliced to unspliced transcripts of MLP measured by RT-qPCR. i Immunoblot analysis of viral and cellular protein levels, with neddylated (\bullet) and unmodified (\circ) forms of Cullin5 indicated. All immunoblots are representative of at least three biological experiments. All graphs show the mean+s.d. with n equals three biological replicates. Statistical significance was calculated using an unpaired, two-tailed Student's t-test, * p < 0.05, ** p < 0.01, *** p < 0.005. Panels d-f with help of AM Price.

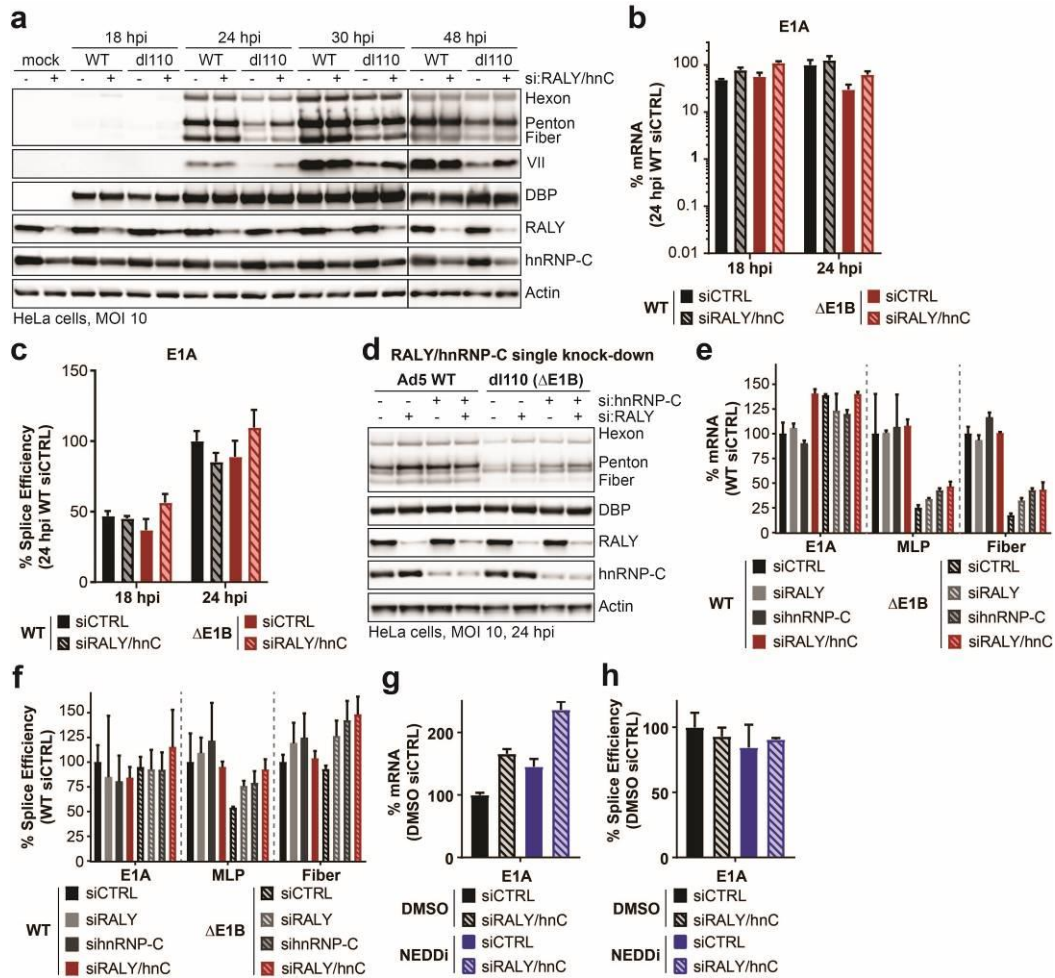


Figure 3.S7 | RALY and hnRNP-C single knock-down rescue late protein, RNA and splice efficiency during infection with Ad Δ E1B. **a-c**, HeLa cells transfected with control (siCTRL) or RALY and hnRNP-C (siRALY/hnC) siRNA 24 h prior to infection with Ad5 WT or Δ E1B (MOI=10), harvested at respective time points. **a**, Extended immunoblot analysis of viral and cellular protein levels. **b**, Bar graph representing spliced RNA levels of viral early transcript E1A measured by RT-qPCR. **c**, Bar graph representing splicing efficiency as defined as the ratio of spliced to unspliced transcripts of E1A measured by RT-qPCR. **d-f**, HeLa cells transfected with control siRNA (siCTRL), siRNA for RALY (siRALY), siRNA for hnRNP-C (sihnRNP-C) or siRNA for both RALY and hnRNP-C (siRALY/hnC) 24 h prior to infection with Ad5 WT or Δ E1B (MOI=10) and harvested at 24 hpi. **d**, Immunoblot analysis of viral and cellular protein levels. **e**, Bar graph representing spliced RNA levels of E1A, MLP and fiber measured by RT-qPCR. **f**, Bar graph representing splicing efficiency as defined as the ratio of spliced to unspliced transcripts of E1A, MLP and fiber measured by RT-qPCR. **g,h**, HeLa cells transfected with control (siCTRL) or RALY and hnRNP-C (siRALY/hnC) siRNA 24 h prior to infection with Ad5 WT (MOI=10), treated with either DMSO or NEDDi at 8 hpi and processed at 24 hpi. **g**, Bar graph representing spliced RNA levels of E1A measured by RT-qPCR. **h**, Bar graph representing splicing efficiency as defined as the ratio of spliced to unspliced transcripts of E1A measured by RT-qPCR. All immunoblots are representative of at least three biological experiments. All graphs show the mean+s.d. with n equals three biological replicates. *Panels b and c with help of AM Price.*

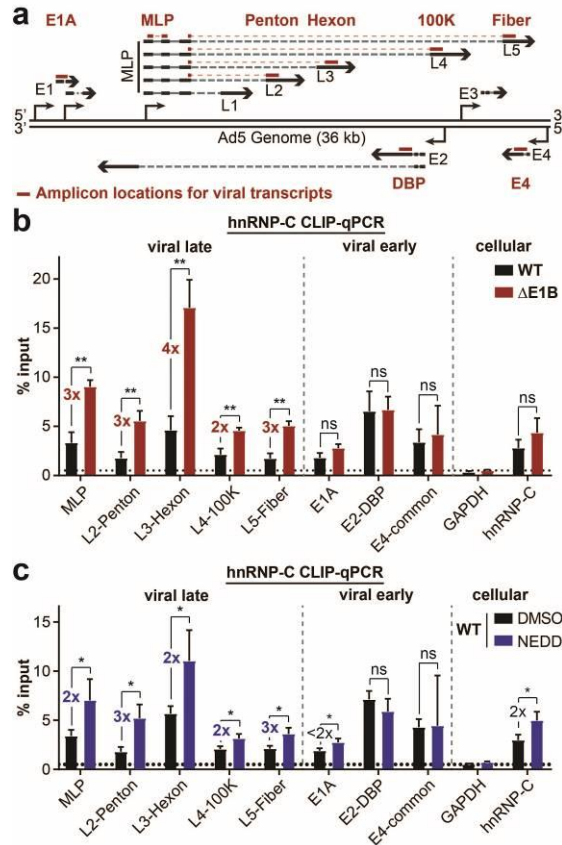


Figure 3.5 | The interaction of hnRNP-C with viral late RNA increases in the absence of a functional viral ubiquitin ligase. **a**, Schematic of the Ad5 genome and viral transcription units. Location of amplicons for viral early (E1A, DBP, E4) and viral late (MLP, Penton, Hexon, 100K, Fiber) are noted. **b**, HeLa cells infected with either WT Ad5 or $\Delta E1B55K$ (MOI=10), UV-crosslinked and harvested at 24 hpi, subjected to hnRNP-C CLIP and RT-qPCR for viral early and late transcripts. GAPDH is a cellular negative control. hnRNP-C is a cellular positive control. **c**, HeLa cells infected with WT Ad5 (MOI=10), treated with either DMSO or NEDDi at 8 hpi, UV-crosslinked and harvested at 24 hpi, subjected to hnRNP-C CLIP and RT-qPCR for viral early and late transcripts. GAPDH is a cellular negative control. hnRNP-C is a cellular positive control. Graphs show mean+s.d, n equals three biological replicates. Statistical significance was calculated using an unpaired, two-tailed Student's t-test, * p < 0.05, ** p < 0.01. *Panels b and c with help of AM Price.*

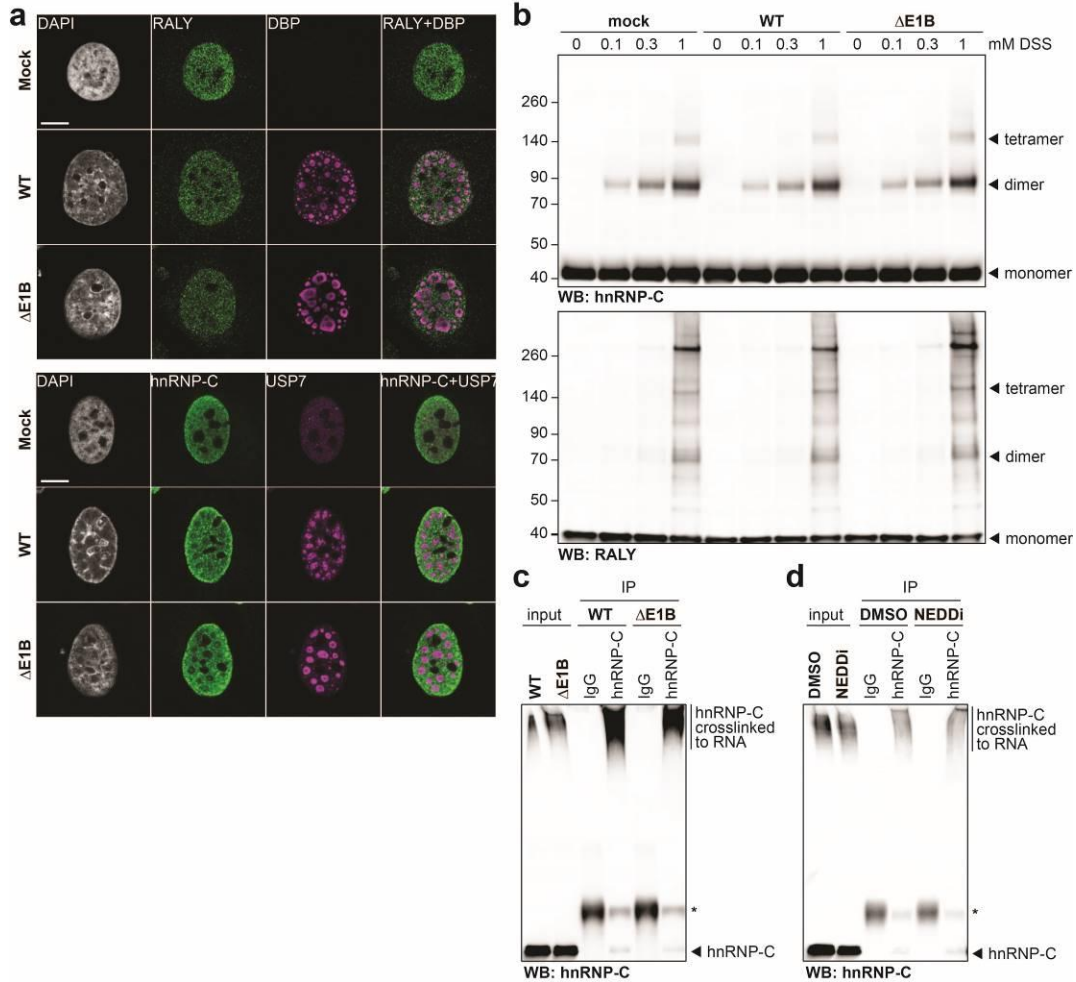


Figure 3.S8 | No dramatic difference in protein localization and protein-complex formation of RALY and hnRNP-C between Ad WT and $\Delta E1B$ infection. **a**, Representative images of immunofluorescence comparing the localization of RALY and hnRNP-C (both green) in mock, Ad WT and $\Delta E1B$ infection of HeLa cells (MOI=10, 24 hpi). Viral replication centers are stained by DBP or USP7 (both magenta) and nuclear DNA by DAPI (grey). Scale bar 10 μ m. **b**, Immunoblot analysis of RALY and hnRNP-C protein complexes formed upon mock, Ad WT and $\Delta E1B$ infection of HeLa cells (MOI=10) and treatment with indicated concentrations of disuccinimidyl suberate (DSS) for 30 min at 24 hpi. Representative of three biological replicates. **c**, Control immunoblot for hnRNP-C CLIP-qPCR shown in Figure 5b. Higher molecular weight complexes stained with hnRNP-C antibody represent hnRNP-C crosslinked to RNA. * marks the antibody heavy chain detected in the IP. Representative of three biological replicates for both CLIP-qPCR and immunoblot analysis thereof. **d**, Control immunoblot for hnRNP-C CLIP-qPCR shown in Figure 5c. Higher molecular weight complexes stained with hnRNP-C antibody represent hnRNP-C crosslinked to RNA. * marks the antibody heavy chain detected in the IP. Representative of three biological replicates for both CLIP-qPCR and immunoblot analysis thereof. *Panel a by M Charman.*

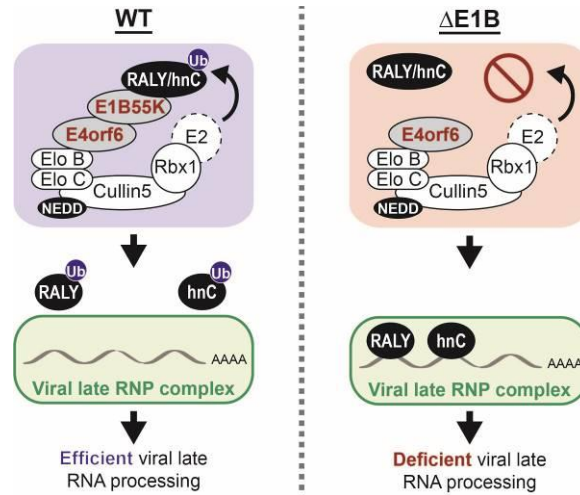


Figure 3.6 | Non-degradative ubiquitination of RNA-binding proteins promotes efficient adenoviral RNA processing. During wild-type (WT) Ad5 infection the E1B55K/E4orf6 complex induces ubiquitination of RNA-binding proteins RALY and hnRNP-C to facilitate efficient viral late RNA processing. Ubiquitination regulates interaction of these host proteins with viral RNA to facilitate viral infection. In the absence of the E1B55K/E4orf6 ubiquitin ligase activity, the RBPs bind to viral late mRNAs and limit RNA processing and protein production. RNP - ribonucleoprotein

3.6 Materials and Methods

3.6.1 Cell culture

All cell lines were obtained from the American Type Culture Collection (ATCC) and cultured at 37°C and 5% CO₂. HeLa (Cat#: ATCC CCL-2), HEK293 (Cat#: ATCC CRL-1573), and U2OS cells (Cat#: ATCC HTB-96) were grown in DMEM (Corning, Cat#: 10-013-CV) supplemented with 10% v/v fetal bovine serum (FBS) (VWR, Cat#: 89510-186) and 1% v/v Pen/Strep (100 U/ml of penicillin, 100 µg/ml of streptomycin, Gibco, Cat#: 15140-122). A549 cells (Cat#: ATCC CCL-185) were maintained in Ham's F-12K medium (Gibco, Cat#: 21127-022) supplemented with 10% v/v FBS and 1% v/v Pen/Strep. Primary like HBEC3-KT (Cat#: ATCC CRL-4051) were grown in Airway Epithelial Cell Basal Medium (Cat#: ATCC PCS-300-030) supplemented with Bronchial Epithelial Cell Growth Kit (Cat#: ATCC PCS-300-040) and 1% v/v Pen/Strep. All cell lines tested negative for mycoplasma using the LookOut Mycoplasma PCR Detection Kit (Sigma-Aldrich).

3.6.2 Viruses and infection

Ad5 wild-type (WT) was purchased from ATCC. The Ad5 E1B55K-deletion mutant dl110 has been described previously²⁴⁵ and was a gift from G. Ketner. The E1 deletion mutant recombinant adenovirus vectors expressing E1B55K (rAd E1B55K)³⁰⁴ and E4orf6 (rAd E4orf6)²²⁴ were obtained from P. Branton. All viruses were propagated on HEK293 cells, purified using two sequential rounds of ultracentrifugation in CsCl gradient and stored in 40% v/v glycerol at -20°C. Viral titers were determined by plaque assay on HEK293 cells for all but rAd E4orf6. For this virus we assumed a plaque forming unit-to-particle ratio of 1:50. All infections were carried out using a multiplicity of infection (MOI) of 10 and harvested at indicated hours post infection (hpi). Infections were performed on monolayers of cells by dilution of the virus in respective low serum growth medium. After 2 h at 37°C additional full serum growth medium was added. For plaque assays, the virus infection media was removed after 2 h and cells were washed 1x in PBS before addition of full serum growth medium.

3.6.3 Plasmids, siRNA and transfection

Full-length RALY with a carboxyl-terminal Flag-tag (cDNA obtained from Dharmacon, Cat#: MHS6278-202857995) and hnRNP-C isoforms 1 and 2 with a carboxyl-terminal Flag-tag (cDNA containing plasmids were a gift from K. Lynch) and RFP were cloned into the pcDNA3.1 vector using the BamHI and XbaI restriction sites. The pRK5 vector encoding Ad5 E4orf6 was generated by subcloning from purified Ad5 DNA as previously described³²⁵. The expression vector for HA-tagged tetra ubiquitin as previously described³²⁶ was a gift from R. Greenberg DNA transfections were performed using the standard protocol for Lipofectamine2000 (Invitrogen).

The following siRNAs were obtained from Dharmacon: non-targeting control (Cat#: D-001206-13-05), RALY (Cat#: M-012392-00-0005) and hnRNP-C (Cat#: M-011869-01-0005; Cat#: L-011869-03-0005 only used for hnRNP-C single knockdown in supplementary Fig. 7). siRNA transfections were performed using the standard protocol for Lipofectamine RNAiMAX (Invitrogen).

3.6.4 Antibodies and inhibitors

The following primary antibodies for viral proteins were obtained: Adenovirus late protein antibody staining Hexon, Penton and Fiber (gift from J. Wilson²⁷⁸, species: rabbit, WB 1:10,000), Protein VII (gift from H. Wodrich³²⁷, Clone: Chimera 2-14, WB 1:200), DBP (gift from A. Levine²⁸⁰, Clone: B6-8, WB 1:1000, IF 1:400), E1B55K (gift from A. Levine³²⁸, Clone: 58K2A6, WB 1:500) and E4orf6 (gift from D. Ornelles³²⁹, Clone: RSA#3, WB 1:500).

The following primary antibodies were used for cellular proteins: MRE11 (Novus Biologicals, Catalog#: NB100-142, WB 1:1000), BLM (Abcam, Catalog#: ab476, WB 1:1000), Cullin5 (Bethyl Laboratories, Catalog#: A302-173A, WB 1:200), Actin (Sigma-Aldrich, Catalog#: A5441-100UL, WB 1:5000), RALY (Bethyl Laboratories, Catalog#: A302-070A, WB 1:1000; Bethyl Laboratories, Catalog#: A302-069A, IF 1:500, IP 5 μ l = 5 μ g), hnRNP-C (Santa Cruz Biotechnology, Catalog#: sc-32308, WB 1:1000, IF 1:1000, IP 25 μ l=5 μ g), Tubulin (Santa Cruz Biotechnology, Catalog#: sc-69969, WB 1:1000), Flag (Sigma-Aldrich, Catalog#: F7425-.2MG, WB 1:1000), Histone H3 (Abcam, Catalog#: ab1791, WB 1:100,000), Ubiquitin (Santa Cruz, Catalog#: sc-9133, IP 10 μ l=2 μ g; Abcam, Catalog#: ab7780, IP 5 μ l), NBS1 (Novus Biologicals, Catalog#: NB100-143, WB

1:1000), RAD50 (GeneTex, Catalog#: GTX70228, WB 1:1000) and USP7 (Bethyl Laboratories, Catalog#: A300-033A, IF 1:500).

Horse radish peroxidase-conjugated (HRP) secondary antibodies for immunoblot were purchased from Jackson Laboratories. Anti-mouse IgG conjugated to HRP for immunoblot of immunoprecipitation samples (used in Fig. 3b) was purchased from Abcam (Cat#: ab131368). Fluorophore-conjugated secondaries for immunofluorescence were purchased from Life Technologies.

Cycloheximide (CHX) was purchased from Calbiochem (Cat#: 293764), dissolved in DMSO to a stock concentration of 25 mM and used at a final concentration of 25 μ M. NEDDylation inhibitor MLN4924 was purchased from Sigma-Aldrich (Cat#: 505477), dissolved in DMSO to a stock concentration of 1 mM and used at a final concentration of 3 μ M. Proteasome inhibitor MG132 was purchased from Sigma-Aldrich (Cat#: 474791) at a concentration of 10 mM in DMSO and used at a final concentration of 20 μ M.

3.6.5 Immunoblotting

Protein samples were prepared using lithium dodecyl sulfate (LDS) loading buffer (NuPage) supplemented with 25 mM dithiothreitol (DTT) and boiled at 95°C for 10 min. Equal amounts of protein lysate were separated by SDS-PAGE and transferred onto a nitrocellulose membrane (Millipore) at 30 V for at least 60 min (overnight for ubiquitination assays). Membranes were stained with Ponceau to confirm equal loading and blocked in 5% w/v milk in TBST supplemented with 0.05% w/v sodium azide. Membranes were incubated with primary antibodies overnight, washed for 30 min in TBST, incubated with HRP-conjugated secondary for 1 h and washed again for 30 min in TBST. Proteins were visualized with Pierce ECL Western Blotting Substrate (Thermo Scientific) and detected using a Syngene G-Box. Images were processed and assembled in Adobe CS6.

3.6.6 Immunofluorescence

HeLa cells were grown on coverslips in 24-well plates, infected with indicated viruses and fixed at 24 hpi in 4% w/v paraformaldehyde in PBS for 10 mins. Cells were permeabilized with

0.5% v/v Triton-X in PBS for 10 mins. The samples were blocked in 3% w/v BSA in PBS (+ 0.05% w/v sodium azide) for 30 mins, incubated with primary antibodies in 3% w/v BSA in PBS (+ 0.05% w/v sodium azide) for 1 h, followed by secondary antibodies and 4,6-diamidino-2-phenylindole (DAPI) for 2 h. Secondary antibodies used were Alexa Fluor α -rabbit 488 and α -mouse 555. Coverslips were mounted onto glass slides using ProLong Gold Antifade Reagent (Cell Signaling Technologies). Immunofluorescence was visualized using a Zeiss LSM 710 Confocal microscope (Cell and Developmental Microscopy Core at UPenn) and ZEN 2011 software. Images were processed in ImageJ and assembled in Adobe CS6.

3.6.7 RNA Fluorescence *in situ* hybridization

RNA FISH was performed following previously established protocols³³⁰, with the following modifications. Thirty-two singly labeled DNA oligonucleotides targeting the Fiber open reading frame were designed using the Stellaris smFISH probe designer and ordered with a 3' mdC-TEG-Amino label from LGC Biosearch. Fiber FISH probes were pooled and labeled with ATTO 647N NHS-Ester (ATTO-TEC, Cat#: AD 647N-31), isopropanol precipitated and purified by HPLC as previously described³³⁰. GAPDH probes labeled with Cy3 were used as a counterstain to demarcate cytoplasmic boundaries and were a kind gift from S. Schaffer³³¹. HeLa cells were grown on coverslips, harvested, fixed, and permeabilized as described for conventional immunofluorescence above. After permeabilization, cells on coverslips were equilibrated in Wash Buffer (2X SSC, 10% formamide) before being inverted over 30 μ l Hybridization Buffer (2X SSC, 10% formamide, 10% dextran sulphate) containing 500 nM Fiber and GAPDH FISH probes and incubated at 37°C in a humidified chamber overnight. The following day coverslips were washed twice with Wash Buffer for 30 minutes at 37°C with DAPI added to the second wash, briefly washed three times at room temperature with 2X SSC, and then affixed to glass slides using clear nail polish. Images were acquired on a Zeiss LSM 710 microscope with ten z-stacks of 0.7 μ m each in the z-direction. Images were deconvoluted by maximum intensity projection in the z-direction using ImageJ. Fiber RNA localization was scored as described in **Figure 3.S1** over 41-

160 individual cells. Representative images were further processed in ImageJ and assembled in Adobe CS6.

3.6.8 RNA isolation and RT-qPCR

Total RNA was isolated from infected cells at the indicated time points using the RNeasy Micro Kit (Qiagen). Complementary DNA (cDNA) was synthesized using 1 µg of input RNA and the High Capacity RNA-to-cDNA Kit (Thermo Fisher). Quantitative PCR was performed by standard protocol using diluted cDNA, primers for different viral and cellular transcripts (see **Supplementary Table 4** for complete list of primers) and SYBR Green (Thermo Scientific) using the QuantStudio 7 Flex Real-Time PCR System (Thermo Scientific). The relative values for each transcript were normalized to a control RNA (actin or HPRT).

3.6.9 Viral genome accumulation by qPCR

Infected cells were harvested by trypsinization at 4 and 24 hpi and total DNA was isolated using the PureLink Genomic DNA kit (Invitrogen). qPCR was performed using primers for the Ad5 DBP and cellular tubulin. Values for DBP were normalized internally to tubulin and to the 4 hpi time point to control for any variations in virus input. qPCR was performed using the standard protocol for SYBR Green and analyzed with the QuantStudio 7 Flex Real-Time PCR System.

3.6.10 Plaque assay

Infected cells seeded in 12-well plates were harvested by scraping at the indicated time points and lysed by three cycles of freeze-thawing. Cell debris was removed from lysates by centrifugation at max speed (21,130 g), 4°C, 5 min. Lysates were diluted serially in DMEM supplemented with 2% v/v FBS and 1% v/v Pen/Strep to infect HEK293 cells seeded in 12-well plates. After incubation for 2 h at 37°C, the infection media was removed, and cells were overlaid with DMEM containing 0.45% w/v SeaPlaque agarose (Lonza) in addition to 2% v/v FBS and 1% v/v Pen/Strep. Plaques were stained using 1% w/v crystal violet in 50% v/v ethanol between 6 to 7 days post-infection.

3.6.11 Immunoprecipitation

Approximately 2×10^7 cells were harvested, washed, pelleted and flash frozen for each immunoprecipitation. For IP of hnRNP-C and RALY 50 μ l of Protein G Dynabeads (Thermo Fisher) per sample were washed 3x in IP buffer (50 mM HEPES pH7.4, 150 mM KCl, 2 mM EDTA, 0.5% v/v NP-40, 0.5 mM DTT, 1x cOmplete Protease Inhibitor Cocktail (Roche)) and incubated with 5 μ g of antibody (α -hnRNP-C or α -RALY) rotating at 4°C for 2h. Cell pellets were resuspended in 1 ml IP buffer and incubated for 1 h on ice. Samples were sonicated with a Diagenode Biorupter on low setting for 30 s on and 30 s off for ten rounds at 4°C and spun at max speed (21,130 g) for 10 min at 4°C. 300 μ l of sample were added to washed beads and incubated rotating at 4°C for 2h. Beads were washed 4x in IP wash (same as above but with only 0.05% v/v NP-40). Samples were eluted in 50 μ l 1x LDS sample buffer with 25 mM DTT by boiling for 10 min at 95°C and further processed for analysis by immunoblot.

The following changes were made to the protocol for IP of E1B55K: IP buffer contained 50 mM Tris-HCl pH7.4, 0.1% v/v Triton X-100, 150 mM NaCl, 50 mM NaF, 1 mM Na_3VO_4 , 1x cOmplete Protease Inhibitor Cocktail.

3.6.12 Denaturing *in vivo* ubiquitination assay

Approximately 1×10^7 cells were washed, pelleted and stored at -80°C for each immunoprecipitation. For HEK293 cells, the pellets were thawed on ice and resuspended in 100 μ l of Lysis buffer (1% w/v SDS, 5 mM EDTA, 10 mM DTT, 1x cOmplete Protease Inhibitor Cocktail) with 1 μ l Benzonase (Sigma-Aldrich) by vortexing. Samples were incubated on ice for 5 min and then further denatured by heating to 95°C for 5 min. 900 μ l of Wash buffer (10 mM Tris-HCl pH 7.4, 1 mM EDTA, 1 mM EGTA, 150 mM NaCl, 1% v/v Triton X-100, 0.2 mM Na_3VO_4 , 1x cOmplete Protease Inhibitor Cocktail), passed 10 times through a 23G syringe and spun at max speed (21,130 g) for 5 min at 4°C. A minimum of 800 μ l of sample was added to 50 μ l washed Pierce Anti-HA Magnetic beads (Thermo Fisher). Sample was incubated with beads rotating for 1 h at 4°C, washed 3x in Wash buffer and eluted in 1x LDS sample buffer with 25 mM DTT for further processing by immunoblot.

The following changes were made to the protocol for HeLa cells: the Lysis buffer contained 1% w/v SDS in PBS, Tris buffered saline with Tween-20 was used as wash buffer, Protein G Dynabeads incubated for 1 h with a mix of both α -ubiquitin antibodies listed above were used for the IP.

3.6.13 De-ubiquitination assay

Approximately 1×10^7 HEK293 cells were washed, pelleted and stored at -80°C for each immunoprecipitation. The pellets were resuspended in 1 ml IP buffer B (20 mM HEPES-KOH pH 7.4, 110 mM potassium acetate, 2 mM MgCl_2 , 0.1% v/v Tween-20, 0.1% v/v Triton X-100, 150 mM NaCl, 1 mM DTT, 0.1 mM PMSF) containing 1x cOmplete Protease Inhibitor Cocktail, 20 μM PR-619 (LifeSensors, Cat#: SI9619-5X5MG), 5 mM 1,10-phenanthroline (LifeSensors, Cat#: SI9649), and 1 $\mu\text{l/ml}$ Benzonase (Sigma-Aldrich). Samples were incubated on ice for 30 min, sonicated with a Diagenode Biorupter on low setting for 30 s on and 30 s off for five rounds at 4°C and spun at max speed (21,130 g) for 5 min at 4°C . 925 μl of sample was added to 100 μl washed Pierce Anti-HA Magnetic beads (Thermo Fisher). Sample was incubated with beads rotating for 2 h at 4°C , washed 3x in IP buffer B, resuspended in 100 μl of IP buffer B and split into three 30 μl aliquots. 1 μl of 20 mM PR-619 was added to sample 1 (untreated), 1 μl of USP2 (LifeSensors, Cat#: DB501) was added to sample 2 (DUB^{PAN}) and 2 μl of OTUB1 (LifeSensors, Cat#: DB201) was added to sample 3 (DUB^{K48}). Samples were incubated at 30°C for a minimum of 1 h. Samples were eluted by addition of 10 μl 4x LDS sample buffer with 100 mM DTT and boiling at 95°C for 10 min for further processing by immunoblotting.

3.6.14 CLIP-qPCR

The CLIP protocol was adapted from existing protocols³³². In short, approximately 2×10^7 cells were crosslinked on ice with 0.8 J/cm^2 UV 254 nm in a UV Stratalinker 2400 (Stratagene), washed in PBS with 2 mM EDTA and 0.2 mM PMSF, flash frozen in liquid nitrogen and stored at -80°C . 50 μl of Protein G Dynabeads per sample were washed 3x in iCLIP lysis buffer A (50 mM Tris-HCl pH 7.4, 10 mM NaCl, 0.2% v/v NP-40, 0.1% w/v SDS, 0.5% w/v Sodium deoxycholate, 1x cOmplete Protease Inhibitor Cocktail), resuspended in 100 μl iCLIP lysis buffer A and

incubated with 5 µg of α -hnRNP-C antibody or 5 µl of Normal Mouse Serum Control (Thermo Fisher) rotating 1 h at 4°C. Cell pellets were resuspended in 1 ml of iCLIP lysis buffer B (same as buffer A but with 1% v/v NP-40 and 11 µl of Murine RNase inhibitor (NEB) per 1 ml) and incubated on ice for 15 min. Samples were sonicated with a Diagenode Biorupter on low setting for 30 s on and 30 s off for five rounds at 4°C. 2 µl of TURBO DNase (Thermo Fisher) were added and samples incubated at 37°C for 6 min. Lysates were cleared by centrifugation at max speed (21,130 g) for 15 min at 4°C and supernatants transferred to a new tube. 300 µl of lysate were added to washed beads and incubated rotating at 4°C for 2 h. Beads were washed 2x in High Salt buffer (50 mM Tris-HCl pH 7.4, 1 M NaCl, 1 mM EDTA, 0.2% v/v NP-40, 0.1% w/v SDS, 0.5% w/v Sodium deoxycholate), 2x in Wash buffer (20 mM Tris-HCl pH 7.4, 10 mM MgCl₂, 0.2% v/v Tween-20) and 2x in Proteinase K buffer (100mM Tris-HCl pH 7.4, 50 mM NaCl, 10 mM EDTA, 0.2% w/v SDS). Beads were resuspended in 50 µl Proteinase K buffer and 10 µl removed and processed for immunoblot analysis. 10 µl of Proteinase K (NEB) and 2 µl Murine RNase Inhibitor were added to the remaining beads or to 30 µl of input (10%) and incubated at 50°C for 1 h. The RNA was extracted using a standard protocol for TRIzol (Thermo Fisher) and further processed for RT-qPCR.

3.6.15 Analyzing protein complexes by crosslinking

Cells were crosslinked using disuccinimidyl suberate (DSS, Thermo Fisher) dissolved to 100 mM in DMSO and further diluted to 0.1 mM, 0.3 mM and 1 mM in PBS. Cells seeded as a monolayer in 6-well plates were washed once with PBS, overlaid with 500 µl with PBS or the different DSS dilutions and incubated at room temperature for 30 min. The reaction was quenched by addition of 500 µl of 20 mM Tris-HCl pH 7.4, washed twice with PBS and further processed for immunoblot analysis.

3.6.16 Mass spectrometry

3.6.16.1 Cell lysis and initial desalting

Approximately 10 mg of input was generated from 5x15 cm plates of HeLa cells transduced with rAd E1B55K and rAd E4orf6 constructs for 0 h (mock), 6 h, 8 h, and 10 h. Each timepoint

was produced in biological triplicate. Cells were harvested with 0.25% Trypsin (Gibco), washed 1x in PBS, flash frozen in liquid nitrogen and stored at -80°C. Pellets were thawed, resuspended in 1 ml of lysis buffer (6 M urea, 2 M thiourea, in 50 mM ammonium bicarbonate pH 8.0) with 1x Halt Protease Cocktail inhibitor solution, and incubated for ~5 min on ice. Samples were then diluted 10-fold in 50 mM ammonium bicarbonate, reduced with 10 mM DTT, alkylated with 20 mM iodoacetamide, and digested with trypsin protease overnight. Digestion was quenched by acidification to pH 2 with trifluoroacetic acid (TFA) and samples were desalted over Waters tC18 SepPak cartridges (Cat#: 036805). A 10% aliquot was set aside for global proteomic analysis and all samples were dried to completion.

3.6.16.2 Di-glycine (K- ϵ -GG) enrichment, fractionation, and desalting

A Cell Signaling PTMScan ubiquitin remnant motif kit (Cat#: 5562) was used to enrich for peptides that had been ubiquitinated. Aliquoted beads were cross-linked for 30 minutes in 100 mM sodium borate and 20 mM dimethyl pimelimidate (Thermo Scientific), following the protocol outlined by Udeshi *et. al.*²¹¹. Tryptic peptides were resuspended in IAP buffer (50 mM MOPS, pH 7.2, 10 mM sodium phosphate, 50 mM NaCl) and immunoprecipitated with the provided antibody for 2 h at 4°C. Samples were eluted in LC-MS grade water (Thermo Fisher) with 0.15% v/v TFA and separated into either 3 high-pH fractions (enriched ubiquitinated peptides) or 7 high-pH fractions (global proteome) over C18 columns (The Nest Group, MicroSpin column C18 silica, part#: SEM SS18V, lot#: 091317). Fractionated samples were desalted a final time over Oligo R3 reverse-phase resin (Thermo Scientific, Cat#:1-1339-03).

3.6.16.3 Data acquisition and search parameters

All solvents used in analysis of MS samples were LC-MS grade. Samples were analyzed with an Easy-nLC system (Thermo Fisher) running 0.1% v/v formic acid (Buffer A) and 80% v/v acetonitrile with 0.1% v/v formic acid (Buffer B), coupled to an Orbitrap Fusion Tribrid mass spectrometer. Peptides were separated using a 75 μ m i.d. silica capillary column packed in-house with Repro-Sil Pur C18-AQ 3 μ m resin and eluted with a gradient of 3-38% Buffer B over 85 minutes. Full MS scans from 300-1500 m/z were analyzed in the Orbitrap at 120,000 FWHM

resolution and 5×10^5 AGC target value, for 50 ms maximum injection time. Ions were selected for MS2 analysis with an isolation window of 2 m/z, for a maximum injection time of 50 ms, to a target AGC of 5×10^4 .

MS raw files were analyzed by MaxQuant software version 1.6.0.16, and MS2 spectra were searched against a target + reverse database with the Andromeda search engine using the Human UniProt FASTA database [9606] (reviewed, canonical entries; downloaded November 2017) and adenovirus serotype 5 UniProt FASTA database (reviewed, canonical entries; downloaded February 2018). The search included variable modifications of methionine oxidation, N-terminal acetylation, and GlyGly on lysine residues, with a fixed modification of carbamidomethyl cysteine. For global proteome samples, iBAQ quantification was performed on unmodified, unique peptides only. Trypsin cleavage was specified with up to 2 missed cleavages allowed. Match between runs was enabled with a retention time alignment window of 20 min and a match time window of 0.7 min. False discovery rate (FDR) was set to 0.01.

3.6.17 Proteomics and bioinformatics analysis

3.6.17.1 Data normalization and filtering

MaxQuant output was filtered to remove identified contaminant and reverse proteins. MaxQuant “Intensity” and “iBAQ”²⁸⁷ label free quantification values were used to measure abundances for the K-ε-GG and WCP data, respectively. Abundances were transformed to log₂ values, with unidentified values assigned as “NA”. K-ε-GG and WCP data were normalized separately. Data were normalized by subtracting the sample medians from log₂ transformed abundances within each sample. Both the KεGG and the WCP datasets were filtered at each timepoint to require identification in at least 2 of 3 replicates to be included in the analysis.

3.6.17.2 Fold change, p-value, and z-score calculations

The fold change across time points was calculated by averaging the log₂ transformed, normalized peptide or protein abundances for each replicate identification within a time point and subtracting the averaged abundance values for compared time points. Hypothesis testing was performed using unpaired, two-tailed Students t-tests. The log₂ transformed, normalized

abundance values were compared for cases in which abundances were quantified for at least two replicates within each time point. A p-value threshold of < 0.05 was required to reject the null hypothesis. Multiple testing correction was not performed. Z-scores were used to measure relative abundances within a time point. Z-scores were calculated by averaging the peptide or protein abundances for each replicate identification within a time point and comparing to the mean and standard deviation of averaged values within that time point.

3.6.17.3 Protein ubiquitin abundance calculation

The di-glycine technique quantifies peptide-based abundance of the K- ϵ -GG modification. In order to quantify protein-based K- ϵ -GG abundance changes, we implemented a calculation to combine the peptide-based fold changes for cases in which multiple K- ϵ -GG peptides comprise a modified protein. If a single K- ϵ -GG peptide was identified for a modified protein, that K- ϵ -GG abundance fold change is representative of the protein-based K- ϵ -GG fold change. For cases in which multiple K- ϵ -GG peptides are quantified for a modified protein, the fold changes of each peptide are weighted by the abundance of that peptide and the weighted fold changes are averaged to calculate the protein-based K- ϵ -GG fold change. In cases for which a peptide was reproducibly uniquely identified in the mock or 10 hour transduction time point, a log₂ fold change of 7, representing the largest fold change identified in the dataset, was assigned to this peptide. The K- ϵ -GG abundance fold changes are normalized by the total protein abundance fold change of the respective protein in the corresponding whole cell proteome. The normalization of the K- ϵ -GG fold change by total protein fold change was performed to identify differentially increased or decreased ubiquitination, beyond what would be expected if modification abundance was driven solely by changes in total protein abundance.

3.6.17.4 K- ϵ -GG and whole cell proteome comparison

The protein-based K- ϵ -GG and corresponding whole cell proteome data were compared to identify proteins that exhibited an increase in K- ϵ -GG abundance and to predict the effect of ubiquitination on total protein abundance. The data integration was performed for protein-based K- ϵ -GG and whole cell proteome quantifications for 10 hours post-transduction compared to

untransduced cells. Proteins that exhibited a protein-based, normalized K-ε-GG log₂ fold change > 1 were classified as being increased in ubiquitination in response to E1B55K/E4orf6 expression. Proteins that exhibited whole cell proteome log₂ fold change greater than the mean fold change +/- 1 standard deviation were classified as increased or decreased in total protein abundance. Proteins for which total protein expression did not deviate more than +/- 1 standard deviation from the mean fold change were classified as unchanged in protein abundance in response to E1B55K/E4orf6 expression. Proteins that were ubiquitinated and decreased in total protein abundance were predicted to be potential substrates of E1B55K/E4orf6 ubiquitin-mediated degradation. Proteins that were ubiquitinated and unchanged in total protein abundance were predicted to be non-degraded substrates of E1B55K/E4orf6.

3.6.17.5 Gene ontology and protein-protein interaction network analysis

The proteins that exhibited increased protein-based ubiquitination were analyzed using the ReactomeFI plug-in (6.1.0)³⁰⁵ within the Cytoscape network visualization software (3.4.0)³³³. The protein-protein interaction network was generated using the Gene Set analysis within the "2016" ReactomeFI network version with "linker genes" included. The network was clustered using the in-built ReactomeFI clustering algorithm. Gene ontology "Molecular Function" analysis was performed within the ReactomeFI application for the entire network as well as for each clustered module. Network node attributes included size, which corresponded to degree of increased ubiquitination, and color, which corresponded to total protein increase or decrease. Network edges were set to non-directed, solid lines for all types of Reactome protein-protein interactions.

3.6.18 Statistics and reproducibility

Each experiment was carried out at least in triplicate with reproducible results. The sample size was chosen to provide enough statistical power apply parametric test (unpaired, two-tailed Student's t-test unless otherwise noted). Details regarding statistical analysis are reported in each figure legend.

CHAPTER 4: Conclusions and future directions

4.1 Summary

Viruses, as obligate intracellular pathogens, rely on altering the host cell environment to create favorable conditions for viral replication and ultimately successful infection of the host (**Figure 4.1a**). Viruses have evolved a myriad of strategies to hijack cellular pathways necessary for viral processes and antagonize immune responses mounted by the host to block infection. Studying these complex interactions between viruses and their host not only provides new insights into viral infection, but also reveals regulatory mechanisms for fundamental cellular processes, enables new strategies for antiviral therapies, and can be used to improve viral-based vectors for oncolytic therapy, gene therapy, and vaccine development. My thesis focuses on Ad, a nuclear-replicating virus and important model system for basic research, and the different strategies used by this pathogen to exploit cellular processes. This work illustrates the complex interaction of Ad with its host cell by examining how this virus manipulates both immune responses and host cell environment in favor of viral propagation.

In Chapter 2, we investigated the hypothesis that a viral histone-like protein such as Ad protein VII can interact with and manipulate host chromatin (**Figure 1.9**). We discovered that protein VII localizes to both viral and host DNA during infection and can bind to host nucleosomes in cells and *in vitro*. Furthermore, we identified PTMs on protein VII reminiscent of modifications found on cellular histones and demonstrated that these PTMs regulate the association of protein VII with host chromatin. We also determined the changes in protein composition of host chromatin caused by protein VII and identified several proteins of the HMGB family, including HMGB1, that are sequestered in chromatin through direct interaction with the Ad histone-like protein. HMGB proteins can function as cellular alarmins upon release from the cell by binding to several immune receptors and activating downstream immune responses. We showed that association with protein VII decreases HMGB1 levels in cell culture supernatant and mouse lungs upon immune stimulation. In a mouse model we also showed that protein VII expression resulted reduced immune cell infiltration. This work demonstrated that protein VII, as a viral histone-like

protein, can indeed manipulate cellular chromatin and revealed a novel association between chromatin composition and modulation of host responses towards viral infection (**Figure 4.1b**)²⁵⁸.

In Chapter 3, we hypothesized that as of yet undiscovered substrates of the E1B55K/E4orf6 complex contribute to the RNA processing phenotype observed upon inhibition of viral-mediated ubiquitination (**Figure 1.13**). We used a combined proteomics approach to identify host proteins ubiquitinated upon E1B55K/E4orf6 expression. We then predicted whether ubiquitination of these host proteins induced degradation or resulted in potential alternative outcomes by determining changes in protein abundance through whole cell proteome profiling. This analysis led to the discovery that RBPs are enriched among proteins that were ubiquitinated by the viral ligase but not decreased in abundance. We then focused on the closely related RBPs RALY and hnRNP-C. We validated that these cellular proteins are ubiquitinated but not degraded upon E1B55K/E4orf6 expression or Ad infection. This makes these host RBPs the first confirmed non-degraded substrates of the Ad ubiquitin ligase. Knockdown of RALY and hnRNP-C using siRNA did not impact WT virus infection but rescued RNA processing, protein production, and progeny production of an E1B55K-deleted mutant virus. We also demonstrated that hnRNP-C associates less with viral late RNA in the absence of a functional viral ubiquitin ligase, when viral RNA processing was attenuated. These data suggest that RALY and hnRNP-C are detrimental to processing of Ad RNA and that ubiquitination relieves this restriction. In this project we not only discovered E1B55K/E4orf6 substrates that explain the RNA processing defect of the mutant viruses, but we also uncovered an unexpected role for non-degradative ubiquitination in Ad infection (**Figure 4.2c**).

These two projects revealed two new aspects of the interaction of Ad and viruses in general with host cells. Our discoveries open up exciting new avenues for research regarding viral histone-like proteins and their impact on host chromatin as well as the role of viral-mediated non-degradative ubiquitination in manipulating the host cell environment. This chapter of my thesis focuses on the broader implications of our work and future directions for both projects.

4.2 Viral histone-like proteins and the manipulation of host chromatin

Several viruses encode proteins that have been proposed to function similar to histones for compaction of viral genomes. However, while it has been shown that cellular histones are very important in context of host chromatin and in association with viral genomes, the impact of viral histone-like proteins on the host genome is unknown. Our work on Ad protein VII is the first time it has been demonstrated that viral histone-like proteins can interact with and manipulate cellular chromatin²⁵⁸. This opens up new areas of research investigating additional viral histone-like proteins and other viral proteins associated with the cellular genome, focusing on how these proteins affect host chromatin structure and function, and the contribution of these processes to virus infection. Accordingly, the assays introduced in Chapter 2 and proposed below could be applied to infection by other viruses to answer some of the following questions: Which viral proteins associate with cellular chromatin? What are the changes in protein composition of cellular chromatin upon infection? What are the overall differences in nuclear architecture during infection and which viral proteins are involved? What is the association between global changes of the nucleus and alterations in chromatin state and gene expression? How do these changes in host chromatin contribute to viral infection?

4.2.1 Potential additional functions mediated by proteins VII

In Chapter 2, we demonstrated that protein VII is sufficient to alter host chromatin structure and that recruitment of HMGB1 decreases inflammation mediated by this alarmin²⁵⁸. Protein VII association with chromatin could fulfill more functions than just suppressing the host immune response and there remain several questions worth addressing. For instance, where in the chromatin does protein VII bind? What consequences does the binding of protein VII have on local chromatin structure and functions such as transcription? How do these changes impact Ad infection?

We propose that protein VII localizes to and changes the chromatin structure of distinct locations in the chromatin. This would allow for directed manipulation of host chromatin functions such as altering transcription, and represent an additional way protein VII could alter the state of

the host cell. This hypothesis could be addressed using protein VII chromatin immunoprecipitation (ChIP) upon Ad infection and in our inducible protein VII-HA cell line as compared to control conditions. Analysis of these data could also identify a potential protein VII binding motif, or determine if this viral protein has a preference for binding near chromatin-associated host factors.

Another question is how protein VII binding changes the state and activity of associated chromatin. Other Ad encoded proteins, such as E1A, E1B55K, and E4orf6, have been demonstrated to alter histone PTMs and host transcription^{47-51,79-81,212,226-228}. Protein VII-mediated changes in cellular gene expression may represent an additional strategy used by Ad to alter the host transcriptome. Dramatic changes to the overall chromatin structure are visible upon protein VII expression by IF. In addition, preliminary experiments measuring chromatin accessibility upon protein VII expression using an assay for transposase-accessible chromatin followed by sequencing (ATAC-Seq)³³⁴ revealed large changes in the openness of chromatin when compared to control conditions (data not shown). Other assays such as Hi-C chromatin conformation capture^{335,336} could be used to further examine the overall impact of protein VII and Ad infection on host chromatin structure. In addition, ChIP assays for specific histone modifications associated with active or repressed chromatin as well as RNA Polymerase II occupancy could be used to provide insight into protein VII-mediated changes in chromatin state. The changes to host chromatin structure and composition could also impact host transcription. To test this, we could use RNA-Seq, comparing control conditions to protein VII expression and Ad infection. All of these data could then be combined with the protein VII ChIP data to correlate changes in chromatin structure, chromatin state, and transcription with protein VII binding. Overall, these data provide a foundation for additional experiments that could identify further functions and consequences of protein VII association with host chromatin.

Our data in Chapter 2 indicate that PTMs on protein VII are important for regulating association of this viral histone-like protein with host chromatin²⁵⁸. As protein VII in virions is not acetylated and the protein VII Δ PTM mutant accumulates in nucleoli, we propose that PTMs

regulate the distinct association of protein VII with host or viral DNA. This could allow for control of the separate functions that protein VII fulfills on cellular and Ad genomes. In addition, PTMs on cellular histones have important functions in the regulation of chromatin⁸⁷⁻⁹⁰ and modifications of protein VII could fulfill a similar purpose. To study the importance of these PTMs for Ad infection, different PTM mutations that either mimic or ablate the ability to modify specific residues within protein VII could be introduced into the sequence of the WT Ad genome. We could then define the impact of these PTM mutations on localization of protein VII during infection. We propose that preventing addition of PTMs on protein VII will lead to predominant association of protein VII with Ad DNA and Ad replication compartments. Conversely, we hypothesize that protein VII mutants containing PTM mimics will interact more with cellular chromatin. We could then examine the effect of these protein VII mutants on different stages of Ad infection, quantifying the impact on viral DNA replication by qPCR, viral protein expression by WB and RT-qPCR, and virus production by plaque assay. By examining the effect of these mutations on the Ad life cycle, we could determine the contribution of PTMs to regulation of different functions of protein VII, including protection of incoming genomes, regulation of initial Ad transcription, manipulation of host chromatin, and packaging of new Ad genomes into viral particles. Ultimately this would allow us to assess the contribution of these protein VII functions to Ad infection in general.

In summary, manipulation of host chromatin by protein VII could further alter chromatin function and ultimately contribute to Ad infection in additional ways. The experiments proposed above would begin to address this hypothesis.

4.2.2 Investigating further functions for protein VII-mediated recruitment of HMGB1 to chromatin

Our data in Chapter 2 demonstrate that sequestration of HMGB1 in chromatin reduces extracellular release of this host alarmin and downstream inflammation²⁵⁸. In addition to its extracellular roles, HMGB1 also functions within cells to regulate nucleosome mobility and transcription factor binding to target DNA sequences²⁶⁰. We proposed that by recruiting HMGB1 to chromatin, protein VII also manipulates these intracellular functions of HMGB1, ultimately supporting Ad infection.

To test this hypothesis, we created an HMGB1 KO cell line using CRISPR/Cas9 and examined whether deletion of HMGB1 impacts any stages of Ad infection. Surprisingly, when we examined Ad WT RNA levels, genome replication, protein levels, and progeny production in HMGB1 WT and KO cells, there were no significant differences (see Appendix II, **Figure A2.5**). Therefore, we conclude that HMGB1 is dispensable for the intracellular steps of Ad infection. Considering HMGB1's role in nucleosome mobility, we proposed that this host protein could be recruited to chromatin to facilitate the large structural changes to the host nucleus observed upon protein VII expression and Ad infection. To test this, we transduced HMGB1 WT and KO cells with vectors for GFP and protein VII-GFP and assessed differences in overall chromatin structure by IF. This revealed that protein VII expression was still able to alter host chromatin in the absence of HMGB1¹⁵¹. In addition, we also tested whether HMGB1 was involved in protein VII-mediated suppression of the DDR. However, upon deletion of HMGB1, protein VII was still able to suppress the DDR¹⁵¹. While dispensable for the overall alteration of the nuclear architecture facilitated by protein VII, HMGB1 may still be important for manipulating chromatin structure at a level that cannot be appreciated by confocal microscopy. To explore this theory, we could repeat the assays introduced in Chapter 4.2.1 that examine the impact of protein VII on chromatin structure and state in the HMGB1 KO cells. These experiments would enable us to determine the contribution of HMGB1 to protein VII-mediated local changes in host chromatin function.

Considering HMGB1's function in facilitating transcription factor binding, sequestration of HMGB1 may also contribute to altering the transcriptional landscape of protein VII expressing cells and we have some evidence to support this hypothesis (see Appendix 2 **Figure A2.6**). We tested this hypothesis by examining the impact of protein VII on induction of the interferon response. We found that expression of protein VII reduces IFN β expression upon stimulation with poly(dA:dT), a repetitive double-stranded DNA sequence that can be recognized by cytosolic DNA sensors and triggers an interferon response (**Figure A2.6a**). This demonstrated that protein VII can alter the expression of at least one host gene. Whether this is achieved through manipulation of transcription or other steps involved in IFN β induction, still needs to be

addressed. We further determined that protein VII localization to chromatin is important for this phenotype, as the nucleolar protein VII Δ PTM mutant (introduced in Chapter 2) is unable to decrease IFN β mRNA levels. This suggests that protein VII suppresses IFN β expression through a chromatin-associated mechanism or that other functions of the PTMs are involved in this phenotype (**Figure A2.6a**). We found that protein VII does not impact signaling downstream of IFN, as expression of ISGs upon IFN β treatment is not decreased in the presence of protein VII (**Figure A2.6b**). We next examined whether HMGB1 is important for protein VII-mediated suppression of IFN β . In HMGB1 KO cells transduced with protein VII-GFP, protein VII expression was unable to suppress IFN β . This indicates that HMGB1 is necessary for suppression of IFN β transcription by protein VII (**Figure A2.6c**). Future experiments could focus on determining which of the cytosolic DNA sensors such as cGAS, IFI16, or AIM2 is antagonized by protein VII in a manner dependent on HMGB1. Through HMGB1-mediated manipulation of cellular transcription, protein VII may also regulate expression of other host genes, potentially altering the immune signals produced by infected cells. This would not have impacted single-cycle infection as discussed previously (see Appendix 2 **Figure A2.5**). Instead, this would be important during *in vivo* infection where Ad needs to counteract antiviral signals produced by infected cells to facilitate efficient spread. The RNA-Seq proposed in Chapter 4.2.1 would reveal protein VII-dependent changes in transcription. Repeating these experiments in HMGB1 KO cells followed by RT-qPCR for transcripts of interest would indicate which of these changes in host gene expression are mediated through the protein VII-HMGB1 interaction. Another option is to analyze the supernatant produced by cells upon infection with Ad by mass spectrometry, comparing control conditions to those with deletion of HMGB1 or protein VII (using the Cre-Lox system introduced in Chapter 2). Host factors released by infected cells only in the absence of protein VII and HMGB1 would represent potential targets of protein VII-mediated transcriptional repression.

Overall, while we have shown that HMGB1 is dispensable for intracellular steps of Ad infection and overall manipulation of host chromatin by protein VII, we have some preliminary data supporting a role for the protein VII-HMGB1 interaction in downregulating host transcription,

including the IFN β gene involved antiviral immune responses. The proposed experiments could form the foundation for identifying additional functions of the protein VII-HMGB1 interaction for Ad infection.

4.3 Non-degradative ubiquitination during viral infection and RNA processing

Our study in Chapter 3 revealed an unexpected function for viral-mediated non-degradative ubiquitination in regulating viral RNA processing. While our work has given some indications into how ubiquitin may alter the interaction of RBPs with RNAs and regulate the processing of these transcripts, many aspects of this phenomenon remain to be elucidated. As many of the RBPs identified in our proteomics analysis were also ubiquitinated in mock conditions, studying viral-mediated regulation of RNA processing may also reveal general regulatory roles for ubiquitination of RBPs in processing of associated target RNAs. In addition, our findings represent one of the first examples of how non-degradative ubiquitination mediated by a viral ubiquitin ligase can alter the host cell environment and support viral infection. This observation opens up opportunities to study the role of non-degradative ubiquitination for different viruses.

4.3.1 Elucidating the difference between processing of early and late Ad RNA

It has been known for a long time that deletion of E1B55K specifically affects processing of Ad late, but not early, RNAs^{60,243-246,251,252}. In Chapter 3 we demonstrated that the E1B55K/E4orf6 complex ubiquitinates RBPs RALY and hnRNP-C without inducing degradation, overcoming a detrimental effect these host proteins have on splicing of viral late transcripts. We also showed that these host RBPs bind more abundantly to viral late, but not early RNA, in the absence of a functional viral ubiquitin ligase. This suggests that viral-mediated ubiquitination could directly alter the specificity of host RBPs for RNA. These data also raise questions of how specificity for binding of viral late transcripts is achieved, what differences exist in processing of individual Ad RNAs, and what role ubiquitination plays in this. Studying how E1B55K/E4orf6-mediated ubiquitination can impact viral late RNAs may also provide insights into regulation of RNA processing in general. As introduced in Chapter 1, one of the major differences between Ad early

and late RNAs is that late transcripts are expressed from one common major late promoter and are then heavily alternatively spliced to at least 14 different ORFs in 5 distinct transcription units with separate poly(A) sites (**Figure 1.4**)¹². We propose that E1B55K/E4orf6-mediated ubiquitination is involved in regulating this complex pattern of alternative splicing. Another difference between Ad transcripts is that late RNAs are only produced after onset of viral genome replication, when E1B55K and E4orf6 levels are high. Early RNAs start to be produced before high levels of the Ad ubiquitin ligase are present and thus hnRNP-C and RALY ubiquitination is low. Therefore, these early RNAs may have evolved to be processed efficiently independent of the ubiquitination status of E1B55K/E4orf6 substrates. In both cases we would expect a differential binding pattern of RALY and hnRNP-C to viral early and late transcripts. In addition, this binding pattern should specifically be altered for viral late RNAs when comparing WT and Δ E1B infection, while early RNAs would remain unchanged.

To test these hypotheses, we plan to define the binding sites of hnRNP-C and RALY in Ad RNAs during WT and Δ E1B infection using eCLIP-Seq³³². These data would allow us to differentiate between various scenarios for the effect of RALY and hnRNP-C binding on RNA processing and what changes are facilitated by ubiquitination of these RBPs. We expect that RALY and hnRNP-C interact with distinct regions of late RNAs when comparing WT and Δ E1B infection. One possibility is that ubiquitination regulates the interaction of RALY and hnRNP-C with specific sites within introns and exons of Ad RNA. There are known roles for hnRNP-C in regulating alternative splicing³⁰⁷. For example, binding sites in exons overlapped with splice acceptor sites and correlated with exon exclusion. Binding to introns was correlated with exon inclusion, potentially by positioning splice acceptor sites in a more favorable conformation³⁰⁷. Considering the many alternative splice forms of the viral late RNAs, regulating the interaction of hnRNP-C with these transcripts may be exceedingly important to prevent this RBP from interfering with generation of the different RNA species. In addition, it has been demonstrated that hnRNP-C can act as a nuclear export inhibitor for bound RNAs³³⁷. Therefore, hnRNP-C may also regulate export in addition to splicing. For example, if hnRNP-C binds within an intron, this

interaction is lost upon splicing and the mRNA could be exported. If the binding site is instead within an exon, the interaction would be retained upon intron removal. Accordingly, the host RBP would need to be removed to facilitate export of the RNA. Both of these scenarios, interfering with splicing and blocking RNA export, are supported by the presence of poly-U stretches, the known binding motif for both hnRNP-C and RALY^{311,338,339}, within exons of several late transcripts. However, these potential binding sites need to be validated using the proposed eCLIP-Seq. In addition, it needs to be determined whether these poly-U stretches are absent in early transcripts or located in introns instead. To further demonstrate the functionality of the different binding sites in Ad early and late RNA, we could mutate or swap the specific regions and test their effect on RNA processing. For example, if we remove hnRNP-C binding sites in viral late RNAs, would their processing become independent of E1B55K/E4orf6 mediated ubiquitination?

To gain more mechanistic insight into the impact of ubiquitination on the ability of RALY and hnRNP-C to bind RNA, we could perform *in vitro* ubiquitination experiments. This assay coupled with RNA electrophoretic mobility shift assay (EMSA) or isothermal titration calorimetry (ITC) could be used to determine changes in affinity for RNA upon ubiquitination. Repeating these experiments with different RALY and hnRNP-C mutants with specific domains have been deleted or the ubiquitination sites abolished would show their contribution to regulation of RNA binding.

We could also visualize the extent of binding of hnRNP-C and RALY to viral early and late RNA by immunofluorescence combined with proximity ligation assay (PLA), and then determine differences between WT and Δ E1B infection. This would also reveal the sites in the nucleus where interaction occurs. Immunofluorescence co-staining for other proteins could show the location of hnRNP-C/RALY-RNA complexes in relation to viral replication centers and other RNA processing factors. We could also determine the localization of ubiquitinated hnRNP-C and RALY by PLA for the RBPs and ubiquitin. This approach would reveal whether this event occurs at a specific site in the nucleus, for example at locations of viral late RNA processing. This could provide further insight into the impact of hnRNP-C and RALY on viral RNA processing and how ubiquitination alters this interaction.

Another hypothesis for the distinct regulation of early and late RNAs is that E1B55K/E4orf6 functions as an RNA-dependent ubiquitin ligase. E1B55K contains predicted RNA-binding domains that have been shown to interact with RNA *in vitro*³⁴⁰. However, this function of E1B55K remains controversial. One study showed a lack of RNA binding for E1B55K during infection and demonstrated that mutations in the RNA-binding domains do not affect infection³⁴¹. Another study, however, found some evidence for interaction of E1B55K with RNA³⁴². We propose that E1B55K interacts specifically with viral late RNAs and facilitates localized ubiquitination of RBPs such as hnRNP-C and RALY, specifically altering their function for processing of Ad late RNAs. This would explain why inhibition of Ad-mediated ubiquitination specifically alters the interaction of hnRNP-C with viral late RNA. This hypothesis could be tested by performing E1B55K CLIP-qPCR or eCLIP-Seq to define the interaction of E1B55K with RNA. These techniques could demonstrate whether E1B55K is able to interact with RNAs and if there is a specificity for binding Ad late RNAs. Another option is to perform PLA for viral RNA and E1B55K. This assay could be used to determine whether E1B55K is recruited to sites of late RNA processing. In addition, this technique would also demonstrate association of E1B55K with RNA even if the interaction is not direct but rather facilitated through additional factors.

An alternative scenario is that the protein composition of complexes associated with viral early and late RNA differs, and that ubiquitination plays a role in regulating which RBPs associate with viral RNAs. To test this hypothesis, we could use a modified version of ChIRP (Chromatin isolation by RNA purification)³⁴³ coupled with mass spectrometry that will allow us to identify proteins specifically associated with Ad early and late RNA species during WT and Δ E1B infection. This would enable us to determine whether E1B55K/E4orf6 substrates differentially interact with early or late RNAs, and how this association changes in the absence of a functional viral ubiquitin ligase. We could then knock down individual components of early and late RNP complexes using siRNA to determine their role in viral RNA processing. Another open question is how Ad achieves selective export of its late RNA over host and early RNAs. By identifying the

proteins associated with different RNA species we may identify the RNA export factors responsible for the phenotype.

The techniques and approaches highlighted in this section would allow us to determine the difference in Ad early and late RNA processing and may give insight into regulation of host RNA processing in general.

4.3.2 Investigating the potential manipulation of host RNA processing by Ad

In Chapter 3, we analyzed the interaction of hnRNP-C with one of its known cellular target RNAs during infection and found a trend towards increased interaction in the absence of a functional Ad ubiquitin ligase. Other viruses have been shown to alter host RNA processing by hijacking host RBPs, such as influenza protein NS1 interacting with NS1-BP and hnRNP family member hnRNP-K³⁴⁴. In addition, ubiquitin and other ubiquitin-like proteins have been implicated in the regulation of host RNA processing. Many cellular RBPs have ubiquitin-binding domains or have been found to be ubiquitinated³²⁰. However, the specific roles ubiquitination of different RBPs plays in facilitating proper RNA processing remains to be elucidated. This raises the question whether Ad infection in general and ubiquitination of RBPs by the E1B55K/E4orf6 complex specifically impact host RNA processing. And if so, could this manipulation of host transcripts be beneficial for viral infection?

We already know of several strategies employed by Ad to manipulate host gene expression. Ad early protein E1A has been demonstrated to alter the host cell transcriptome, modulating the cellular environment in a proviral manner⁴⁷⁻⁵¹. In addition, E1B55K and E4orf6 were shown to block p53-dependent transcription, either through their ubiquitin ligase activity or independent of each other^{79-81,212,226-228}. Therefore, manipulation of host transcripts through Ad-mediated ubiquitination could represent another layer of host gene expression control. To determine the impact of Ad on the host transcriptome, we performed an initial RNA-Seq experiment comparing mock and Ad WT infection. Our preliminary analysis revealed large changes in both general RNA abundances and specific splicing events between the conditions (data not shown). To determine which of these differences are dependent on E1B55K/E4orf6-mediated ubiquitination, we could

perform RNA-Seq focusing on host RNAs under mock, Ad WT, and Ad Δ E1B infection conditions, ideally over a time course. By cross-referencing Ad ubiquitin ligase substrates with potential motifs identified through bioinformatics analysis in altered RNA, we could reveal links between RNA processing and ubiquitination of RBPs by E1B55K/E4orf6. To test the importance of the identified RBPs for Ad, we could perform an siRNA knockdown screen and monitor the impact of the specific host factors on Ad WT and Ad Δ E1B infection by Western blot or IF. To test the importance of specific splice events, we could use Morpholino antisense oligos to block specific splice isoforms and assay the effect on Ad infection.

In the case of hnRNP-C and RALY specifically, the eCLIP-Seq experiment proposed in Chapter 4.3.1 above could reveal changes in interaction of these RBPs with cellular RNAs under mock, Ad WT, and Ad Δ E1B conditions. The analysis of these data could reveal whether Ad infection changes the interaction of these RBPs with host RNAs and the potential role for ubiquitination in this process. This technique could also be used to investigate the alterations in RNA-binding patterns of any additional RBPs discovered in the RNA-Seq experiment. An alternative approach to identify host RBPs involved in regulating host RNA splicing during infection could be ChIRP-MS comparing the RNA-associated proteome for those transcripts most significantly altered and those unaffected upon Ad infection. This may reveal specific host RBPs that differentially associate with the altered but not the unaltered host RNAs when comparing mock, Ad WT, and Ad Δ E1B infection. The manipulation of host RNA processing goes beyond the manipulation of RNA splicing and should also include investigation of the block in host RNA export that occurs during the late stage of infection. The ChIRP-MS data could reveal export-related proteins that associate with all host RNA species specifically during infection with Ad WT but not the other conditions.

The approaches described above could help to determine whether and how Ad infection alters host RNA levels and processing. These experiments could also reveal a potential role for E1B55K/E4orf6-mediated ubiquitination in this process. In addition, Ad could function as a tool to understand how ubiquitination of RBPs could affect RNA processing in general.

4.3.3 Exploitation of additional host pathways by Ad-mediated ubiquitination

Our approach to identify novel substrates of E1B55K/E4orf6 introduced in Chapter 3 allows for identification of both degradative and non-degradative ubiquitination. This allowed us to perform a comprehensive analysis of Ad-mediated manipulation of the host cell environment through ubiquitination. In addition to identifying RBPs as a major target of Ad-mediated ubiquitination, our data also highlight other pathways that may be redirected using this strategy. These novel Ad ubiquitin ligase substrates include transmembrane proteins (such as EGFR, CAR), protein chaperones (several heat shock proteins), other components of the host ubiquitin machinery (DUBs such as USP5, USP16, and USP25), proteins directing intracellular transport (several members of the RAB family), proteins involved in metabolism (such as citrate synthase as a component of the TCA cycle), and host factors important for antigen presentation (TAP1, TAP2).

Manipulation of all these different cellular components could be beneficial for Ad infection. We could use a secondary screen to determine which of these ubiquitinated host proteins are of functional importance for Ad infection. Proteins that decrease in protein abundance upon ubiquitination likely represent antiviral host factors that are downregulated by the virus to overcome a host response. For these proteins, a suitable strategy is siRNA mediated knockdown or CRISPR/Cas9 mediated knockout followed by infection with WT Ad and different mutants. Western blot analysis could then be used to identify any impact on viral protein levels. For those host factors that are substrates for non-degradative ubiquitination the situation is more complex. While we saw a rescue for Δ E1B virus infection upon knockdown of RALY and hnRNP-C, this may not be the case for other proteins in this category. A better strategy would be to conduct several screens that include overexpression of the respective protein, expression of a version with K-to-R mutation of the ubiquitin sites, or even CRISPR mutation of the respective endogenous genes in addition to an siRNA screen. Combining the data of these screens could allow us to determine the importance of these proteins for Ad infection and inform which of these candidates merit further investigation.

Another approach to determine which pathways are manipulated by Ad is to identify substrates that are ubiquitinated by different Ad serotypes. Overlap in ubiquitinated proteins or targeted networks would highlight those important for viral infection. We could use a similar mass spectrometry strategy as introduced in Chapter 3 to compare the ubiquitinome and whole cell proteome during infection with human serotypes Ad5 WT, Ad5 Δ E1B, Ad4, and Ad35 in primary-like human bronchial epithelial cells (HBEC3-KT). Furthermore, we could also analyze ubiquitination of host proteins facilitated by the distantly related mouse Ad serotype MAV-1 in mouse embryonic fibroblasts (MEF). We could use the results of these experiments to verify the E1B55K/E4orf6-dependent ubiquitination events during Ad5 infection that we have identified in Chapter 3. In addition, there are other Ad5 proteins that can induce ubiquitination. For example, E4orf3 recruits host proteins to PML nuclear bodies and functions as a SUMO-ligase^{58,63,64,235,345-347}. This can induce ubiquitination of E4orf3 interaction partners through PML resident STUBLs (SUMO-targeted ubiquitin ligases)³⁴⁸. These substrates of Ad-mediated ubiquitination would not have been identified by our initial mass spectrometry experiment in Chapter 3 as we only examined changes in ubiquitination upon E1B55K and E4orf6 expression. The additional serotypes in this proposed experiment have been shown to possess different substrate specificities for ubiquitin-mediated degradation^{239,240,349}. Subsequently, it is likely that these serotypes will also show additional differences in viral-mediated ubiquitination. Comparing the ubiquitinome of these different serotypes will highlight common pathways manipulated by Ad serotypes. In particular, the comparison with the distantly related MAV-1 could highlight these conserved targets. In addition, this approach could also reveal any serotype-specific manipulation of the host environment. Depending on the outcome, this analysis may be expanded to other Ad serotypes with different tissue tropism that would allow us to probe tissue specific use of ubiquitination during Ad infection.

Overall, the experiments highlighted in this section would support a more comprehensive understanding of the role of Ad-mediated ubiquitination in shaping the host cell environment.

4.3.4 The role of non-degradative ubiquitination for viral infection

Our research revealed that Ad can use the same viral protein complex to facilitate both degradative and non-degradative ubiquitination in order to manipulate the host cell environment. We have used a similar proteomics approach to identify substrates ubiquitinated by the HSV-1 E3 ubiquitin ligase ICP0. Preliminary data analysis indicates that ICP0 can also generate both degradative and non-degradative ubiquitination (53 predicted degraded and 142 predicted non-degraded substrates). In both cases, non-degradative ubiquitination appears to be the predominant form of ubiquitination facilitated by these viral ubiquitin ligases. This highlights the possibility that non-degradative ubiquitination is abundantly used by viruses, especially since ICP0 and the E1B55K/E4orf6 complex belong to different types of viral E3 ubiquitin ligases (Type I for ICP0, Type II for E1B55K/E4orf6; see Chapter 1.4.2)¹. Most other studies that examined viral mediated ubiquitination were not designed in such a way that would have allowed for identification of non-degradative ubiquitination. Consequently, we are likely missing insights into many ubiquitin-mediated functions during virus infection. This is particularly interesting as non-degradative ubiquitin chains have very diverse functions and would allow for more targeted manipulation of the host cell environment than proteasomal degradation alone. Using our approach of combining the di-glycine remnant profiling to define the ubiquitinome combined with whole cell proteome analysis (or similar strategies) would allow identification of non-degraded substrates of viral ubiquitin ligases and should be considered in future studies to allow more thorough study of viral-mediated ubiquitination. These studies could also provide new insights into the function of ubiquitin by identifying different pathways that are regulated by ubiquitination, or reveal new roles of ubiquitin in those instances. There is a particularly large potential for defining new functions of the less commonly used ubiquitin-chain types, which have remained understudied so far.

Viral E3 ubiquitin ligases also represent a useful tool to understand the determinants for degradative and non-degradative ubiquitination facilitated by the same ubiquitin ligase. There is increasing evidence that many cellular ubiquitin ligases, such as Cullin complexes, can facilitate

different types of ubiquitination³²¹⁻³²³. The Ad E1B55K/E4orf6 complex or other viral ubiquitin ligases could be used to define how this is regulated. For example, our lab has previously used a large array of E1B55K mutants to determine different residues important for MRN and p53 ubiquitination and subsequent degradation²¹⁹. This resource could allow us to determine whether degraded and non-degraded substrates interact with different residues and domains of E1B55K and potentially reveal patterns that are involved in regulating the different ubiquitination outcomes. Cullin complexes, such as the one hijacked by E1B55K/E4orf6, commonly associate with E2 proteins that facilitate degradative K48 ubiquitination¹⁹⁶. However, we have shown that non-K48 ubiquitin is associated with RALY and hnRNP-C during Ad infection. Therefore, additional E2 proteins must exist that can function with Cullin complexes to facilitate ubiquitination. These E2 proteins could be identified using the Ad ubiquitin ligase, either through siRNA mediated knockdown of different E2 proteins and probing for loss of RALY and hnRNP-C ubiquitination, or by IP of the viral proteins and identification of interacting proteins by mass spectrometry. The latter approach would also reveal if other proteins are involved in regulating ubiquitination of different substrates. For example, a study published earlier this year showed that HIV protein Vif, which hijacks a host Cullin complex, can also recruit a second E3 ubiquitin ligase to ubiquitinate substrates using a E1-E2-E3/E3-substrate ubiquitination mechanism³⁵⁰.

The experiments discussed in this section highlight the potential of studying viral-mediated non-degradative ubiquitination for increasing our understanding of virus-host interaction and revealing new roles for ubiquitination in regulating cellular processes. These studies could also provide new targets for antiviral therapies as preventing non-degradative ubiquitination or inhibiting host proteins manipulated by viruses through this strategy may be less disruptive than the inhibition of the proteasome.

4.4 Implications for oncolytic virus design

Oncolytic viruses, such as Ad-based vectors, are commonly designed with two aims in mind. The first is specific replication of the viral vector in cancer cells followed by cell lysis. The second

is production of an immune signal that can overcome the anti-inflammatory environment created by the cancer cells and induce the immune system to attack the cancer cells. Both projects described in Chapter 2 and 3 of this thesis can inform better design of oncolytic Ad vectors, addressing both of these aims.

While protein VII is dispensable for virion assembly and genome packaging, it is essential for uncoating in the endosome of the next cells¹⁵³. Because of this important function in propagation of infection, protein VII is present in Ad-based vectors. Sequestration of HMGB1 in host chromatin by protein VII reduces inflammation in response to the virus. While this is beneficial for WT Ad infection, it is unfavorable for the purpose of an oncolytic virus. Therefore, it would be ideal to separate the role of protein VII in packaging viral genomes from the anti-inflammatory sequestration of HMGB1 in chromatin. We discovered that while protein VII from human Ad serotypes interacts with HMGB1, protein VII from murine serotype MAV-1 does not (See Appendix 2 **Figure A2.1**). MAV-1 protein VII still fulfills its role in packaging of Ad genomes, and as such separates the function in virion assembly from HMGB1 sequestration. Therefore, one strategy to increase the immunogenicity of Ad oncolytic vectors could be to replace the human Ad protein VII with its murine counterpart. This would enable HMGB1 release during infection without compromising virion propagation. An alternative approach could be to mutate human Ad protein VII to ablate HMGB1-binding. We have used the difference in HMGB1 binding between human and murine protein VII to map the region of human Ad protein VII that interacts with this host factor (See Appendix 2 **Figure A2.2**). These data could be used as a starting point to create more refined human Ad protein VII mutants that function normally in virion assembly but do not interact with HMGB1.

The initial theory of using Ad as an oncolytic vector was based on $\Delta E1B$ viruses and the idea that these Ad mutants could replicate more efficiently in cells with defective p53. It has now been demonstrated that the oncolytic potential of these viruses is independent of the p53 status but rather relies on altered RNA processing^{241,242}. Many cancer cells exhibit altered processing of RNA and exhibit changes in expression in many of the RBPs identified in our study in Chapter

3^{351,352}. The insight into interaction of E1B55K/E4orf6-mediated ubiquitination and viral RNA processing will allow us to better define biomarkers that could predict which cells support replication of an Ad vector lacking E1B55K and therefore better target the use of these oncolytic viruses. In addition, we could further define which residues in E1B55K facilitate the interaction with RALY and hnRNP-C (or additional RBPs). This would enable the creation of mutant viruses that encode a E1B55K mutant protein that still facilitates the degradation of DDR proteins and p53 but does not ubiquitinate RBPs and therefore would still be dependent on altered RNA processing in cancer cells.

Overall, a better understanding of how Ad interacts with its host cell will enable the design of better Ad-based vectors for treating disease.

4.5 Concluding remarks

Ad has long been recognized as an excellent tool for studying virus-host interactions as well as elucidating fundamental cellular processes. The work presented in this thesis reveals previously unknown strategies used by Ad to manipulate the host chromatin and RNA processing in favor of viral infection. Our findings and experimental approaches could serve as the basis for further research into the role of viral histone-like proteins and their impact on host chromatin structure as well as function, and the study of viral-mediated ubiquitination, especially non-degradative ubiquitination. In addition, our work could be expanded to further improve Ad-based vectors used in oncolytic therapy and to investigate the regulation of host processes such as splicing and chromatin structure.

APPENDIX

Appendix 1: Differential Salt Fractionation of Nuclei to Analyze Chromatin-associated Proteins from Cultured Mammalian Cells

This chapter has been published as:

Herrmann C, Avgousti DC, Weitzman MD. Differential Salt Fractionation of Nuclei to Analyze Chromatin-associated Proteins from Cultured Mammalian Cells. *Bio Protoc* **7** (2017). **PMID: 28845440**.³⁵³

A1.1 Abstract

Nucleosomes are the core units of cellular chromatin and are comprised of 147 base pairs (bp) of DNA wrapped around an octamer of histone proteins. Proteins such as chromatin remodelers, transcription factors, and DNA repair proteins interact dynamically with chromatin to regulate access to DNA, control gene transcription, and maintain genome integrity. The extent of association with chromatin changes rapidly in response to stresses, such as immune activation, oxidative stress, or viral infection, resulting in downstream effects on chromatin conformation and transcription of target genes. To elucidate changes in the composition of proteins associated with chromatin under different conditions, we adapted existing protocols to isolate nuclei and fractionate cellular chromatin using a gradient of salt concentrations. The presence of specific proteins in different salt fractions can be assessed by Western blotting or mass spectrometry, providing insight into the degree to which they are associated with chromatin.

A1.2 Background

Many chromatin-associated proteins are insoluble under low salt conditions because of their charged-based interaction with DNA or histones. Since salt disrupts charged-based protein-DNA and protein-protein interactions, chromatin-associated proteins become more soluble with increasing concentration of NaCl²⁶⁷. Proteins strongly bound to DNA are expected to elute with

high salt whereas loosely bound proteins, such as transcription factors, will elute with low salt. We are specifically interested in how virus infection alters the composition of factors associated with the cellular chromatin. Nuclear replicating viruses, such as adenovirus, herpes simplex virus, and Epstein-Barr virus, dramatically alter the appearance of the host chromatin during infection^{155,156,158,258}. We hypothesized that these changes in appearance are partly due to differences in protein composition of host chromatin. Changes in host chromatin could reflect antiviral defenses mounted by the cell or active manipulation by the virus. To compare association of proteins with chromatin in uninfected and infected cells we developed this protocol to fractionate nuclei using a salt gradient (**Figure A1.1**). In this protocol we isolate nuclei, digest the DNA down to mono-nucleosome length, and then wash the nuclei with increasing concentrations of salt, collecting each fraction for analysis by Western blotting. We recently used this protocol to elucidate changes to cellular chromatin during infection with adenovirus²⁵⁸. We now present this protocol as a general approach to monitor association of proteins with chromatin under a wide range of perturbing conditions.

A1.3 Materials and Reagents

Note: Comparable reagents from different suppliers may be used for the protocol.

1. 150 mm tissue culture dishes (Corning, Falcon®, catalog number: 353025)
2. 15 ml centrifuge tube (Corning, catalog number: 430790)
3. 5 ml pipettes (VWR, catalog number: 89130-908)
4. Transfer pipette (Denville Scientific, catalog number: P7222)
5. 30 ml glass tube (Corning, Corex®, catalog number: 1-8445-30)
Note: This product has been discontinued.
6. 1.7 ml microcentrifuge tubes (VWR, catalog number: 87003-294)
7. Pipette tips
 - 0.1-10 µl (Corning, catalog number: 4153)
 - 1-200 µl (Corning, catalog number: 4126)
 - 100-1,000 µl (Corning, catalog number: 4129)
8. 250 ml sterile disposable filter units with 0.2 µm PES membrane (Thermo Fisher Scientific, Thermo Scientific™, catalog number: 568-0020) (used for Buffer I and Buffer II)

9. 60 ml syringe (BD, catalog number: 309653) (used for Buffer IV.80, IV.150, IV.300 and IV.600)
10. 25 mm syringe filter (Pall, catalog number: 4612) (used for Buffer IV.80, IV.150, IV.300 and IV.600)
11. A549 cells (ATCC, catalog number: CCL-185)
12. Ham's F-12K cell culture media (Thermo Fisher Scientific, Gibco™, catalog number: 21127-022)
13. Fetal bovine serum (FBS) (VWR, catalog number: 89510-182)
14. Penicillin-streptomycin (Pen/Strep) (Thermo Fisher Scientific, Gibco™, catalog number: 15140-122)
15. Trypsin-EDTA (0.25%) (Thermo Fisher Scientific, Gibco™, catalog number: 25200-056)
16. Phosphate buffered saline (PBS) (Mediatech, catalog number: 21-030-CM)
17. Liquid nitrogen
18. NP-40/IGEPAL® CA-630 (Sigma-Aldrich, catalog number: I8896) (10% stock solution in H₂O)
19. Phenylmethanesulfonyl fluoride (PMSF) (Sigma-Aldrich, catalog number: P7626) (0.1 M stock solution in isopropanol)
20. 1,4-dithiothreitol (DTT) (Sigma-Aldrich, catalog number: 10197777001) (1 M stock solution in HEPES buffer, pH 7.75)
21. Protease inhibitor cocktail (Roche Diagnostics, catalog number: 11697498001) (prepared as 50xstock solution in H₂O according to manufacturer instructions)
22. Micrococcal nuclease (MNase) (Sigma-Aldrich, catalog number: N3755) (0.2 U/μl stock solution in H₂O)
23. Ethylene glycol-bis(2-aminoethylether)-N,N,N',N'-tetraacetic acid (EGTA) (Sigma-Aldrich, catalog number: E3889) (0.1 mM stock solution in H₂O, pH = 10)
24. PCR purification kit (QIAGEN, catalog number: 28104)
25. Orange G (Sigma-Aldrich, catalog number: O3756) (0.35% [w/v] orange G with 30% [w/v] sucrose in H₂O for 6x stock solution)
26. 100 bp DNA ladder (New England Biolabs, catalog number: N3231)
27. Broad range protein ladder (Thermo Fisher Scientific, Thermo Scientific™, catalog number: 26623)
28. GelRed nucleic acid gel stain (Biotum, catalog number: 41003)
29. LDS sample buffer (4x) (Thermo Fisher Scientific, Novex™, catalog number: NP0007)
30. Sucrose (Fisher Scientific, catalog number: BP220-1)
31. Potassium chloride (KCl) (Sigma-Aldrich, catalog number: P9541) (1 M stock solution in H₂O)
32. Sodium chloride (NaCl) (Sigma-Aldrich, catalog number: S9625) (5 M stock solution in H₂O)

33. Magnesium chloride hexahydrate ($\text{MgCl}_2 \cdot 6\text{H}_2\text{O}$) (Sigma-Aldrich, catalog number: M2670) (1 M stock solution in H_2O)
34. Trizma base (Sigma-Aldrich, catalog number: T1503) (1 M stock solution in H_2O adjusted to pH 7.4 with HCl)
35. UltraPure agarose (Thermo Fisher Scientific, Invitrogen™, catalog number: 16500500)
36. Hydrochloric acid 6.0 N solution (HCl) (Fisher Scientific, catalog number: MK-H168-4)
37. Calcium chloride dihydrate ($\text{CaCl}_2 \cdot 2\text{H}_2\text{O}$) (Sigma-Aldrich, catalog number: C5080) (0.5 M stock solution in H_2O)
38. Triton X-100 (Sigma-Aldrich, catalog number: T8787)
39. HEPES (Sigma-Aldrich, catalog number: H3375) (1 M stock solution in H_2O adjusted to pH 7.9 with NaOH)
40. Sodium hydroxide (NaOH) (AMRESCO, catalog number: M137)
41. Buffer I.A and I.B (see Recipes)
42. Buffer II (see Recipes)
43. Buffer III.A and III.B (see Recipes)
44. Buffer IV.80, IV.150, IV.300 and IV.600 (see Recipes)
45. Hypotonic buffer (see Recipes)

A1.4 Equipment

Note: Equipment with similar properties may be used for the protocol, however, we recommend using a specific kind of reusable centrifuge tubes (listed in 5) to ensure high quality isolation of nuclei.

1. CO_2 incubator for cell culture (BINDER, catalog number: 9040-0082)
2. Benchtop centrifuge (Beckman Coulter, model: Allegra X-14R)
3. Rotors for benchtop centrifuge (Beckman Coulter, models: SX4750 for tissue culture and FX6100 for 10,000 \times ; g spins, or seminal rotors suitable for high speeds)
4. Adapters for FX6100 rotor (Beckman Coulter, catalog number: 392830)
5. 30 ml reusable centrifuge tubes (Sigma-Aldrich, catalog number: T2793)
6. Tabletop centrifuge 5424 R (Eppendorf, model: 5424 R)
7. 1 ml tissue grinder (Dounce homogenizer) with tight fitting pestle (Ace Glass Incorporated, catalog number: 8343-01)
8. Water bath (Fisher Scientific, model: Isotemp™ Digital-Control Water Baths Model 215, catalog number: 15-462-15Q)
9. Tube rotator (VWR, catalog number: 10136-084)

10. Pipettes

- 1-10 μ l (Gilson, catalog number: F144055P)
- 2-20 μ l (Gilson, catalog number: F144056M)
- 20-200 μ l (Gilson, catalog number: F144058M)
- 100-1,000 μ l (Gilson, catalog number: F144059M)

11. Agarose gel electrophoresis systems (Thermo Fisher Scientific, Thermo Scientific™, model: Owl EasyCast B1A system)
12. Fluorescence and chemiluminescence gel imaging system (Syngene, model: G:BOX Chemi XT4)
13. Heat block (Fisher Scientific, model: Isotemp™ Digital Dry Baths/Block Heaters, catalog number: 88-860-022)
14. Protein electrophoresis apparatus (Bio-Rad Laboratories, model: Mini-PROTEAN® Tetra Vertical Electrophoresis Cell for Mini Precast Gels, catalog number: 1658005)
15. Western blot apparatus (Thermo Fisher Scientific, model: SureLock™ Mini-Cell Electrophoresis System)

A1.5 Software

1. ImageJ (freely available from National Institutes of Health, <https://imagej.nih.gov.proxy.library.upenn.edu/ij/>)

A1.6 Procedure

A1.6.A Cell culture

Note: This protocol was optimized for nuclear isolation and chromatin fractionation of roughly 4×10^7 A549 cells (for A549 cells that is approximately two 100% confluent 150 mm cell culture dishes). This number of cells was chosen for efficient nuclear isolation as described in Procedure B. This protocol can be used for other cell types but should be optimized accordingly.

1. For each condition, grow roughly 4×10^7 A549 cells in F-12K media with 10% FBS and 1% Pen/Strep.

Note: Time treatments such that the required cell number is reached at time of harvest.

2. Harvest cells using trypsin and combine into one 15 ml tube per condition.

3. Centrifuge for 2 min, 500 × *g*, room temperature using benchtop centrifuge (Allegra X-14R with rotor SX4750).
4. Wash cells once with 10 ml of PBS and centrifuge again for 2 min, 500 × *g*, room temperature.
5. Aspirate as much of the supernatant as possible without disturbing the cell pellet.
6. Flash freeze samples in liquid nitrogen.
7. Store samples at −80 °C until ready to process.

A1.6.B Nuclear isolation

Note: This section describes two alternative methods for nuclear isolation. The procedure detailed in B1 yields a clean nuclear fraction but B2 is recommended for highly mobile nuclear proteins that are lost from the nuclear fraction when mild detergents are used as described in B1 (see example in **Figure A1.2**).

1. Nuclear isolation using mild detergent and sucrose cushion.

Note: This section describes permeabilizing the cell membrane using a mild detergent (NP-40), followed by separation of the nuclei from cytoplasmic debris by sucrose cushion. The sucrose cushion consists of a layer with 1.2 M sucrose at the bottom (Buffer II) and a layer with 0.32 M sucrose on top (Buffer I, **Figure A1.3A**). The nuclei are more dense than the 1.2 M sucrose buffer and will pellet at the bottom of the tube while the less dense cytoplasmic debris will remain in the upper sucrose layer (**Figure A1.3B**).

- a. Thaw cells on ice (about 10 min until pellet is loose).
- b. In the meantime, prepare one aliquot each of Buffer I.A and I.B by addition of PMSF, DTT, and protease inhibitor cocktail immediately before use (see Recipes for final concentrations). Add NP-40 to Buffer I.B.
- c. Gently resuspend cells in 2 ml of Buffer I.A using a 5 ml pipette. Avoid the formation of bubbles.
- d. Set aside 50 µl of the cell suspension in a new tube labeled 'cells fraction'.
- e. Add 2 ml of Buffer I.B containing NP-40 to the 2 ml of cell suspension and mix gently by inverting the tube 2-3 times.
- f. Incubate samples on ice for 10 min. Mix gently by inverting after 5 min.
- g. Pipette 8 ml of ice-cold Buffer II into 30 ml reusable centrifuge tubes (one per sample).
- h. Carefully layer cell suspension onto Buffer II (**Figure A1.3A**).

- i. If the number of tubes is even, balance the tubes with Buffer I.A before centrifugation. If the number of tubes is uneven, use an additional tube containing water as balance.
- j. Centrifuge for 20 min, $10,000 \times g$, 4°C using benchtop centrifuge (Allegra X-14R with rotor FX6100) with low brakes (deceleration setting 1 for this centrifuge model, 5-10 min of deceleration for other centrifuge models) to avoid disruption of pellet.
Note: Use the adapters listed in the Equipment section under 4 to fit the 30 ml reusable centrifuge tubes into the FX6100 rotor. The nuclei form a dense pellet at the bottom of the tube while the cytoplasmic debris remains in the upper sucrose layer, **Figure A1.3C**.
- k. Carefully remove the supernatant using a transfer pipette. Keep pellet containing the nuclei and proceed to Procedure C.

2. Nuclear isolation by manual disruption

Note: Using mild detergents such as NP-40 for nuclear isolation is important to ensure that the nuclear membrane remains largely intact. In some cases, highly mobile nuclear proteins such as HMGB1²⁷³ may diffuse out of the nucleus upon isolation with this method. To prevent loss of these proteins from the nuclear fraction, we adapted an alternative method that relies on a hypotonic buffer and subsequent manual disruption of the cell membrane using a Dounce homogenizer. The short centrifugation times in this step minimize diffusion of these proteins out of the nuclei (**Figure A1.2**).

- a. Thaw cells on ice (about 10 min until pellet is loose).
- b. Gently resuspend cells in 1 ml of hypotonic buffer and transfer into a 1.7 ml tube using a P1000 pipette with the tip cut (or wide orifice pipette tips) to avoid disrupting the cellular membranes.
- c. Set aside 25 μl of the cell suspension in a new tube as 'cells fraction'.
Note: This is proportional to the 50 μl aliquot taken from 2 ml of cell suspension in step B1.
- d. Incubate on ice for 30 min.
- e. Pre-cool the Dounce homogenizer and the pestle on ice for at least 5 min.
- f. Transfer the cell suspension to cold Dounce homogenizer using a transfer pipette.
- g. Disrupt the cell membrane using 40 strokes of the tight-fitting pestle. Minimize the formation of bubbles.
- h. Transfer sample to 1.7 ml tube using a transfer pipette.
- i. Centrifuge for 5 min, $1,500 \times g$, 4°C using a tabletop centrifuge.

- j. Carefully remove the supernatant using a P1000 pipette. Transfer supernatant and label as 'cytosol fraction' if desired. Keep pellet containing the nuclei and proceed to Procedure C.

Note: The nuclei form a loose pellet at the bottom of the tube that can be easily disturbed. The cytoplasmic fraction in step B1 is too dilute to isolate as a result of the sucrose cushion.

A1.6.C Micrococcal nuclease digestion

Note: In this step the DNA is digested to the length of mono-nucleosomes (roughly 150 bp) using MNase. While partial MNase digest in combination with nuclear fractionation by salt gradient can be used to separate euchromatin from heterochromatin²⁶⁷, our protocol aims to identify global association of proteins with chromatin and does not distinguish between different types of chromatin. Subsequently, it is important that the DNA is completely digested into mono-nucleosomes to break up chromatin and allow for elution of all soluble proteins in Procedure D (**Figure A1.4**). EGTA is used instead of EDTA to stop the MNase digestion as EGTA preferentially chelates Ca²⁺ ions that are necessary for MNase enzymatic activity but does not impact Mg²⁺ ions important for protein-protein interactions. Proteins loosely bound to chromatin elute during MNase digest and can be detected in the supernatant collected in this section of the protocol.

1. Prepare and cool Buffer III.A and III.B.
2. Add 400 µl Buffer III.A to the nuclei.
3. Gently resuspend the nuclei using a P1000 pipette with the tip cut (or wide orifice pipette tips) to avoid disrupting the nuclear membranes.
4. Add 5 µl of MNase (1 U) and incubate at 37 °C (in a water bath) for 30 min.
5. Mix every 10 min by gently inverting the tube 2-3 times.
6. After 30 min add 25 µl of ice-cold 0.1 M EGTA to stop the digest.
7. Set aside a 60 µl aliquot of the nuclear suspension as 'nuclei fraction' and for DNA isolation to confirm the sufficient digest of DNA (described in Procedure E).
8. Centrifuge for 10 min, 400 ×; g, 4 °C.
9. Transfer supernatant to fresh tube and label 'MNase fraction'.
10. Wash the nuclei once by resuspending them in 400 µl Buffer III.B.
11. Centrifuge again for 10 min, 400 ×; g, 4 °C. Discard the supernatant.

A1.6.D Chromatin fractionation

Note: In this step the nuclei are further fractionated using buffers with increasing amounts of NaCl. Proteins only weakly bound to DNA are expected to be soluble under low salt conditions and will elute from nuclei in the buffers with low NaCl concentration. Proteins tightly bound to chromatin only become soluble under high salt conditions and only elute from nuclei in the buffers with high NaCl concentration.

1. Gently resuspend the nuclei in 400 μ l Buffer IV.80 using a P1000 pipette with the tip cut (or wide orifice pipette tips).
2. Rotate at 4 °C for 30 min.
3. Centrifuge for 10 min, 400 \times ; *g*, 4 °C.
4. Transfer supernatant to fresh tube and label '80 mM fraction'.
5. Repeat steps D1-D4 with Buffer IV.150, IV.300 and IV.600 in that order. Keep the supernatants as fractions '150 mM', '300 mM' and '600 mM', respectively.
6. Prepare samples for Western blot immediately (see Table A.1) or store at -20 °C.

A1.6.E DNA isolation and DNA gel

Note: In this step DNA is isolated from the samples after MNase digestion to test the length of DNA fragments. The goal is to digest the DNA down to mono-nucleosome level of around 150 bp to ensure optimal chromatin fractionation (**Figure A1.4**). It is important that orange G or another small molecular weight dye is used for loading the DNA. Commonly used DNA loading dyes such as bromophenol blue run around the same size as 150 bp of DNA and may obscure the results.

1. Dilute 10 μ l of the 'nuclei' fraction in 90 μ l H₂O for better DNA purification.
2. Use a PCR purification kit to isolate the DNA from this sample following the kit instructions. Elute the DNA in 30 μ l of H₂O.
3. Take out 5 μ l (about 5 μ g) of DNA and add 1 μ l of 6 \times Orange G. Keep the rest of the DNA on ice until results are finalized or freeze at -20 °C.
4. Run samples and a 100 bp ladder on a 2% agarose gel containing 1 \times GelRed at 100 V for 1 h.
5. Visualize the DNA using gel imager and check for prominent DNA band of around 150 bp with minimal DNA laddering (Figure 4).

A1.6.F Verifying the quality of nuclear fractionation by Western blot

Note: The quality of the nuclear fractionation can be analyzed using SDS-PAGE combined with Western blotting (Figure 1G). Efficient nuclear isolation can be tested by probing for proteins such as tubulin that are only found in the cytoplasm. The quality of chromatin fractionation can be tested by probing for histone proteins such as histone H3 or proteins expected to bind histone tails such as bromodomain containing protein Brd1³⁵⁴. The interaction of the histone H3 and Brd1 with chromatin should only be disrupted under high salt conditions. In addition, proteomics can be performed to identify changes to global chromatin composition under different conditions. Further details concerning mass spectrometry of salt fractions can be found in (Avgousti et al., 2016²⁵⁸).

1. Prepare samples for analysis by Western blotting according to Table 1.
2. Denature samples at 95 °C (in a heat block) for 10 min.
3. Analyze 15 µl of each sample via SDS-PAGE and Western blot. Probe for tubulin and histone H3 as controls.

A1.7 Data analysis

To compare the association of a protein of interest with chromatin under different conditions, the samples should be run on the same SDS-PAGE gel and Western blot as different exposures may confound the interpretation. Expected results for various proteins are described here to aid in data analysis, though each protein of interest tested should be considered separately. The 'cells' fraction represents the total amount of protein in a sample for relative comparison with other fractions. A cytoplasmic protein such as tubulin should only be present in the 'cells' fraction (**Figure 1G**). Nuclear proteins should also be present in the 'nuclei' fraction as seen for H3 and Brd1 (**Figure 1G**). The band intensity for the remaining fractions represents the solubility of nuclear proteins under these conditions. H3 and Brd1 have the highest band intensity in the '600 mM' fraction, signifying greater solubility under high salt conditions typical for chromatin-associated proteins. For HMGB1 the highest band intensity can be observed for the 'MNase' and '80 mM' fraction, indicating solubility under low salt conditions, suggesting weak association with chromatin. Differences in band intensity for different fractions can be quantified using ImageJ

(freely available from National Institutes of Health, <https://imagej.nih.gov.proxy.library.upenn.edu/ij/>).

Details concerning data analysis for mass spectrometry of salt fractions can be found in (Avgousti et al., 2016²⁵⁸).

A1.8 Notes

This protocol is suitable to compare changes in the chromatin-associated proteome under different conditions. We have used this method to show changes to cellular chromatin during infection with adenovirus²⁵⁸.

A1.9 Figures

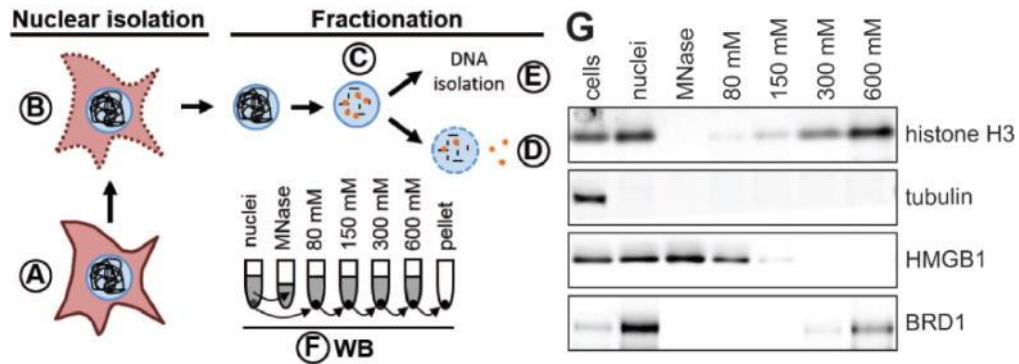


Figure A1.1 | Schematic of nuclear fractionation and example Western blot. **A.** Roughly 4×10^7 cells are prepared per condition. **B.** Plasma membranes are permeabilized and nuclei are isolated either by sucrose cushion (step B1) or using a Dounce homogenizer (step B2). **C.** DNA is digested to mono-nucleosome length using MNase. Proteins loosely bound to chromatin elute during this step. **D.** The chromatin is further fractionated by washing the nuclei in buffers with increasing salt concentration. **E.** The DNA is isolated from nuclei to confirm digestion of the cellular genome to 150 bp fragments. **F.** The quality of fractionation is tested using SDS-PAGE and Western blot (WB) for control proteins (e.g., tubulin, histone H3). The grey colored supernatants (and the pellet in case of the nuclei) represent the samples used for Western blot analysis. **G.** Example Western blot analysis of chromatin fractionation. Tubulin is found only in the cytoplasmic fraction and is a suitable control to test the quality of nuclear isolation. Histone H3 is a component of cellular chromatin and only elutes from nuclei in buffers with high salt. HMGB1 is a highly mobile nuclear protein and thus elutes during MNase digest and under lower salt conditions. Brd1 directly binds to histone tails and elutes under high salt conditions.

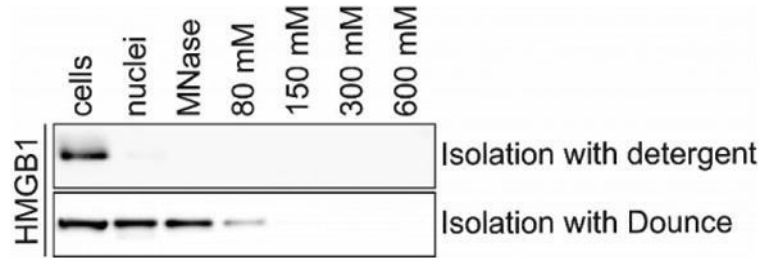


Figure A1.2 | Fractionation of nuclear protein HMGB1 can differ depending on the method of nuclear isolation. Western blot of chromatin fractionation of A549 cells using different methods of nuclear isolation. HMGB1 is lost from nuclei during nuclear isolation B1 using NP-40 and a sucrose cushion. HMGB1 is retained in the nuclear fraction during isolation of nuclei with the alternative method described in step B2.

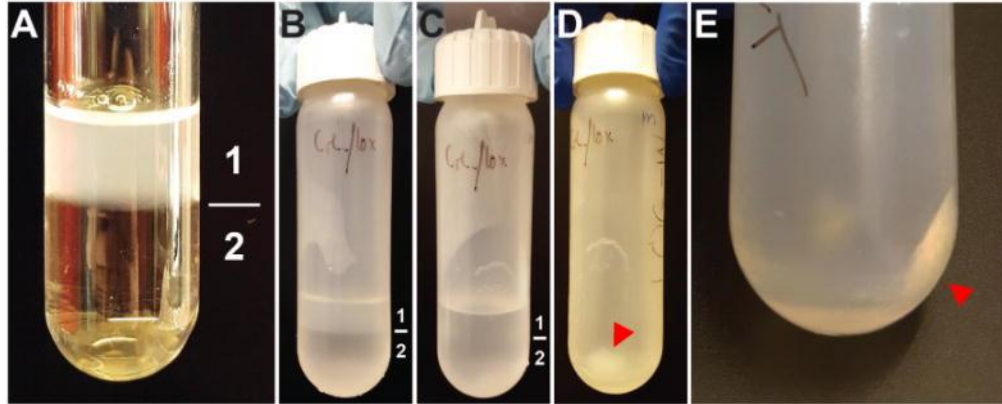


Figure A1.3 | Intermediate steps of nuclear isolation. **A**, Layers of the sucrose cushion. 1 = cells resuspended in Buffer I containing 0.32 M sucrose. 2 = Buffer II containing 1.2 M sucrose. Clear glass tube was used for better visibility of the two layers. **B**, Layers of sucrose cushion as seen before the centrifugation step in the 30 ml reusable tube. Layer 1 = Buffer I. Layer 2 = Buffer II. **C**, Layers of sucrose cushion as seen after the centrifugation step in the 30 ml reusable tube. Layer 1 = Buffer I. Layer 2 = Buffer II. **D** and **E**, Pellet of nuclei after spin at 10,000 \times *g* indicated by red arrow. The buffers were removed before these pictures were taken.

Fraction	Sample	H₂O	4x LDS sample buffer with 10% DTT
cells (from B1)	10 µl	20 µl	10 µl
cells (from B2)	5 µl	25 µl	10 µl
nuclei	10 µl	20 µl	10 µl
MNase	30 µl	-	10 µl
80 mM	30 µl	-	10 µl
150 mM	30 µl	-	10 µl
300 mM	30 µl	-	10 µl
600 mM	30 µl	-	10 µl

Table A1.1 | Preparation of different fractions for Western blot.

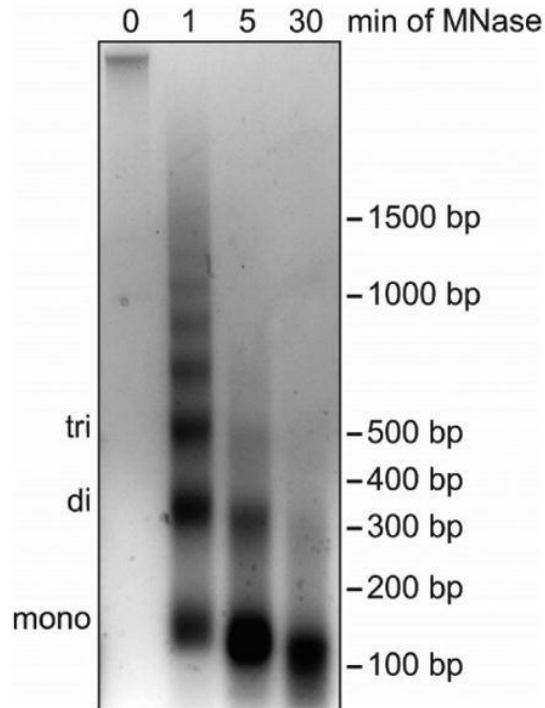


Figure A1.4 | Digestion of cellular DNA using MNase. Agarose gel analysis of DNA extracted from nuclei during a time course of MNase treatment. The position of DNA bands corresponding to mono-, di- and tri-nucleosomes are indicated on the left while the DNA size in base pairs (bp) is indicated on the right. Without MNase digestion (0 min), cellular DNA barely enters the agarose gel because of the large size of the DNA molecules. After 1 min of MNase digestion, DNA fragments show the characteristic banding pattern of multiples of 150 bp. After 5 min the DNA fragments correspond to one to three nucleosomes in length. After 30 min most DNA fragments are close to 150 bp, indicating the desired digestion of cellular DNA necessary for optimal chromatin fractionation. The high concentration of DNA causes the slightly lower shift of the mono-nucleosome band. The nuclei used for this time course were isolated using method B.1. No differences in MNase digestion efficiency have been observed with nuclei isolated using method B.2.

A1.10 Recipes

1. Buffer I.A and I.B

- 0.32 M sucrose
- 60 mM KCl
- 15 mM NaCl
- 5 mM MgCl₂
- 0.1 mM EGTA
- 15 mM Tris pH 7.4
- Filtered and stored at 4 °C
- Add fresh:
- 0.5 mM DTT
- 0.1 mM PMSF
- 1× protease inhibitor cocktail
- Add only to Buffer I.B:
- 0.1% NP-40

2. Buffer II

- 1.2 M sucrose
- 60 mM KCl
- 15 mM NaCl
- 5 mM MgCl₂
- 0.1 mM EGTA
- 15 mM Tris pH 7.4
- Filtered and stored at 4 °C
- Add fresh:
- 0.5 mM DTT
- 0.1 mM PMSF
- 1× protease inhibitor cocktail

3. Buffer III.A and III.B

- 10 mM Tris pH 7.4
- 2 mM MgCl₂
- 0.1 mM PMSF
- Add only to Buffer III.A:
- 5 mM CaCl₂

4. Buffer IV.80, IV.150, IV.300 and IV.600
 - 10 mM Tris pH 7.4
 - 2 mM MgCl₂
 - 2 mM EGTA
 - 0.1% Triton X-100
 - Add the following concentrations of NaCl to the individual buffers:
 - 70 mM Buffer IV.80
 - 140 mM Buffer IV.150
 - 290 mM Buffer IV.300
 - 590 mM Buffer IV.600
 - Filtered and stored at 4 °C
 - Add fresh: 0.1 mM PMSF
5. Hypotonic buffer
 - 10 mM HEPES pH 7.9
 - 1.5 mM MgCl₂
 - 10 mM KCl
 - 0.1 mM PMSF
 - 0.5 mM DTT

Appendix 2: Mapping the protein VII-HMGB1 interaction and determining the role of HMGB1 for intracellular steps of Ad infection

A2.1 Introduction

We have demonstrated that histone-like protein VII from human Adenovirus 5 (Ad5) localizes to and alters cellular chromatin²⁵⁸. Furthermore, this viral protein sequesters members of the HMGB family of proteins in chromatin, preventing their release upon immune stimulation, and downstream inflammatory response mediated through these host alarmins. In addition to the role in the immune response, HMGB1 also fulfills several functions within the host cell²⁶⁰. HMGB1 can bind to and bend DNA, facilitating both nucleosome mobility and the binding of transcription factors to their target genes. As such, HMGB1 is involved in regulating chromatin structure, DDR, and transcription²⁶⁰. We hypothesized that by immobilizing HMGB1 in chromatin, protein VII manipulates these intracellular functions of HMGB1. This could contribute to the changes in host chromatin structure, DDR, and, potentially, transcription facilitated by protein VII^{151,258}. Ultimately, manipulation of the cell intrinsic functions of HMGB1 could represent another strategy employed by protein VII to support Ad infection. To test this, we further characterized the interaction of protein VII with HMGB1 and defined the domains in both proteins that facilitate binding. We also created HMGB1 KO cell lines using CRISPR/Cas9 and determined the consequence of HMGB1 deletion on different stages of Ad infection. We further used these HMGB1 KO cell lines to determine the contribution of HMGB1 to protein VII mediated changes in nuclear structure and DDR inhibition (these experiments have been published as part of Avgousti et al., JVI, 2017¹⁵¹ and will not part of this chapter). We also investigated the impact of protein VII on expression of IFN β and ISGs upon immune activation, and examined the role of HMGB1 in this process.

A2.2 Results

A2.2.1 Protein VII from human but not mouse adenovirus immobilizes HMGB1 in chromatin

In our initial study of protein VII functions in host chromatin, we tested how conserved the interaction between protein VII and HMGB1 is among different Ad serotypes. Infections by all human serotypes examined resulted in chromatin retention of HMGB1. However, when we infected mouse embryonic fibroblasts (MEFs) with mouse adenovirus serotype MAV-1 we discovered that HMGB1 does not become immobilized in chromatin during infection with this Ad serotype (**Figure A2.1a**). To verify that this phenotype is not caused by differences in cell type or infection between the mouse and human adenovirus, we created an A549 cell line encoding inducible of MAV-1 protein VII. We then compared HMGB1 retention by chromatin fractionation followed by Western blot for control, Ad5 protein VII-HA, and MAV-1 protein VII-HA. This analysis revealed that only the expression of Ad5 protein VII-HA leads to the retention of HMGB1 in high-salt chromatin fractions, consistent with the results observed during infection (**Figure A2.1b**). We also compared the impact of the different protein VII versions on chromatin structure and changes in HMGB1 localization. Under control conditions, HMGB1 has a pan-nuclear localization with enrichment in nucleoli. Expression of Ad5 protein VII-HA altered the nuclear architecture, as shown previously²⁵⁸, and caused changes in HMGB1 localization to distinct structures in the nucleus that overlap with protein VII staining. MAV-1 protein VII-HA was also able to alter nuclear morphology, even though this pattern was distinct from the one induced by the Ad5 version. HMGB1 does not co-localize with the mouse protein VII-HA. Instead the host protein seems to be excluded from the areas with the highest levels of MAV-1 protein VII-HA (**Figure A2.1c**). These experiments demonstrated that protein VII from human and mouse adenovirus serotypes differ in their ability to bind and sequester HMGB1 in chromatin.

A2.2.2 The N-terminus of Ad5 protein VII binds to HMGB1

After confirming that protein VII from Ad5 but not MAV-1 immobilized HMGB1 in chromatin, we wanted to use this difference between the two viral proteins to map the interaction of Ad5 protein VII with HMGB1. We first determined the homology between the human and mouse version of protein VII and revealed only limited sequence identity between them, with the highest overlap in the N-terminal region (**Figure A2.2a**). We then made four different chimeras between Ad5 and

MAV-1 protein VII to test which domain of human protein VII can interact with HMGB1 (**Figure A2.2b**). When we introduced these chimeras into our inducible A549 system, we discovered that all of the chimeras induce changes in nuclear architecture, indicating that these chimeric viral histone-like proteins retain their ability to alter host chromatin (**Figure A2.2c**). Interestingly, the localization of the chimeras inside the nucleus was not the same. Chimeras 1 and 2 localized to distinct areas within the nucleus, reminiscent of WT MAV-1 protein, while chimeras 3 and 4 were more nucleoplasmic, similar to WT Ad5 protein VII (**Figure A2.1c**). Regarding HMGB1, only the first two chimeras were able to induce relocalization of HMGB1 while for the last two HMGB1 appeared to be excluded from areas of protein VII accumulation (visualized in **Figure A2.2c**, summarized in **Figure A2.2b**). We concluded that the Ad5 protein VII N-terminus interact with HMGB1 as this domain is shared between chimeras 1 and 2. To confirm this, we generated a construct for Ad5 protein VII amino acids 1-66 tagged with GFP. We then expressed this truncated version of protein VII in A549 cells, performed a GFP-IP, and probed for HMGB1 co-immunoprecipitation by Western blot. This showed that amino acids 1-66 of Ad5 protein VII can pull-down HMGB1, similar to or better than full-length human protein VII (**Figure A2.2d**).

A2.2.3 Ad5 protein VII interacts with the HMGB1 A-box in cells

After determining that the Ad5 protein VII N-terminus is responsible for binding to HMGB1, we wanted to determine which domain of HMGB1 is involved in this interaction. HMGB1 has three distinct domains: the A-box, the B-box, and the acidic tail²⁶⁰. We created GFP tagged versions of these different domains and combinations thereof (**Figure A2.3a**). All of these HMGB1 constructs showed a pan-nuclear pattern when transfected into control A549 cells. Upon induction of Ad5 protein VII expression, only HMGB1 constructs containing the A-box were relocalized to the protein VII pattern (visualized in **Figure A2.3b**, summarized in **Figure A2.3a**). Next, we wanted to confirm that protein VII can immobilize the HMGB1 A-box in chromatin. We expressed the A-box-GFP construct in control or protein VII expressing cells and performed FRAP. In control cells, the fluorescence of the bleached spot is rapidly recovered, indicating that the HMGB1 A-box is highly mobile in these cells. Upon expression of protein VII the signal upon bleaching recovered much

slower, demonstrating that under these conditions the HMGB1 A-box is immobilized (**Figure A2.3c**). These experiments indicate that in cells interaction between protein VII and the HMGB1 A-box is sufficient to retain the host protein in chromatin.

A2.2.4 Protein VII binds to the HMGB1 acidic tail *in vitro*

To confirm the interaction between protein VII and the HMGB1 A-box *in vitro*, we created several HMGB1 constructs for the separate domains tagged with GST and purified them from bacteria (**Figure A2.4a**). We then incubated these GST-HMGB1 constructs with purified protein VII-His, performed a GST pull-down and probed for interaction by both Coomassie staining and Western blot. Surprisingly, only the full-length HMGB1 and the acidic C-terminus were able to pull-down protein VII-His, but not the HMGB1 A-box (**Figure A2.4b**). These results demonstrate that while the HMGB1 A-box is sufficient for protein VII interaction in cells, *in vitro* it is the acidic HMGB1 C-terminus that directly binds to protein VII.

A2.2.5 HMGB1 knockout does not impact any stage of Ad infection

To determine the contribution of intracellular functions of HMGB1 to adenovirus infection, we used CRISPR/Cas9 to create several HMGB1 knockout (KO) cell lines. We confirmed HMGB1 deletion by both Western blot for the protein and RT-qPCR for RNA (**Figure A2.5a**). We then compared expression of Ad proteins over a time course of infection with Ad WT in the HMGB1 WT and several KO cell lines. While KO1 showed a decrease in production of late proteins (Hexon, Penton, Fiber, and protein VII), we did not observe this reduction in the other two KO cell lines (**Figure A2.5b**). As these cell lines were generated from single cells, we concluded that HMGB1 KO1 possessed additional background mutations that caused the decrease in viral late protein production, and used KO2 and KO3 for all other assays. We then tested the effect of HMGB1 KO on viral RNA production by RT-qPCR, genome replication by qPCR, and progeny production by plaque assays (**Figure A2.5c-e**). All these experiments were carried out over a time course for both HMGB1 KO2 and KO3 as compared to the parental cell line. None of these experiments displayed any significant difference for the examined stages of Ad infection upon

HMGB1 deletion. We therefore concluded that protein VII-mediated recruitment of HMGB1 does not directly contribute to Ad infection during a single infectious cycle.

A2.2.6 Protein VII expression suppresses $\text{INF}\beta$ expression in an HMGB1-dependent manner

Even though HMGB1 was dispensable for Ad replication, we hypothesized that it may contribute to infection by supporting a protein VII function in the genome that would not be apparent through assays that only look at a single infectious cycle. To test this hypothesis, we first wanted to define any additional functions of the Ad viral histone-like protein. We found that in addition to altering nuclear architecture, protein VII on host chromatin can suppress induction of the DDR, reminiscent to its function on viral genomes^{144,151}. When we repeated these assays in HMGB1 KO cell lines we observed that protein VII was still able to suppress the DDR. In addition, we also noticed that even upon deletion of HMGB1, protein VII still able to alter nuclear morphology. This indicates that both of these protein VII functions, the suppression of the DDR and changing host chromatin, are HMGB1-independent¹⁵¹.

As protein VII directly binds to and alters cellular chromatin, we proposed that this could impact the cellular transcription, including expression of antiviral proteins. We therefore tested whether protein VII could alter the expression of cellular genes involved in the immune response. We transfected control and protein VII expressing cells with the dsDNA analog poly(dA:dT) and measured induction of $\text{INF}\beta$ at baseline and 8 hours post-treatment. We discovered that protein VII expression dramatically reduced $\text{INF}\beta$ RNA levels at both time points, indicating that protein VII interferes with the immune response towards dsDNA, the same molecular danger signal that is introduced into cells during Ad infection (**Figure A2.6a**). To determine whether chromatin association was necessary for this effect of protein VII, we repeated the experiment in the protein VII Δ PTM cell line. This protein VII mutant protein localizes to nucleoli and does not alter nuclear morphology. Expression of protein VII Δ PTM did not cause a no significant reductions in $\text{INF}\beta$ expression compared to control cells (**Figure A2.6a**). This suggests that protein VII needs to be associated with host chromatin to suppress the immune response, even though other functions of the PTMs may also contribute to the phenotype.

We proposed that protein VII may also interfere with expression of other immune genes downstream of IFN β . Therefore, we treated control and protein VII cells with type I IFN and measured the level of induction for several ISGs. None of the examined ISGs showed significant differences in RNA levels upon protein VII expression (**Figure A2.6b**). We therefore concluded that protein VII specifically blocks IFN β expression.

Next, we wanted to determine whether HMGB1 contributes to the suppression of IFN β production. We transduced WT and HMGB1 KO cells with control or protein VII-GFP encoding vectors and transfected them with poly(dA:dT) to induce an immune response. While protein VII-GFP was able to decrease IFN β RNA levels in the parental cells, there was no significant difference in HMGB1 KO cells.

In conclusion, our data revealed that while HMGB1 is dispensable for virus replication, suppression of the DDR, and large-scale changes in nuclear morphology, this host protein may contribute to protein VII-mediated suppression of IFN β upon dsDNA-mediated stimulation of host immune responses.

A2.3 Discussion

In this project, we further characterized the interaction between Ad5 protein VII and HMGB1. In addition, we also examined the importance of HMGB1 for Ad infection and the contribution to protein VII functions. We determined that the protein VII N-terminus is sufficient for binding to HMGB1. However, our experiments to define which part of HMGB1 is bound by protein VII were contradictory. In cells, the HMGB1 A-box is sufficient for relocalization by protein VII. Yet this HMGB1 domain does not bind to protein VII *in vitro*. Instead the HMGB1 acidic tail can pull down protein VII *in vitro*, but not in cells. This indicates that likely both domains contribute to protein VII-HMGB1 binding, but additional factors determine their specific contribution for the interaction. Both the HMGB1 A-box and protein VII have DNA binding capability. Therefore, DNA may facilitate the interaction observed in cells. To test this, we can add DNA to the *in vitro* binding assay and determine whether the HMGB1 A-box can pull down protein VII under those

conditions. In addition, other host proteins may contribute to the interaction. We can assess this hypothesis by determining the HMGB1 and protein VII interactome by IP-MS and identify proteins that bind to both. These proteins would be likely candidates for regulating the protein VII-HMGB1 interaction in cells. As for investigating the impact of HMGB1 on protein VII functions, we have preliminary evidence that protein suppresses expression of IFN β upon detection of dsDNA by the host cell and that HMGB1 is required for this response. The contribution of HMGB1 to suppression of IFN β expression is discussed in detail in Chapter 4.2.2 of this thesis. In summary, in this chapter we further characterized the protein VII-HMGB1 interaction and started to explore additional functions for this association.

A2.4 Figures

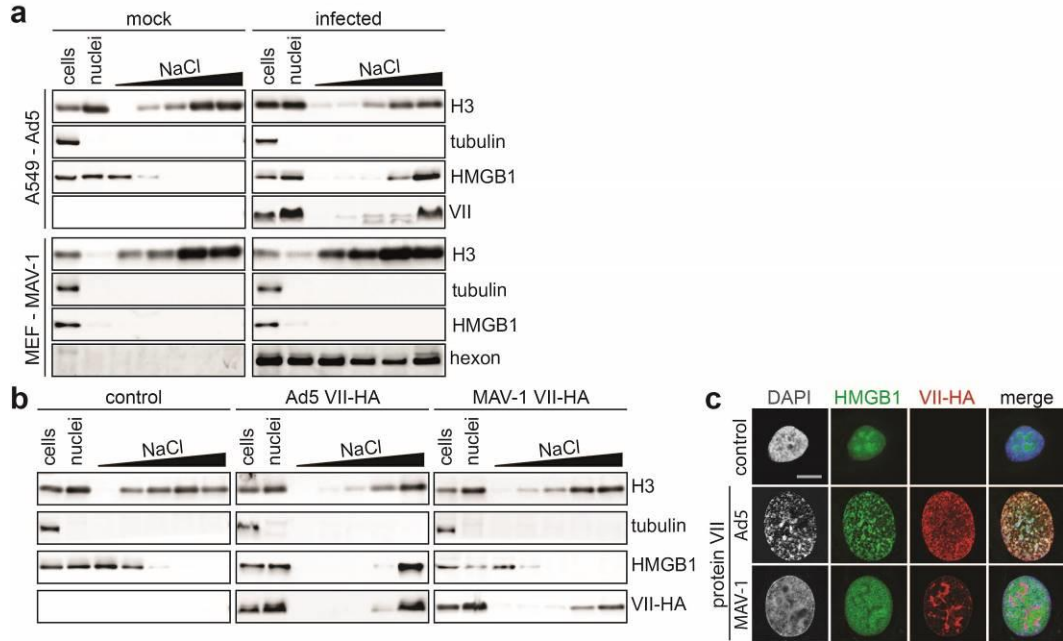


Figure A2.1 | The Ad5 but not MAV-1 protein VII interacts with HMGB1. **a**, Nuclear fractionation of A549 or MEF cells under mock conditions or infected with human Ad5 and mouse MAV-1 showing differential retention of HMGB1 in high-salt chromatin fractions during infection with different viruses. Fractionation was performed using increasing molarity of salt followed by Western blot for different cellular and viral proteins. 24 hpi, Ad5 MOI = 20, MAV-1 MOI = 5. **b**, Expression of Ad5 but not MAV-1 protein VII leads to retention of HMGB1 in chromatin. Nuclear fractionation of A549 cells under control conditions or treated with doxycycline for 4 days to induce expression of different protein VII-HA variants followed by Western blot analysis of indicated proteins. **c**, IF experiment corresponding to **b** showing colocalization of HMGB1 (green) with Ad5 but not MAV-1 protein VII-HA (red). Scale bar = 10 μ m, DAPI in blue.

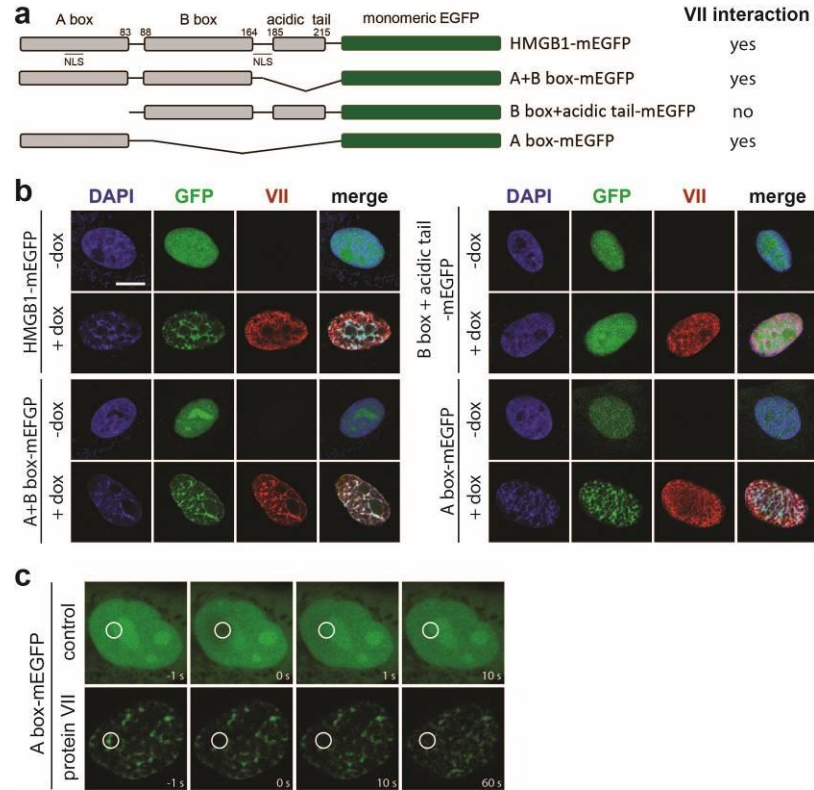


Figure A2.3 | Protein VII interacts with the HMGB1 A-box in cells. **a**, Schematic for the different HMGB1-mEGFP constructs and their behavior in regards to redistribution by protein VII. **b**, IF of different HMGB1-mEGFP in A549 cells containing an inducible copy of Ad5 protein VII-HA (red). Cells were treated with doxycycline for 4 days to induce expression of the viral protein and transfected with the different GFP constructs 24 hours prior to fixation. Scale bar = 10 μ m, DAPI in blue. **c**, FRAP recovery for A box-mEGFP in the presence and absence of protein VII. A549 cells were treated with doxycycline for 4 days to induce protein VII expression and transfected with A box-mEGFP 24 hours before experiment. Circle denotes area of interest that was bleached by the laser.

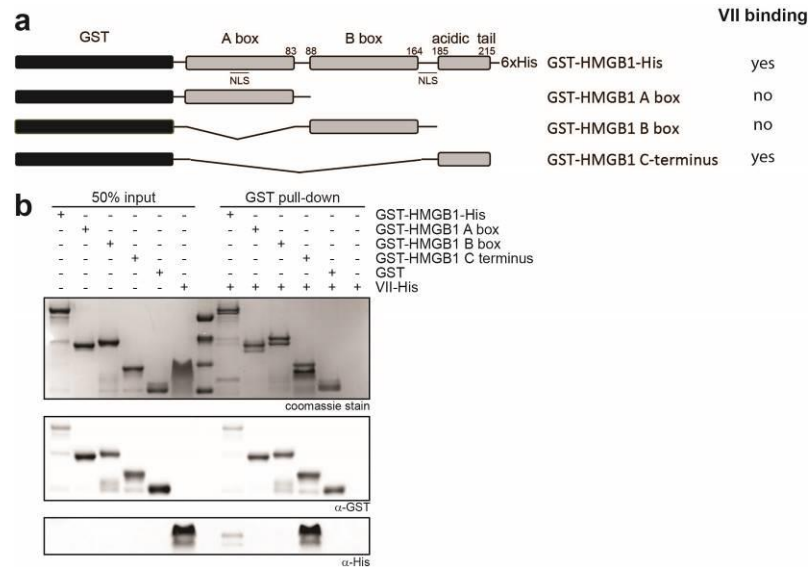


Figure A2.4 | HMGB1 C-terminus interacts with protein VII in vitro. **a**, Schematic of different GST-HMGB1 constructs and summary of interaction with protein VII in vitro. **b**, Western blot analysis of GST IP of different HMGB1 constructs shows pull down of protein VII by full-length HMGB1 and the HMGB1 C-terminus.

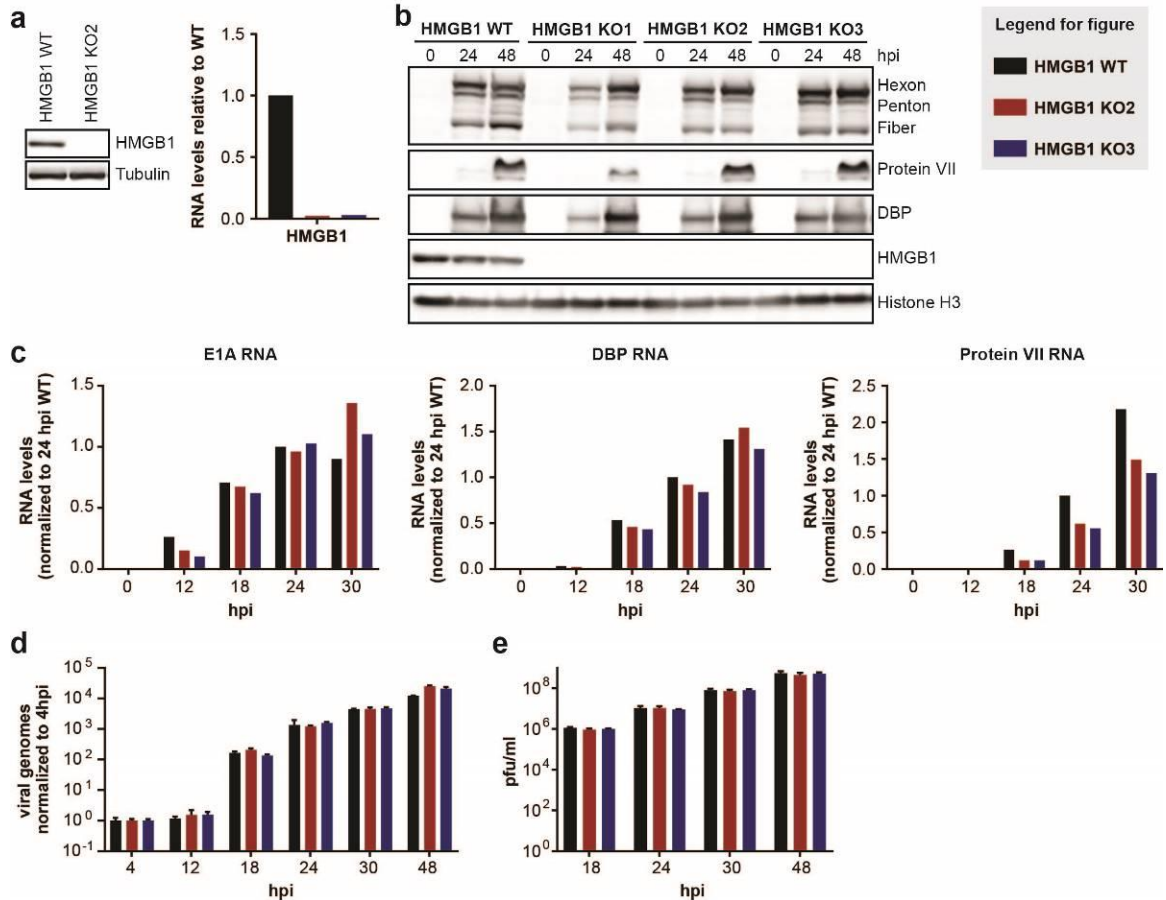


Figure A2.5 | Deletion of HMGB1 does not impact Ad5 infection. **a**, Verification of HMGB1 deletion by CRISPR/Cas9 in A549 cells by Western blot (left) for HMGB1 protein levels and RT-qPCR (right) for HMGB1 mRNA comparing the parental cell line to the KO cell lines. **b-e**, Infection of HMGB1 WT or HMGB1 KO cell lines with Ad5 WT virus at MOI of 10 for indicated times. **b**, Western blot showing that levels of different viral proteins are similar in HMGB1 WT and two out of three HMGB1 KO cells. **c**, RT-qPCR for different viral RNAs over a time course with comparable levels between HMGB1 WT and KO cell lines. **d**, qPCR for viral genomes in HMGB1 WT and KO cells with no significant differences over a time course of infection. **e**, plaque assay for infection viral particles produced from HMGB1 WT and KO cells over a time course with no significant differences between cell lines.

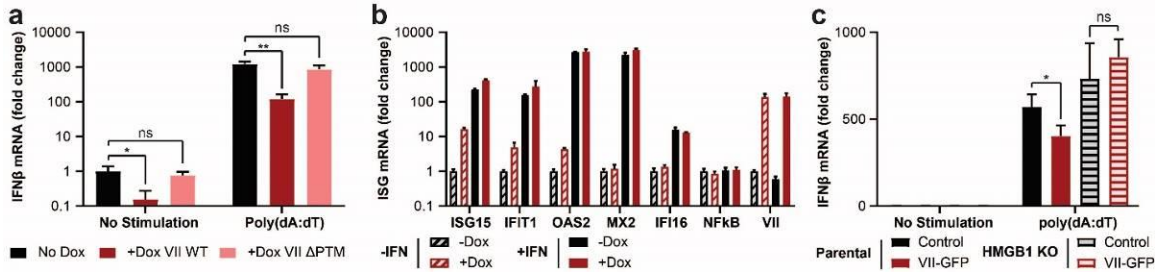


Figure A2.6 | Protein VII suppresses IFN β expression through HMGB1. **a**, RT-qPCR showing decreased IFN β mRNA levels upon expression of protein VII WT but not Δ PTM mutant. A549 cells were treated with doxycycline for 4 days to induce expression of either protein VII WT or protein VII Δ PTM, transfected with poly(dA:dT) for 8 h, and RNA extracted for RT-qPCR. **b**, RT-qPCR results for different interferon stimulated genes (ISGs) upon treatment with type I IFN for 24 h showing no decrease upon expression of protein VII induced by doxycycline treatment of A549 cells for 4 days. NF κ B serves as a negative control since it is upstream of IFN expression, and VII verifies the expression of protein VII. Values are normalized to untreated parental. **c**, RT-qPCR results showing that deletion of HMGB1 counteracts protein VII-mediated suppression of IFN β mRNA upon poly(dA:dT) treatment of A549 cells for 8 h. For all experiments shown is mean+s.d., n = 3 biological replicates. * p < 0.05, ** p < 0.01, ns = not significant. *Data courtesy of NJ Pancholi.*

A2.5 Methods

The work of this Appendix is based on results from Chapter 2 and only methods not used in that chapter will be described here. Please refer to Chapter 2 for all other methods.

A2.5.1 Cells and viruses

The HMGB1 KO cell line was made using the CRISPR/Cas9 system and has been described previously (PMID: 28794020). MEF were purchased from ATCC and cultured in DMEM with 10% FBS and 1% Penn/Strep. MAV-1 was a kind gift of K Spindler and infections were performed using the same standard methods used for Ad5.

A2.5.2 Cloning of protein VII and HMGB1 constructs

MAV-1 protein VII was cloned from genomic DNA isolated from MEFs infected with MAV-1. For generation of the different protein VII inducible cell lines, the respective coding sequences were introduced into the inducible plasmid cassette with a C-terminal HA tag using restriction enzymes BsrGI and AgeI. Protein VII-GFP, protein VII 1-66-GFP, and the different GFP tagged versions of HMGB1 were cloned into a pmEGFP-N1 vector using XmaI and AgeI. The GST-tagged version of HMGB1 were cloned into a pGEX 6p3 vector using XhoI and EcoRI. For all, positive clones were selected in DH5 α cells and sequenced. All primer sequences are available upon request.

A2.5.3 Purification of HMGB1 constructs

The HMGB1 constructs were transformed into BL21 (DE3) cells (NEB C25271). BL21 cells were inoculated from overnight cultures and grown to an optical density of 0.5-0.6 OD₂₆₀ nm, induced with 0.1 mM isopropyl- β -D-thiogalactoside (IPTG; Sigma) and harvested after 4 h at 37 °C. Cells were in 28 ml of chilled lysis buffer (50 mM Tris-HCl pH 8, 10 mM NaCl, 2 mM MgCl₂, 1 mM PMSF, 2.5 μ g/ml aprotinin, 2.5 μ g/ml leupeptin and pepstatin, 0.05% NP-40) and incubated on ice for 10-20 minutes. Cells incubated with 0.5 mg/ml Lysozyme and 25 U/ml benzonase (Sigma E1014) for 30 min at RT and 30 min on ice. Then 7 ml of 5 M NaCl was added to a final concentration of 1 M. Cells were disrupted by sonication using a Thermo Fischer Sonic Dismembrator at output of low for 10 s (1 s sonication with 1 s break, 18% output) which was

repeated twice. Samples were spun at 27,000 g for 20 min at 4 °C. 3x200 µl glutathione agarose beads were prepared per sample by washing with 5 ml of cold lysis buffers three times. 10-12 ml of supernatant from the lysed bacteria was transferred into each tube (1 vol. bed of 100 vol. lysate) and rotated for at 4°C for at least 3 h. Beads were spun at 700 g for 2 min at 4 °C, washed twice with 5-10 ml of Wash Buffer (50 mM Tris-HCl pH 8, 500 mM NaCl, 2 mM MgCl₂, 1 mM PMSF, 2.5 µg/ml aprotinin, 0.05% NP-40) and spun again. Beads were washed once with 5 ml of elution buffer (50 mM Tris-HCl pH 8, 150 mM NaCl without glutathione), spun again, and transferred to a 1.5 ml microfuge tube. 300 µl of elution buffer with 3.07 mg reduced glutathione per 1 ml was added to the beads, followed by rotation at 4°C for 10 minutes and spun at 4000 rpm at 4°C for 1 minute in tabletop microcentrifuge. Supernatant was removed and spun at 13000 rpm at 4°C for 10 min. The elution was repeated twice.

For purification of the GST-HMGB1-His construct only a His-tag purification was performed before the GST-tag purification. For this 3x200 µl of Cobalt-beads were washed three times with 5 ml cold lysis buffer. For protein binding 5 mM imidazole was added to the bacteria supernatant. 10 ml supernatant each were added to the beads, rotated at 4°C for at least 1 h, and spun at 4000 g for 3 min at 4 °C. The beads were washed four times with 5-10 ml wash buffer 2 (50 mM Tris-HCl pH 8, 0.5 M NaCl, 2 mM MgCl₂, 1 mM PMSF, 0.05% NP-40, 10 mM imidazole) and combined in one tube. 1 ml of elution buffer 2 (50 mM Tris-HCl pH 8, 500 mM NaCl, 300 mM imidazole) and spun at 4000 g at 4°C for 3 minutes. The elution was repeated three times and then further processed by GST purification.

A2.5.4 In vitro binding assay for HMGB1 and protein VII interaction

The different GST-HMGB1 constructs were combined with recombinant protein-VII-His at equimolar ratios and incubated at 4 °C for 1 h. Complexes were then mixed with glutathione agarose beads (Thermo Scientific Product # 16100) to bind the GST-HMGB1 constructs and any associated protein, and washed three times in the binding buffer (50 mM Tris pH 8, 300 mM NaCl, 0.1% IGEPAL). The beads were then boiled in sample buffer, separated on an SDS-PAGE and visualized by Coomassie staining or further processed for Western blot.

A2.5.5 Interferon stimulation

For stimulation with DNA the cells were transfected with with 1 ug/mL poly(dA:dT)/LyoVec (Invivogen tlr1-patc) by addition to regular media. The cells were collected 8 h post stimulation and processed for RT-qPCR. For ectopic treatment with interferon the cells with 1000 units/mL universal type I IFN (PBL Assay Science), collected 24 h post treatment and processed for RT-qPCR.

BIBLIOGRAPHY

- 1 Dybas JM, Herrmann C, Weitzman MD. Ubiquitination at the interface of tumor viruses and DNA damage responses. *Curr Opin Virol* **32**, 40-47 (2018).
- 2 Jensen S, Thomsen AR. Sensing of RNA viruses: a review of innate immune receptors involved in recognizing RNA virus invasion. *J Virol* **86**, 2900-2910 (2012).
- 3 Ma Z, Ni G, Damania B. Innate Sensing of DNA Virus Genomes. *Annual review of virology* **5**, 341-362 (2018).
- 4 Ni G, Ma Z, Damania B. cGAS and STING: At the intersection of DNA and RNA virus-sensing networks. *PLoS pathogens* **14**, e1007148 (2018).
- 5 Daugherty MD, Malik HS. Rules of engagement: molecular insights from host-virus arms races. *Annu Rev Genet* **46**, 677-700 (2012).
- 6 Berk AJ. Recent lessons in gene expression, cell cycle control, and cell biology from adenovirus. *Oncogene* **24**, 7673-7685 (2005).
- 7 Knipe DM, Lieberman PM, Jung JU, McBride AA, Morris KV, Ott M, Margolis D, Nieto A, Nevels M, Parks RJ, Kristie TM. Snapshots: chromatin control of viral infection. *Virology* **435**, 141-156 (2013).
- 8 Lieberman PM. Chromatin organization and virus gene expression. *J Cell Physiol* **216**, 295-302 (2008).
- 9 Isaacson MK, Ploegh HL. Ubiquitination, ubiquitin-like modifiers, and deubiquitination in viral infection. *Cell host & microbe* **5**, 559-570 (2009).
- 10 Luo H. Interplay between the virus and the ubiquitin-proteasome system: molecular mechanism of viral pathogenesis. *Curr Opin Virol* **17**, 1-10 (2016).
- 11 Rowe WP, Huebner RJ, Gilmore LK, Parrott RH, Ward TG. Isolation of a cytopathogenic agent from human adenoids undergoing spontaneous degeneration in tissue culture. *Proc Soc Exp Biol Med* **84**, 570-573 (1953).
- 12 Knipe DM, Howley PM. *Fields virology*. 6th edn, (Wolters Kluwer/Lippincott Williams & Wilkins Health, 2013).
- 13 Davison AJ, Benko M, Harrach B. Genetic content and evolution of adenoviruses. *The Journal of general virology* **84**, 2895-2908 (2003).
- 14 Yamamoto Y, Nagasato M, Yoshida T, Aoki K. Recent advances in genetic modification of adenovirus vectors for cancer treatment. *Cancer Sci* **108**, 831-837 (2017).
- 15 Afkhami S, Yao Y, Xing Z. Methods and clinical development of adenovirus-vectored vaccines against mucosal pathogens. *Mol Ther Methods Clin Dev* **3**, 16030 (2016).
- 16 Wold WS, Toth K. Adenovirus vectors for gene therapy, vaccination and cancer gene therapy. *Curr Gene Ther* **13**, 421-433 (2013).
- 17 Lee CS, Bishop ES, Zhang R, Yu X, Farina EM, Yan S, Zhao C, Zheng Z, Shu Y, Wu X, Lei J, Li Y, Zhang W, Yang C, Wu K, Wu Y, Ho S, Athviraham A, Lee MJ, Wolf JM, Reid RR, He TC. Adenovirus-Mediated Gene Delivery: Potential Applications for Gene and Cell-Based Therapies in the New Era of Personalized Medicine. *Genes Dis* **4**, 43-63 (2017).
- 18 Liu H, Jin L, Koh SB, Atanasov I, Schein S, Wu L, Zhou ZH. Atomic structure of human adenovirus by cryo-EM reveals interactions among protein networks. *Science* **329**, 1038-1043 (2010).
- 19 Reddy VS, Natchiar SK, Stewart PL, Nemerow GR. Crystal structure of human adenovirus at 3.5 Å resolution. *Science* **329**, 1071-1075 (2010).
- 20 San Martin C. Latest insights on adenovirus structure and assembly. *Viruses* **4**, 847-877 (2012).
- 21 Maizel JV, Jr., White DO, Scharff MD. The polypeptides of adenovirus. II. Soluble proteins, cores, top components and the structure of the virion. *Virology* **36**, 126-136 (1968).
- 22 van Oostrum J, Burnett RM. Molecular composition of the adenovirus type 2 virion. *J Virol* **56**, 439-448 (1985).
- 23 Chatterjee PK, Vayda ME, Flint SJ. Adenoviral protein VII packages intracellular viral DNA throughout the early phase of infection. *EMBO J* **5**, 1633-1644 (1986).

- 24 Vayda ME, Rogers AE, Flint SJ. The structure of nucleoprotein cores released from adenovirions. *Nucleic Acids Res* **11**, 441-460 (1983).
- 25 Anderson CW, Young ME, Flint SJ. Characterization of the adenovirus 2 virion protein, mu. *Virology* **172**, 506-512 (1989).
- 26 Russell WC, Laver WG, Sanderson PJ. Internal components of adenovirus. *Nature* **219**, 1127-1130 (1968).
- 27 Smart JE, Stillman BW. Adenovirus terminal protein precursor. Partial amino acid sequence and the site of covalent linkage to virus DNA. *The Journal of biological chemistry* **257**, 13499-13506 (1982).
- 28 Van der Vliet PC. Adenovirus DNA replication. *Current topics in microbiology and immunology* **199 (Pt 2)**, 1-30 (1995).
- 29 Cotten M, Weber JM. The adenovirus protease is required for virus entry into host cells. *Virology* **213**, 494-502 (1995).
- 30 Greber UF, Webster P, Weber J, Helenius A. The role of the adenovirus protease on virus entry into cells. *EMBO J* **15**, 1766-1777 (1996).
- 31 Ostapchuk P, Yang J, Auffarth E, Hearing P. Functional interaction of the adenovirus IVa2 protein with adenovirus type 5 packaging sequences. *J Virol* **79**, 2831-2838 (2005).
- 32 Nemerow GR, Stewart PL. Role of alpha(v) integrins in adenovirus cell entry and gene delivery. *Microbiol Mol Biol Rev* **63**, 725-734 (1999).
- 33 Summerford C, Bartlett JS, Samulski RJ. AlphaVbeta5 integrin: a co-receptor for adeno-associated virus type 2 infection. *Nat Med* **5**, 78-82 (1999).
- 34 Philipson L, Lonberg-Holm K, Pettersson U. Virus-receptor interaction in an adenovirus system. *J Virol* **2**, 1064-1075 (1968).
- 35 Bergelson JM, Cunningham JA, Droguett G, Kurt-Jones EA, Krithivas A, Hong JS, Horwitz MS, Crowell RL, Finberg RW. Isolation of a common receptor for Coxsackie B viruses and adenoviruses 2 and 5. *Science* **275**, 1320-1323 (1997).
- 36 Gaggar A, Shayakhmetov DM, Lieber A. CD46 is a cellular receptor for group B adenoviruses. *Nat Med* **9**, 1408-1412 (2003).
- 37 Chardonnet Y, Dales S. Early events in the interaction of adenoviruses with HeLa cells. I. Penetration of type 5 and intracellular release of the DNA genome. *Virology* **40**, 462-477 (1970).
- 38 Greber UF, Willetts M, Webster P, Helenius A. Stepwise dismantling of adenovirus 2 during entry into cells. *Cell* **75**, 477-486 (1993).
- 39 Dales S, Chardonnet Y. Early events in the interaction of adenoviruses with HeLa cells. IV. Association with microtubules and the nuclear pore complex during vectorial movement of the inoculum. *Virology* **56**, 465-483 (1973).
- 40 Bremner KH, Scherer J, Yi J, Vershinin M, Gross SP, Vallee RB. Adenovirus transport via direct interaction of cytoplasmic dynein with the viral capsid hexon subunit. *Cell host & microbe* **6**, 523-535 (2009).
- 41 Greber UF, Suomalainen M, Stidwill RP, Boucke K, Ebersold MW, Helenius A. The role of the nuclear pore complex in adenovirus DNA entry. *EMBO J* **16**, 5998-6007 (1997).
- 42 Hearing P, Shenk T. The adenovirus type 5 E1A transcriptional control region contains a duplicated enhancer element. *Cell* **33**, 695-703 (1983).
- 43 Nevins JR, Ginsberg HS, Blanchard JM, Wilson MC, Darnell JE, Jr. Regulation of the primary expression of the early adenovirus transcription units. *J Virol* **32**, 727-733 (1979).
- 44 Winberg G, Shenk T. Dissection of overlapping functions within the adenovirus type 5 E1A gene. *EMBO J* **3**, 1907-1912 (1984).
- 45 Pelka P, Ablack JN, Torchia J, Turnell AS, Grand RJ, Mymryk JS. Transcriptional control by adenovirus E1A conserved region 3 via p300/CBP. *Nucleic Acids Res* **37**, 1095-1106 (2009).
- 46 Bagchi S, Raychaudhuri P, Nevins JR. Adenovirus E1A proteins can dissociate heteromeric complexes involving the E2F transcription factor: a novel mechanism for E1A trans-activation. *Cell* **62**, 659-669 (1990).

- 47 Ferrari R, Gou D, Jawdekar G, Johnson SA, Nava M, Su T, Yousef AF, Zemke NR, Pellegrini M, Kurdistani SK, Berk AJ. Adenovirus small E1A employs the lysine acetylases p300/CBP and tumor suppressor Rb to repress select host genes and promote productive virus infection. *Cell host & microbe* **16**, 663-676 (2014).
- 48 Fonseca GJ, Thillainadesan G, Yousef AF, Ablack JN, Mossman KL, Torchia J, Mymryk JS. Adenovirus evasion of interferon-mediated innate immunity by direct antagonism of a cellular histone posttranslational modification. *Cell host & microbe* **11**, 597-606 (2012).
- 49 Leonard GT, Sen GC. Effects of adenovirus E1A protein on interferon-signaling. *Virology* **224**, 25-33 (1996).
- 50 Anderson KP, Fennie EH. Adenovirus early region 1A modulation of interferon antiviral activity. *J Virol* **61**, 787-795 (1987).
- 51 Ackrill AM, Foster GR, Laxton CD, Flavell DM, Stark GR, Kerr IM. Inhibition of the cellular response to interferons by products of the adenovirus type 5 E1A oncogene. *Nucleic Acids Res* **19**, 4387-4393 (1991).
- 52 Cuconati A, White E. Viral homologs of BCL-2: role of apoptosis in the regulation of virus infection. *Genes Dev* **16**, 2465-2478 (2002).
- 53 Blackford AN, Grand RJ. Adenovirus E1B 55-kilodalton protein: multiple roles in viral infection and cell transformation. *J Virol* **83**, 4000-4012 (2009).
- 54 Coenjaerts FE, van der Vliet PC. Adenovirus DNA replication in a reconstituted system. *Methods Enzymol* **262**, 548-560 (1995).
- 55 van der Vliet PC, Levine AJ. DNA-binding proteins specific for cells infected by adenovirus. *Nat New Biol* **246**, 170-174 (1973).
- 56 Dekker J, Kanellopoulos PN, Loonstra AK, van Oosterhout JA, Leonard K, Tucker PA, van der Vliet PC. Multimerization of the adenovirus DNA-binding protein is the driving force for ATP-independent DNA unwinding during strand displacement synthesis. *EMBO J* **16**, 1455-1463 (1997).
- 57 Lichtenstein DL, Toth K, Doronin K, Tollefson AE, Wold WS. Functions and mechanisms of action of the adenovirus E3 proteins. *Int Rev Immunol* **23**, 75-111 (2004).
- 58 Tauber B, Dobner T. Molecular regulation and biological function of adenovirus early genes: the E4 ORFs. *Gene* **278**, 1-23 (2001).
- 59 Weitzman MD. Functions of the adenovirus E4 proteins and their impact on viral vectors. *Front Biosci* **10**, 1106-1117 (2005).
- 60 Bridge E, Ketner G. Redundant control of adenovirus late gene expression by early region 4. *J Virol* **63**, 631-638 (1989).
- 61 Huang MM, Hearing P. Adenovirus early region 4 encodes two gene products with redundant effects in lytic infection. *J Virol* **63**, 2605-2615 (1989).
- 62 Lallemand-Breitenbach V, de The H. PML nuclear bodies. *Cold Spring Harb Perspect Biol* **2**, a000661 (2010).
- 63 Carvalho T, Seeler JS, Ohman K, Jordan P, Pettersson U, Akusjarvi G, Carmo-Fonseca M, Dejean A. Targeting of adenovirus E1A and E4-ORF3 proteins to nuclear matrix-associated PML bodies. *J Cell Biol* **131**, 45-56 (1995).
- 64 Doucas V, Ishov AM, Romo A, Juguilon H, Weitzman MD, Evans RM, Maul GG. Adenovirus replication is coupled with the dynamic properties of the PML nuclear structure. *Genes Dev* **10**, 196-207 (1996).
- 65 Weiden MD, Ginsberg HS. Deletion of the E4 region of the genome produces adenovirus DNA concatemers. *Proceedings of the National Academy of Sciences of the United States of America* **91**, 153-157 (1994).
- 66 Ou HD, Kwiatkowski W, Deerinck TJ, Noske A, Blain KY, Land HS, Soria C, Powers CJ, May AP, Shu X, Tsien RY, Fitzpatrick JA, Long JA, Ellisman MH, Choe S, O'Shea CC. A structural basis for the assembly and functions of a viral polymer that inactivates multiple tumor suppressors. *Cell* **151**, 304-319 (2012).
- 67 Stracker TH, Carson CT, Weitzman MD. Adenovirus oncoproteins inactivate the Mre11-Rad50-NBS1 DNA repair complex. *Nature* **418**, 348-352 (2002).

- 68 Pombo A, Ferreira J, Bridge E, Carmo-Fonseca M. Adenovirus replication and transcription sites are spatially separated in the nucleus of infected cells. *EMBO J* **13**, 5075-5085 (1994).
- 69 Reyes ED, Kulej K, Pancholi NJ, Akhtar LN, Avgousti DC, Kim ET, Bricker DK, Spruce LA, Koniski SA, Seeholzer SH, Isaacs SN, Garcia BA, Weitzman MD. Identifying Host Factors Associated with DNA Replicated During Virus Infection. *Mol Cell Proteomics* **16**, 2079-2097 (2017).
- 70 Thomas GP, Mathews MB. DNA replication and the early to late transition in adenovirus infection. *Cell* **22**, 523-533 (1980).
- 71 Shaw AR, Ziff EB. Transcripts from the adenovirus-2 major late promoter yield a single early family of 3' coterminal mRNAs and five late families. *Cell* **22**, 905-916 (1980).
- 72 Chen PH, Ornelles DA, Shenk T. The adenovirus L3 23-kilodalton proteinase cleaves the amino-terminal head domain from cytokeratin 18 and disrupts the cytokeratin network of HeLa cells. *J Virol* **67**, 3507-3514 (1993).
- 73 Tollefson AE, Scaria A, Hermiston TW, Ryerse JS, Wold LJ, Wold WS. The adenovirus death protein (E3-11.6K) is required at very late stages of infection for efficient cell lysis and release of adenovirus from infected cells. *J Virol* **70**, 2296-2306 (1996).
- 74 Berget SM, Moore C, Sharp PA. Spliced segments at the 5' terminus of adenovirus 2 late mRNA. *Proceedings of the National Academy of Sciences of the United States of America* **74**, 3171-3175 (1977).
- 75 Berk AJ. Discovery of RNA splicing and genes in pieces. *Proceedings of the National Academy of Sciences of the United States of America* **113**, 801-805 (2016).
- 76 Trentin JJ, Yabe Y, Taylor G. The quest for human cancer viruses. *Science* **137**, 835-841 (1962).
- 77 Endter C, Dobner T. Cell transformation by human adenoviruses. *Current topics in microbiology and immunology* **273**, 163-214 (2004).
- 78 Graham FL, Smiley J, Russell WC, Nairn R. Characteristics of a human cell line transformed by DNA from human adenovirus type 5. *The Journal of general virology* **36**, 59-74 (1977).
- 79 Kao CC, Yew PR, Berk AJ. Domains required for in vitro association between the cellular p53 and the adenovirus 2 E1B 55K proteins. *Virology* **179**, 806-814 (1990).
- 80 Braithwaite AW, Blair GE, Nelson CC, McGovern J, Bellett AJ. Adenovirus E1b-58 kD antigen binds to p53 during infection of rodent cells: evidence for an N-terminal binding site on p53. *Oncogene* **6**, 781-787 (1991).
- 81 Lin J, Chen J, Elenbaas B, Levine AJ. Several hydrophobic amino acids in the p53 amino-terminal domain are required for transcriptional activation, binding to mdm-2 and the adenovirus 5 E1B 55-kD protein. *Genes Dev* **8**, 1235-1246 (1994).
- 82 Sarnow P, Ho YS, Williams J, Levine AJ. Adenovirus E1b-58kd tumor antigen and SV40 large tumor antigen are physically associated with the same 54 kd cellular protein in transformed cells. *Cell* **28**, 387-394 (1982).
- 83 Weitzman MD, Lilley CE, Chaurushiya MS. Genomes in conflict: maintaining genome integrity during virus infection. *Annu Rev Microbiol* **64**, 61-81 (2010).
- 84 Pancholi NJ, Price AM, Weitzman MD. Take your PIKK: tumour viruses and DNA damage response pathways. *Philosophical transactions of the Royal Society of London. Series B, Biological sciences* **372** (2017).
- 85 Weitzman MD, Fradet-Turcotte A. Virus DNA Replication and the Host DNA Damage Response. *Annual review of virology* **5**, 141-164 (2018).
- 86 Luftig MA. Viruses and the DNA Damage Response: Activation and Antagonism. *Annual review of virology* **1**, 605-625 (2014).
- 87 Bannister AJ, Kouzarides T. Regulation of chromatin by histone modifications. *Cell Res* **21**, 381-395 (2011).
- 88 Gates LA, Foulds CE, O'Malley BW. Histone Marks in the 'Driver's Seat': Functional Roles in Steering the Transcription Cycle. *Trends Biochem Sci* **42**, 977-989 (2017).

- 89 Zhang T, Cooper S, Brockdorff N. The interplay of histone modifications - writers that read. *EMBO Rep* **16**, 1467-1481 (2015).
- 90 Kouzarides T. Chromatin modifications and their function. *Cell* **128**, 693-705 (2007).
- 91 Dixon JR, Jung I, Selvaraj S, Shen Y, Antosiewicz-Bourget JE, Lee AY, Ye Z, Kim A, Rajagopal N, Xie W, Diao Y, Liang J, Zhao H, Lobanenkov VV, Ecker JR, Thomson JA, Ren B. Chromatin architecture reorganization during stem cell differentiation. *Nature* **518**, 331-336 (2015).
- 92 Smale ST, Tarakhovskiy A, Natoli G. Chromatin contributions to the regulation of innate immunity. *Annu Rev Immunol* **32**, 489-511 (2014).
- 93 Meshorer E, Misteli T. Chromatin in pluripotent embryonic stem cells and differentiation. *Nature reviews. Molecular cell biology* **7**, 540-546 (2006).
- 94 Schlesinger S, Meshorer E. Open Chromatin, Epigenetic Plasticity, and Nuclear Organization in Pluripotency. *Dev Cell* **48**, 135-150 (2019).
- 95 Lau CM, Adams NM, Geary CD, Weizman OE, Rapp M, Pritykin Y, Leslie CS, Sun JC. Epigenetic control of innate and adaptive immune memory. *Nat Immunol* **19**, 963-972 (2018).
- 96 Cutter AR, Hayes JJ. A brief review of nucleosome structure. *FEBS letters* **589**, 2914-2922 (2015).
- 97 Luger K, Rechsteiner TJ, Flaus AJ, Wayne MM, Richmond TJ. Characterization of nucleosome core particles containing histone proteins made in bacteria. *Journal of molecular biology* **272**, 301-311 (1997).
- 98 Malik HS, Henikoff S. Phylogenomics of the nucleosome. *Nat Struct Biol* **10**, 882-891 (2003).
- 99 Allan J, Mitchell T, Harborne N, Bohm L, Crane-Robinson C. Roles of H1 domains in determining higher order chromatin structure and H1 location. *Journal of molecular biology* **187**, 591-601 (1986).
- 100 Hansen JC. Conformational dynamics of the chromatin fiber in solution: determinants, mechanisms, and functions. *Annu Rev Biophys Biomol Struct* **31**, 361-392 (2002).
- 101 Deaton AM, Bird A. CpG islands and the regulation of transcription. *Genes Dev* **25**, 1010-1022 (2011).
- 102 Arnaudo AM, Garcia BA. Proteomic characterization of novel histone post-translational modifications. *Epigenetics Chromatin* **6**, 24 (2013).
- 103 Kouzarides T. SnapShot: Histone-modifying enzymes. *Cell* **131**, 822 (2007).
- 104 Jackson SP. Sensing and repairing DNA double-strand breaks. *Carcinogenesis* **23**, 687-696 (2002).
- 105 Burma S, Chen BP, Murphy M, Kurimasa A, Chen DJ. ATM phosphorylates histone H2AX in response to DNA double-strand breaks. *The Journal of biological chemistry* **276**, 42462-42467 (2001).
- 106 Clapier CR, Iwasa J, Cairns BR, Peterson CL. Mechanisms of action and regulation of ATP-dependent chromatin-remodelling complexes. *Nature reviews. Molecular cell biology* **18**, 407-422 (2017).
- 107 Varshavsky AJ, Nedospasov SA, Schmatchenko VV, Bakayev VV, Chumackov PM, Georgiev GP. Compact form of SV40 viral minichromosome is resistant to nuclease: possible implications for chromatin structure. *Nucleic Acids Res* **4**, 3303-3325 (1977).
- 108 Favre M, Breitbart F, Croissant O, Orth G. Chromatin-like structures obtained after alkaline disruption of bovine and human papillomaviruses. *J Virol* **21**, 1205-1209 (1977).
- 109 Milavetz B. Hyperacetylation and differential deacetylation of histones H4 and H3 define two distinct classes of acetylated SV40 chromosomes early in infection. *Virology* **319**, 324-336 (2004).
- 110 Saper G, Kler S, Asor R, Oppenheim A, Raviv U, Harries D. Effect of capsid confinement on the chromatin organization of the SV40 minichromosome. *Nucleic Acids Res* **41**, 1569-1580 (2013).

- 111 Balakrishnan L, Gefroh A, Milavetz B. Histone H4 lysine 20 mono- and tri-methylation define distinct biological processes in SV40 minichromosomes. *Cell cycle (Georgetown, Tex.)* **9**, 1320-1332 (2010).
- 112 Wu S, Rice JC. A histone methylation code for SV40 minichromosomes. *Cell cycle (Georgetown, Tex.)* **9**, 1235-1236 (2010).
- 113 Cliffe AR, Knipe DM. Herpes simplex virus ICP0 promotes both histone removal and acetylation on viral DNA during lytic infection. *J Virol* **82**, 12030-12038 (2008).
- 114 Oh J, Fraser NW. Temporal association of the herpes simplex virus genome with histone proteins during a lytic infection. *J Virol* **82**, 3530-3537 (2008).
- 115 Herrera FJ, Triezenberg SJ. VP16-dependent association of chromatin-modifying coactivators and underrepresentation of histones at immediate-early gene promoters during herpes simplex virus infection. *J Virol* **78**, 9689-9696 (2004).
- 116 Knipe DM, Cliffe A. Chromatin control of herpes simplex virus lytic and latent infection. *Nat Rev Microbiol* **6**, 211-221 (2008).
- 117 Wang QY, Zhou C, Johnson KE, Colgrove RC, Coen DM, Knipe DM. Herpesviral latency-associated transcript gene promotes assembly of heterochromatin on viral lytic-gene promoters in latent infection. *Proceedings of the National Academy of Sciences of the United States of America* **102**, 16055-16059 (2005).
- 118 Gunther T, Grundhoff A. The epigenetic landscape of latent Kaposi sarcoma-associated herpesvirus genomes. *PLoS pathogens* **6**, e1000935 (2010).
- 119 Toth Z, Maglinte DT, Lee SH, Lee HR, Wong LY, Brulois KF, Lee S, Buckley JD, Laird PW, Marquez VE, Jung JU. Epigenetic analysis of KSHV latent and lytic genomes. *PLoS pathogens* **6**, e1001013 (2010).
- 120 Symons J, Cameron PU, Lewin SR. HIV integration sites and implications for maintenance of the reservoir. *Curr Opin HIV AIDS* **13**, 152-159 (2018).
- 121 Castro-Gonzalez S, Colomer-Lluch M, Serra-Moreno R. Barriers for HIV Cure: The Latent Reservoir. *AIDS Res Hum Retroviruses* **34**, 739-759 (2018).
- 122 Deeks SG. HIV: Shock and kill. *Nature* **487**, 439-440 (2012).
- 123 Van Lint C, Emiliani S, Ott M, Verdin E. Transcriptional activation and chromatin remodeling of the HIV-1 promoter in response to histone acetylation. *EMBO J* **15**, 1112-1120 (1996).
- 124 Wightman F, Ellenberg P, Churchill M, Lewin SR. HDAC inhibitors in HIV. *Immunol Cell Biol* **90**, 47-54 (2012).
- 125 Archin NM, Liberty AL, Kashuba AD, Choudhary SK, Kuruc JD, Crooks AM, Parker DC, Anderson EM, Kearney MF, Strain MC, Richman DD, Hudgens MG, Bosch RJ, Coffin JM, Eron JJ, Hazuda DJ, Margolis DM. Administration of vorinostat disrupts HIV-1 latency in patients on antiretroviral therapy. *Nature* **487**, 482-485 (2012).
- 126 McBride AA, Sakakibara N, Stepp WH, Jang MK. Hitchhiking on host chromatin: how papillomaviruses persist. *Biochim Biophys Acta* **1819**, 820-825 (2012).
- 127 You J. Papillomavirus interaction with cellular chromatin. *Biochim Biophys Acta* **1799**, 192-199 (2010).
- 128 Zhirnov OP, Klenk HD. Histones as a target for influenza virus matrix protein M1. *Virology* **235**, 302-310 (1997).
- 129 Garcia-Robles I, Akarsu H, Muller CW, Ruigrok RW, Baudin F. Interaction of influenza virus proteins with nucleosomes. *Virology* **332**, 329-336 (2005).
- 130 Takizawa N, Watanabe K, Nouno K, Kobayashi N, Nagata K. Association of functional influenza viral proteins and RNAs with nuclear chromatin and sub-chromatin structure. *Microbes Infect* **8**, 823-833 (2006).
- 131 Marazzi I, Ho JS, Kim J, Manicassamy B, Dewell S, Albrecht RA, Seibert CW, Schaefer U, Jeffrey KL, Prinjha RK, Lee K, Garcia-Sastre A, Roeder RG, Tarakhovskiy A. Suppression of the antiviral response by an influenza histone mimic. *Nature* **483**, 428-433 (2012).
- 132 Gibson W, Roizman B. Compartmentalization of spermine and spermidine in the herpes simplex virion. *Proceedings of the National Academy of Sciences of the United States of America* **68**, 2818-2821 (1971).

- 133 Lischwe MA, Sung MT. A histone-like protein from adenovirus chromatin. *Nature* **267**, 552-554 (1977).
- 134 Mirza MA, Weber J. Structure of adenovirus chromatin. *Biochim Biophys Acta* **696**, 76-86 (1982).
- 135 Corden J, Engelking HM, Pearson GD. Chromatin-like organization of the adenovirus chromosome. *Proceedings of the National Academy of Sciences of the United States of America* **73**, 401-404 (1976).
- 136 Tweeten KA, Bulla LA, Consigli RA. Characterization of an extremely basic protein derived from granulosis virus nucleocapsids. *J Virol* **33**, 866-876 (1980).
- 137 Wang M, Tuladhar E, Shen S, Wang H, van Oers MM, Vlak JM, Westenberg M. Specificity of baculovirus P6.9 basic DNA-binding proteins and critical role of the C terminus in virion formation. *J Virol* **84**, 8821-8828 (2010).
- 138 Anderson CW, Baum PR, Gesteland RF. Processing of adenovirus 2-induced proteins. *J Virol* **12**, 241-252 (1973).
- 139 Komatsu T, Haruki H, Nagata K. Cellular and viral chromatin proteins are positive factors in the regulation of adenovirus gene expression. *Nucleic Acids Res* **39**, 889-901 (2011).
- 140 Matsumoto K, Nagata K, Ui M, Hanaoka F. Template activating factor I, a novel host factor required to stimulate the adenovirus core DNA replication. *The Journal of biological chemistry* **268**, 10582-10587 (1993).
- 141 Gyurcsik B, Haruki H, Takahashi T, Mihara H, Nagata K. Binding modes of the precursor of adenovirus major core protein VII to DNA and template activating factor I: implication for the mechanism of remodeling of the adenovirus chromatin. *Biochemistry* **45**, 303-313 (2006).
- 142 Okuwaki M, Nagata K. Template activating factor-I remodels the chromatin structure and stimulates transcription from the chromatin template. *The Journal of biological chemistry* **273**, 34511-34518 (1998).
- 143 Johnson JS, Osheim YN, Xue Y, Emanuel MR, Lewis PW, Bankovich A, Beyer AL, Engel DA. Adenovirus protein VII condenses DNA, represses transcription, and associates with transcriptional activator E1A. *J Virol* **78**, 6459-6468 (2004).
- 144 Karen KA, Hearing P. Adenovirus core protein VII protects the viral genome from a DNA damage response at early times after infection. *J Virol* **85**, 4135-4142 (2011).
- 145 Haruki H, Okuwaki M, Miyagishi M, Taira K, Nagata K. Involvement of template-activating factor I/SET in transcription of adenovirus early genes as a positive-acting factor. *J Virol* **80**, 794-801 (2006).
- 146 Komatsu T, Nagata K. Replication-uncoupled histone deposition during adenovirus DNA replication. *J Virol* **86**, 6701-6711 (2012).
- 147 Giberson AN, Davidson AR, Parks RJ. Chromatin structure of adenovirus DNA throughout infection. *Nucleic Acids Res* **40**, 2369-2376 (2012).
- 148 Chen J, Morral N, Engel DA. Transcription releases protein VII from adenovirus chromatin. *Virology* **369**, 411-422 (2007).
- 149 Ross PJ, Kennedy MA, Christou C, Risco Quiroz M, Poulin KL, Parks RJ. Assembly of helper-dependent adenovirus DNA into chromatin promotes efficient gene expression. *J Virol* **85**, 3950-3958 (2011).
- 150 Giberson AN, Saha B, Campbell K, Christou C, Poulin KL, Parks RJ. Human adenoviral DNA association with nucleosomes containing histone variant H3.3 during the early phase of infection is not dependent on viral transcription or replication. *Biochem Cell Biol* **96**, 797-807 (2018).
- 151 Avgousti DC, Della Fera AN, Otter CJ, Herrmann C, Pancholi NJ, Weitzman MD. Adenovirus Core Protein VII Downregulates the DNA Damage Response on the Host Genome. *J Virol* **91** (2017).
- 152 Chelius D, Huhmer AF, Shieh CH, Lehmborg E, Traina JA, Slattery TK, Pungor E, Jr. Analysis of the adenovirus type 5 proteome by liquid chromatography and tandem mass spectrometry methods. *J Proteome Res* **1**, 501-513 (2002).

- 153 Ostapchuk P, Suomalainen M, Zheng Y, Boucke K, Greber UF, Hearing P. The adenovirus major core protein VII is dispensable for virion assembly but is essential for lytic infection. *PLoS pathogens* **13**, e1006455 (2017).
- 154 Oudet P, Gross-Bellard M, Chambon P. Electron microscopic and biochemical evidence that chromatin structure is a repeating unit. *Cell* **4**, 281-300 (1975).
- 155 Chiu YF, Sugden AU, Sugden B. Epstein-Barr viral productive amplification reprograms nuclear architecture, DNA replication, and histone deposition. *Cell host & microbe* **14**, 607-618 (2013).
- 156 Simpson-Holley M, Colgrove RC, Nalepa G, Harper JW, Knipe DM. Identification and functional evaluation of cellular and viral factors involved in the alteration of nuclear architecture during herpes simplex virus 1 infection. *J Virol* **79**, 12840-12851 (2005).
- 157 Ihalainen TO, Niskanen EA, Jylhava J, Paloheimo O, Dross N, Smolander H, Langowski J, Timonen J, Vihinen-Ranta M. Parvovirus induced alterations in nuclear architecture and dynamics. *PLoS One* **4**, e5948 (2009).
- 158 Lam YW, Evans VC, Heesom KJ, Lamond AI, Matthews DA. Proteomics analysis of the nucleolus in adenovirus-infected cells. *Mol Cell Proteomics* **9**, 117-130 (2010).
- 159 Komander D, Rape M. The ubiquitin code. *Annu Rev Biochem* **81**, 203-229 (2012).
- 160 Yau R, Rape M. The increasing complexity of the ubiquitin code. *Nat Cell Biol* **18**, 579-586 (2016).
- 161 Akutsu M, Dikic I, Bremm A. Ubiquitin chain diversity at a glance. *J Cell Sci* **129**, 875-880 (2016).
- 162 McDowell GS, Philpott A. Non-canonical ubiquitylation: mechanisms and consequences. *Int J Biochem Cell Biol* **45**, 1833-1842 (2013).
- 163 Husnjak K, Dikic I. Ubiquitin-binding proteins: decoders of ubiquitin-mediated cellular functions. *Annu Rev Biochem* **81**, 291-322 (2012).
- 164 Kulathu Y, Komander D. Atypical ubiquitylation - the unexplored world of polyubiquitin beyond Lys48 and Lys63 linkages. *Nature reviews. Molecular cell biology* **13**, 508-523 (2012).
- 165 Thrower JS, Hoffman L, Rechsteiner M, Pickart CM. Recognition of the polyubiquitin proteolytic signal. *EMBO J* **19**, 94-102 (2000).
- 166 Tanaka K. The proteasome: overview of structure and functions. *Proc Jpn Acad Ser B Phys Biol Sci* **85**, 12-36 (2009).
- 167 Grice GL, Nathan JA. The recognition of ubiquitinated proteins by the proteasome. *Cell Mol Life Sci* **73**, 3497-3506 (2016).
- 168 Xu P, Duong DM, Seyfried NT, Cheng D, Xie Y, Robert J, Rush J, Hochstrasser M, Finley D, Peng J. Quantitative proteomics reveals the function of unconventional ubiquitin chains in proteasomal degradation. *Cell* **137**, 133-145 (2009).
- 169 Johnson ES, Ma PC, Ota IM, Varshavsky A. A proteolytic pathway that recognizes ubiquitin as a degradation signal. *The Journal of biological chemistry* **270**, 17442-17456 (1995).
- 170 Matsumoto ML, Wickliffe KE, Dong KC, Yu C, Bosanac I, Bustos D, Phu L, Kirkpatrick DS, Hymowitz SG, Rape M, Kelley RF, Dixit VM. K11-linked polyubiquitination in cell cycle control revealed by a K11 linkage-specific antibody. *Mol Cell* **39**, 477-484 (2010).
- 171 Karin M, Ben-Neriah Y. Phosphorylation meets ubiquitination: the control of NF-[kappa]B activity. *Annu Rev Immunol* **18**, 621-663 (2000).
- 172 Gerlach B, Cordier SM, Schmukle AC, Emmerich CH, Rieser E, Haas TL, Webb AI, Rickard JA, Anderton H, Wong WW, Nachbar U, Gangoda L, Warnken U, Purcell AW, Silke J, Walczak H. Linear ubiquitination prevents inflammation and regulates immune signalling. *Nature* **471**, 591-596 (2011).
- 173 Tokunaga F, Sakata S, Saeki Y, Satomi Y, Kirisako T, Kamei K, Nakagawa T, Kato M, Murata S, Yamaoka S, Yamamoto M, Akira S, Takao T, Tanaka K, Iwai K. Involvement of linear polyubiquitylation of NEMO in NF-kappaB activation. *Nat Cell Biol* **11**, 123-132 (2009).

- 174 Liu P, Gan W, Su S, Hauenstein AV, Fu TM, Brasher B, Schwerdtfeger C, Liang AC, Xu M, Wei W. K63-linked polyubiquitin chains bind to DNA to facilitate DNA damage repair. *Sci Signal* **11** (2018).
- 175 Lee BL, Singh A, Mark Glover JN, Hendzel MJ, Spyrapoulos L. Molecular Basis for K63-Linked Ubiquitination Processes in Double-Strand DNA Break Repair: A Focus on Kinetics and Dynamics. *Journal of molecular biology* **429**, 3409-3429 (2017).
- 176 Erpapazoglou Z, Walker O, Haguenaer-Tsapis R. Versatile roles of k63-linked ubiquitin chains in trafficking. *Cells* **3**, 1027-1088 (2014).
- 177 Piper RC, Dikic I, Lukacs GL. Ubiquitin-dependent sorting in endocytosis. *Cold Spring Harb Perspect Biol* **6** (2014).
- 178 Back S, Gorman AW, Vogel C, Silva GM. Site-Specific K63 Ubiquitinomics Provides Insights into Translation Regulation under Stress. *J Proteome Res* **18**, 309-318 (2019).
- 179 Silva GM, Vogel C. Mass spectrometry analysis of K63-ubiquitinated targets in response to oxidative stress. *Data Brief* **4**, 130-134 (2015).
- 180 Morris JR, Solomon E. BRCA1 : BARD1 induces the formation of conjugated ubiquitin structures, dependent on K6 of ubiquitin, in cells during DNA replication and repair. *Hum Mol Genet* **13**, 807-817 (2004).
- 181 Durcan TM, Tang MY, Perusse JR, Dashti EA, Aguilera MA, McLelland GL, Gros P, Shaler TA, Faubert D, Coulombe B, Fon EA. USP8 regulates mitophagy by removing K6-linked ubiquitin conjugates from parkin. *EMBO J* **33**, 2473-2491 (2014).
- 182 Ordureau A, Sarraf SA, Duda DM, Heo JM, Jedrychowski MP, Sviderskiy VO, Olszewski JL, Koerber JT, Xie T, Beausoleil SA, Wells JA, Gygi SP, Schulman BA, Harper JW. Quantitative proteomics reveal a feedforward mechanism for mitochondrial PARKIN translocation and ubiquitin chain synthesis. *Mol Cell* **56**, 360-375 (2014).
- 183 Gatti M, Pinato S, Maiolica A, Rocchio F, Prato MG, Aebersold R, Penengo L. RNF168 promotes noncanonical K27 ubiquitination to signal DNA damage. *Cell reports* **10**, 226-238 (2015).
- 184 Wang Q, Liu X, Cui Y, Tang Y, Chen W, Li S, Yu H, Pan Y, Wang C. The E3 ubiquitin ligase AMFR and INSIG1 bridge the activation of TBK1 kinase by modifying the adaptor STING. *Immunity* **41**, 919-933 (2014).
- 185 Fei C, Li Z, Li C, Chen Y, Chen Z, He X, Mao L, Wang X, Zeng R, Li L. Smurf1-mediated Lys29-linked nonproteolytic polyubiquitination of axin negatively regulates Wnt/beta-catenin signaling. *Mol Cell Biol* **33**, 4095-4105 (2013).
- 186 Yuan WC, Lee YR, Lin SY, Chang LY, Tan YP, Hung CC, Kuo JC, Liu CH, Lin MY, Xu M, Chen ZJ, Chen RH. K33-Linked Polyubiquitination of Coronin 7 by Cul3-KLHL20 Ubiquitin E3 Ligase Regulates Protein Trafficking. *Mol Cell* **54**, 586-600 (2014).
- 187 Hoege C, Pfander B, Moldovan GL, Pyrowolakis G, Jentsch S. RAD6-dependent DNA repair is linked to modification of PCNA by ubiquitin and SUMO. *Nature* **419**, 135-141 (2002).
- 188 Li M, Brooks CL, Wu-Baer F, Chen D, Baer R, Gu W. Mono- versus polyubiquitination: differential control of p53 fate by Mdm2. *Science* **302**, 1972-1975 (2003).
- 189 Mashtalir N, Daou S, Barbour H, Sen NN, Gagnon J, Hammond-Martel I, Dar HH, Therrien M, Affar el B. Autodeubiquitination protects the tumor suppressor BAP1 from cytoplasmic sequestration mediated by the atypical ubiquitin ligase UBE2O. *Mol Cell* **54**, 392-406 (2014).
- 190 Mevissen TET, Komander D. Mechanisms of Deubiquitinase Specificity and Regulation. *Annu Rev Biochem* **86**, 159-192 (2017).
- 191 Lilley CE, Chaurushiya MS, Boutell C, Everett RD, Weitzman MD. The intrinsic antiviral defense to incoming HSV-1 genomes includes specific DNA repair proteins and is counteracted by the viral protein ICP0. *PLoS pathogens* **7**, e1002084 (2011).
- 192 Lilley CE, Chaurushiya MS, Boutell C, Landry S, Suh J, Panier S, Everett RD, Stewart GS, Durocher D, Weitzman MD. A viral E3 ligase targets RNF8 and RNF168 to control histone ubiquitination and DNA damage responses. *EMBO J* **29**, 943-955 (2010).

- 193 Everett RD, Freemont P, Saitoh H, Dasso M, Orr A, Kathoria M, Parkinson J. The disruption of ND10 during herpes simplex virus infection correlates with the Vmw110- and proteasome-dependent loss of several PML isoforms. *J Virol* **72**, 6581-6591 (1998).
- 194 Gu H, Roizman B. The degradation of promyelocytic leukemia and Sp100 proteins by herpes simplex virus 1 is mediated by the ubiquitin-conjugating enzyme UbcH5a. *Proceedings of the National Academy of Sciences of the United States of America* **100**, 8963-8968 (2003).
- 195 Glass M, Everett RD. Components of promyelocytic leukemia nuclear bodies (ND10) act cooperatively to repress herpesvirus infection. *J Virol* **87**, 2174-2185 (2013).
- 196 Nguyen HC, Wang W, Xiong Y. Cullin-RING E3 Ubiquitin Ligases: Bridges to Destruction. *Subcell Biochem* **83**, 323-347 (2017).
- 197 Yu X, Yu Y, Liu B, Luo K, Kong W, Mao P, Yu XF. Induction of APOBEC3G ubiquitination and degradation by an HIV-1 Vif-Cul5-SCF complex. *Science* **302**, 1056-1060 (2003).
- 198 Stopak K, de Noronha C, Yonemoto W, Greene WC. HIV-1 Vif blocks the antiviral activity of APOBEC3G by impairing both its translation and intracellular stability. *Mol Cell* **12**, 591-601 (2003).
- 199 Harris RS, Bishop KN, Sheehy AM, Craig HM, Petersen-Mahrt SK, Watt IN, Neuberger MS, Malim MH. DNA deamination mediates innate immunity to retroviral infection. *Cell* **113**, 803-809 (2003).
- 200 Zhang H, Yang B, Pomerantz RJ, Zhang C, Arunachalam SC, Gao L. The cytidine deaminase CEM15 induces hypermutation in newly synthesized HIV-1 DNA. *Nature* **424**, 94-98 (2003).
- 201 Mangeat B, Turelli P, Caron G, Friedli M, Perrin L, Trono D. Broad antiretroviral defence by human APOBEC3G through lethal editing of nascent reverse transcripts. *Nature* **424**, 99-103 (2003).
- 202 Scheffner M, Huibregtse JM, Vierstra RD, Howley PM. The HPV-16 E6 and E6-AP complex functions as a ubiquitin-protein ligase in the ubiquitination of p53. *Cell* **75**, 495-505 (1993).
- 203 Scheffner M, Werness BA, Huibregtse JM, Levine AJ, Howley PM. The E6 oncoprotein encoded by human papillomavirus types 16 and 18 promotes the degradation of p53. *Cell* **63**, 1129-1136 (1990).
- 204 Huibregtse JM, Scheffner M, Howley PM. A cellular protein mediates association of p53 with the E6 oncoprotein of human papillomavirus types 16 or 18. *Embo j* **10**, 4129-4135 (1991).
- 205 Saridakis V, Sheng Y, Sarkari F, Holowaty MN, Shire K, Nguyen T, Zhang RG, Liao J, Lee W, Edwards AM, Arrowsmith CH, Frappier L. Structure of the p53 binding domain of HAUSP/USP7 bound to Epstein-Barr nuclear antigen 1 implications for EBV-mediated immortalization. *Mol Cell* **18**, 25-36 (2005).
- 206 Sheng Y, Saridakis V, Sarkari F, Duan S, Wu T, Arrowsmith CH, Frappier L. Molecular recognition of p53 and MDM2 by USP7/HAUSP. *Nat Struct Mol Biol* **13**, 285-291 (2006).
- 207 Faust TB, Li Y, Bacon CW, Jang GM, Weiss A, Jayaraman B, Newton BW, Krogan NJ, D'Orso I, Frankel AD. The HIV-1 Tat protein recruits a ubiquitin ligase to reorganize the 7SK snRNP for transcriptional activation. *Elife* **7** (2018).
- 208 Faust TB, Li Y, Jang GM, Johnson JR, Yang S, Weiss A, Krogan NJ, Frankel AD. PJA2 ubiquitinates the HIV-1 Tat protein with atypical chain linkages to activate viral transcription. *Sci Rep* **7**, 45394 (2017).
- 209 Duncan LM, Piper S, Dodd RB, Saville MK, Sanderson CM, Luzio JP, Lehner PJ. Lysine-63-linked ubiquitination is required for endolysosomal degradation of class I molecules. *EMBO J* **25**, 1635-1645 (2006).
- 210 Xu G, Paige JS, Jaffrey SR. Global analysis of lysine ubiquitination by ubiquitin remnant immunoaffinity profiling. *Nature biotechnology* **28**, 868-873 (2010).
- 211 Udeshi ND, Mertins P, Svinkina T, Carr SA. Large-scale identification of ubiquitination sites by mass spectrometry. *Nat Protoc* **8**, 1950-1960 (2013).

- 212 Querido E, Blanchette P, Yan Q, Kamura T, Morrison M, Boivin D, Kaelin WG, Conaway RC, Conaway JW, Branton PE. Degradation of p53 by adenovirus E4orf6 and E1B55K proteins occurs via a novel mechanism involving a Cullin-containing complex. *Genes Dev* **15**, 3104-3117 (2001).
- 213 Harada JN, Shevchenko A, Shevchenko A, Pallas DC, Berk AJ. Analysis of the adenovirus E1B-55K-anchored proteome reveals its link to ubiquitination machinery. *J Virol* **76**, 9194-9206 (2002).
- 214 Rubenwolf S, Schutt H, Nevels M, Wolf H, Dobner T. Structural analysis of the adenovirus type 5 E1B 55-kilodalton-E4orf6 protein complex. *J Virol* **71**, 1115-1123 (1997).
- 215 Sarnow P, Hearing P, Anderson CW, Halbert DN, Shenk T, Levine AJ. Adenovirus early region 1B 58,000-dalton tumor antigen is physically associated with an early region 4 25,000-dalton protein in productively infected cells. *J Virol* **49**, 692-700 (1984).
- 216 Blanchette P, Kindsmuller K, Groitl P, Dallaire F, Speiseder T, Branton PE, Dobner T. Control of mRNA export by adenovirus E4orf6 and E1B55K proteins during productive infection requires E4orf6 ubiquitin ligase activity. *J Virol* **82**, 2642-2651 (2008).
- 217 Blanchette P, Cheng CY, Yan Q, Ketner G, Ornelles DA, Dobner T, Conaway RC, Conaway JW, Branton PE. Both BC-box motifs of adenovirus protein E4orf6 are required to efficiently assemble an E3 ligase complex that degrades p53. *Mol Cell Biol* **24**, 9619-9629 (2004).
- 218 Cheng CY, Blanchette P, Branton PE. The adenovirus E4orf6 E3 ubiquitin ligase complex assembles in a novel fashion. *Virology* **364**, 36-44 (2007).
- 219 Schwartz RA, Lakdawala SS, Eshleman HD, Russell MR, Carson CT, Weitzman MD. Distinct requirements of adenovirus E1b55K protein for degradation of cellular substrates. *J Virol* **82**, 9043-9055 (2008).
- 220 Goodrum FD, Shenk T, Ornelles DA. Adenovirus early region 4 34-kilodalton protein directs the nuclear localization of the early region 1B 55-kilodalton protein in primate cells. *J Virol* **70**, 6323-6335 (1996).
- 221 Orazio NI, Naeger CM, Karlseder J, Weitzman MD. The adenovirus E1b55K/E4orf6 complex induces degradation of the Bloom helicase during infection. *J Virol* **85**, 1887-1892 (2011).
- 222 Baker A, Rohleder KJ, Hanakahi LA, Ketner G. Adenovirus E4 34k and E1b 55k oncoproteins target host DNA ligase IV for proteasomal degradation. *J Virol* **81**, 7034-7040 (2007).
- 223 Dallaire F, Blanchette P, Groitl P, Dobner T, Branton PE. Identification of integrin alpha3 as a new substrate of the adenovirus E4orf6/E1B 55-kilodalton E3 ubiquitin ligase complex. *J Virol* **83**, 5329-5338 (2009).
- 224 Querido E, Marcellus RC, Lai A, Charbonneau R, Teodoro JG, Ketner G, Branton PE. Regulation of p53 levels by the E1B 55-kilodalton protein and E4orf6 in adenovirus-infected cells. *J Virol* **71**, 3788-3798 (1997).
- 225 Shen Y, Kitzes G, Nye JA, Fattaey A, Hermiston T. Analyses of single-amino-acid substitution mutants of adenovirus type 5 E1B-55K protein. *J Virol* **75**, 4297-4307 (2001).
- 226 Higashino F, Pipas JM, Shenk T. Adenovirus E4orf6 oncoprotein modulates the function of the p53-related protein, p73. *Proceedings of the National Academy of Sciences of the United States of America* **95**, 15683-15687 (1998).
- 227 Steegenga WT, Shvarts A, Riteco N, Bos JL, Jochemsen AG. Distinct regulation of p53 and p73 activity by adenovirus E1A, E1B, and E4orf6 proteins. *Mol Cell Biol* **19**, 3885-3894 (1999).
- 228 Dobner T, Horikoshi N, Rubenwolf S, Shenk T. Blockage by adenovirus E4orf6 of transcriptional activation by the p53 tumor suppressor. *Science* **272**, 1470-1473 (1996).
- 229 Lamarche BJ, Orazio NI, Weitzman MD. The MRN complex in double-strand break repair and telomere maintenance. *FEBS letters* **584**, 3682-3695 (2010).
- 230 Brosh RM, Jr. DNA helicases involved in DNA repair and their roles in cancer. *Nature reviews. Cancer* **13**, 542-558 (2013).

- 231 Lieber MR. The mechanism of double-strand DNA break repair by the nonhomologous DNA end-joining pathway. *Annu Rev Biochem* **79**, 181-211 (2010).
- 232 Lakdawala SS, Schwartz RA, Ferenchak K, Carson CT, McSharry BP, Wilkinson GW, Weitzman WD. Differential Requirements of the C Terminus of Nbs1 in Suppressing Adenovirus DNA Replication and Promoting Concatemer Formation. *J Virol* **82**, 8362-8372 (2008).
- 233 Boyer J, Rohleder K, Ketner G. Adenovirus E4 34k and E4 11k inhibit double strand break repair and are physically associated with the cellular DNA-dependent protein kinase. *Virology* **263**, 307-312 (1999).
- 234 Carson CT, Schwartz RA, Stracker TH, Lilley CE, Lee DV, Weitzman MD. The Mre11 complex is required for ATM activation and the G2/M checkpoint. *Embo j* **22**, 6610-6620 (2003).
- 235 Evans JD, Hearing P. Distinct roles of the Adenovirus E4 ORF3 protein in viral DNA replication and inhibition of genome concatenation. *J Virol* **77**, 5295-5304 (2003).
- 236 Jayaram S, Bridge E. Genome concatenation contributes to the late gene expression defect of an adenovirus E4 mutant. *Virology* **342**, 286-296 (2005).
- 237 Mathew SS, Bridge E. The cellular Mre11 protein interferes with adenovirus E4 mutant DNA replication. *Virology* **365**, 346-355 (2007).
- 238 Dallaire F, Blanchette P, Branton PE. A proteomic approach to identify candidate substrates of human adenovirus E4orf6-E1B55K and other viral cullin-based E3 ubiquitin ligases. *J Virol* **83**, 12172-12184 (2009).
- 239 Cheng CY, Gilson T, Dallaire F, Ketner G, Branton PE, Blanchette P. The E4orf6/E1B55K E3 ubiquitin ligase complexes of human adenoviruses exhibit heterogeneity in composition and substrate specificity. *J Virol* **85**, 765-775 (2011).
- 240 Pancholi NJ, Weitzman MD. Serotype-specific restriction of wild-type adenoviruses by the cellular Mre11-Rad50-Nbs1 complex. *Virology* **518**, 221-231 (2018).
- 241 Goodrum FD, Ornelles DA. p53 status does not determine outcome of E1B 55-kilodalton mutant adenovirus lytic infection. *J Virol* **72**, 9479-9490 (1998).
- 242 O'Shea CC, Johnson L, Bagus B, Choi S, Nicholas C, Shen A, Boyle L, Pandey K, Soria C, Kunich J, Shen Y, Habets G, Ginzinger D, McCormick F. Late viral RNA export, rather than p53 inactivation, determines ONYX-015 tumor selectivity. *Cancer Cell* **6**, 611-623 (2004).
- 243 Babiss LE, Ginsberg HS, Darnell JE, Jr. Adenovirus E1B proteins are required for accumulation of late viral mRNA and for effects on cellular mRNA translation and transport. *Mol Cell Biol* **5**, 2552-2558 (1985).
- 244 Pilder S, Moore M, Logan J, Shenk T. The adenovirus E1B-55K transforming polypeptide modulates transport or cytoplasmic stabilization of viral and host cell mRNAs. *Mol Cell Biol* **6**, 470-476 (1986).
- 245 Babiss LE, Ginsberg HS. Adenovirus type 5 early region 1b gene product is required for efficient shutoff of host protein synthesis. *J Virol* **50**, 202-212 (1984).
- 246 Halbert DN, Cutt JR, Shenk T. Adenovirus early region 4 encodes functions required for efficient DNA replication, late gene expression, and host cell shutoff. *J Virol* **56**, 250-257 (1985).
- 247 Cuesta R, Xi Q, Schneider RJ. Adenovirus-specific translation by displacement of kinase Mnk1 from cap-initiation complex eIF4F. *EMBO J* **19**, 3465-3474 (2000).
- 248 Cuesta R, Xi Q, Schneider RJ. Structural basis for competitive inhibition of eIF4G-Mnk1 interaction by the adenovirus 100-kilodalton protein. *J Virol* **78**, 7707-7716 (2004).
- 249 Dolph PJ, Racaniello V, Villamarin A, Palladino F, Schneider RJ. The adenovirus tripartite leader may eliminate the requirement for cap-binding protein complex during translation initiation. *J Virol* **62**, 2059-2066 (1988).
- 250 Dolph PJ, Huang JT, Schneider RJ. Translation by the adenovirus tripartite leader: elements which determine independence from cap-binding protein complex. *J Virol* **64**, 2669-2677 (1990).
- 251 Sandler AB, Ketner G. Adenovirus early region 4 is essential for normal stability of late nuclear RNAs. *J Virol* **63**, 624-630 (1989).

- 252 Bridge E, Ketner G. Interaction of adenoviral E4 and E1b products in late gene expression. *Virology* **174**, 345-353 (1990).
- 253 Hung G, Flint SJ. Normal human cell proteins that interact with the adenovirus type 5 E1B 55kDa protein. *Virology* **504**, 12-24 (2017).
- 254 Evans VC, Barker G, Heesom KJ, Fan J, Bessant C, Matthews DA. De novo derivation of proteomes from transcriptomes for transcript and protein identification. *Nat Methods* **9**, 1207-1211 (2012).
- 255 Fu YR, Turnell AS, Davis S, Heesom KJ, Evans VC, Matthews DA. Comparison of protein expression during wild-type, and E1B-55k-deletion, adenovirus infection using quantitative time-course proteomics. *The Journal of general virology* **98**, 1377-1388 (2017).
- 256 Iconomou M, Saunders DN. Systematic approaches to identify E3 ligase substrates. *Biochem J* **473**, 4083-4101 (2016).
- 257 Pierce NW, Kleiger G, Shan SO, Deshaies RJ. Detection of sequential polyubiquitylation on a millisecond timescale. *Nature* **462**, 615-619 (2009).
- 258 Avgousti DC, Herrmann C, Kulej K, Pancholi NJ, Sekulic N, Petrescu J, Molden RC, Blumenthal D, Paris AJ, Reyes ED, Ostapchuk P, Hearing P, Seeholzer SH, Worthen GS, Black BE, Garcia BA, Weitzman MD. A core viral protein binds host nucleosomes to sequester immune danger signals. *Nature* **535**, 173-177 (2016).
- 259 Elde NC, Malik HS. The evolutionary conundrum of pathogen mimicry. *Nat Rev Microbiol* **7**, 787-797 (2009).
- 260 Kang R, Chen R, Zhang Q, Hou W, Wu S, Cao L, Huang J, Yu Y, Fan XG, Yan Z, Sun X, Wang H, Wang Q, Tsung A, Billiar TR, Zeh HJ, 3rd, Lotze MT, Tang D. HMGB1 in health and disease. *Mol Aspects Med* **40**, 1-116 (2014).
- 261 Lotze MT, Tracey KJ. High-mobility group box 1 protein (HMGB1): nuclear weapon in the immune arsenal. *Nat Rev Immunol* **5**, 331-342 (2005).
- 262 Paschos K, Allday MJ. Epigenetic reprogramming of host genes in viral and microbial pathogenesis. *Trends Microbiol* **18**, 439-447 (2010).
- 263 Ferrari R, Berk AJ, Kurdistani SK. Viral manipulation of the host epigenome for oncogenic transformation. *Nat Rev Genet* **10**, 290-294 (2009).
- 264 Wykes SM, Krawetz SA. The structural organization of sperm chromatin. *The Journal of biological chemistry* **278**, 29471-29477 (2003).
- 265 Lin S, Garcia BA. Examining histone posttranslational modification patterns by high-resolution mass spectrometry. *Methods Enzymol* **512**, 3-28 (2012).
- 266 Shechter D, Dormann HL, Allis CD, Hake SB. Extraction, purification and analysis of histones. *Nat Protoc* **2**, 1445-1457 (2007).
- 267 Teves SS, Henikoff S. Salt fractionation of nucleosomes for genome-wide profiling. *Methods Mol Biol* **833**, 421-432 (2012).
- 268 Falk SJ, Guo LY, Sekulic N, Smoak EM, Mani T, Logsdon GA, Gupta K, Jansen LE, Van Duyne GD, Vinogradov SA, Lampson MA, Black BE. Chromosomes. CENP-C reshapes and stabilizes CENP-A nucleosomes at the centromere. *Science* **348**, 699-703 (2015).
- 269 White AE, Hieb AR, Luger K. A quantitative investigation of linker histone interactions with nucleosomes and chromatin. *Sci Rep* **6**, 19122 (2016).
- 270 Fedor MJ, Daniell E. Acetylation of histone-like proteins of adenovirus type 5. *J Virol* **35**, 637-643 (1980).
- 271 Robinson CM, Singh G, Lee JY, Dehghan S, Rajaiya J, Liu EB, Yousuf MA, Betensky RA, Jones MS, Dyer DW, Seto D, Chodosh J. Molecular evolution of human adenoviruses. *Sci Rep* **3**, 1812 (2013).
- 272 Scaffidi P, Misteli T, Bianchi ME. Release of chromatin protein HMGB1 by necrotic cells triggers inflammation. *Nature* **418**, 191-195 (2002).
- 273 Sapojnikova N, Maman J, Myers FA, Thorne AW, Vorobyev VI, Crane-Robinson C. Biochemical observation of the rapid mobility of nuclear HMGB1. *Biochim Biophys Acta* **1729**, 57-63 (2005).
- 274 Lu B, Nakamura T, Inouye K, Li J, Tang Y, Lundback P, Valdes-Ferrer SI, Olofsson PS, Kalb T, Roth J, Zou Y, Erlandsson-Harris H, Yang H, Ting JP, Wang H, Andersson U,

- Antoine DJ, Chavan SS, Hotamisligil GS, Tracey KJ. Novel role of PKR in inflammasome activation and HMGB1 release. *Nature* **488**, 670-674 (2012).
- 275 Koziol-White CJ, Damera G, Panettieri RA, Jr. Targeting airway smooth muscle in airways diseases: an old concept with new twists. *Expert Rev Respir Med* **5**, 767-777 (2011).
- 276 Ueno H, Matsuda T, Hashimoto S, Amaya F, Kitamura Y, Tanaka M, Kobayashi A, Maruyama I, Yamada S, Hasegawa N, Soejima J, Koh H, Ishizaka A. Contributions of high mobility group box protein in experimental and clinical acute lung injury. *Am J Respir Crit Care Med* **170**, 1310-1316 (2004).
- 277 Khandelia P, Yap K, Makeyev EV. Streamlined platform for short hairpin RNA interference and transgenesis in cultured mammalian cells. *Proceedings of the National Academy of Sciences of the United States of America* **108**, 12799-12804 (2011).
- 278 Kozarsky KF, Jooss K, Donahee M, Strauss JF, 3rd, Wilson JM. Effective treatment of familial hypercholesterolaemia in the mouse model using adenovirus-mediated transfer of the VLDL receptor gene. *Nat Genet* **13**, 54-62 (1996).
- 279 Le LP, Le HN, Nelson AR, Matthews DA, Yamamoto M, Curiel DT. Core labeling of adenovirus with EGFP. *Virology* **351**, 291-302 (2006).
- 280 Reich NC, Sarnow P, Duprey E, Levine AJ. Monoclonal antibodies which recognize native and denatured forms of the adenovirus DNA-binding protein. *Virology* **128**, 480-484 (1983).
- 281 Das S, MacDonald K, Chang HY, Mitzner W. A simple method of mouse lung intubation. *J Vis Exp*, e50318 (2013).
- 282 Jeyaseelan S, Chu HW, Young SK, Worthen GS. Transcriptional profiling of lipopolysaccharide-induced acute lung injury. *Infect Immun* **72**, 7247-7256 (2004).
- 283 Nick JA, Young SK, Brown KK, Avdi NJ, Arndt PG, Suratt BT, Janes MS, Henson PM, Worthen GS. Role of p38 mitogen-activated protein kinase in a murine model of pulmonary inflammation. *J Immunol* **164**, 2151-2159 (2000).
- 284 Zaret K. Micrococcal nuclease analysis of chromatin structure. *Curr Protoc Mol Biol* **Chapter 21**, Unit 21 21 (2005).
- 285 Wessel D, Flugge UI. A method for the quantitative recovery of protein in dilute solution in the presence of detergents and lipids. *Anal Biochem* **138**, 141-143 (1984).
- 286 Cox J, Mann M. MaxQuant enables high peptide identification rates, individualized p.p.b.-range mass accuracies and proteome-wide protein quantification. *Nature biotechnology* **26**, 1367-1372 (2008).
- 287 Schwanhauser B, Busse D, Li N, Dittmar G, Schuchhardt J, Wolf J, Chen W, Selbach M. Global quantification of mammalian gene expression control. *Nature* **473**, 337-342 (2011).
- 288 Tanaka Y, Tawaramoto-Sasanuma M, Kawaguchi S, Ohta T, Yoda K, Kurumizaka H, Yokoyama S. Expression and purification of recombinant human histones. *Methods* **33**, 3-11 (2004).
- 289 Hasson D, Panchenko T, Salimian KJ, Salman MU, Sekulic N, Alonso A, Warburton PE, Black BE. The octamer is the major form of CENP-A nucleosomes at human centromeres. *Nat Struct Mol Biol* **20**, 687-695 (2013).
- 290 Sekulic N, Bassett EA, Rogers DJ, Black BE. The structure of (CENP-A-H4)₂ reveals physical features that mark centromeres. *Nature* **467**, 347-351 (2010).
- 291 Kulej K, Avgousti DC, Weitzman MD, Garcia BA. Characterization of histone post-translational modifications during virus infection using mass spectrometry-based proteomics. *Methods* **90**, 8-20 (2015).
- 292 Cooper PR, Panettieri RA, Jr. Steroids completely reverse albuterol-induced beta(2)-adrenergic receptor tolerance in human small airways. *J Allergy Clin Immunol* **122**, 734-740 (2008).
- 293 Zacharias DA, Violin JD, Newton AC, Tsien RY. Partitioning of lipid-modified monomeric GFPs into membrane microdomains of live cells. *Science* **296**, 913-916 (2002).
- 294 Blumenthal D, Goldstien L, Edidin M, Gheber LA. Universal Approach to FRAP Analysis of Arbitrary Bleaching Patterns. *Sci Rep* **5**, 11655 (2015).
- 295 Oh E, Akopian D, Rape M. Principles of Ubiquitin-Dependent Signaling. *Annu Rev Cell Dev Biol* **34**, 137-162 (2018).

- 296 Petroski MD, Deshaies RJ. Function and regulation of cullin-RING ubiquitin ligases. *Nature reviews. Molecular cell biology* **6**, 9-20 (2005).
- 297 Woo JL, Berk AJ. Adenovirus ubiquitin-protein ligase stimulates viral late mRNA nuclear export. *J Virol* **81**, 575-587 (2007).
- 298 Cathomen T, Weitzman MD. A functional complex of adenovirus proteins E1B-55kDa and E4orf6 is necessary to modulate the expression level of p53 but not its transcriptional activity. *J Virol* **74**, 11407-11412 (2000).
- 299 Soucy TA, Smith PG, Milhollen MA, Berger AJ, Gavin JM, Adhikari S, Brownell JE, Burke KE, Cardin DP, Critchley S, Cullis CA, Doucette A, Garnsey JJ, Gaulin JL, Gershman RE, Lublinsky AR, McDonald A, Mizutani H, Narayanan U, Olhava EJ, Peluso S, Rezaei M, Sintchak MD, Talreja T, Thomas MP, Traore T, Vyskocil S, Weatherhead GS, Yu J, Zhang J, Dick LR, Claiborne CF, Rolfe M, Bolen JB, Langston SP. An inhibitor of NEDD8-activating enzyme as a new approach to treat cancer. *Nature* **458**, 732-736 (2009).
- 300 Hori T, Osaka F, Chiba T, Miyamoto C, Okabayashi K, Shimbara N, Kato S, Tanaka K. Covalent modification of all members of human cullin family proteins by NEDD8. *Oncogene* **18**, 6829-6834 (1999).
- 301 Schwechheimer C. NEDD8-its role in the regulation of Cullin-RING ligases. *Curr Opin Plant Biol* **45**, 112-119 (2018).
- 302 Tudek A, Schmid M, Jensen TH. Escaping nuclear decay: the significance of mRNA export for gene expression. *Curr Genet* **65**, 473-476 (2019).
- 303 Stewart M. Polyadenylation and nuclear export of mRNAs. *The Journal of biological chemistry* **294**, 2977-2987 (2019).
- 304 Marcellus RC, Teodoro JG, Charbonneau R, Shore GC, Branton PE. Expression of p53 in Saos-2 osteosarcoma cells induces apoptosis which can be inhibited by Bcl-2 or the adenovirus E1B-55 kDa protein. *Cell Growth Differ* **7**, 1643-1650 (1996).
- 305 Fabregat A, Jupe S, Matthews L, Sidiropoulos K, Gillespie M, Garapati P, Haw R, Jassal B, Korninger F, May B, Milacic M, Roca CD, Rothfels K, Sevilla C, Shamovsky V, Shorser S, Varusai T, Viteri G, Weiser J, Wu G, Stein L, Hermjakob H, D'Eustachio P. The Reactome Pathway Knowledgebase. *Nucleic Acids Res* **46**, D649-D655 (2018).
- 306 www.proteinatlas.org.
- 307 Konig J, Zarnack K, Rot G, Curk T, Kayikci M, Zupan B, Turner DJ, Luscombe NM, Ule J. iCLIP reveals the function of hnRNP particles in splicing at individual nucleotide resolution. *Nat Struct Mol Biol* **17**, 909-915 (2010).
- 308 McCloskey A, Taniguchi I, Shinmyozu K, Ohno M. hnRNP C tetramer measures RNA length to classify RNA polymerase II transcripts for export. *Science* **335**, 1643-1646 (2012).
- 309 Zarnack K, Konig J, Tajnik M, Martincorena I, Eustermann S, Stevant I, Reyes A, Anders S, Luscombe NM, Ule J. Direct competition between hnRNP C and U2AF65 protects the transcriptome from the exonization of Alu elements. *Cell* **152**, 453-466 (2013).
- 310 Cornella N, Tebaldi T, Gasperini L, Singh J, Padgett RA, Rossi A, Macchi P. The hnRNP RALY regulates transcription and cell proliferation by modulating the expression of specific factors including the proliferation marker E2F1. *The Journal of biological chemistry* **292**, 19674-19692 (2017).
- 311 Rossi A, Moro A, Tebaldi T, Cornella N, Gasperini L, Lunelli L, Quattrone A, Viero G, Macchi P. Identification and dynamic changes of RNAs isolated from RALY-containing ribonucleoprotein complexes. *Nucleic Acids Res* **45**, 6775-6792 (2017).
- 312 Bondy-Chorney E, Baldwin RM, Didillon A, Chabot B, Jasmin BJ, Cote J. RNA binding protein RALY promotes Protein Arginine Methyltransferase 1 alternatively spliced isoform v2 relative expression and metastatic potential in breast cancer cells. *Int J Biochem Cell Biol* **91**, 124-135 (2017).
- 313 van Eekelen C, Ohlsson R, Philipson L, Mariman E, van Beek R, van Venrooij W. Sequence dependent interaction of hnRNP proteins with late adenoviral transcripts. *Nucleic Acids Res* **10**, 7115-7131 (1982).

- 314 Tenzer S, Moro A, Kuharev J, Francis AC, Vidalino L, Provenzani A, Macchi P. Proteome-wide characterization of the RNA-binding protein RALY-interactome using the in vivo-biotinylation-pulldown-quant (iBioPQ) approach. *J Proteome Res* **12**, 2869-2884 (2013).
- 315 Chahal JS, Flint SJ. Timely synthesis of the adenovirus type 5 E1B 55-kilodalton protein is required for efficient genome replication in normal human cells. *J Virol* **86**, 3064-3072 (2012).
- 316 Bridge E, Pettersson U. Nuclear organization of adenovirus RNA biogenesis. *Exp Cell Res* **229**, 233-239 (1996).
- 317 Aspegren A, Rabino C, Bridge E. Organization of splicing factors in adenovirus-infected cells reflects changes in gene expression during the early to late phase transition. *Exp Cell Res* **245**, 203-213 (1998).
- 318 Huang M, Rech JE, Northington SJ, Flicker PF, Mayeda A, Krainer AR, LeStourgeon WM. The C-protein tetramer binds 230 to 240 nucleotides of pre-mRNA and nucleates the assembly of 40S heterogeneous nuclear ribonucleoprotein particles. *Mol Cell Biol* **14**, 518-533 (1994).
- 319 Vassileva MT, Matunis MJ. SUMO modification of heterogeneous nuclear ribonucleoproteins. *Mol Cell Biol* **24**, 3623-3632 (2004).
- 320 Chanarat S, Mishra SK. Emerging Roles of Ubiquitin-like Proteins in Pre-mRNA Splicing. *Trends Biochem Sci* **43**, 896-907 (2018).
- 321 Chan CH, Li CF, Yang WL, Gao Y, Lee SW, Feng Z, Huang HY, Tsai KK, Flores LG, Shao Y, Hazle JD, Yu D, Wei W, Sarbassov D, Hung MC, Nakayama KI, Lin HK. The Skp2-SCF E3 ligase regulates Akt ubiquitination, glycolysis, herceptin sensitivity, and tumorigenesis. *Cell* **149**, 1098-1111 (2012).
- 322 Lee SW, Li CF, Jin G, Cai Z, Han F, Chan CH, Yang WL, Li BK, Rezaeian AH, Li HY, Huang HY, Lin HK. Skp2-dependent ubiquitination and activation of LKB1 is essential for cancer cell survival under energy stress. *Mol Cell* **57**, 1022-1033 (2015).
- 323 Zhang Q, Karnak D, Tan M, Lawrence TS, Morgan MA, Sun Y. FBXW7 Facilitates Nonhomologous End-Joining via K63-Linked Polyubiquitylation of XRCC4. *Mol Cell* **61**, 419-433 (2016).
- 324 Bischoff JR, Kirn DH, Williams A, Heise C, Horn S, Muna M, Ng L, Nye JA, Sampson-Johannes A, Fattaey A, McCormick F. An adenovirus mutant that replicates selectively in p53-deficient human tumor cells. *Science* **274**, 373-376 (1996).
- 325 Grifman M, Chen NN, Gao GP, Cathomen T, Wilson JM, Weitzman MD. Overexpression of cyclin A inhibits augmentation of recombinant adeno-associated virus transduction by the adenovirus E4orf6 protein. *J Virol* **73**, 10010-10019 (1999).
- 326 Sobhian B, Shao G, Lilli DR, Culhane AC, Moreau LA, Xia B, Livingston DM, Greenberg RA. RAP80 targets BRCA1 to specific ubiquitin structures at DNA damage sites. *Science* **316**, 1198-1202 (2007).
- 327 Komatsu T, Dacheux D, Kreppel F, Nagata K, Wodrich H. A Method for Visualization of Incoming Adenovirus Chromatin Complexes in Fixed and Living Cells. *PLoS One* **10**, e0137102 (2015).
- 328 Sarnow P, Sullivan CA, Levine AJ. A monoclonal antibody detecting the adenovirus type 5-E1b-58Kd tumor antigen: characterization of the E1b-58Kd tumor antigen in adenovirus-infected and -transformed cells. *Virology* **120**, 510-517 (1982).
- 329 Chiba I, Takahashi T, Nau MM, D'Amico D, Curiel DT, Mitsudomi T, Buchhagen DL, Carbone D, Piantadosi S, Koga H, et al. Mutations in the p53 gene are frequent in primary, resected non-small cell lung cancer. Lung Cancer Study Group. *Oncogene* **5**, 1603-1610 (1990).
- 330 Raj A, van den Bogaard P, Rifkin SA, van Oudenaarden A, Tyagi S. Imaging individual mRNA molecules using multiple singly labeled probes. *Nat Methods* **5**, 877-879 (2008).
- 331 Shaffer SM, Dunagin MC, Torborg SR, Torre EA, Emert B, Krepler C, Beqiri M, Sproesser K, Brafford PA, Xiao M, Eggan E, Anastopoulos IN, Vargas-Garcia CA, Singh A, Nathanson KL, Herlyn M, Raj A. Rare cell variability and drug-induced reprogramming as a mode of cancer drug resistance. *Nature* **546**, 431-435 (2017).

- 332 Van Nostrand EL, Pratt GA, Shishkin AA, Gelboin-Burkhart C, Fang MY, Sundararaman B, Blue SM, Nguyen TB, Surka C, Elkins K, Stanton R, Rigo F, Guttman M, Yeo GW. Robust transcriptome-wide discovery of RNA-binding protein binding sites with enhanced CLIP (eCLIP). *Nat Methods* **13**, 508-514 (2016).
- 333 Shannon P, Markiel A, Ozier O, Baliga NS, Wang JT, Ramage D, Amin N, Schwikowski B, Ideker T. Cytoscape: a software environment for integrated models of biomolecular interaction networks. *Genome Res* **13**, 2498-2504 (2003).
- 334 Buenrostro JD, Giresi PG, Zaba LC, Chang HY, Greenleaf WJ. Transposition of native chromatin for fast and sensitive epigenomic profiling of open chromatin, DNA-binding proteins and nucleosome position. *Nat Methods* **10**, 1213-1218 (2013).
- 335 Hakim O, Misteli T. SnapShot: Chromosome confirmation capture. *Cell* **148**, 1068 e1061-1062 (2012).
- 336 Lieberman-Aiden E, van Berkum NL, Williams L, Imakaev M, Ragoczy T, Telling A, Amit I, Lajoie BR, Sabo PJ, Dorschner MO, Sandstrom R, Bernstein B, Bender MA, Groudine M, Gnirke A, Stamatoyannopoulos J, Mirny LA, Lander ES, Dekker J. Comprehensive mapping of long-range interactions reveals folding principles of the human genome. *Science* **326**, 289-293 (2009).
- 337 Tan JH, Kajiwara Y, Shahied L, Li J, McAfee JG, LeStourgeon WM. The bZIP-like motif of hnRNP C directs the nuclear accumulation of pre-mRNA and lethality in yeast. *Journal of molecular biology* **305**, 829-838 (2001).
- 338 Wan L, Kim JK, Pollard VW, Dreyfuss G. Mutational definition of RNA-binding and protein-protein interaction domains of heterogeneous nuclear RNP C1. *The Journal of biological chemistry* **276**, 7681-7688 (2001).
- 339 Cienikova Z, Damberger FF, Hall J, Allain FH, Maris C. Structural and mechanistic insights into poly(uridine) tract recognition by the hnRNP C RNA recognition motif. *J Am Chem Soc* **136**, 14536-14544 (2014).
- 340 Horridge JJ, Leppard KN. RNA-binding activity of the E1B 55-kilodalton protein from human adenovirus type 5. *J Virol* **72**, 9374-9379 (1998).
- 341 Kato SE, Huang W, Flint SJ. Role of the RNA recognition motif of the E1B 55 kDa protein in the adenovirus type 5 infectious cycle. *Virology* **417**, 9-17 (2011).
- 342 Tejera B, Lopez RE, Hidalgo P, Cardenas R, Ballesteros G, Rivillas L, French L, Amero C, Pastor N, Santiago A, Groitl P, Dobner T, Gonzalez RA. The human adenovirus type 5 E1B 55kDa protein interacts with RNA promoting timely DNA replication and viral late mRNA metabolism. *PLoS One* **14**, e0214882 (2019).
- 343 Chu C, Quinn J, Chang HY. Chromatin isolation by RNA purification (ChIRP). *J Vis Exp* (2012).
- 344 Thompson MG, Munoz-Moreno R, Bhat P, Roytenberg R, Lindberg J, Gazzara MR, Mallory MJ, Zhang K, Garcia-Sastre A, Fontoura BMA, Lynch KW. Co-regulatory activity of hnRNP K and NS1-BP in influenza and human mRNA splicing. *Nat Commun* **9**, 2407 (2018).
- 345 Sohn SY, Hearing P. Mechanism of Adenovirus E4-ORF3-Mediated SUMO Modifications. *mBio* **10** (2019).
- 346 Sohn SY, Hearing P. The adenovirus E4-ORF3 protein functions as a SUMO E3 ligase for TIF-1gamma sumoylation and poly-SUMO chain elongation. *Proceedings of the National Academy of Sciences of the United States of America* **113**, 6725-6730 (2016).
- 347 Sohn SY, Bridges RG, Hearing P. Proteomic analysis of ubiquitin-like posttranslational modifications induced by the adenovirus E4-ORF3 protein. *J Virol* **89**, 1744-1755 (2015).
- 348 Bridges RG, Sohn SY, Wright J, Leppard KN, Hearing P. The Adenovirus E4-ORF3 Protein Stimulates SUMOylation of General Transcription Factor TFII-I to Direct Proteasomal Degradation. *mBio* **7**, e02184-02115 (2016).
- 349 Goodman DE, Pretto CD, Krepostman TA, Carnahan KE, Spindler KR. Enhanced Replication of Mouse Adenovirus Type 1 following Virus-Induced Degradation of Protein Kinase R (PKR). *mBio* **10** (2019).
- 350 Huttenhain R, Xu J, Burton LA, Gordon DE, Hultquist JF, Johnson JR, Satkamp L, Hiatt J, Rhee DY, Baek K, Crosby DC, Frankel AD, Marson A, Harper JW, Alpi AF, Schulman BA,

- Gross JD, Krogan NJ. ARIH2 Is a Vif-Dependent Regulator of CUL5-Mediated APOBEC3G Degradation in HIV Infection. *Cell host & microbe* **26**, 86-99 e87 (2019).
- 351 Wang BD, Lee NH. Aberrant RNA Splicing in Cancer and Drug Resistance. *Cancers (Basel)* **10** (2018).
- 352 Sveen A, Kilpinen S, Ruusulehto A, Lothe RA, Skotheim RI. Aberrant RNA splicing in cancer; expression changes and driver mutations of splicing factor genes. *Oncogene* **35**, 2413-2427 (2016).
- 353 Herrmann C, Avgousti DC, Weitzman MD. Differential Salt Fractionation of Nuclei to Analyze Chromatin-associated Proteins from Cultured Mammalian Cells. *Bio Protoc* **7** (2017).
- 354 Sanchez R, Meslamani J, Zhou MM. The bromodomain: from epigenome reader to druggable target. *Biochim Biophys Acta* **1839**, 676-685 (2014).